Phase transitions in systems of hard anisotropic particles on lattices

By

Joyjit Kundu

PHYS10201004005

The Institute of Mathematical Sciences, Chennai

A thesis submitted to the

Board of Studies in Physical Sciences

In partial fulfillment of requirements

For the Degree of

DOCTOR OF PHILOSOPHY

of

HOMI BHABHA NATIONAL INSTITUTE

January, 2015

Homi Bhabha National Institute

Recommendations of the Viva Voce Board

As members of the Viva Voce Board, we certify that we have read the dissertation prepared by Joyjit Kundu entitled “Phase transitions in systems of hard anisotropic particles on lattices" and recommend that it maybe accepted as fulfilling the dissertation requirement for the Degree of Doctor of Philosophy.

_____ Date:

Chair - Purusattam Ray

_____ Date:

Guide/Convener - Rajesh Ravindran

_____ Date:

Member 1 - Pinaki Chaudhuri (replacing Gautam I. Menon)

_____ Date:

Member 2 - Ronojoy Adhikari

_____ Date:

External Examiner - Kedar Damle

Final approval and acceptance of this dissertation is contingent upon the candidate’s submission of the final copies of the dissertation to HBNI.

I hereby certify that I have read this dissertation prepared under my direction and recommend that it may be accepted as fulfilling the dissertation requirement.

Date:

Place: Guide

STATEMENT BY AUTHOR

This dissertation has been submitted in partial fulfillment of requirements for an advanced degree at Homi Bhabha National Institute (HBNI) and is deposited in the Library to be made available to borrowers under rules of the HBNI.

Brief quotations from this dissertation are allowable without special permission, provided that accurate acknowledgement of source is made. Requests for permission for extended quotation from or reproduction of this manuscript in whole or in part may be granted by the Competent Authority of HBNI when in his or her judgement the proposed use of the material is in the interests of scholarship. In all other instances, however, permission must be obtained from the author.

Joyjit Kundu

DECLARATION

I, hereby declare that the investigation presented in the thesis has been carried out by me. The work is original and has not been submitted earlier as a whole or in part for a degree / diploma at this or any other Institution / University.

Joyjit Kundu

ACKNOWLEDGEMENTS

First, I would like to thank my supervisor Prof. Rajesh Ravindran for his wonderful guidance, continuous encouragement, support and patience throughout my stay at The Institute of Mathematical Sciences (IMSc). I have found him more as a friend who has always given me the freedom to discuss about any idea. I must say that apart from learning Statistical Mechanics from him, I have been enriched by his scientific ethics, and way of working. His excellent ideas have helped immensely to build up this thesis. I thank him for being so approachable.

I am thankful to my collaborators Porf. Deepak Dhar, Prof. J. F. Stilck, and Trisha Nath. In particular, I would like to thank Prof. Deepak Dhar for his valuable comments, ideas, suggestions regarding my research work. Discussions with him have always been beneficial for me. I am grateful to Prof. Gautam Menon, Prof. Purusattam Ray, and Prof. Ronojoy Adhikari for their constructive criticisms and insightful remarks as members of my doctoral committee.

Life at IMSc would not have been joyful without my friends and colleagues. I would especially like to thank Nirmalya, Subhadeep, Tuhin, Sudhir, Abhrajit, Pinaki, Krishanu, Prateep, and Gaurav. These guys have really made my stay at IMSc wonderful and memorable.

I also thank Dr. Pinaki Chaudhuri, Dr. S. R. Hassan, Soumyajyoti Biswas, Arghya Dutta, Saurabh Niyogi, Abhijit Chakraborty for being around me whenever I needed.

I would like to thank the High-Performance Computing facility at IMSc. Most of the simulations for my work have been carried out on the supercomputing machine Annapurna. I take this opportunity to thank P. Mangalapandi for helping me out in this regard.

I am also grateful to IMSc administration and librarians for all their support during my stay.

Finally, I would like to express my gratitude to my parents and my (would be) wife. It would not have been possible for me to reach this level without their constant support, understanding and unconditional love.

List of Publications arising from the thesis

- **Journal**

1. **Phase transitions in systems of hard rectangles with non-integer aspect ratio**

   Joyjit Kundu and R. Rajesh

   Eur. Phys. J. B **88**, 133 (2015)

2. **Asymptotic behavior of the isotropic-nematic and nematic-columnar phase boundaries for the system of hard rectangles on a square Lattice**

   Joyjit Kundu and R. Rajesh

   Phys. Rev. E **91**, 012105 (2015)

3. **Phase transitions in a system of hard rectangles on the square lattice**

   Joyjit Kundu and R. Rajesh

   Phys. Rev. E **89**, 052124 (2014)

4. **Reentrant disordered phase in a system of repulsive rods on a Bethe-like lattice**

   Joyjit Kundu and R. Rajesh

   Phys. Rev. E **88**, 012134 (2013)

5. **Nematic-disordered phase transition in systems of long rigid rods on two-dimensional lattices**

   Joyjit Kundu, R. Rajesh, Deepak Dhar, Jürgen F. Stilck

   Phys. Rev. E **87**, 032103 (2013)

- **Conferences**

1. **A Monte carlo algorithm for studying phase transition in systems of hard rigid rods**

   Joyjit Kundu, R. Rajesh, Deepak Dhar, Jürgen F. Stilck

   AIP Conf. Proc. **1447**, 113 (2012)

Other Publications

- **Journal**

1. [‡]**High-activity expansion for the columnar phase of the hard rectangle gas**

   Trisha Nath, Joyjit Kundu, and R. Rajesh

   To appear in J. Stat. Phys, June 2015 (*arXiv:1411.7831*)

[‡]Not included in thesis

Contents

Synopsis

Entropy is a measure of disorder in a system. Usually, ordering transitions lead to a decrease in entropy. Entropy-driven phase transitions, on the other hand, are interesting and counter-intuitive as they lead to increase in visible order with gain in entropy. Examples of systems undergoing entropy-driven phase transitions from disordered to ordered phases with different broken symmetries include colloids of polymethyl methacrylate (PMMA) [1], tobacco mosaic virus [2], fd virus [3], silica particles [4], boehmite particles [5], Brownian square platelets [6], and banana-shaped molecules [7].

Hard-core models or systems with only excluded volume interactions are minimal models to study entropy-driven ordering transitions. For example, hard spheres in continuum undergo a fluid–solid transition with increasing packing fraction as seen in experiments with colloidal PMMA [8, 9]. The phase transitions in a system of hard rods are significant for more complex systems like liquid crystals [10, 11, 12]. Hard-core lattice gas models of particles of different shapes have direct realization in the adsorption of gas molecules on metal surfaces [13, 14].

Consider systems of hard anisotropic particles. Long hard rods in three dimensions undergo a discontinuous transition from an isotropic fluid phase to an orientationally ordered nematic phase with increasing density [11, 15, 16]. Further increase of density may lead to phases with translational order, like the smectic and solid phases [12]. Hard needles in two-dimensional continuum undergo a Kosterlitz-Thouless-type transition into a nematic phase with quasi-long-range orientational order [17]. Systems of hard rectangles with short aspect ratio in continuum may exhibit tetratic and solid-like phases [18, 19].

Compared to the continuum problems, the systems of hard rods or rectangles on lattices are less well-understood. It may be heuristically argued that the maximal density phase for hard rectangles on lattices does not posses orientational order [10, 20]. Both the low

and high-density phases being disordered, it remained unclear till recently whether the system may ever exhibit an ordered phase [10]. In this thesis, we focus on the model of hard rectangles on lattices.

The Model of hard rectangles: Consider a monodispersed system of hard rectangles of size $m \times mk$, where the aspect ratio $k > 1$, on a square lattice with periodic boundary conditions. Generalization to the other lattices is straight forward. Each rectangle may be oriented along the horizontal or vertical direction. A horizontal (vertical) rectangle occupies mk lattice sites along the x (y)-axis and m lattice sites along the y (x)-axis. No two rectangles may overlap or equivalently each site may be occupied atmost by one rectangle. We associate an activity $z = e^{\mu}$ to each rectangle, where μ is the chemical potential. The grand canonical partition function for the system is

$$\mathcal{Z} = \sum_{n_h, n_v} C(n_h, n_v)\, z^{n_h + n_v}, \tag{1}$$

where $C(n_h, n_v)$ is the number of distinct configurations with n_h horizontal and n_v vertical rectangles. The fraction of occupied sites $\rho = m^2 k \, \langle n_h + n_v \rangle / L^2$ will be referred as density, where L is the system size.

Known results: When $m = 1$, the system corresponds to that of hard rods on lattices. The dimer model ($k = 2$) does not undergo any phase transition and remains disordered at all densities [21, 22, 23]. Recently, the existence of an intermediate density nematic phase having only orientational order and, hence, a transition from a low-density disordered (LDD) to the nematic phase has been shown both numerically for $k \geq 7$ [20] and rigorously for $k \gg 1$ [24]. The LDD–nematic phase transition was found to be in the Ising universality class for the square lattice and in the three-state Potts universality class for the triangular lattice [25]. If the heuristic argument of the high-density phase being orientationally disordered is correct, there should be a second transition from the nematic to a high-density disordered (HDD) phase. However, it is difficult to equilibrate the system at high densities using Monte Carlo algorithms with local evaporation and deposition

moves as the system gets stuck in long lived metastable states. Therefore, establishing the existence and determining the nature of the HDD phase have remained open problems. The only exact solution that exists is for hard rods on the random locally tree-like layered lattice [26]. On this lattice, while the LDD–nematic transition exists, the second transition is absent. There are very few studies for $m > 1$. Simulations of hard parallelepipeds on cubic lattice show layered and columnar phases, but no nematic phase [27]. However, the complete phase diagram has remained unexplored. The limit $m \to \infty$, keeping k fixed corresponds to the system of oriented rectangles of aspect ratio k in continuum, known as the Zwanzig model. From truncated virial expansion [15] and within a Bethe approximation [28], it was predicted that this model would undergo a disordered–nematic phase transition with increasing density [15].

Is there an efficient algorithm that allows the study of hard-core systems close to full packing? What are the possible phases and the $\rho - k$ phase diagram for different m? What is the nature of the phase transitions between the different phases? In this thesis we systematically address these questions. Below, we summarize the main results.

The Monte carlo algorithm: We implement an efficient Monte carlo algorithm to study systems of extended hard particles on lattices. Here, we describe the algorithm for hard rectangles of size $m \times mk$ on a square lattice. Starting with an valid configuration, a row (or a column) is chosen at random. First, all the horizontal (vertical) rectangles whose bottom-left corners are on that row (column) are evaporated, keeping the remaining rectangles as they are. The row (column) now consists of intervals of empty sites, separated by sites which are either already occupied by rectangles or can not be occupied due to the hard-core constraint. Next, the empty intervals of the row (column) are refilled by deposition of horizontal (vertical) rectangles with the correct equilibrium grand canonical probabilities. The calculation of these probabilities reduces to a solvable one-dimensional problem. In addition to the evaporation-deposition move, we also implement a flip move. In this move, a site is picked up at random. If the chosen site is the bottom-left corner of

a square plaquette of size $mk \times mk$ consisting of k aligned horizontal (vertical) rectangles, the plaquette is replaced by a similar plaquette of k vertical (horizontal) rectangles. One Monte Carlo move corresponds to $2L$ evaporation-deposition and L^2 plaquette flip moves.

This algorithm is easily parallelizable. The evaporation and deposition of rectangles in rows or columns separated by m are independent of each other, and may be done simultaneously by passing them into different processors. Similarly, the flip move may also be parallelized by dividing the lattice of size L^2 into L^2/m^2k^2 blocks of size $mk \times mk$. For rods of size 1×7, this algorithm allows to simulate system sizes upto 2576 and densities upto 0.99, while algorithms with local moves are restricted to $L < 200$ and densities upto 0.85 [20].

The algorithm is easily generalized to particles of different shapes. Other implementations of this algorithm include lattice gas model of particles with exclusion of several next-nearest-neighbor sites [29, 30], mixtures of hard squares and dimers [31].

Hard rods ($m = 1$): Implementing the above algorithm for the hard rod system ($m = 1$) on the square and triangular lattices, we demonstrate the existence of the HDD phase on both the lattices for $k = 7$. The metastability of the nematic order at high densities is quantitatively described using classical nucleation theory. The transition from the nematic to the HDD phase with increasing density is found to be continuous on both the lattices. On the square lattice, our best estimates of the critical exponents for this transition are $\beta/\nu = 0.22 \pm 0.07$, $\gamma/\nu = 1.56 \pm 0.07$, and $\alpha/\nu = 0.22 \pm 0.07$. These exponents differ from those of the two-dimensional Ising model. To better understand the nature of the HDD phase, we study the correlations, cluster size distribution, stack distribution and the formation of bound states of vacancies. Interestingly, we find the existence of a crossover length scale $\xi^* \gtrsim 1400$ on the square lattice. For distances smaller than ξ^*, correlations appear to decay algebraically and we can not rule out a crossover to Ising universality class at length scales $\gg \xi^*$. The stack distribution remains exponential at all densities. We find that the vacancies in the HDD phase, similar to the LDD phase, do not form a

bound state. Thus, it remains unclear from Monte Carlo simulations whether the HDD phase is a reentrant LDD phase. On the triangular lattice the critical exponents for the second transition are consistent with the first transition that belongs to the three-state Potts universality class.

Repulsive rods on a Bethe-like lattice: To investigate whether the HDD phase is a reentrant LDD phase, we study a model where rods are allowed to intersect, but with an energy cost, adding an extra dimension to the phase diagram. We solve the model exactly on the random locally tree-like layered lattice (RLTL), a lattice that was introduced in Ref. [26] to study the disordered–nematic transition for hard rods of finite length k. We briefly describe the RLTL for coordination number $q = 4$. Generalization to the larger even values of q is straight forward. Consider a collection of M layers, each having N sites. A layer m is connected to the adjacent layer $(m-1)$ by N bonds of type X and N bonds of type Y. Each site in the mth layer is connected with randomly chosen sites in the $(m-1)$-th layer by an X bond and a Y bond. A rod of length k, called as k-mer, occupies $(k-1)$ consecutive bonds of same type. Rods on X (Y) type of bonds will be called x-mers (y-mers). When $q = 4$, a site may either be empty, or occupied by a single rod, or occupied simultaneously by an x-mer and a y-mer. We assign a weight u for each site that is simultaneously occupied by an x-mer and a y-mer. When $q = 6$, there are three types of bonds and each site may be occupied by atmost three k-mers of different types. An additional weight v is associated to such sites. The partition function is defined as the weighted average over all rod-configurations as well as bond-configurations.

We show that when $k \geq 4$ and $u < u_c$, the system undergoes two phase transition with increasing density: first from a LDD to a nematic phase and second, from the nematic to a HDD phase [see Fig. 1]. When $q = 4$, both the transitions are continuous and found to be in the mean field Ising universality class [see Fig. 1 (A)]. For $q = 6$, the first transition is discontinuous, while the nature of the second transition depends on the length of the rods and the intersection parameters. The phase coexistence region at a discontinuous

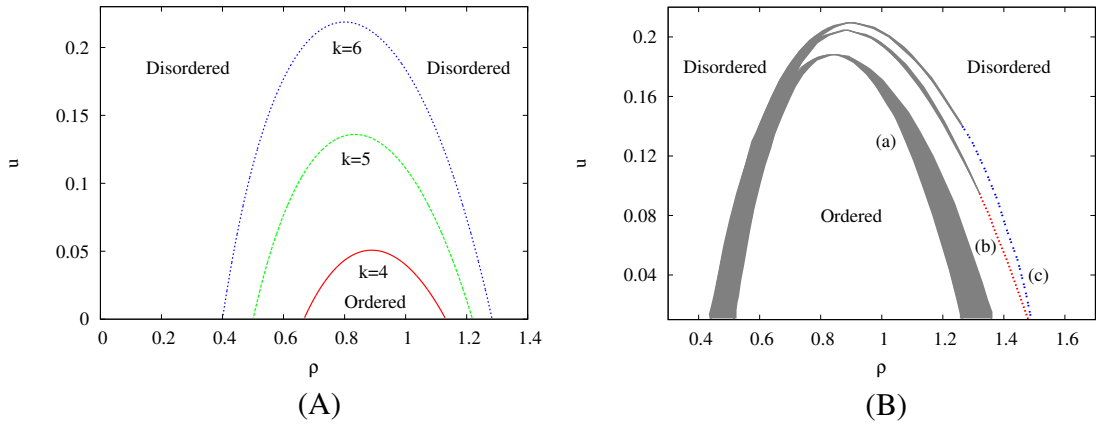

Figure 1: Phase diagram when (A) $q = 4$ for different values of k and, (B) $q = 6$ and $k = 7$: (a) $v = u^2$, (b) $v = u^3$, and (c) $v = u^4$. Lines stand for continuous transitions and shaded region denotes phase coexistence at a discontinuous transition.

transition is shown by the shaded region in Fig. 1(B). Beyond a critical value u_c, no phase transition is observed, where $u_c < 1$ for any finite k. The $u - \rho$ phase diagram in Fig. 1 shows that it is always possible to continuously transform the LDD phase into the HDD phase without crossing any phase boundary, implying that the LDD and HDD phases are qualitatively similar.

Hard Rectangles with integer aspect ratio ($m \geq 2$, $k \in \mathbb{N}$): For hard rectangles of size $m \times mk$ with $m \geq 2$ and integer k, we find that the system may exist in four distinct phases: a low-density isotropic phase (I) in which the rectangles have neither orientational nor translational order, a nematic (N) phase in which the rectangles have orientational order but no translational order, a columnar (C) phase that has orientational order and partial translational order along the direction perpendicular to the preferred orientation and a sublattice (S) phase with complete spatial order, but no orientational order. Figure 2 shows the phase diagram for $m = 2$, obtained from Monte carlo simulations. The high-density (HD) phase is a S phase for $k \geq 2$ and C phase for $k = 1$ (hard square). When $m = 2$, $k = 2, 3$, the system undergoes a direct transition from the I to the S phase with increasing density. For $4 \leq k < 7$, there exists two transitions: first from the I phase to the C phase and second from the C to the S phase. When $k \geq 7$, with increasing density, the system transits successively from I to N to C to S phases. The I-N, N-C and

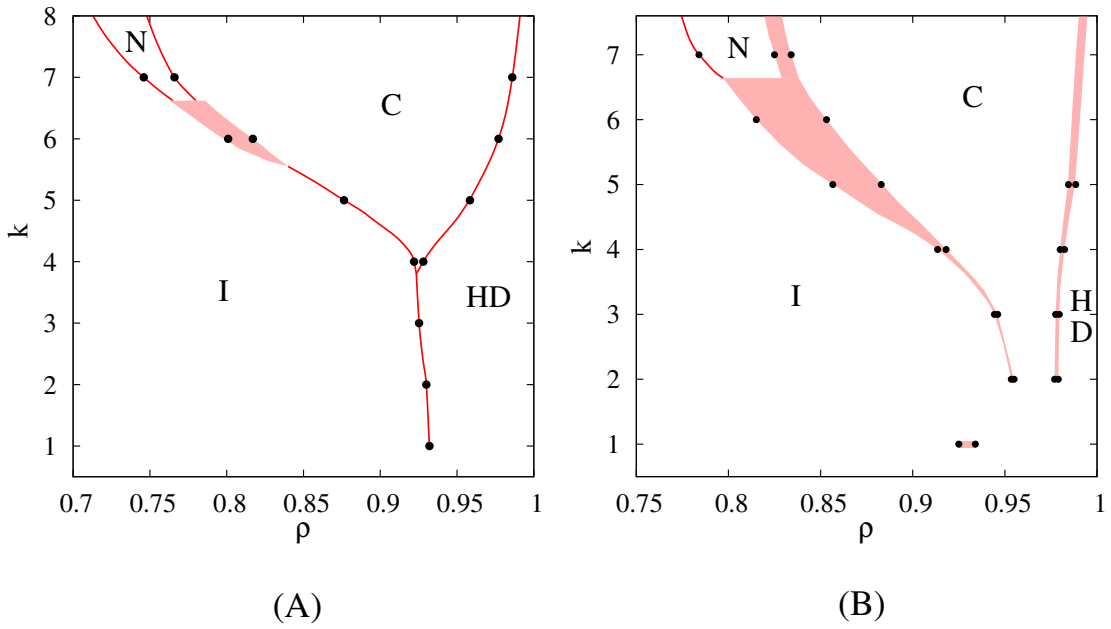

Figure 2: Phase diagram for integer k, when (A) $m = 2$ and, (B) $m = 3$. The data points are from simulation, while the continuous lines and shaded portions are guides to the eye. The shaded portion denotes regions of phase coexistence. The HD phase is a C phase for k = 1 and a S phase for k > 1.

C-S transitions are found to be continuous. The I-C transition is continuous for $k = 5$, and discontinuous for $k = 6$. Universality classes and the critical exponents for different transitions are summarized in Table 1. When $m = 3$, there exists no direct transition from the I to the S phase [see Fig. 2(B)]. For $2 \leq k < 7$, the system may exist in I, C or S phases depending on the density. When $k \geq 7$, the system undergoes I-N, N-C and C-S transitions with increasing density. All the transitions except the I-N transition, are found to be discontinuous. The I-N transition continues to be in the Ising universality class. We expect that the phase diagram for $m \geq 4$ is qualitatively similar to that for $m = 3$.

Hard Rectangles with non-integer aspect ratio ($m \geq 2$, $k \notin \mathbb{N}$): We also determine the phase diagram of the hard rectangle system when the aspect ratio k is a non-integer. The existence of a low-density I phase, an intermediate density N and C phases, and a high-density (HD) phase is observed. The HD phase has no orientational or positional order when the length and width of the rectangles are mutually prime (e.g. rectangles of size 2×5), otherwise, it is conjectured to be a sublattice phase (e.g rectangles of size 4×6).

Transition	k	*Universality class*	ν
I-S	2	Ashkin-Teller	1.18 ± 0.06
I-S	3	Ashkin-Teller	1.23 ± 0.07
I-C	5	Ashkin-Teller	0.82 ± 0.06
I-C	6	First order	
C-S	5	Ashkin-Teller	0.83 ± 0.06
I-N	7	Ising	1.00
N-C	7	Ising	1.00

Table 1: Table showing nature of different phase transitions for $2 \times 2k$ rectangles, where k is a integer. For the Ashkin-Teller and Ising universality classes, $\beta/\nu = 1/8$, $\gamma/\nu = 7/4$.

The system does not exhibit any phase transitions when $k < k_{min}(m)$. For $k_{min}(m) \leq k < k_c$, existence of an intermediate density C phase is observed. We find that $k_{min}(m = 2) = 11/2$ and $k_{min}(m = 3) = 13/3$. When $m = 2$, unlike the case of integer k, we find that the I-C transition is discontinuous when it exists. When $k \geq k_c$ for any m, an N phase exists and the system is expected to undergo three successive transitions with increasing density: first from the I to the N phase, second from the N to the C phase and third, from the C to the HD phase. We find, $20/3 < k_c \leq 7$. Both the I-N and N-C transitions belong to the Ising universality class for $m = 2$. We could not access the transition from the C phase to the HD phase due to difficulties with equilibration. The phase diagram of the system for $m \geq 3$ is expected to be qualitatively similar to that for $m = 2$.

Asymptotic behavior of the phase boundaries for hard rectangles: The asymptotic behavior of the I-N, N-C and C-S phase boundaries is studied using Monte carlo simulations and analytical calculations. Simulating systems up to $k = 60$ for $m = 1$ and $k = 56$ for $m = 2$ and 3, we show that the critical density for the I-N transition $\rho_c^{I-N} \approx A_1/k$, when $k \gg 1$, where A_1 is independent of m and equals to 4.80 ± 0.05. The N-C phase boundary is studied numerically for $m = 2$ and k up to 24. We obtain the critical density $\rho_c^{N-C} \approx 0.73 + 0.23k^{-1}$ for large k. Binder cumulant for the N-C transition is found to be non-universal and decreases as k^{-1} for $k \gg 1$. However, the critical exponents belong to the Ising universality class for all k. Numerical simulations of the C-S phase transitions for large k is constrained by large relaxation times at high densities. The I-N

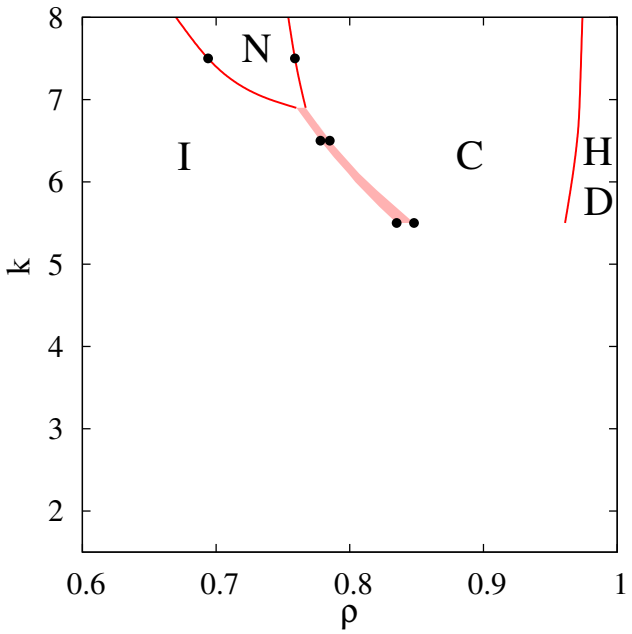

Figure 3: Phase diagram for the system of rectangles of size $2 \times 2k$, where k is a non-integer. The data points are from simulation, while the continuous lines and shaded portions are guides to the eye. The shaded portion denotes regions of phase coexistence.

phase boundary is calculated analytically from the virial expansion truncated at the second virial coefficient and a Bethe approximation. Within both the theories, we obtain $\rho_c^{I-N} \approx A_1/k$ for $k \gg 1$, where $A_1 = 2$. In this case, truncated virial theory is not exact in the limit $k \to \infty$. In particular, we find that all the even virial coefficients contributes in the limit $k \to \infty$. For the N-C transition, within a Bethe approximation, we obtain $\rho_c^{N-C}(m) \approx A_2(m) + A_3(m)\, k^{-1}$, with $A_2(m = 2) \approx 0.59$ and $A_3(m = 2) \approx 0.15$, which is qualitatively in agreement with the numerical finding. The C-S phase boundary is studied by estimating the entropies of the C and S phases. By comparing the entropies of these two phases , we obtain $\rho_c^{C-S} \approx 1 - A_4/mk^2$ for $k \gg 1$, where A_4 is a constant.

List of Figures

List of Tables

Chapter 1

Introduction

Phase transitions in equilibrium systems continue to be an active and fascinating area of research in Statistical Physics. Common examples of phase transitions in nature are the liquid–vapor and the liquid–solid transitions. While the liquid–solid transition in three dimensions is first order in nature, the liquid–vapor transition may be first order or second order. At a first order or discontinuous transition, the first derivatives of the free energy are discontinuous. In a second order or continuous phase transition, the first derivatives remain continuous, but the second derivatives of the free energy diverge. A second order transition is characterized by the divergence of the correlation length at the critical point. Near a critical point, the singular behavior of the thermodynamic quantities is universal and is determined by a set of critical exponents and universal scaling functions. The universality class of a continuous phase transition does not depend on many of the microscopic details of the particular system, rather it depends on factors like symmetry of the Hamiltonian, symmetry of the order parameter and dimensionality of the system. For instance, the critical exponents of the liquid–vapor transition belongs to the Ising universality class describing the ferromagnetic-paramagnetic transition in magnets.

In a phase transition, the free energy is minimized by two different phases on either side of the critical value of a control parameter like temperature or density. Usually, an ordered

phase has lower entropy than a disordered phase and a system undergoes a transition to such an ordered phase when the lowering of energy outweighs the loss in entropy. Thus, they are energy driven. On the other hand, there are entropy-driven ordering transitions in which there is no significant change of internal energy. Such transitions are particularly interesting and counter-intuitive as they lead to increase in visible order with increase of microscopic disorder, resulting in the gain in entropy [32]. Examples of entropy-driven transitions include the fluid–solid transition in colloids of polymethyl methacrylate (PMMA) [1], transition to various liquid crystalline phases like nematic, smectic, and cholesteric phases in systems of tobacco mosaic virus [33, 2], fd virus [3, 34], silica particles [35, 4], boehmite particles [5], banana-shaped molecules [7], and ordering transitions in adsorbed monolayer of gas particles on metal surfaces [13, 36, 37]. Entropy-driven crystal-crystal transitions may be realized in Brownian square platelets [6].

Systems with only hard-core or excluded volume interactions are minimal models to study entropy-driven transitions. For example, liquid–solid transition in colloidal polymethyl methacrylate (PMMA) may be modelled by the hard sphere system in continuum that exhibits a discontinuous transition from a liquid phase to a crystal phase with increasing packing fraction [8, 9]. Systems of hard rods or sphero-cylinders can reproduce the liquid, nematic, smectic and solid phases as seen in more complex systems like liquid crystals [10, 11, 12]. The phase behavior of two-dimensional Brownian square platelets may be reproduced by studying the model of rounded hard squares [38]. Hard-core lattice gas models have direct realizations in adsorptions of gas particles on metal surfaces and are studied to explain the phase diagram of the monolayers of adsorbed gas particles [13, 36, 39, 40, 37, 14]. The (100) and (110) planes of fcc crystals have square and rectangular symmetry and may be treated with lattice statistics if the adsorbate-adsorbate interaction is negligible with respect to the periodic variation of the corrugation potential of the underlying substrate [37]. For example, the monolayer of chlorine (Cl) on Ag(100) undergoes a continuous transition, belonging to the Ising universality class, to a spatially ordered structure $c(2 \times 2)$ with increasing coverage [13]. The critical coverage for this

transition is quite close to that of the hard square model, which also undergoes a similar transition [41, 42, 43]. Lattice gas model with repulsive interaction up to forth nearest neighbor has been used to study the phase behavior of selenium adsorbed on Ni(100) [36].

In addition to its relevance for entropy-driven transitions, hard-core lattice gas models are closely related to directed and undirected animals [44, 45, 46] and the Yang-Lee singularity [47], have applications in frustrated antiferromagnetic quantum spin systems [48, 49], short-range resonating valence bond physics [50], combinatorial problems [51, 52], glass transitions [53, 54, 55], granular media [56], self-assembly of nano particles on monolayers [57], thermodynamics of linear adsorbates [58, 59], and in establishing rigorous results [21, 60, 22, 23, 24]. Differently shaped particles that have been studied include dimers [61, 62, 63, 64, 21, 60, 22, 23, 65], trimers [66, 67], squares [41, 68, 69, 70, 71, 72, 73, 14, 74, 75], hexagons [76, 77, 78], triangles [66], tetrominoes [79, 57], discs [80, 29] and mixtures [31]. Despite sustained interests, exact solution exists only for hard hexagons [76] and related models [81]. Thus, it is important to study different shapes using simulations and approximate methods in order to develop phenomenology, leading to better understanding. The integrability of the hard hexagon and non-integrability of the hard square model has recently been studied in detail using zeros of partition function [82]. In this thesis, we focus on models of anisotropic hard particles.

1.1 Models of anisotropic hard particles

1.1.1 Continuum models

Solution of hard long rods in three dimensions undergoes a discontinuous transition from an isotropic phase to an orientationally ordered nematic phase with increasing density [11]. In the nematic phase, particles do not have positional order. The loss of orientational entropy in the nematic phase is compensated by the gain in positional entropy, as the ex-

cluded volume becomes negligible when the rods are aligned. This was shown by a virial expansion. The second virial coefficient was obtained by averaging the excluded volume over all orientations, or for an ordered arrangement of particles, over their equilibrium distribution of orientations. The orientational distribution was determined by the condition of minimum free energy. The third and higher virial coefficients may be neglected in the limit of infinite aspect ratio. Thus, this calculation is exact only for infinitely thin and long rods, or else restricted to low concentrations for rods with finite aspect ratio. Subsequently, the existence of a smectic phase, a columnar phase and a solid phase was shown to arise from pure hard-core exclusion at high densities [83, 84, 85, 12]. Complete phase diagram of the system of hard sphero-cylinders in three dimensions was determined using computer simulations [12]. Polydispersity in the length of the sphero-cylinders leads to the destabilization of the smectic phase towards nematic phase at low densities and columnar phase at high densities [86]. Experimental realizations include tobacco mosaic virus [2], fd virus [3, 87, 34], silica colloids [35, 4], boehmite particles [88, 5] and DNA origami nanoneedles on lipid membranes [89].

In two-dimensional continuum, system of hard needles (limit of infinite aspect ratio) undergoes Kosterlitz-Thouless-type (KT) transition to a nematic phase with quasi-long-range orientational order at high densities [90, 91, 92, 17]. Model of hard sphero-cylinders confined to lie in a plane, exhibits isotropic, nematic, and solid phases (with quasi long-range translational order) as the density is varied. When the aspect ratio is small, the system directly transits from the isotropic into the solid phase [93]. Experiment with hard rectangles of aspect ratio ~ 6.4 shows a KT transition from an isotropic to a nematic phase. Surprisingly, the existence of an intermediate tetratic phase with four fold orientational symmetry was also observed [19]. Monte carlo simulations of the system of hard rectangles with aspect ratio 2 exhibits tetratic liquid and tetratic solid phases with quasi-long-range order [18]. Existence of an intermediate tetratic phase between the isotropic liquid and two-dimensional solid phases for the system of hard squares was shown using Monte carlo simulations in Ref. [94].

1.1.2 Discrete models

Although the continuum models are well studied, the phenomenology is, however, less clear when the orientations are discrete, and the positions are either on a lattice or in the continuum. Flory introduced a lattice based mean field theory of the hard rod problem that handles higher densities better [16]. In this calculation, the rods are a set of points on a lattice. To describe a tilted rod, the rod is replaced by a set of smaller units, each unit being still oriented in the same lattice direction, but displaced in the perpendicular direction. When all rods are parallel, the partition function can be calculated exactly. The Flory calculation is useful for a dense highly ordered phase and complements the Onsager calculation for low densities. Within this approximation, the isotropic–nematic transition is confirmed, though the estimates for the critical density are roughly double to that of Onsager's estimates.

For oriented (restricted orientation) cuboids of size $d \times d \times l$ in the continuum, higher order virial coefficients can be calculated. In the limit $d/l \to 0$, the n^{th} virial coefficient is proportional to $(l^d\rho)^{n-1}$, except for the third virial coefficient being equal to zero. Working in the limit $d/l \to 0$ keeping $l^2 d$ a constant, it can be shown that the isotropic–nematic transition occurs up to the seventh virial coefficient [15]. However, early simulations of semi-flexible polymers on lattices were inconclusive about the existence of a nematic phase [95]. Later, using scaled particle theory it was predicted that, in addition to the the nematic phase, the system would exhibit inhomogeneous phases like smectic, columnar and plastic solid (orientationally disordered) phases [96]. System of hard lines ($d = 0$) with discrete orientations in two dimensions was shown numerically to undergo an Ising like transition from an isotropic to a nematic phase with increasing density [97]. But there exists no numerical investigation for the complete phase diagram of rectangles with finite aspect ratio (l/d).

Polydispersed Zwanzig model was studied using virial expansion [98] which predicts the experimental observations like broadening of phase coexistence region with increas-

ing polydispersity and strong fractionation effect in the system of sterically stabilized boehmite particles [88, 5].

In this thesis, we discuss the models of monodispersed anisotropic particles in two dimensions where both the space and orientation are discrete.

1.1.3 Hard rectangle gas on lattices

We consider systems of monodispersed hard rectangles of size $m \times mk$ on lattices, where each rectangle occupies m consecutive lattice sites along the short axis and mk lattice sites along the long axis such that k is the aspect ratio. The rectangles may orient along different possible lattice directions. The system of hard rectangles on lattices represents a class of general hard-core lattice gas models. The limiting cases when either the aspect ratio $k = 1$ (hard squares) or $m = 1$ (hard rods) are better studied. When $k = 1$ (hard squares), the system is known to undergo a transition from an isotropic phase to a columnar phase at high density [29]. For hard squares, columnar phase corresponds to the phase having partial translational order (only along one lattice direction). On the square lattice, the transition from isotropic to the columnar phase is continuous, belonging to the Ashkin-Teller universality class for $m = 2$ [99, 29, 80, 100, 74, 30] and discontinuous for $m = 3$ [80, 29].

When $m = 1$, each rod occupies k consecutive lattice sites along a fixed lattice direction and will be called k-mers. For $m = 1$, $k = 2$, the system corresponds to the well studied monomer-dimer model, which may be realized in the adsorption of diatomic molecules on a $2d$ substrate. It has been shown rigorously that the monomer-dimer partition function has its zeros on the imaginary axis for any non negative dimer activities, implying that the system does not undergo any phase transitions as a function of monomer (empty sites) density on any lattice [21, 60, 22, 23]. However, the system of hard dimers with additional interaction of disallowing nearest neighbor occupation leads to a discontinuous transition

to an ordered phase [78]. Similarly, system of dimers with aligning interaction gives rise to a rich phase diagram involving a KT transition and a line of Ashkin-Teller criticality between different phases [101]. The fully packed hard dimer problem on planar lattices may be solved exactly using Pfaffian techniques [61, 63, 62], allowing the calculation of the correlation functions of two test monomers [64, 102]. It was shown using general perturbation theory for Pfaffians that in the limit of zero monomer density, the correlations decay algebraically on a bipartite lattice [64], while on the triangular lattice, correlations are short-ranged at full packing [103].

The fully packed critical phase of the hard dimer model in two dimensions may studied by mapping it to a height model [104, 105]. The height mapping breaks down at nonzero monomer densities. After integrating out the short distance fluctuations, the coarse-grained height model may be represented as a Coulomb gas, where the height field is conjugate to the electric charge density and dual magnetic charges correspond to a dislocation in the height field [65]. But this approach relies on the exact solution to determine the renormalized coupling, which is needed for the calculation of exponents [106]. However, one may determine the coupling using transfer matrix calculation or Monte carlo simulations [107]. System of closed packed dimers with interaction between the neighboring dimers has also been studied using Coulomb gas method [107, 108]. Recently, the non integrable interacting dimer model has been studied rigorously by combining discrete holomorphicity and constructive renormalization group methods [109]. Using a local gauge field generalization of the height representation and Monte carlo simulations for the system of hard dimers, it was shown that the critical coulomb phase exists even on higher dimensional bipartite lattices, but not on the non-bipartite lattices like fcc and Fisher lattices [110]. Hard trimer ($m = 1$ and $k = 3$) packing on a square lattice also admits height representation, where the height variable is a two-dimensional vector [67], but there exist no exact solution to fix the couplings. The problem of determining the corresponding couplings analytically for k-mers is still open.

For $m = 1$ and $k \geq 2$, it may be heuristically argued that the maximal density phase is orientationally disordered on lattices [20], making it uncertain whether a pure lattice model may ever exhibit a nematic phase [10]. This argument may be constructed by estimating the entropy of a nematic and a disordered phase near full packing. The calculation of entropy of a fully aligned nematic phase at density ρ (fraction of occupied sites) reduces to a solvable one-dimensional problem. Consider a system with only horizontal rods on a square lattice of size $L \times L$ with periodic boundary conditions. On average, each row contains $\rho L/k$ number of rods and $L(1-\rho)$ number of empty sites. The number of ways of arranging them on a row is

$$\Omega_{nem}(L,\rho) = \frac{\left[L(1-\rho)+\frac{\rho L}{k}\right]!}{[L(1-\rho)]!\left[\frac{\rho L}{k}\right]!}. \tag{1.1}$$

For L rows, the total number of ways of arrangement is Ω_{nem}^{L}. Hence, the entropy per site in the thermodynamic limit $L \to \infty$ is given by

$$\mathcal{S}_{nem}(\rho) = \left(1-\rho+\frac{\rho}{k}\right)\log\left(1-\rho+\frac{\rho}{k}\right) - (1-\rho)\log(1-\rho) - \frac{\rho}{k}\log\frac{\rho}{k}. \tag{1.2}$$

When $\rho = 1-\epsilon$, $\epsilon \to 0$, one may obtain $\mathcal{S}_{nem}$ as perturbation expansion in powers of ϵ as,

$$\mathcal{S}_{nem}(\rho = 1-\epsilon) = \epsilon \log\frac{1}{\epsilon k} + \epsilon + \text{ higher-order terms in } \epsilon. \tag{1.3}$$

It can be easily seen from the above equation that $\mathcal{S}_{nem} \to 0$, as $\rho \to 1$ or $\epsilon \to 0$.

A lower bound of the disordered phase entropy at full packing may be estimated by breaking the lattice into L^2/k^2 blocks of size $k \times k$. Each of these blocks may be covered by k-mers in two ways: either by k horizontal rods or k vertical rods. Thus the total number of ways to cover the lattice is $2^{L^2/k^2}$, leading to the entropy of the disordered phase per site $\mathcal{S}_{dis}(\rho = 1) \geq \frac{1}{k^2}\log 2$. A better estimate of the lower bound on $\mathcal{S}_{dis}(\rho = 1)$ may be derived in the following way [20]. One may break the lattice of size $L \times L$ into L/k strips of size $k \times L$. Consider F_L be the number of ways of covering a strip of size $k \times L$ with

k-mers. The left most column of the strip may be occupied either by a vertical rod or by the heads of k horizontal rods. Hence, F_L satisfies the following recursion relation

$$F_L = F_{L-1} + F_{L-k}. \tag{1.4}$$

It implies $F_L \approx \lambda^L$, where λ is the largest root of the equation

$$\lambda^k - \lambda^{k-1} - 1 = 0. \tag{1.5}$$

Solution of this equation has the following asymptotic expression for $k \gg 1$,

$$\lambda = 1 + \frac{\log k}{k} - \frac{\log\log k}{k} + \frac{\log\log k}{k \log k} + \text{higher-order terms}. \tag{1.6}$$

As there are L/k number of strips, the total number of ways of covering the lattice of size $L \times L$ with k-mers is given by $\Omega = [F_L]^{L/k} \approx \lambda^{L^2/k}$. Therefore, the the entropy per site of the disordered phase at full packing in the thermodynamic limit $L \to \infty$ is,

$$\begin{aligned} \mathcal{S}_{dis}(\rho = 1) &= \frac{1}{L^2} \log \Omega \\ &\geq \frac{\log k}{k^2},\ k \gg 1. \end{aligned} \tag{1.7}$$

For densities close to 1 ($\rho = 1 - \epsilon$), the correction term to $\mathcal{S}_{dis}(\rho = 1)$ may be estimated by removing ϵ/k fraction of rods at random from the fully packed state. Here, the entropy of the holes is ignored, assuming that they form bound states. This gives the entropy of the disordered phase close to the full packing to be approximately

$$\mathcal{S}_{dis}\,(\rho = 1 - \epsilon) \approx \mathcal{S}_{dis}\,(\rho = 1) - \frac{1}{k}[\epsilon \log \epsilon + (1 - \epsilon)\log(1 - \epsilon)],\ \ k \gg 1. \tag{1.8}$$

Clearly at $\rho = 1$ or $\epsilon = 0$, the disordered phase entropy ($\approx \log k/k^2$) is larger than the nematic phase entropy (which is zero), favouring orientational disorder at full packing.

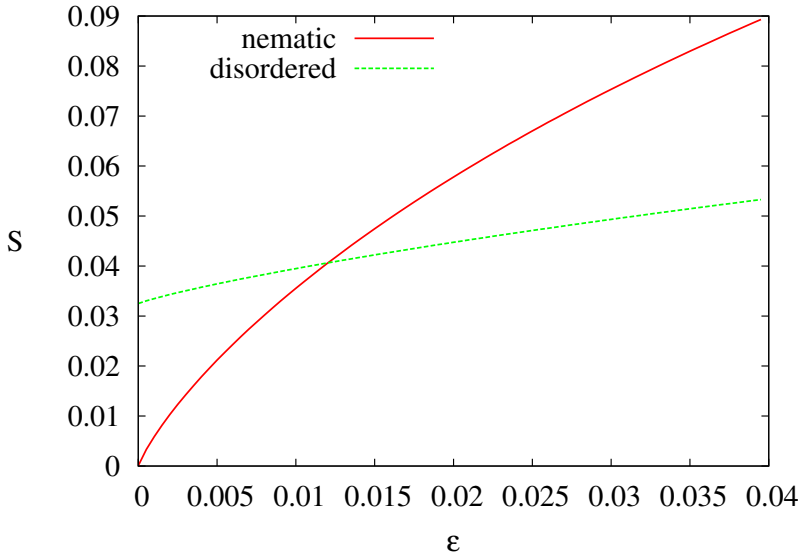

Figure 1.1: Entropy per site for nematic and disordered phases given by Eq. (1.3) and Eq. (1.8) respectively, as a function of $\epsilon = 1 - \rho$ when k = 8 [20].

Recently, the existence of a transition from the low-density disordered phase to an intermediate density nematic phase for the system of k-mers on the square lattice has been shown numerically for $k \geq 7$. In addition, using the above entropic argument it was predicted that the nematic phase would exist for the range of densities $\rho_1^* < \rho < \rho_2^*$. Beyond ρ_2^*, the phase would be orientationally disordered [20]. For $\rho = 1 - \epsilon$, from Eq. (1.3) and Eq. (1.8) one may verify that the the entropies for nematic and disordered phases become equal at $\epsilon \approx C/k^2$ (see Fig. 1.1), which predicts the existence of a second transition from the nematic to a disordered phase at critical density $\rho_2^* \approx 1 - C/k^2$ [20].

The existence of the nematic phase, and hence the first transition from the low-density disordered to the nematic phase has been proved rigorously for $k \gg 1$ [24]. In this proof, at first, the system of rods is mapped to a contour model of effective Ising spins. Coarse-graining of the lattice is done by dividing it into squares of size $\ell \sim k/2$, such that only rods of the same orientation can have their centers within the same square. Hence each square can be of three types: first, +1, if it contains centers of horizontal rods, second, −1, if it contains the centers of vertical rods, and otherwise 0, if empty, which is very unlikely to occur. The values associated to each squares may be thought as

different spin values for the coarse-grained system. Such squares with opposite spins have strong repulsive interaction due to the hard-core constraint. A typical spin configuration consists of domains of type $+1$ and -1, separated by contours containing zeros or pairs of neighboring opposite spins. This contour theory is not invariant under the $\mathbb{Z}^2$ symmetry, therefore, instead of Peierl's argument, cluster expansion methods by Pirogov and Sinai were applied to complete the proof.

The first transition from the low-density disordered to the nematic phase for the system of monodispersed long rods has also been studied in detail through Monte carlo simulations with local moves [25, 111, 112, 113]. Comparison between the configurational entropy and the entropy of the fully aligned nematic phase predicts that the nematic phase would appear only when $k \geq k_{min} = 7$ on both the square [113] and triangular lattices [112]. In addition, it was estimated that $0.87 \leq \rho_2^* \leq 0.93$ for $k = 7$ for the square lattice, and an approximate functional form for the entropy as a function of the density was proposed [113]. The critical density for the first transition was predicted to be $\rho_1^* \propto 1/k$ [112, 114]. On the square lattice, the transition is numerically found to be in the Ising [25], or equivalently in the liquid-gas universality class [97], and on the triangular and honeycomb lattices, it is in the three-state Potts model universality class [25, 111].

If the high density phase is orientationally disordered, there has to be a second transition from the intermediate density nematic phase to the high-density disordered phase. To distinguish between the two phases without nematic order, we refer to the first as low-density disordered (LDD) phase and the second as high-density disordered (HDD) phase. In Ref. [113], it was shown using the Monte carlo simulations with deposition, evaporation, diffusion and rotation moves that the nematic order parameter comes down with increasing the density for $k = 7$. But the algorithm is still not efficient enough to confirm the existence of the HDD phase or perform quantitative studies of the second transition. Numerical studies are difficult because of the large relaxation times of the nearly jammed configurations at high densities.

Recently, the model was exactly solved on a random locally tree-like layered lattice and the existence of an disordered–nematic transition was shown. On this lattice, k_{min} is a function of the coordination number and is equal to 4 when the coordination number is 4. But the second transition is absent in this model. [26].

A related model of polydispersed long hard rods ($m = 1$) on the square lattice was solved by mapping the partition function of the system into that of the nearest neighbor two-dimensional Ising model [115]. In this model, the activity of a rod of length k is $q/(2q)^k$. It is shown that for small enough q, a nematic phase exists. A generalization of this model has recently been studied in Ref. [116], using transfer matrix method. The model allows rods of length k with weight $z_i^{k-2} z_e^2$, where z_i (z_e) is the activity for an internal (endpoint) monomer. The choice $z_e = \sqrt{z_i/2}$ reduces to the previous model [115]. For a fixed z_e, the system undergoes a transition to a nematic phase with increasing z_i. The transition belongs to the two-dimensional Ising universality class. However, the second transition to the high-density disordered phase is absent in this model. Phase diagram of a mixture of hard squares ($k = 1$) and dimers ($m = 1$, $k = 2$) on a square lattice has recently been studied using Monte carlo simulations and coulomb gas method. At full packing, the system undergoes a Kosterlitz-Thouless transition from a columnar phase to a power law correlated phase. For nonzero density of vacancies, a line of Ashkin-Teller criticality separates the columnar phase from a disordered fluid phase [31].

There are very few studies for $m > 1$. Simulations of monodispersed hard parallelepipeds on cubic lattice show layered and columnar phases, but no nematic phase [27]. When $m \to \infty$, keeping k fixed, the lattice model is equivalent to the model of oriented rectangles in two-dimensional continuum, also known as the Zwanzig model [15]. For oriented lines in the continuum ($k \to \infty$), a nematic phase exists at high density [97].

The phase diagram of the system for arbitrary m and k has been difficult to determine, primarily due to the lack of an efficient Monte Carlo algorithm. In general, numerical studies of extended objects are constrained by the fact that it is difficult to equilibrate the

system at high densities using Monte Carlo algorithms with local moves as the system gets trapped in metastable states and requires correlated moves of several particles to access different configurations.

1.2 Overview of the thesis

Is there any efficient algorithm to study the system of hard extended objects on lattices? Can one show the existence of the nematic–disordered phase transition at high densities for the system of monodispersed hard rods? If it exists, what is the nature of this transition? Are the low-density and high-density disordered phases different from each other? What is the phase diagram of hard rectangles of arbitrary size?

In this thesis, we will address the above questions using numerical simulations, exact calculation, Bethe approximation, virial expansion and arguments based on estimation of entropies. The rest of the thesis is organized as follows.

In **Chapter 2**, we present a Monte carlo algorithm for studying equilibrium properties of extended objects having only excluded volume interactions. The algorithm does not suffer from slow-down due to jamming even at densities close to the maximum possible. We describe the algorithm by implementing it for the system of hard rods ($m = 1$) and also generalize it for the system of hard rectangles of size $m \times mk$. In addition to overcome jamming at high packing densities, it is easily parallelized, which makes it suitable for studying hard-core systems with particles of other shapes, and also in higher dimensions. We discuss various methods to parallelize the program, that allows us to perform large scale simulations.

In **Chapter 3**, we study the transition from the nematic phase to the high-density disordered phase in systems of long rigid rods ($m = 1$) of length k on the square and triangular lattices. The existence of a second transition is shown for $k = 7$ on both the lattices. Metastability of the nematic order at high densities is explained within the classical nu-

cleation theory of Kolmogorov-Johnson-Mehl-Avrami. We study correlations in the high-density disordered phase, and find evidence of a crossover length scale $\xi^* \gtrsim 1400$, on the square lattice. For distances smaller than ξ^*, correlations appear to decay algebraically. Our best estimates of the critical exponents on the square lattice differ from those of the Ising model, but we cannot rule out a crossover to Ising universality class at length scales $\gg \xi^*$. On the triangular lattice, the estimated critical exponents are consistent with those of the two-dimensional three-state Potts universality class.

In **Chapter 4**, we solve exactly a model of monodispersed rigid rods of length k with repulsive interactions on the random locally tree-like layered lattice to throw light on the high-density disordered phase. For $k \geq 4$, we show that with increasing density, the system undergoes two phase transitions: first from a low-density disordered phase to an intermediate density nematic phase and second from the nematic phase to a high-density re-entrant disordered phase. When the coordination number is 4, both the phase transitions are continuous and in the mean field Ising universality class. For even coordination number larger than 4, the first transition is found to be discontinuous while the nature of the second transition depends on the rod length k and the interaction parameters. We argue that the low-density disordered and the high-density disordered phases are qualitatively similar.

In **Chapter 5**, the phase diagram of a system of monodispersed hard rectangles of size $m \times mk$ on a square lattice is numerically determined for $m = 2, 3$ and integer aspect ratio $k = 1, 2, \ldots, 7$. We show the existence of a disordered isotropic phase, a nematic phase with orientational order, a columnar phase with orientational and partial translational order, and a solid-like sublattice phase with complete translational order, but no orientational order. In particular we show that for $k \geq 7$, the system undergoes three entropy-driven phase transitions with increasing density: first, from a low-density isotropic phase to an intermediate density nematic phase, second, from the nematic phase to a columnar phase and third, from the columnar to a high-density sublattice phase. The nature of the different

phase transitions are established and the critical exponents for the continuous transitions are determined using finite size scaling.

In **Chapter 6**, we investigate, using Monte Carlo simulations, the phase diagram of a system of hard rectangles of size $m \times mk$ on a square lattice when the aspect ratio k is a non-integer. The existence of a disordered isotropic phase, a nematic phase with only orientational order, a columnar phase with orientational and partial translational order, and a high-density phase with no orientational order is shown. The high-density phase is a solid-like sublattice phase only if the length and width of the rectangles are not mutually prime, else, it is an isotropic phase. The minimum value of k beyond which the nematic and columnar phases exist are determined for $m = 2$ and 3. The nature of the transitions between different phases is determined, and the critical exponents are numerically obtained for the continuous transitions.

In **Chapter 7**, asymptotic behavior of phase boundaries of the hard rectangle system is determined both numerically and analytically using Monte carlo simulations, entropy estimates, Bethe approximation and virial expansion for large m and k. We find the critical density for the isotropic–nematic transition $\rho_c^{I-N} \approx A_1 k^{-1}$, where A_1 is independent of m and the transition density for the nematic–columnar transition $\rho_c^{N-C} \approx A_2(m) + A_3(m)k^{-1}$ for $k \gg 1$. Based on estimates of entropy for the columnar and sublattice phases, we obtain $\rho_c^{C-S} \approx 1 - A_4/mk^2$ for $k \gg 1$, where A_4 is a constant. We estimate the value of A_1, A_2, and A_3 numerically and also within the corresponding approximate theories. In addition, we observe that the critical Binder cumulant for the nematic–columnar phase transition is non-universal and decreases as k^{-1} for $k \gg 1$. However, the transition is shown to be in the Ising universality class.

Finally, in **Chapter 8**, we present the principal conclusions that emerge from the work in this thesis, as well as open problems.

Chapter 2

A Monte carlo algorithm for studying systems of hard particles on lattices

2.1 Introduction

In this chapter, we present a Monte carlo algorithm that is efficient in simulating systems of hard particles with large excluded volume on lattices, even at densities close to the full packing. This algorithm overcomes the difficulties of slow relaxation time at high densities, faced by the algorithms with local moves. Here, we describe the algorithm for the system of hard rectangles of size $m \times mk$ on a square lattice, though it may easily be generalized to particles of different shape. The model of hard rectangles is described in Sec. 2.2. Section 2.3 contains a review of the Monte carlo algorithms that were used earlier to study the system of hard rectangles. In Sec. 2.4, we describe the Monte carlo algorithm with non-local moves that we have used in this thesis, by illustrating its implementation for the system of hard rods and rectangles. Section 2.5 contains a discussion about various High Performance Computing techniques that are useful to parallelize the program. Section 2.6 contains summary of the results and discussion. The content of this chapter is published in Ref. [117, 118, 119].

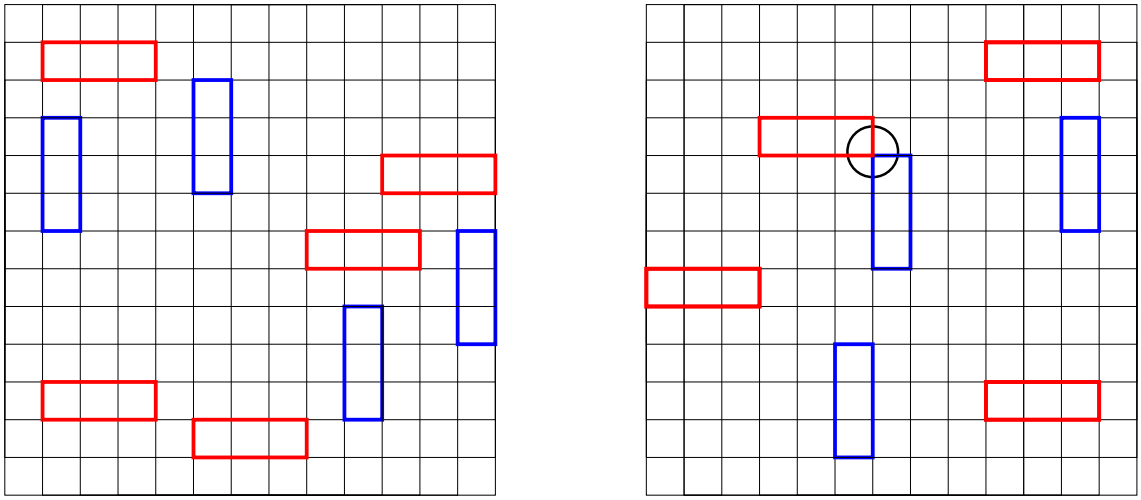

(a) (b)

Figure 2.1: (a) A valid configuration of horizontal and vertical rectangles of size 2×4, (b) a configuration that is disallowed due to the hard-core constraint.

2.2 Model

We define the model on a square lattice of size $L \times L$ with periodic boundary conditions. Consider a system of monodispersed hard rectangles of size $m \times mk$ such that the aspect ratio is k. Each rectangle may have two possible orientations: either horizontal or vertical. A horizontal (vertical) rectangle occupies mk lattice sites along the x (y)-axis and m lattice sites along the y (x)-axis. No two rectangles may overlap or equivalently each site may be occupied atmost by one rectangle. Fig. 2.1 shows a system of hard rectangles of size 2×4, where $m = 2$ and $k = 2$. We associate an activity z_h to each horizontal rectangle and z_v to each vertical rectangle. The corresponding chemical potentials are denoted by μ_h and μ_v respectively, where $z_h = e^{\mu_h}$ and $z_v = e^{\mu_v}$. The grand canonical partition function for the system is

$$\mathcal{Z} = \sum_{N_h, N_v} C(N_h, N_v)\, z_h^{N_h}\, z_v^{N_v}, \tag{2.1}$$

where $C(N_h, N_v)$ is the number of distinct configurations with N_h horizontal and N_v vertical rectangles. Fraction of occupied sites or density is defined as

$$\rho = \frac{m^2 k\,(N_h + N_v)}{L^2}. \tag{2.2}$$

The case $m = 1$ corresponds to the system of hard rods. Straight rods occupying k consecutive sites along any one lattice direction will be called k-mers. A k-mer may be either horizontal (x-mer) or vertical (y-mer). The bottom-left corner of a k-mer will be called its head.

2.3 Algorithms with deposition-evaporation move

We, first, briefly review the grand-canonical Monte carlo algorithm with local moves for simulating the system of hard rods ($m = 1$) on the square lattice [20]. Starting with an arbitrary configuration, deposition of a new rod is attempted with probability p or evaporation of an existing rod is attempted with probability $(1 - p)$. In the deposition move, horizontal or vertical orientation is chosen with probability $1/2$. Next, a site is picked up at random and deposition of a rod is attempted along the chosen direction. The deposition is successful only if k consecutive lattice sites along that particular direction, starting from the chosen site, are empty. Otherwise, the deposition attempt is rejected. In the evaporation attempt, again a site is chosen at random. If the site is the head of a rod, it is evaporated. This dynamics does not conserve the number of rods. The probability of deposition attempt p is related to the activity z through the detailed balance condition as $z = p/2(1 - p)$. Using this algorithm, the existence of a nematic phase at intermediate densities was shown for the system of hard rods of length $k \geq 7$ on the square lattice [20]. However, it is not possible to equilibrate the system for densities beyond 0.85 for $k = 7$, making the algorithm unsuitable for studying high densities.

In addition to the evaporation-deposition move, diffusional and rotational relaxations were also implemented [113]. In the diffusion move, a randomly chosen rod is translated to one of the neighboring positions, if permitted by the hard-core constraint. In the rotation move, a k-mer is rotated by $\pi/2$ about its head, provided the new position does not have any overlap with other rods. Implementing this algorithm for hard rods ($m = 1$, $k = 7$),

it was shown that the nematic order gradually decreases with increasing density [113]. But a clear evidence of the existence of a high-density disordered phase and hence, the second transition was lacking as the algorithm suffers from large relaxation times at high densities, making it unsuitable for a detailed study.

Apart from algorithms with local moves, cluster algorithms were implemented for the hard-core systems. Classical hard-core monomer-dimer model on lattices has been studied using a cluster algorithm, called as pocket algorithm [120]. The algorithm is as follows: starting with an arbitrary configuration, a symmetry axis and a dimer is picked at random. Then the dimer is reflected with respect to the chosen symmetry axis and deposited to the new position. If it overlaps with other existing dimers, they are reflected similarly with respect to the symmetry axis. This process continues until the final configuration has no overlapping dimers. Reflection about any diagonal axis changes the number of horizontal or vertical dimers and any horizontal or vertical axis allows the dimers to move through the different winding number sectors. On the square lattice, the algorithm may be shown to be ergodic if the symmetry axis passes through sites of the lattice. In three dimensions, symmetry planes are chosen for reflection [110]. Although, this algorithm works in any dimension for different lattices and arbitrary doping with monomers, it is not efficient enough to study the system of longer rods. For longer rods there are large number of overlaps, increasing the time taken for achieving a valid configuration through reflection.

Cluster algorithm has also been implemented for the system of oriented lines ($k \to \infty$, keeping m fixed) in the continuum, allowing the study of the system at high densities [97]. Width of the lines being zero, two lines of same orientation can not have any overlap. But each line has a square shaped depletion zone which is not allowed to contain any centers of lines with perpendicular orientation due to the hard-core constraint. The algorithm is as follows. Starting with an initial configuration, deposition or evaporation of a horizontal or vertical line is attempted with equal probability. In the deposition attempt, a horizontal

(vertical) line is placed at a random position. It may lead to overlap with several vertical (horizontal) lines. If the number of overlapping vertical (horizontal) lines is larger than a parameter δ, specified by the fugacity of the vertical (horizontal) lines, the attempt is rejected, otherwise it is accepted with some weight depending on fugacities and number of particles. In the evaporation attempt, a randomly chosen horizontal (vertical) line is evaporated and a number of vertical (horizontal) lines, chosen at random between 0 and δ, is distributed over the depletion zone of the evaporated line. If any of the vertical (horizontal) lines intersect with the existing horizontal (vertical) lines, the move is rejected, otherwise accepted with certain weight. This cluster move is associated with a biased sampling method [121] to make it more efficient. But this algorithm works only for hard lines. Although this system exhibits orientational ordering at high densities, it can not have any spatial order by construction.

2.4 The Monte carlo algorithm

2.4.1 Hard rods

In this section we describe an efficient Monte carlo algorithm consisting of non-local moves by implementing it for the system of hard rods ($m = 1$). The algorithm is defined as follows: given a valid configuration, first, a row is chosen at random. All x-mers lying on that row are removed without moving any of the y-mers [see Fig. 2.2(a)]. The chosen row now consists of sets of contiguous empty sites, separated from each other by sites occupied by y-mers [shown by cross symbols in Fig. 2.2(b)]. All the empty intervals of the row are now reoccupied with x-mers. Each interval may be reoccupied independently of each other and the problem reduces to that of occupying an interval of some given length ℓ of a one-dimensional lattice with k-mers with correct probabilities. These probabilities may be obtained by solving a one-dimensional problem.

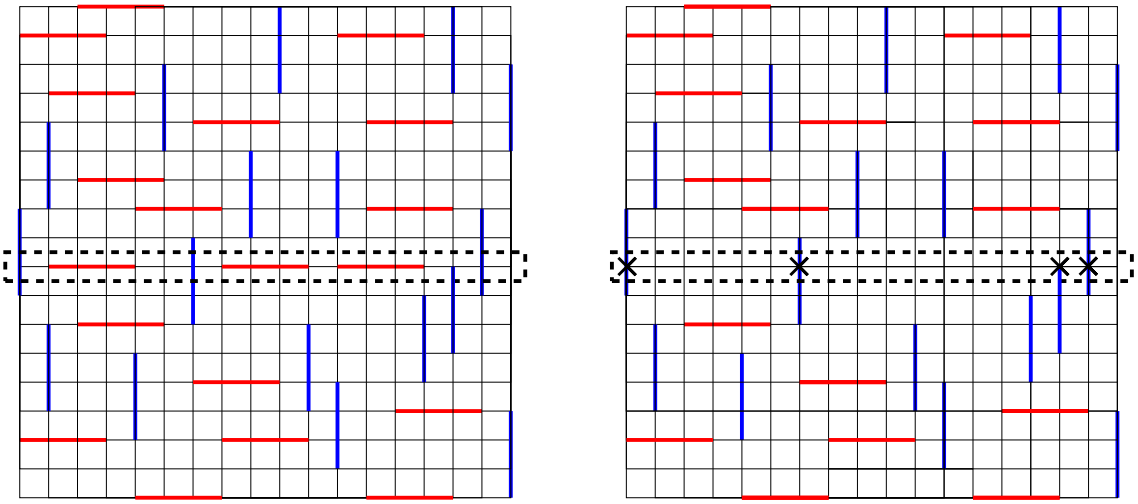

(a) (b)

Figure 2.2: An illustration of the Monte Carlo algorithm for the system of rods of length $k = 4$: (a) Initial configuration of x-mres (shown by red color) and y-mers (shown by blue color). The chosen row is enclosed by a dashed line, (b) configuration after the evaporation of the x-mers from the row, enclosed by the dashed line. Each interval now consists of contiguous empty sites, separated from each other by the sites occupied by the y-mers, denoted by cross symbols. The sites, marked with cross symbols, cannot be occupied by the horizontal rods in the new configuration.

Let the grand canonical partition function of a system of hard rods on a one-dimensional lattice of ℓ sites with open boundary conditions be denoted by $\Omega_o(z;\ell)$. The partition functions $\Omega_o(z;\ell)$ obeys the following simple recursion relation,

$$\Omega_o(z;\ell) = z\Omega_o(z;\ell-k) + \Omega_o(z;\ell-1), \text{ when } \ell \geq k, \tag{2.3a}$$

$$\Omega_o(z;\ell) = 1, \text{ when } \ell = 0, 1, \ldots, k-1. \tag{2.3b}$$

The solution of this recursion relation is $\Omega_o(z;\ell) = \sum_{i=1}^{k} a_i \lambda_i^{\ell}$, where λ_i's are independent of ℓ. The a_i's are determined by the boundary conditions 2.3(b). Once Eq. (2.3) is solved for $\Omega_o(z;\ell)$, all the equilibrium probabilities can be calculated exactly. The probability that the left most site of an open chain of length ℓ is occupied by the left most site of an x-mer is

$$p_\ell = z\,\frac{\Omega_o(z;\ell-k)}{\Omega_o(z;\ell)}, \tag{2.4}$$

and the probability of it is being empty is $(1 - p_\ell)$. If occupied, we move to the k-th

neighbor along the chain and reduce the length of the interval by k, and if not occupied, we consider the immediate neighbor to the right and reduce the length of the interval by one.

With periodic boundary conditions, the recursion relations have to be modified. Let $\Omega_p(z;\ell)$ be the partition function of a one-dimensional lattice of length ℓ with periodic boundary conditions. It is easy to see that

$$\Omega_p(z;\ell) \quad = \quad kz\Omega_o(z;\ell-k) + \Omega_o(z;\ell-1). \tag{2.5}$$

When $\Omega_o(z;\ell)$ is known, the computation of $\Omega_p(z;\ell)$ is straightforward. The probability that a site of an empty row of length L is occupied by an x-mer is

$$p_L = k\, z\, \frac{\Omega_o(z;L-k)}{\Omega_p(z;L)}. \tag{2.6}$$

We use a list of stored values of the relevant probabilities $\{p_\ell\}$ for all $\ell = 1,\ldots,L$, to reduce the computation time. It can be easily seen that the evaporation or reoccupation of x-mers in any row is independent of the other rows. Hence at each time step, all the x-mers can be evaporated and then redeposited simultaneously in all the rows with the equilibrium grand canonical weights.

Following the evaporation of and reoccupation of x-mers, we repeat the procedure with y-mers. Keeping x-mers fixed, all y-mers are evaporated and the columns are then re-occupied with y-mers. A Monte Carlo move corresponds to one set of evaporation and reoccupation of both x-mers and y-mers.

We check for equilibration by starting the simulation with two different initial configurations and making sure that the final equilibrium state is independent of the initial condition: one configuration is a fully nematic state, where all rods are oriented either along horizontal or vertical direction and the other is a random configuration where x-mers and y-mers are placed randomly.

2.4.2 Hard rectangles

Here, we generalize the algorithm for the system of hard rectangles of size $m \times mk$. The bottom-left corner of a rectangle will be called its head. Given a valid configuration of rectangles, in a single move, a row or a column is chosen at random. If a row is chosen, then all horizontal rectangles whose heads lie in that row are removed, leaving the other rectangles untouched. The emptied row now consists of two kinds of sites: forbidden sites that cannot be occupied with the horizontal rectangles having their heads on that row due to the presence of vertical rectangles in the same row or due to rectangles with heads in the neighboring $(m-1)$ rows, and sites that may be reoccupied by horizontal rectangles in a valid configuration. An example illustrating the forbidden sites is shown in Fig. 2.3(a). It is clear that the sites that may be occupied are divided into intervals of contiguous empty sites. The problem of occupation of the emptied row with a new configuration of rectangles with heads on the same row, now reduces to the problem of occupying the empty intervals. The empty intervals may be occupied independently of each other, as the occupation of one is not affected by the configuration of rectangles in the remaining ones. Thus, the reoccupation of the emptied row with horizontal rectangles reduces to a problem of occupying a one-dimensional interval with rods of length mk. The calculation of equilibrium probabilities is same as discussed in Sec. 2.4.1. If a column is chosen instead of a row, then a similar operation is performed for the vertical rectangles whose heads lie on that column.

In addition to the above evaporation-deposition move, we find that the autocorrelation time is reduced considerably by introducing a flip move. At first, we describe the flip move for integer k. In this move, a site (i, j) is picked at random. If it is occupied by the head of a horizontal rectangle, then we check whether $(i, j+m), (i, j+2m), \ldots, (i, j+[k-1]m)$ sites are occupied by the heads of horizontal rectangles. If that is the case, we call this set of k aligned rectangles a rotatable plaquette of horizontal rectangles. In the flip move such a rotatable plaquette of size $mk \times mk$, containing k horizontal rectangles, is replaced

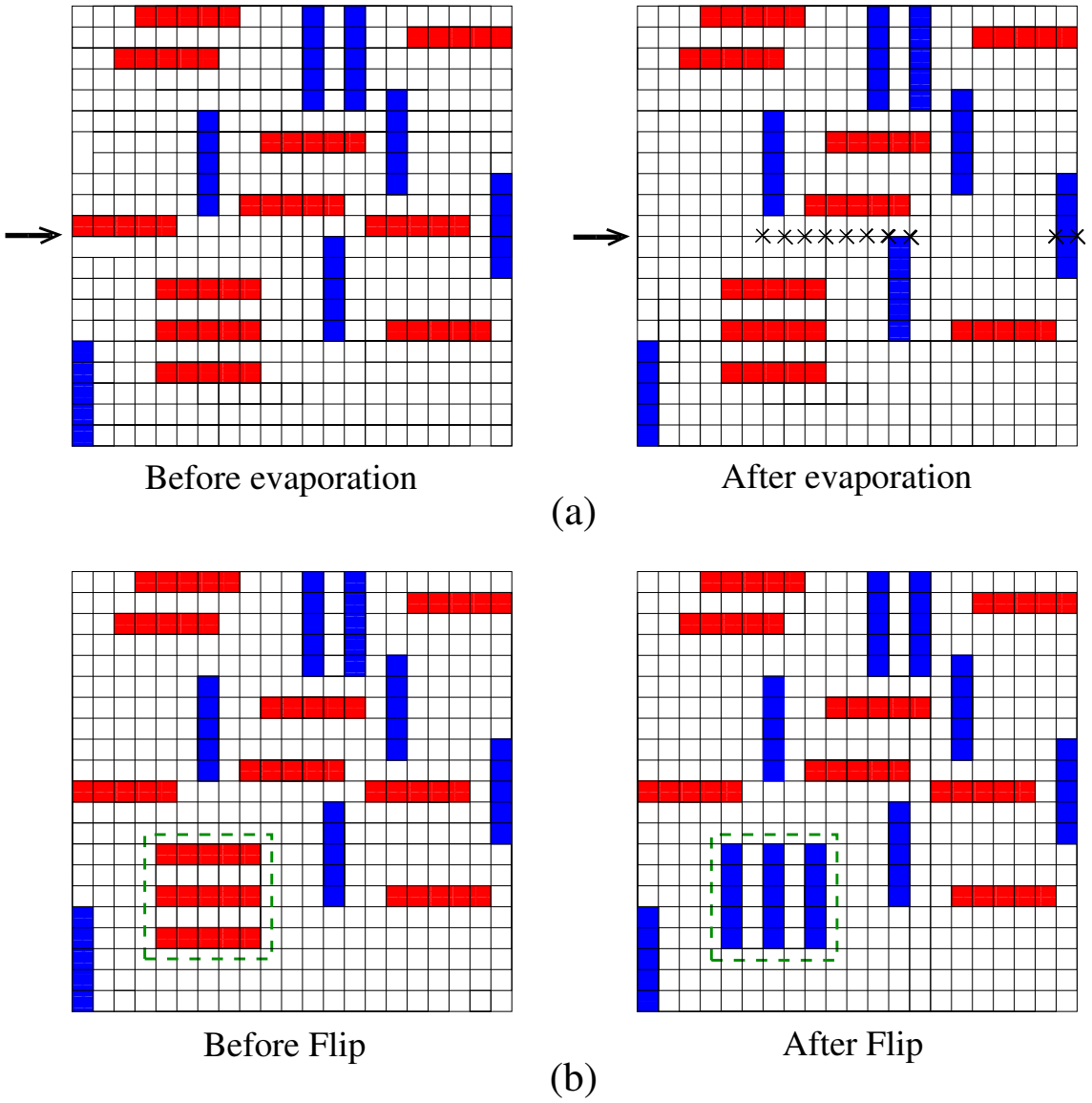

Figure 2.3: An illustration of the Monte Carlo algorithm for the system of rectangles: (a) Configurations before and after the evaporation of horizontal rectangles with heads on a particular row (denoted by an arrow). Sites denoted by cross symbols cannot be occupied by the horizontal rectangles with their heads on that row in the new configuration. (b) An example of the flip move for rectangles of size 2×6. A rotatable or flippable plaquette of size 6×6, consisting of three aligned rectangles, is shown by the dashed line. After the flip move, the horizontal rectangles become vertical.

by a similar plaquette of k vertical rectangles. An example of the flip move is shown in Fig. 2.3(b). If (i, j) is occupied by the head of a vertical rectangle and a rotatable plaquette of vertical rectangles is present, then it is replaced by a plaquette of k aligned horizontal rectangles. When k is non-integer, a square plaquette consisting of ℓ aligned horizontal (vertical) rectangles is replaced by a similar plaquette of ℓ vertical (horizontal) rectangles, where ℓ is the ratio of the least common multiple of m and mk to m. In general, a rotatable plaquette is of size $R \times R$, where R is the least common multiple of m and mk. A Monte Carlo move corresponds to $2L$ evaporation-deposition moves and L^2 flip moves. It is easy to check that the algorithm obeys detailed balance. While going through each interval on the rows or columns, we erase the old configuration and reoccupy with a new one obeying equilibrium grand canonical probabilities as expressed in Eq. (2.4) and (2.6). The flip move trivially satisfies the detailed balance condition. For any $\rho < 1$, there is always a nonzero probability to achieve any configuration from any initial configuration, implying that the algorithm is ergodic. At any finite z, the evaporation-deposition move by itself can sample the entire configuration space. The flip move is non-ergodic by itself and samples a particular sector of the configuration space. However, its inclusion makes the sampling more efficient. At full coverage, only the flip move is applicable and thus, the algorithm is not ergodic.

2.5 Parallelization using High Performance Computing

The algorithm is easily parallelizable since the evaporation or reoccupation of horizontal (vertical) rectangles in the rows (columns) that are separated by m, is independent of each other and can be done simultaneously. The flip move is parallelized by dividing the lattice into L^2/R^2 blocks of size $R \times R$. The flipping of each of these blocks is independent of the others and may therefore be performed simultaneously. We flip a rotatable plaquette with probability $1/2$.

The above discussed Monte carlo algorithm may be parallelized using various High Performance Computing (HPC) techniques. In case of CPU based parallel computing, we have used Message Passing Interface (MPI) and Open Multi-Processing (OpenMP). MPI is a specification of message passing libraries and addresses the message-passing parallel programming model. It runs on distributed, shared and hybrid memory architectures, but the programming model acts as a distributed memory model. We carry out our simulations on the supercomputing machine Annapurna (Intel Nehalem 2.93 GHz) at The Institute of Mathematical Sciences. It has 128 nodes, each node is having 8 cores. All the nodes have their own private memory space. Within each node, the memory is shared among the 8 cores. In MPI, each core possesses its own copy of the data and does not get affected by other cores. Data transfer among the different nodes is much slower than that within a node. Maximum efficiency may be achieved by balancing the number of nodes and the amount of data transfer among them. We observe maximum efficiency while using single node, presumably due to the overhead of node to node transfer.

On the other hand, OpenMP is a shared-memory application programming interface (API) and simply a compiler extension to parallelize the existing source code. It is based on instructions that can be added in the sequential code to share the work among different cores [122]. Thus, it is much simpler to use than MPI. Being restricted to the shared memory, with OpenMP, one can not go beyond one node. In contrast to MPI, in this case, the data need not to be transferred among different cores within a node, as the shared data can be accessed or updated by any core. Thus, OpenMP runs faster than MPI within a single node.

CUDA or Compute Unified Device Architecture is used as a framework for general purpose parallel computing on Graphics processing unit (GPU), and CUDA C is an language developed to facilitate GPU computing. GPU has a massively parallel architecture consisting of thousands of efficient cores designed for handling multiple tasks simultaneously. For example in case of the hard rod problem, if we consider a lattice of size 1000×1000,

all the 1000 rows or columns may be updated parallely. GPU turns out to be very efficient for simulating large system sizes and it has opened up the possibility of studying three-dimensional systems. Details about GPU computing may be found in Ref. [123].

2.6 Summary and discussion

We presented an efficient Monte Carlo algorithm that is able to overcome jamming at high densities to study the phase transitions in a system of extended hard particles on lattices. The algorithm is more efficient than algorithms with only local moves. In addition to overcoming jamming at high packing densities, it is easily parallelized, which makes it suitable for studying the high densities for large system sizes, and also higher-dimensional systems. All Monte Carlo simulations presented in this thesis have been done using a parallelized version of the algorithm. Other implementations of this algorithm include lattice gas model of particles with exclusion of several next-nearest-neighbor sites [29, 30], mixtures of hard squares and dimers [31]. The algorithm, described in Ref. [31], works efficiently even at full packing and can be generalized to similar problems. In this case, the corresponding equilibrium probabilities are not stored, but they are calculated at every time step using transfer-matrix method.

Chapter 3

Phase transitions in systems of hard rods on two-Dimensional lattices

3.1 Introduction

In this chapter, we study the system of hard rods ($m = 1$) of length k on two-dimensional lattices using the efficient Monte carlo algorithm. Existence of an intermediate density nematic phase and hence a transition from a low-density disordered (LDD) to the nematic phase has recently been shown numerically for $k \geq 7$ [20, 25] and rigorously for $k \gg 1$ [24]. But the study at high densities were restricted due to the slow relaxation time of local algorithms. Implementing the efficient Monte carlo algorithm, as discussed in the previous chapter, we show that the equilibrium high-density phase for the system has no order, implying the existence of a second transition from the nematic to the high-density disordered (HDD) phase for $k \geq 7$. We study this nematic–disordered transition on the square and the triangular lattice for $k = 7$ in detail. We also investigate the nature of the high-density disordered phase. Using lattices of size up to $L = 2576$, we find evidence of power-law decay of orientational correlations between rods at high densities for distances $r \leq \xi^* \approx 1400$, where ξ^* is a characteristic length scale of the system. Correlations appear

to decay faster for distances $r \gtrsim \xi^*$, but we have limited data in this regime, and cannot rule out a power-law decay, even for $r \gg \xi^*$.

Regarding the critical behavior near the phase transition on the square and triangular lattices, for $k = 7$, our results show that the transition is continuous and occurs for $\rho_2^* = 0.917 \pm .015$ ($\mu_c = 5.57 \pm .02$) on the square lattice, and for $\rho_2^* = 0.905 \pm .010$ ($\mu_c = 5.14 \pm 0.05$) on the triangular lattice, where μ_c is the critical chemical potential. For comparison, $\rho_1^* \approx 0.745$ on the square lattice [112]. On the square lattice, our best estimates of the effective critical exponents differ from those of the Ising universality class, with exponents $\nu = 0.90 \pm 0.05$, $\beta/\nu = 0.22 \pm 0.07$, $\gamma/\nu = 1.56 \pm 0.07$ and $\alpha/\nu = 0.22 \pm 0.07$. However, it appears that these are only effective exponents, and a cross over to the Ising exponents ($\alpha/\nu = 0, \beta/\nu = 0.125, \gamma/\nu = 1.75$, and $\nu = 1$) at larger length scales can not be ruled out. On the triangular lattice, our estimates of critical exponents for the second transition are $\nu = 0.83 \pm 0.04, \beta/\nu = 0.13 \pm 0.02, \gamma/\nu = 1.73 \pm 0.04$ and $\alpha/\nu = 0.40 \pm 0.05$, consistent with those of the three-state Potts model universality class ($\nu = 5/6, \beta/\nu = 2/15, \gamma/\nu = 26/15$, and $\alpha/\nu = 2/5$).

In this chapter, we study the model, introduced in Sec. 2.2 when $m = 1$. The plan of this chapter is as follows. In Sec. 3.2, we redefine the model of hard rods on lattices. In Sec. 3.3, we use the Monte carlo algorithm, discussed in the previous chapter, to show that at high activities, the nematic phase is unstable to creation of bubbles of HDD phase, and that the decay of the nematic order parameter to zero is well described quantitatively by the classical nucleation theory of Kolmogorov-Johnson-Mehl-Avrami. Section 3.4 is devoted to study different properties of the HDD phase: the two point correlations, cluster size distributions, susceptibility, size distribution of structures that we call 'stacks', and the formation of bound states of vacancies. The critical behavior near the second transition from the nematic phase to the HDD phase is studied in Sec. 3.5 for both the square and triangular lattices, by determining the numerical values of the critical exponents. Section 3.6 summarizes the main results. The content of this chapter is published

in Ref. [118].

3.2 Model and the Monte carlo algorithm

To make the chapter self-contained, we redefine the model on the square lattice (See Sec. 2.2). Generalization to the triangular lattice is straightforward. Consider a square lattice of size $L \times L$ with periodic boundary conditions. Rods occupying k consecutive lattice sites along any lattice direction are called as k-mers. A k-mer, can be either horizontal (x-mer) or vertical (y-mer). A lattice site can have at most one k-mer passing through it. An activity $z = e^{\mu}$ is associated with each k-mer, where μ is the chemical potential. Density or the fraction of occupied sites is given by $\rho = n_h + n_v$, where n_h and n_v are the fraction of sites occupied by the x-mers and y-mers respectively.

We simulate the system in the constant μ grand canonical ensemble using an efficient algorithm that involves cluster moves. The implementation of the algorithm for the system of hard rods is described in detail in Sec. 2.4.1. Numerical simulations in this chapter are performed without incorporating the flip move in the algorithm.

3.3 Metastability of the nematic phase for large activities

We first verify that, for large activities, the nematic phase is unstable to the growth of the HDD phase. In Fig. 3.1(a)–(c), we show snapshots of the system of rods of length $k = 7$ in equilibrium on a square lattice at low, intermediate and high densities. For the high-density snapshot, the initial configuration had full nematic order, but the system relaxed to a disordered phase. A similar disordered phase is also seen for the triangular lattice at high densities (see Fig. 3.2). In Fig. 3.3, we show the temporal evolution of the order parameter Q, defined as $Q = \langle n_h - n_v \rangle / \langle n_h + n_v \rangle$. For all values of μ, the initial configuration had full nematic order. For $\mu = 3.89$, at large times, the system relaxes to an

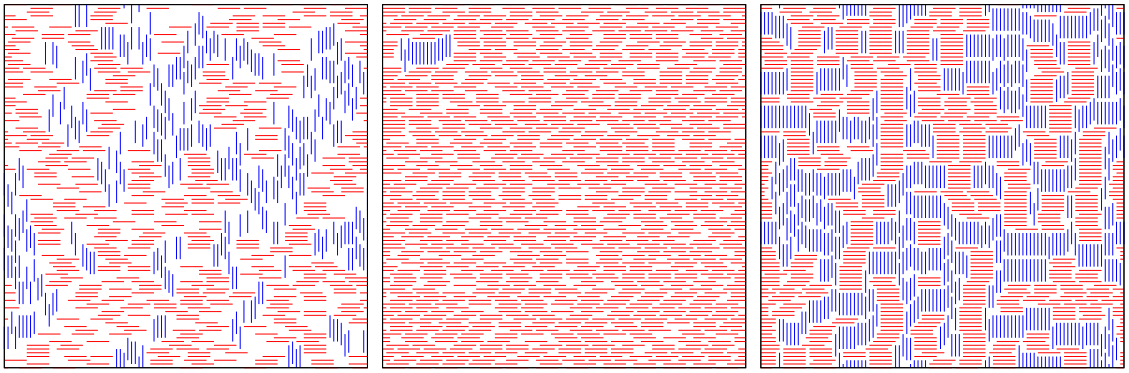

Figure 3.1: Typical configurations of the system in equilibrium at densities (a) $\rho \approx 0.66$ ($\mu = 0.41$) (b) $\rho \approx 0.89$ ($\mu = 4.82$), and (c) $\rho \approx 0.96$ ($\mu = 7.60$) on a square lattice. Here, $k = 7$ and $L = 98$.

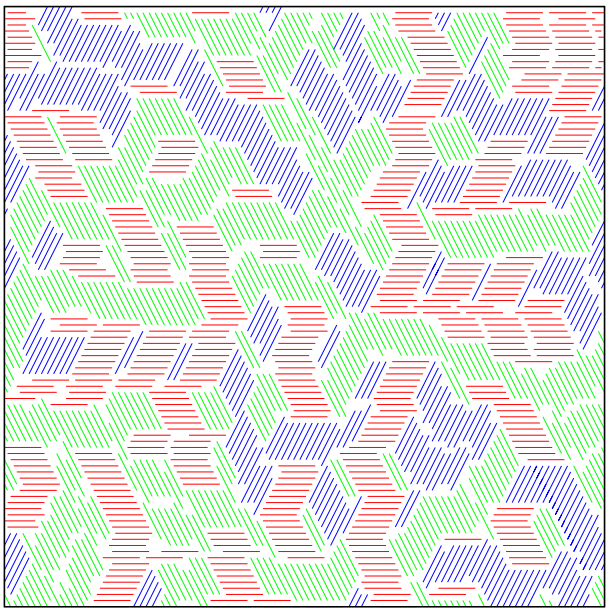

Figure 3.2: A typical configuration of the system in equilibrium at density $\rho \approx 0.96$ ($\mu = 7.60$) on a triangular lattice. Here, $k = 7$ and $L = 98$.

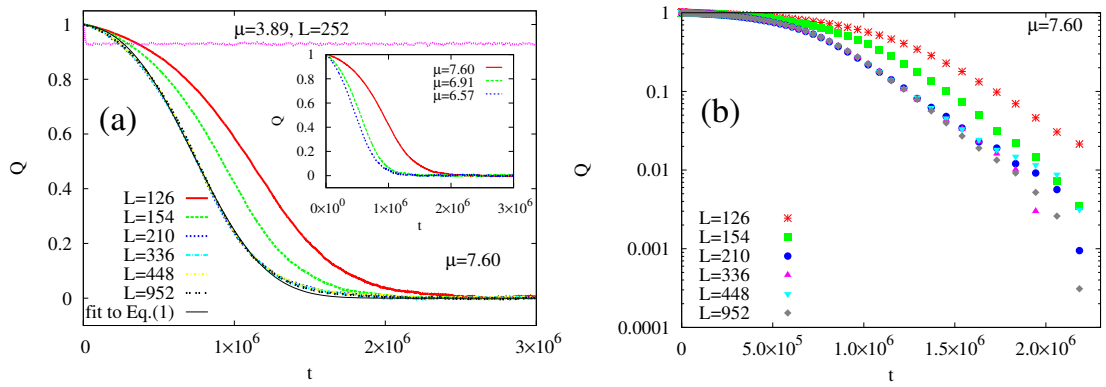

Figure 3.3: (a) Evolution of the order parameter Q for the square lattice as a function of time (Monte Carlo steps), starting from a fully ordered state for two different values of μ: $\mu = 3.89$ ($\rho \approx 0.867$), and $\mu = 7.60$ ($\rho \approx 0.957$). The best fit of the data to Eq. (3.1) with additional subleading terms is also shown. Inset: Data for different chemical potentials, all corresponding to HDD phase for $L = 154$ and $k = 7$. The densities corresponding to these values of μ are approximately 0.957, 0.948, 0.941. (b) Variation of Q with time t for $\mu = 7.60$ in semi-log scale, exhibiting the exponential decay of Q when $t > t^*$ as described in Eq. (3.1).

equilibrium state with a nonzero nematic order. However, for larger $\mu = 7.60$, the nematic order decreases with time to zero. Figure 3.4 shows how how for large μ value, the system evolves from an initial configuration with full nematic order to the equilibrium disordered phase with time. Figure 3.4 (a) shows the snapshot of a fully ordered phase ($Q = 1$) at $T = 2 \times 10^4$, and Fig. 3.4 (f) shows the HDD phase ($Q \approx 0$) at $T = 2 \times 10^6$. Interestingly, we find that the average lifetime of the metastable state *decreases* with increasing system size, and saturates to a L independent value for $L \gtrsim 200$ (see Fig. 3.3).

Naively, faster relaxation for larger systems may appear unexpected, but is easily explained using the well-known nucleation theory of Kolmogorov-Johnson-Mehl-Avrami [124, 125]. We assume that critical droplets of the stable phase are created with a small uniform rate ϵ per unit time per unit area, and once formed, the droplet radius grows at a constant rate v. Then, the probability that any randomly chosen site is still not invaded by the stable phase is given by $\exp[-\epsilon \int_0^t dt' V(t')]$, where $V(t')$ is the area of the region such that a nucleation event within this area will reach the origin before time t'. The area $V(t')$ is given by $V(t') = \pi v^2 t'^2$ when the droplet is smaller than the size of the lattice. For time

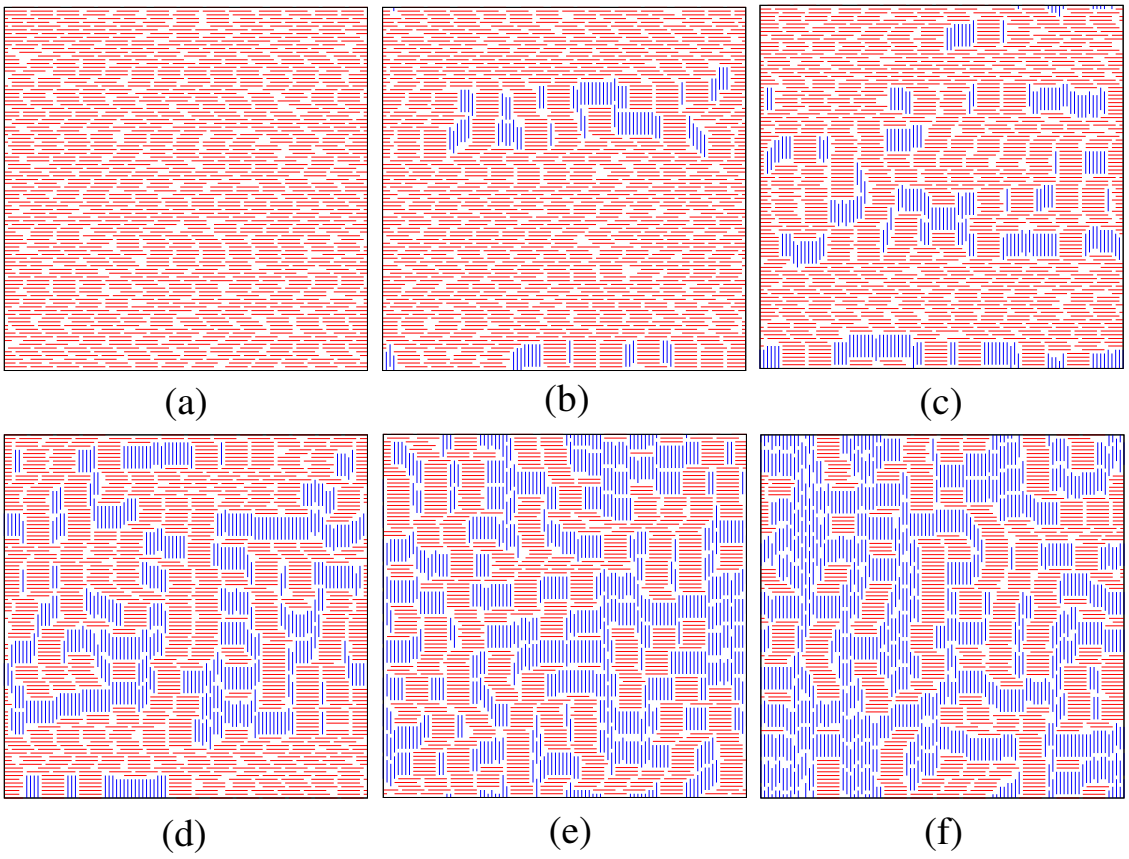

Figure 3.4: Snapshots of the system of hard rods at different Monte carlo steps t: (a) $t = 2 \times 10^4$, (b) $t = 3 \times 10^5$, (c) $t = 6 \times 10^5$, (d) $t = 8 \times 10^5$, (e) $t = 1.2 \times 10^6$, and (f) $t = 2.0 \times 10^6$. The data are for $k = 7$, $L = 98$, and $\mu = 7.60$ ($\rho \approx 0.96$).

t' greater than this characteristic time t^*, we have $V(t') = L^2$. If the droplet does not grow equally fast in all directions, we take suitably defined average over directions to define v^2. Thus, we obtain

$$\begin{aligned} Q(t) &= \exp\left[-\frac{\pi}{3}\epsilon v^2 t^3\right], \text{ for } t < t^*, \\ &= \exp\left[-\pi\epsilon v^2 t^{*2}\left(t - \frac{2t^*}{3}\right)\right], \text{ for } t > t^*. \end{aligned} \tag{3.1}$$

We see that with this choice, both $Q(t)$ and its derivative are continuous at $t = t^*$. Since

$V(t')$ should tend to L^2 for large t', we get the crossover scale t^* given by

$$t^* = \frac{L}{v\sqrt{\pi}}. \tag{3.2}$$

The crossover lattice size L^* beyond which the average lifetime of the metastable state becomes independent of L can then be estimated from the above to be

$$L^* \sim \left(\frac{3\sqrt{\pi}v}{\epsilon}\right)^{1/3}. \tag{3.3}$$

Fitting the numerical data in Fig. 3.3 (a) to Eq. (3.1) we obtain $\epsilon = (2.1 \pm 0.2) \times 10^{-10}$ and $v = (5.5 \pm 0.7) \times 10^{-5}$ for $\mu = 7.60$. From Eq. (3.3), we then obtain the crossover scale $L^* \sim 110$, of the same order as the numerically observed value of $L^* \sim 200$. The difference is presumably due to simplifying approximations made in the theory, e.g., neglecting the dependence of the mean velocity of growth on the direction of growth, or the curvature of the interface, etc. Figure 3.3 (b) shows the exponential decay of Q for $t > t^*$.

We can also estimate v directly from simulations of a system with an initial configuration where half the sample is in the nematic phase and the other half is in the equilibrium disordered phase at that μ. For $\mu = 7.60$, we find that this velocity increases slowly with L, and tends to a limiting value $\approx 1.0 \times 10^{-4}$ for $L \geq 784$, reasonably close to the velocity obtained from fitting data to Eq. (3.1). For decreasing chemical potential μ, we find that both the velocity v and nucleation rate ϵ increase.

3.4 Nature of the high-density disordered phase

There is a one-to-one correspondence between fully packed k-mer configurations and a restricted solid on solid height model with vector-valued heights [126, 127]. The height fluctuations at large length scales are well-described by a Gaussian model, and at full packing the orientation-orientation correlation function decays as a power-law with dis-

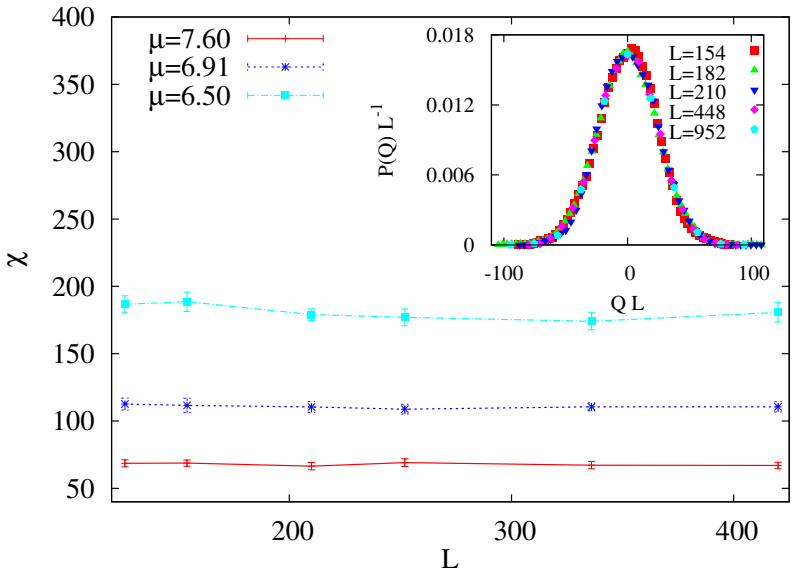

Figure 3.5: Susceptibility χ for the square lattice as a function of L for three values of μ, all in the HDD phase. There is no anomalous dependence on L. Inset: The scaled probability distribution for the order parameter $P(Q)$ for different L's collapse when plotted against QL. The data are for $\mu = 5.95$.

tance. The exponent of this power law has been estimated for the case $k = 3$ by exact diagonalization studies [67]. If these correlations are not destroyed by small density of vacancies for large k, then the correlations in the HDD phase would be long-ranged, qualitatively different from the known exponential decay of correlations in the LDD phase. In this section, we test this possibility by studying the susceptibility χ, the order parameter correlation function $C_{SS}(i, j)$, the cluster size distribution $F(s)$, and the size distribution of structures that we call stacks. We also examine the formation of bound states of vacancies.

The susceptibility is defined as $\chi = L^2\langle(n_h - n_v)^2\rangle / \langle n_h + n_v\rangle^2$. Figure 3.5 shows the variation of χ with L, for three different values of μ in the HDD phase. χ tends to a finite nonzero value for large L, hence, if the correlations are a power law, then the decay exponent is larger than 2. From the central limit theorem, it follows that the order parameter Q should scale as L^{-1}. This is confirmed in the inset of Fig. 3.5, where the scaled probability distributions for different L's collapse onto one curve when plotted against QL.

The order parameter correlation function $C_{SS}(i, j)$ is defined as follows. Given a configu-

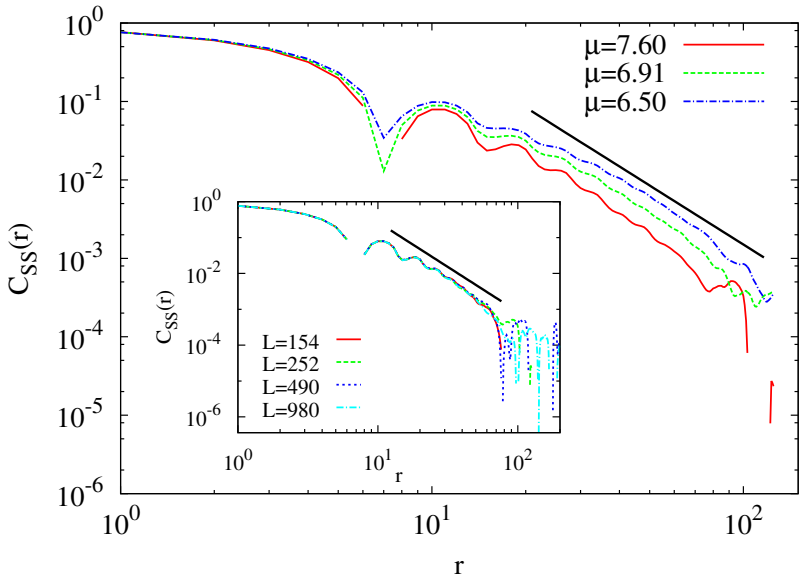

Figure 3.6: Order parameter correlations $C_{SS}(r)$ for the square lattice as a function of r, measured along the x- and y-axes, for three different values of μ, all corresponds to the HDD phase. The system size is $L = 252$. Inset: The dependence of $C_{SS}(r)$ on L is shown for $\mu = 7.60$. The solid lines are power laws $r^{-2.5}$, intended only as guides to the eye.

ration, we assign to each site (i, j) a variable $S_{i,j}$, where $S_{i,j} = 1$ if (i, j) is occupied by an x-mer, $S_{i,j} = -1$ if (i, j) is occupied by an y-mer, and $S_{i,j} = 0$ if (i, j) is empty. Then,

$$C_{SS}(i, j) = \langle S_{0,0} S_{i,j} \rangle. \tag{3.4}$$

Figure 3.6 shows the variation of $C_{SS}(r)$ with separation r along the x- and y- axes, for different chemical potentials and systems sizes. In the HDD phase, the correlation function has an oscillatory dependence on distance with period k, and for $r \gg k$, appears to decrease as a power law $r^{-\eta}$, with $\eta > 2$. Given the limited range of r available $7 \ll r \ll L/2$, it is difficult to get an accurate estimate of the exponent η.

The long-range correlations in the HDD phase are better studied by looking at the large-scale properties of connected clusters of parallel rods. For instance, it is known that the exponent characterizing the decay of cluster size distribution of critical Fortuin–Kasteleyn clusters [128] in the q-state Potts model [129, 130] has a non-trivial dependence on q. We denote all sites occupied by x-mers by 1 and the rest by zero. For our problem, we define

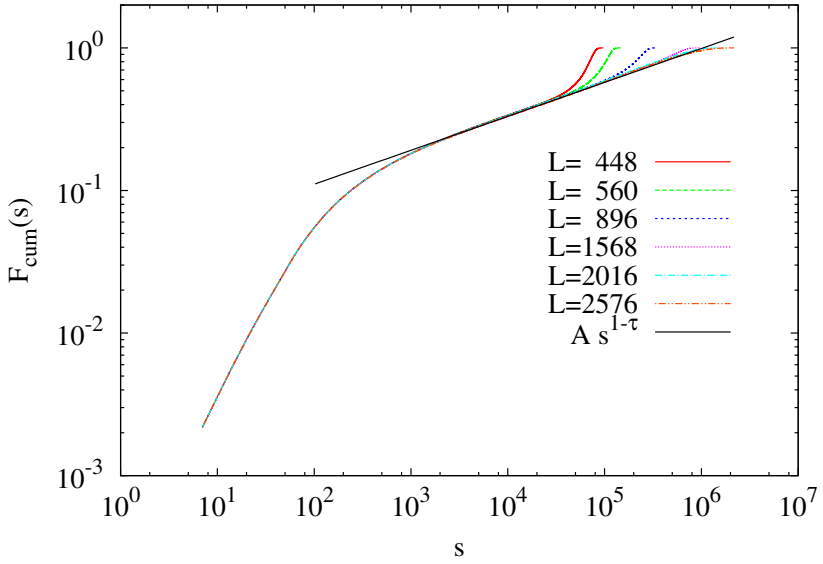

Figure 3.7: $F_{cum}(s)$, the probability that a randomly chosen 1 (a site occupied by an x-mer) belongs to a connected cluster of size $\leq s$, in the HDD phase ($\mu = 7.60$) for different system sizes. The data are for the square lattice.

a cluster as a set of 1's connected by nearest neighbor bonds. Let $F(s)$ be the probability that a randomly chosen 1 belongs to a cluster of s sites. Clearly, $F(s)$ is zero, unless s is a multiple of k. Let the cumulative distribution function be $F_{cum}(s) = \sum_{s'=1}^{s} F(s')$.

In Fig. 3.7, we plot $F_{cum}(s)$ in the HDD phase for different system sizes on the square lattice. We find that for intermediate range of s, for $10^3 \ll s \ll 10^6$, $F_{cum}(s) \simeq As^{1-\tau}$, with $\tau < 1$. For $\mu = 7.60$, we estimate the numerical values to be $A = 0.037$ and $\tau = 0.762$. For small system sizes (up to $L = 1568$), $F_{cum}(s)$ has a system-size dependent cutoff. The L-independent cutoff s^* is determined by the condition $As^{*1-\tau} \approx 1$, giving $s^* \approx 1.04 \times 10^6$. The density of 1's being roughly 0.48, we expect to observe s^* only when L exceeds a characteristic length scale $\xi^* \sim 1400$. This is indeed seen in Fig. 3.7.

In the HDD phase, $F_{cum}(s)$ depends weakly on μ (see Fig. 3.8). The power law exponent τ is estimated to be 0.778 ($\mu = 6.50$), 0.767 ($\mu = 6.91$) and 0.762 ($\mu = 7.60$). It appears that τ decreases slowly with increasing μ, while s^* decreases with increasing μ.

One qualitative feature of the HDD phase is the appearance of large groups of parallel rods, worm-like in appearance, nearly aligned in the transverse direction. This is clearly

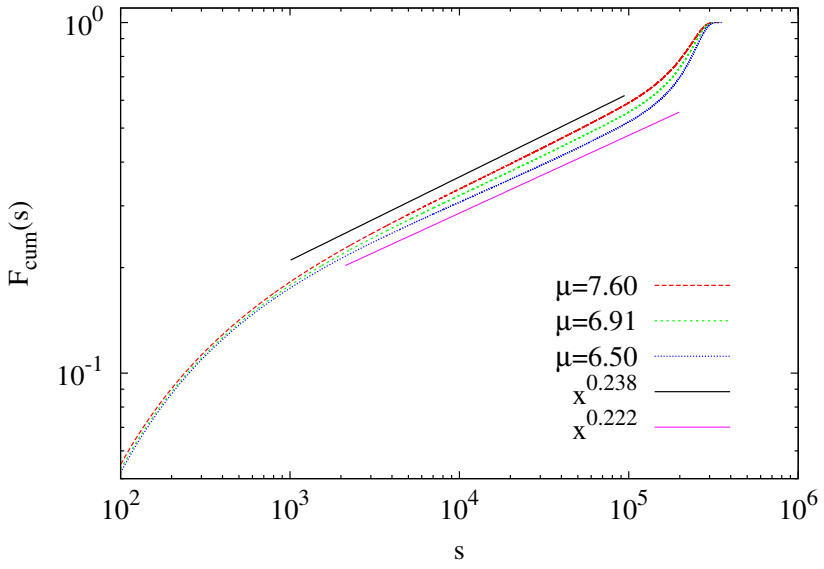

Figure 3.8: $F_{cum}(s)$, the probability that a randomly chosen 1 (a site occupied by an x-mer) belongs to a connected cluster of size $\leq s$, for different values of μ, all corresponding to the HDD phase. The curves appear to have weakly density dependent power-law exponents.

seen in Fig. 3.1(c). We call these groups stacks. To be precise, we define a stack as follows: two neighboring parallel k-mers are said to belong to the same stack if the number of nearest-neighbor bonds between them is greater than $k/2$. A stack is the maximal cluster of rods that can be so constructed. By this definition, a stack has a linear structure without branching, with some transverse fluctuations allowed. Size of a stack is defined by the number of rods present in it. Examples of stacks on square and triangular lattices are shown in Fig. 3.9. Any given configuration of rods is uniquely broken up into a collection of disjoint stacks.

There are a noticeable number of large stacks in the HDD phase. We measured the stack size distribution $D(s_1)$, the number of stacks of size s_1 per site of the lattice, in all the three phases and at the transition points (see Fig. 3.10). Interestingly, we found that this distribution is nearly exponential in all the three phases, as well as at the critical points, and there is no indication of any power-law tail in this function. It implies the absence of any local spatial ordering of parallel rods in HDD phase and thus, it is indistinguishable from the LDD phase in this respect. In the HDD phase, the mean stack size $\langle s_1 \rangle$ is

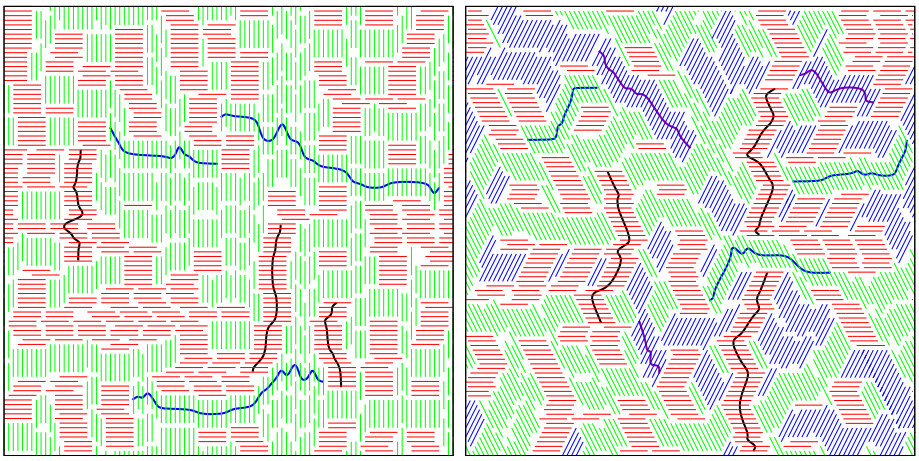

Figure 3.9: Some examples of the different types of stacks, shown here as rods joined by wiggly lines, for (a) square lattice and (b) triangular lattice. The snapshots are for $\mu = 7.60$, corresponding to the HDD phase. Rods of different orientations are shown in different colors for easy visualization.

approximately 12, for both square and triangular lattices, and is only weakly dependent on the density. For this average stack size, the size of the cluster of occupied sites is $s = 12 \times k = 84$. Presumably, this might be the reason of having a L independent knee like structure in the distribution of $F_{cum}(s)$ around $s \approx 80 - 90$ (see Fig. 3.7).

It was suggested in Ref. [20] that the second phase transition may be viewed as a binding-unbinding transition of k species of vacancies. For studying such a characterization, we break the square lattice into k sublattices. A site (x, y) belongs to the i-th sublattice if $x + y = i \ (mod\ k)$, where $i = 0, 1, \ldots, k - 1$. In a typical configuration with a low density of vacant sites, it was argued that the vacancies would form bound states of k vacancies, one from each sublattice. The HDD phase can then be described as a weakly interacting gas of such bound states if the typical distance between two bound states is much larger than the mean size of a bound state.

Let d_{ij} be the Euclidean distance between a randomly picked vacant site on the i-th sublattice, and the vacant site nearest to it on the j-th sublattice. The average of d_{ij}, averaged over all pairs (ij), with $i \neq j$, will be denoted by $\bar{d}_{ij}$, and $\bar{d}_{ii}$ will denote the value of d_{ii},

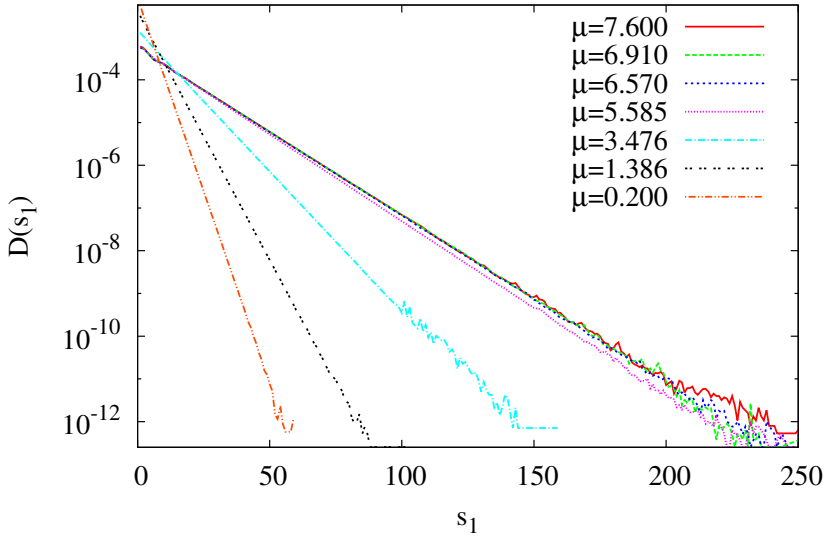

Figure 3.10: Stack distribution in the LDD phase ($\mu = 0.200$), intermediate density nematic phase ($\mu = 3.476$), HDD phase ($\mu = 7.600$), and at two critical points ($\mu = 1.3863$, 5.57) are shown. Data are for $L = 280$, $k = 7$, and the square lattice.

averaged over i.

In Fig. 3.11, we show the variation of $\bar{d}_{ij}$ and $\bar{d}_{ii}$ with density ρ. We see that $\bar{d}_{ii}$ and $\bar{d}_{ij}$, both vary approximately as $(1-\rho)^{-1/2}$, with $\bar{d}_{ii} \approx 1.18\bar{d}_{ij}$. The data are for $L = 168$ and $k = 7$. There is no noticeable dependence of the data on L. We see no signature of $\bar{d}_{ij}$ saturating to a finite value, for the densities up to 0.995, when $\bar{d}_{ij} \simeq 35$.

We conclude that the bound state, if exists at all, is very weakly bound. Near ρ_2^*, the typical spacing between vacancies is much less than the size of the bound state, and the transition can not be treated as binding-unbinding transition when the average distance between bound states becomes comparable to their size.

3.5 Critical behavior near the second transition

We now discuss the critical behavior near the second transition. Several thermodynamic quantities are of interest. We define the order parameter variable q_1 for the square lattice

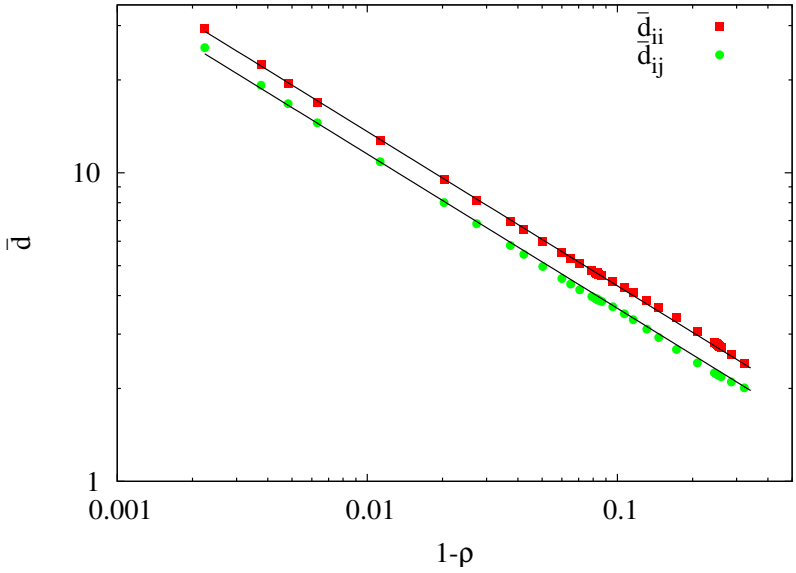

Figure 3.11: The average spacing between vacancies $\bar{d}_{ii}$ and $\bar{d}_{ij}$, on the square lattice as a function of density ρ. The solid lines show the functions $K(1-\rho)^{-1/2}$, for $K = 1.36$ and 1.15. The data are for $L = 168$ and $k = 7$.

as $q_1 = n_h - n_v$. For the triangular lattice, $\rho = n_1 + n_2 + n_3$ and $q_1 = n_1 + \omega\, n_2 + \omega^2\, n_3$, where ω is the complex cube-root of unity, and n_i ($i = 1, 2, 3$) is the fraction of sites occupied by the k-mers oriented along i-th lattice directions. The averaged order parameter Q, its second moment χ, compressibility κ, and Binder cumulant U are defined as

$$Q = \frac{\langle |q_1| \rangle}{\langle \rho \rangle}, \tag{3.5a}$$

$$\chi = \frac{L^2 \langle |q_1|^2 \rangle}{\langle \rho \rangle^2}, \tag{3.5b}$$

$$\kappa = L^2 \left[\langle \rho^2 \rangle - \langle \rho \rangle^2 \right], \tag{3.5c}$$

$$U = 1 - \frac{\langle |q_1|^4 \rangle}{a \langle |q_1|^2 \rangle^2}, \tag{3.5d}$$

where $a = 3$ for square lattice and $a = 2$ for triangular lattice. Q is zero in the LDD and HDD phases and nonzero in the nematic phase.

The data used for estimating the critical exponents are for $k = 7$, and for five different system sizes $L = 154$, 210, 336, 448, and 952 for the square lattice and $L = 210$, 336, 448, and 560 for the triangular lattice. The system is equilibrated for 10^7 Monte Carlo

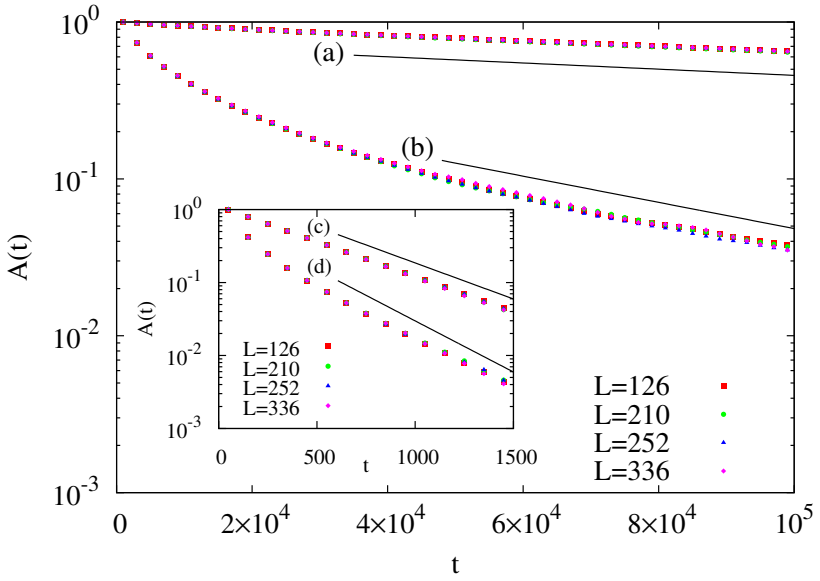

Figure 3.12: The temporal variation of the autocorrelation functions for (a) the global order parameter q_1 and (b) the local order parameter S. The data are for $\mu = 7.60$ and the autocorrelation times corresponding to the solid lines are (a)220000 and (b) 52000 Monte carlo steps. Inset: Data as above but in the LDD phase ($\mu = 0.20$), with (c) corresponding to $A_{q_1q_1}(t)$ (d) corresponding to $A_{SS}(t)$. The autocorrelation times are (c) 440 and (d) 310. All data are for $k = 7$.

steps for each μ, following which the data are averaged over 3×10^8 Monte Carlo steps. These times are larger than the largest autocorrelation times that we encounter, obtained by measuring the autocorrelation function

$$A_{q_1q_1}(t) = \frac{\langle q_1(\tau)q_1(\tau + t)\rangle}{\langle q_1^2\rangle}, \tag{3.6}$$

where the averaging is done over the reference time τ. The function $A_{SS}(t)$ for the local order parameter is defined similarly. The largest autocorrelation time is for the largest density and is close to 2.2×10^5 Monte Carlo steps (see Fig. 3.12). To estimate errors, the measurement is broken up into 10 statistically independent blocks.

The quantities in Eq. (3.5) are determined as a function of μ using Monte Carlo simulations. The nature of the second transition from the ordered nematic phase to the HDD phase is determined by the singular behavior of U, Q, χ, and κ near the critical point. Let $\epsilon = (\mu - \mu_c)/\mu_c$, where μ_c is the critical chemical potential. The singular behavior

is characterized by the critical exponents ν, β, γ, and α, defined by $Q \sim (-\epsilon)^{\beta}$, $\epsilon < 0$, $\chi \sim |\epsilon|^{-\gamma}$ and $\kappa \sim |\epsilon|^{-\alpha}$, and $\xi^* \sim |\epsilon|^{-\nu}$, where ξ^* is the correlation length and $|\epsilon| \to 0$. Here, the density ρ is at the same footing as energy in a typical spin model, and the chemical potential $\mu = \mu_h = \mu_v$ is like temperature. The order parameter would be coupled to the symmetry breaking field ($\sim \mu_h - \mu_v$) between the two orientations. Thus, the scaling of the compressibility κ or the second derivative of the free energy with respect to μ is given by the specific heat exponent α. The exponents are obtained by finite size scaling of the different quantities near the critical point:

$$U \simeq f_U(\epsilon L^{1/\nu}), \tag{3.7a}$$

$$Q \simeq L^{-\beta/\nu} f_Q(\epsilon L^{1/\nu}), \tag{3.7b}$$

$$\chi \simeq L^{\gamma/\nu} f_\chi(\epsilon L^{1/\nu}), \tag{3.7c}$$

$$\kappa \simeq L^{\alpha/\nu} f_\kappa(\epsilon L^{1/\nu}), \tag{3.7d}$$

where f_U, f_Q, f_χ, and f_κ are scaling functions.

3.5.1 Square lattice

We first present results for the square lattice. The data for the Binder cumulant U for different system sizes intersect at $\mu_c = 5.57 \pm .02$ (see Fig. 3.13). The density at this value of chemical potential is $\rho_2^* = 0.917 \pm .015$, consistent with the variational estimate $0.87 \le \rho_2^* \le 0.93$ in Ref. [113]. The value of U at the transition lies in the range 0.56 to 0.59. This is not very different from the value for the Ising transition $U_c \approx 0.61$ [131]. The data for different system sizes collapse when scaled as in Eq. (3.7a) with $\nu = 0.90 \pm .05$ (see inset of Fig. 3.13). To compare with the first transition from the LDD phase to the nematic phase, $\rho_1^* = 0.745 \pm 0.010$, and the numerical estimate for the exponent ν is consistent with the known exact Ising value 1 [25].

The data for order parameter, χ and κ for different system sizes are shown in Figs. 3.14,

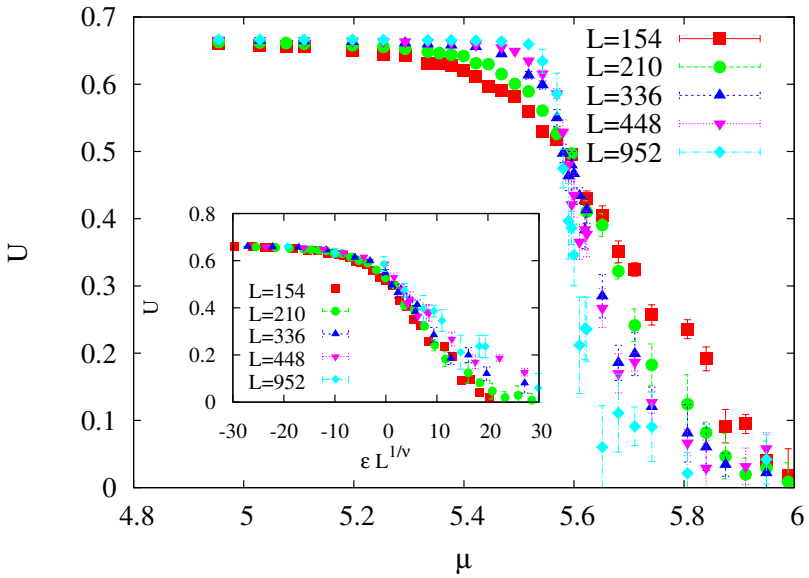

Figure 3.13: The Binder cumulant U as a function of chemical potential μ for different lattice sizes of a square lattice. The curves intersect at $\mu_c = 5.57 \pm .02$. Inset: Data collapse for square lattices when U is plotted against $\epsilon L^{1/\nu}$ with $\nu = 0.90$ and $\epsilon = (\mu - \mu_c)/\mu_c$.

3.15 and 3.16 respectively. Q decreases to zero at high densities. Our best estimates of effective critical exponents are $\beta/\nu = 0.22 \pm 0.07$ (see inset of Fig. 3.14). $\gamma/\nu = 1.56 \pm 0.07$ (see inset of Fig. 3.15), and $\alpha/\nu = 0.22 \pm 0.07$ (see inset of Fig. 3.16). The estimated error bars are our subjective estimates, based on the goodness of fit. These differ substantially from the values of the exponents of the two-dimensional Ising model ($\nu = 1, \beta = 1/8, \gamma = 7/4, \alpha = 0$). However, as discussed in Sec. 3.4, it seems like there is a characteristic length scale $\xi^* \sim 1400$ in the HDD phase, and we cannot say much about the asymptotic value the critical exponents at length scales $L \gg \xi^*$.

3.5.2 Triangular lattice

For the triangular lattice, we find that the second transition is continuous with $\mu_c = 5.147 \pm .050$ and $\rho_2^* = 0.905 \pm .010$. The data for U, Q, χ, and κ for different system sizes collapse onto one scaling curve when scaled as in Eq. (3.7) with exponents that are indistinguishable from those of the three-state Potts model (see Fig. 3.17,3.18, 3.19,3.20) ($\nu = 5/6$, $\beta/\nu = 2/15$, $\gamma/\nu = 26/15$ and $\alpha/\nu = 2/5$). We estimate $\nu = 0.83 \pm 0.04$,

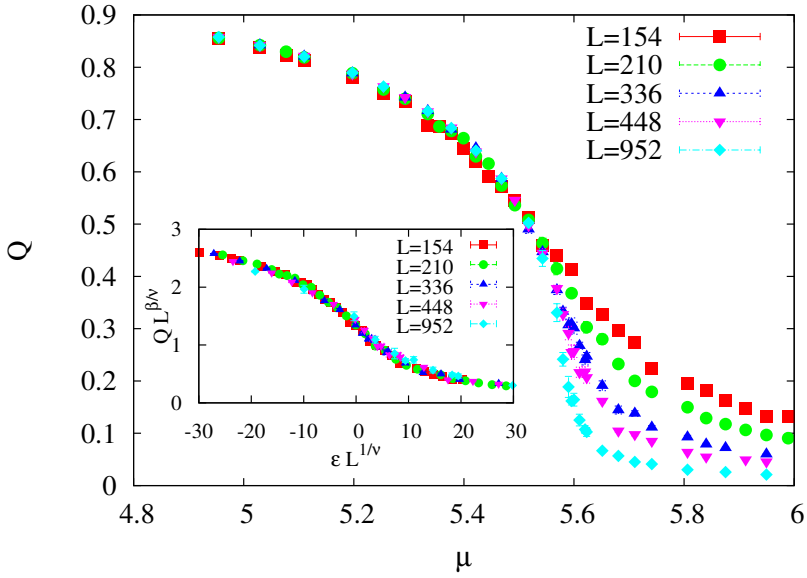

Figure 3.14: The variation of the order parameter Q with chemical potential μ for different systems sizes of a square lattice. Inset: Data collapse for square lattices when scaled Q is plotted against $\epsilon L^{1/\nu}$ with $\nu = 0.90$, $\beta/\nu = 0.22$ and $\epsilon = (\mu - \mu_c)/\mu_c$.

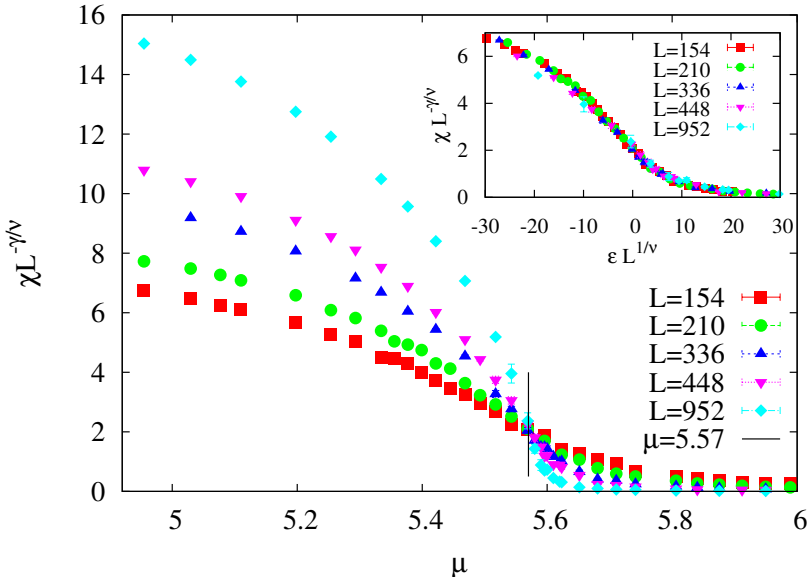

Figure 3.15: The variation of χ with chemical potential μ for different system sizes of a square lattice. The curves cross at μ_c when χ is scaled by $L^{-\gamma/\nu}$, with $\gamma/\nu = 1.56$. Inset: Data collapse for square lattices when $\chi L^{-\gamma/\nu}$ is plotted against $\epsilon L^{1/\nu}$ with $\nu = 0.90$, and $\epsilon = (\mu - \mu_c)/\mu_c$.

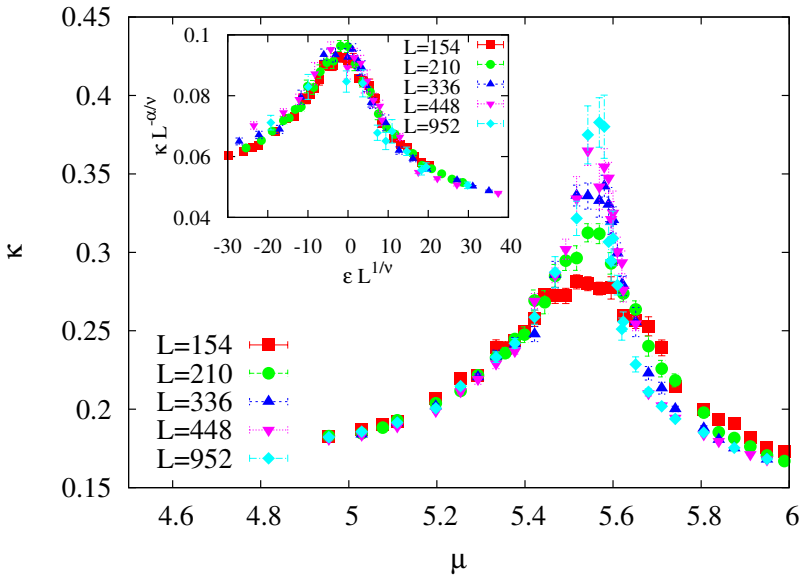

Figure 3.16: The variation of compressibility κ with chemical potential μ for different system sizes of a square lattice. Inset: Data collapse for square lattices when the scaled κ is plotted against $\epsilon L^{1/\nu}$ with $\nu = 0.90$, $\alpha/\nu = 0.22$, and $\epsilon = (\mu - \mu_c)/\mu_c$.

$\beta/\nu = 0.13 \pm 0.02$, $\gamma/\nu = 1.73 \pm 0.04$ and $\alpha/\nu = 0.40 \pm 0.05$. From symmetry, one can argue that there is only one type of surface tension as it is the same between the different ordered phases (where majority of the rods are oriented along one of the thee possible lattice directions). Thus, we can relate this with the three-state Potts model having $\mathbb{Z}_3$ symmetry and a unique surface tension energy between different spins.

As in the case of the square lattice, we probe the correlations in the triangular lattice by looking at the large-scale properties of connected clusters of parallel rods. We denote all sites occupied by horizontal rods by 1 and the rest by zero. In Fig. 3.21, $F(s)$, the probability that a randomly chosen 1 belongs to a cluster of s sites, is shown for different system sizes L in the HDD phase. Unlike the square lattice case, here, there is no extended regime of s where $F(s)$ seems to grow as a power of s. This suggests that for the triangular lattice, the HDD and LDD phases are qualitatively similar, and the HDD phase has a finite correlation length ~ 60.

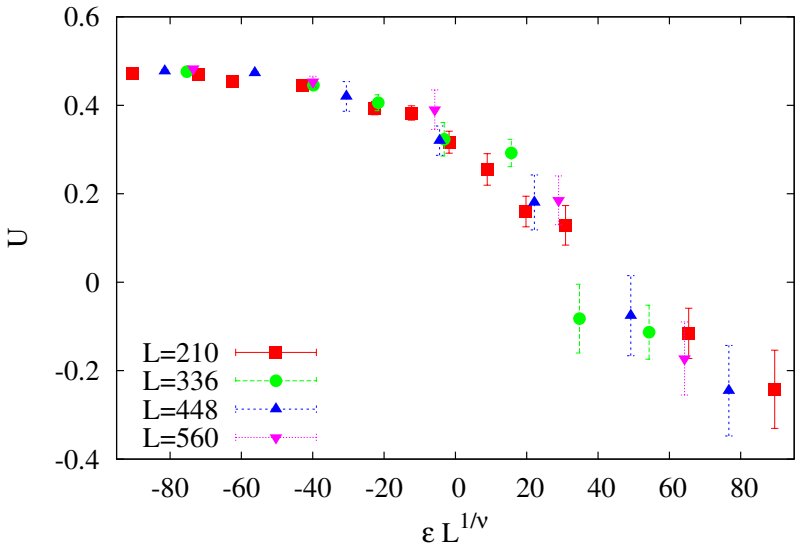

Figure 3.17: Data collapse for triangular lattices when U is plotted against $\epsilon L^{1/\nu}$ with $\mu_c = 5.147$ and $\nu = 5/6$, where $\epsilon = (\mu - \mu_c)/\mu_c$.

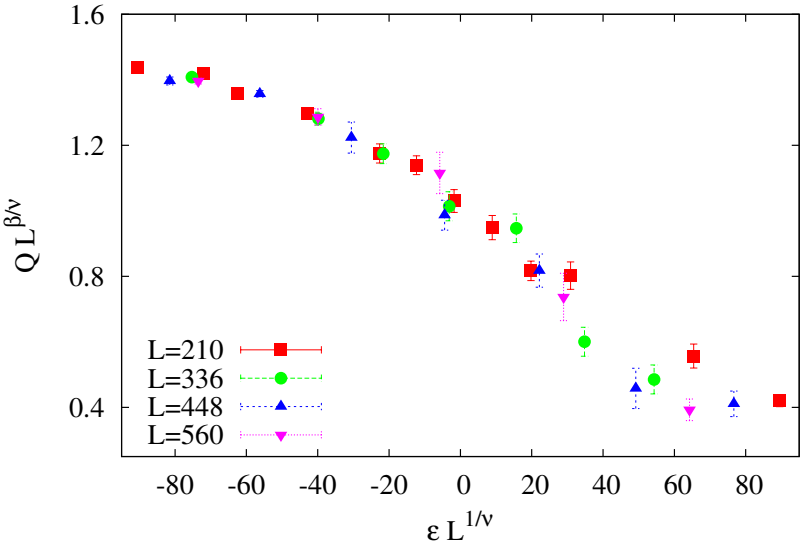

Figure 3.18: Data collapse for triangular lattices when scaled Q is plotted against $\epsilon L^{1/\nu}$ with $\mu_c = 5.147$, $\nu = 5/6$ and $\beta/\nu = 2/15$.

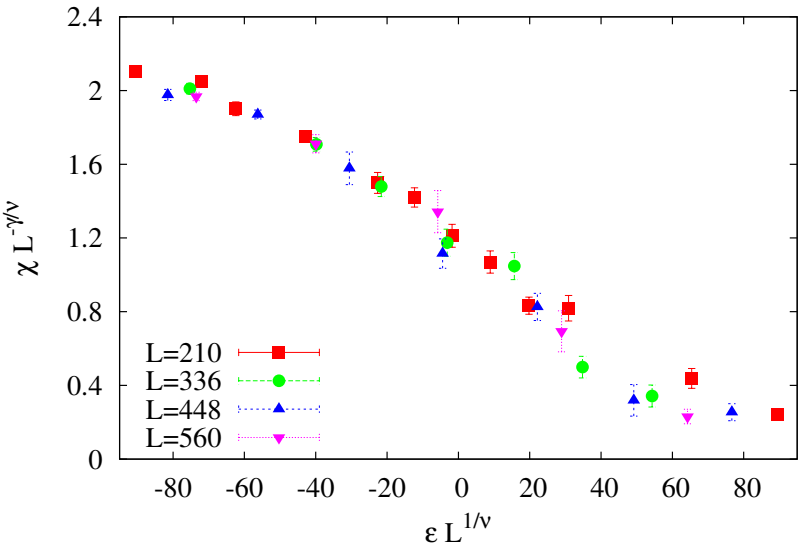

Figure 3.19: Data collapse for triangular lattices when scaled χ is plotted against $\epsilon L^{1/\nu}$ with $\mu_c = 5.147$, $\nu = 5/6$ and $\gamma/\nu = 26/15$.

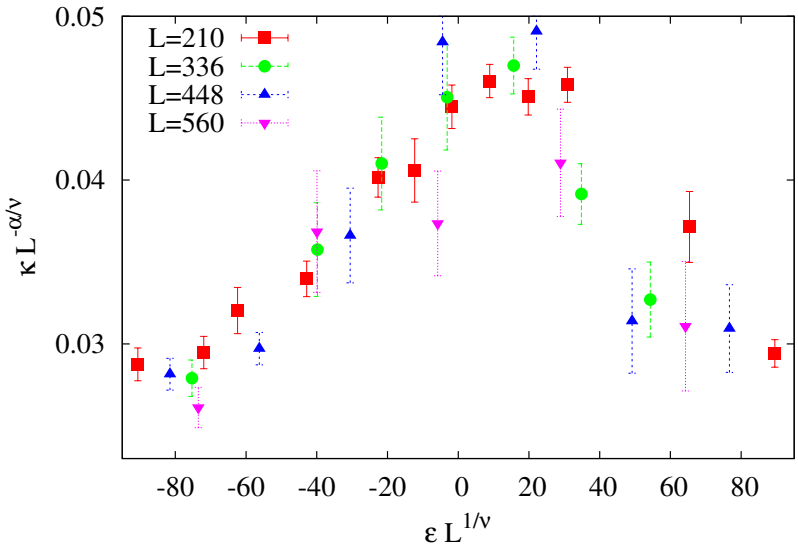

Figure 3.20: Data collapse for triangular lattices when scaled κ is plotted against $\epsilon L^{1/\nu}$ with $\mu_c = 5.147$, $\nu = 5/6$ and $\alpha/\nu = 2/5$.

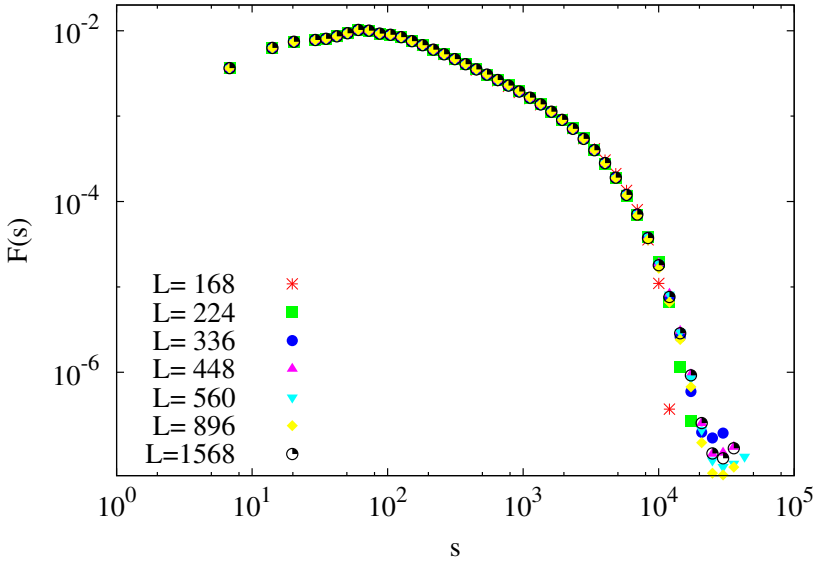

Figure 3.21: $F(s)$, the probability that a randomly chosen site belongs to a s-site connected cluster of horizontal rods in the HDD phase for different system sizes of the triangular lattice.

3.6 Summary and discussion

In this chapter, we studied the problem of hard, rigid rods on two-dimensional square and triangular lattices, using the efficient Mote carlo algorithm. We showed the existence of a second transition from the ordered nematic phase to a disordered phase as the packing density is increased. By studying the order parameter, its second moment, compressibility and Binder cumulant, we find that the second transition is continuous on both square and triangular lattices. We also investigated the nature of correlations in the HDD phase by measuring distribution of connected clusters of parallel rods, as well as the distribution of stacks.

We are not able to give a very clear answer to the question whether the HDD and LDD phases are qualitatively different, or not. But the available evidence suggests that while the HDD phase has a large correlation length ξ^*, it is not qualitatively different. This is based on the evidence that vacancies in the HDD phase do not form a bound state. In that sense, a k-mer system with $k = 7$, at high densities is similar to the $k = 2$ case, where also,

the monomers do not form a bound state, and unbound monomers lead to an exponential decay of correlations at any nonzero vacancy density.

An interesting feature of the HDD phase is the appearance of a large characteristic length scale $\xi^* \sim 1400$ on the square lattice, as inferred from the fact that the cluster size distribution seems to follow a power law distribution $F(s) \sim s^{-\tau}$, with $\tau < 1$ for $s < \xi^{*2}$. The amplitude of this power-law term is rather small. This is related to the fact that for the k-mer problem, various perturbation series involve terms like k^{-k} [20], which then leads to large correlation lengths. The HDD phase has power-law correlations at least for lengths up to ξ^*.

For the triangular lattice, the correlation length ξ^* is much smaller, as near the critical point, clusters of each type of rods cover only about a third of the sites, which is substantially below the corresponding percolation threshold.

On the square lattice, our best estimates of the numerical values of the critical exponents are different from those of the Ising universality class. However, because the correlation lengths in the HDD phase are large and no clear distinction between the LDD and the HDD phases are found, we cannot rule out a crossover to the Ising universality class at larger length scales. For the triangular lattice with $k = 7$, the estimated exponents for second transition are consistent with those of two-dimensional three-state Potts universality class.

Chapter 4

Repulsive Rods on a Bethe-like lattice

4.1 Introduction

On two-dimensional lattices, the system of hard rods undergoes two entropy-driven transitions: first from a low-density disordered (LDD) phase to an intermediate density nematic phase, and second from the nematic phase to a high-density disordered (HDD) phase. On the square lattice, the second transition is continuous with effective critical exponents that are different from the two-dimensional Ising exponents, though a crossover to the Ising universality class at large length scales could not be ruled out (see Sec. 3.6). This raises the question whether the LDD and HDD phases are same or different.

In this chapter, we ask whether there is a solvable model of k-mers that shows two transitions with increasing density and throws light on the HDD phase? The hard-core k-mer problem was solved exactly on the random locally tree-like layered lattice (RLTL), a Bethe-like lattice [26]. This lattice was introduced because a uniform nematic order is unstable on the more conventional Bethe lattice when the coordination number is larger than 4. However, on the RLTL, while a stable nematic phase exists for all even coordination numbers greater than or equal to four, the second transition is absent for hard rods [26]. Here we relax the hard-core constraint and allow k-mers of different orientations to inter-

sect at a lattice site. Weights $u, v, \ldots$ are associated with sites that are occupied by two, three, $\ldots$ k-mers. When the weights are zero, we recover the hard rod problem. We solve this model on the RLTL and show that for a range of $u, v, \ldots$, the system undergoes two transitions as the density is increased: first from a LDD phase to a nematic phase and second from the nematic phase to a HDD phase. For coordination number $q = 4$, the two transitions are continuous and belong to the mean field Ising universality class. For $q \geq 6$, where q is an even integer, while the first transition is first order, the second transition is first order or continuous depending on the values of $k, u, v, \ldots$.. In all cases, it is possible to continuously transform the LDD phase into the HDD phase in the ρ–interaction parameters phase diagram without crossing any phase boundary, showing that the LDD and HDD phases are qualitatively similar, and hence the HDD phase is a reentrant LDD phase.

The rest of the chapter is organized as follows. In Sec. 4.2, we recapitulate the construction of RLTL and formulate the model of rods on this lattice. In Sec. 4.3, we derive the analytic expression for free energy for fixed density of horizontal and vertical k-mers on the 4-coordinated RLTL. It is shown that the system undergoes two continuous phase transitions for $k \geq 4$. In Sec. 4.4, the free energy is computed for coordination number $q = 6$, and the dependence of the nature of the transition on the different parameters are detailed. Section 4.5 summarizes the main results of this work. The content of this chapter is published in Ref. [132].

4.2 The RLTL and definition of the model

The RLTL was introduced in Ref. [26]. In this section, we recapitulate its construction for coordination number $q = 4$. Generalization to larger even values of q is straightforward. Consider a collection of M layers, each having N sites. Each site in layer m is connected to the sites in layer $(m - 1)$ by two bonds. To distinguish between two orientations, the

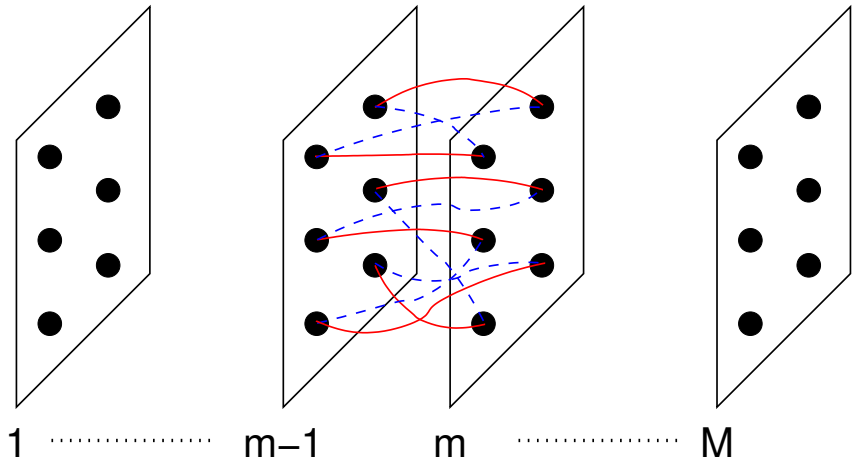

Figure 4.1: Schematic diagram of the RLTL with $N = 6$ sites per layer and coordination number 4. A typical bond configuration between layers $m - 1$ and m is shown with X bonds in red (solid) lines and Y bonds in blue (dotted) lines.

bonds are divided into two types: X and Y. Each site in the m-th layer is connected with exactly one randomly chosen site in the $(m - 1)$-th layer with a bond of type X. Similarly, bonds of type Y are also connected by random pairing of sites in the two adjacent layers. Hence, the total number of such possible pairing between two layers is $(N!)^2$. A typical bond configuration is shown in Fig. 4.1. For a q-coordinated lattice with periodic boundary conditions, the total number of different possible graphs is $(N!)^{qM/2}$, and with open boundary conditions there are $(N!)^{q(M-1)/2}$ different possible graphs. In the thermodynamic limit, the RLTL contains few short loops and locally resembles a Bethe lattice.

We consider a system of monodispersed rods of length k on the RLTL. A k-mer occupies $(k - 1)$ consecutive bonds of same type. Rods on X (Y) type of bonds will be called x-mers (y-mers). Weights e^{μ_1} and e^{μ_2} are associated with each x-mer and y-mer, where μ's are chemical potentials. Linear rods comprising of k monomers are placed on the RLTL such that a site can be occupied by utmost two k-mers. Two k-mers of the same type can not intersect. A weight u is associated with every site that is occupied by two k-mers of different types. The limiting case $u = 0$ corresponds to the hard-core problem. For even $q \geq 6$, a site can be occupied by utmost $q/2$ k-mers, each of different type.

For a given bond configuration $\mathcal{R}$, let $Z_{\mathcal{R}}(M, N)$ denote the partition function, the weighted sum over all possible rod configurations. We, then, define the average partition function as

$$Z_{av}(M, N) = \frac{1}{N_{\mathcal{R}}} \sum_{\mathcal{R}} Z_{\mathcal{R}}(M, N), \tag{4.1}$$

where $N_{\mathcal{R}}$ is the number of different bond configurations on the lattice. In the thermodynamic limit the mean free energy per site is obtained by

$$f = -\lim_{M,N\to\infty} \frac{1}{MN} \ln Z_{av}, \tag{4.2}$$

where the temperature and Boltzmann constant have been set equal to 1.

4.3 k-mers on RLTL with coordination number $q = 4$

In this section, we calculate the free energy of the system on the RLTL of coordination number 4 for fixed u and fixed densities of x-mers and y-mers. The phase diagram of the system is obtained by minimizing the free energy with respect to x-mer and y-mer densities for a fixed total density.

4.3.1 Calculation of free energy

To calculate the partition function, consider the operation of adding the m-th layer, given the configuration up to the $(m-1)$-th layer. The number of ways of adding the m-th layer is denoted by C_m. C_m will be a function of the number of x-mers and y-mers passing through the m-th layer and the number of intersections between x-mers and y-mers at the m-th layer.

Let x_m (y_m) be the number of x-mers (y-mers) whose left most sites or heads are in the m-th layer. X_m and Y_m are the number of sites in the m-th layer occupied by x-mers and

y-mers respectively, but where the site is not the head of the k-mer. Clearly,

$$X_m = \sum_{j=1}^{k-1} x_{m-j},\ Y_m = \sum_{j=1}^{k-1} y_{m-j},\ 1 \le m \le M, \tag{4.3}$$

with $x_m = y_m = 0$, for $m \le 0$. To have all k-mer fully contained within the lattice for open boundary condition we need to impose, $x_m = y_m = 0$ for, $m \ge M - k + 2$.

In a k-mer, let h denote its head or left most site and b denote the other $k-1$ sites. Then, we define Γ^m_{ij}, where $i, j = h, b$, to be the number of intersections at the m-th layer between site i of an x-mer and site j of a y-mer. For instance, Γ^m_{hh} is the number of sites in the m-th layer, occupied simultaneously by the heads of an x-mer and a y-mer. Given $\{x_m\}$, $\{y_m\}$ and $\{\Gamma^m_{ij}\}$, the calculation of C_m reduces to an enumeration problem.

Now we derive the expression for C_m. C_m is the total number of ways of connecting the X- and Y-bonds from the $(m-1)$-th layer to the m-th layer consistent with the number of x-mers, y-mers, and intersections at the m-th layer. In the $(m-1)$-th layer, there are X_m and Y_m sites occupied by x-mers and y-mers that extend to the m-th layer. These X_m bonds of type X have to be connected to X_m different sites out of the N sites in the m-th layer. This can be done in

$$\frac{N!}{(N - X_m)!}$$

ways. Among the Y_m bonds of type Y, Γ^m_{bb} of them are connected to sites occupied by an x-mer and the remaining $Y_m - \Gamma^m_{bb}$ bonds are connected to empty sites in the m-th layer. The number of ways of connecting the Y bonds is a product of the two enumerations and is equal to

$$\frac{Y_m! X_m!}{\Gamma^m_{bb}!(Y - \Gamma^m_{bb})!(X_m - \Gamma^m_{bb})!} \times \frac{(N - X_m)!}{(N - X_m - Y_m + \Gamma^m_{bb})!}.$$

Now connect the remaining $(N - X_m)$ free bonds of type X and $(N - Y_m)$ free bonds of type Y to sites in layer m that are not occupied by x-mers and y-mers respectively. This can be

done in

$$(N - X_m)!(N - Y_m)!$$

ways.

We have to now assign sites to x_m and y_m heads in layer m. Out of x_m (y_m) heads, Γ^m_{hb} (Γ^m_{bh}) of them will be on sites already occupied by only a y-mer (x-mer). The number of ways of doing this is

$$\frac{(X_m - \Gamma^m_{bb})!}{\Gamma^m_{bh}!(X_m - \Gamma^m_{bb} - \Gamma^m_{bh})!} \times \frac{(Y_m - \Gamma^m_{bb})!}{\Gamma^m_{hb}!(Y_m - \Gamma^m_{bb} - \Gamma^m_{hb})!}.$$

There are $(N - X_m - Y_m + \Gamma^m_{bb})$ sites in the m-th layer which are unoccupied so far. They can be divided into four groups: Γ^m_{hh} sites, each occupied by the heads of an x-mer and a y-mer, $(x_m - \Gamma^m_{hh} - \Gamma^m_{hb})$ sites occupied by only a head of an x-mer, $(y_m - \Gamma^m_{hh} - \Gamma^m_{bh})$ sites occupied by only a head of a y-mer, and $(N - X_m - Y_m - x_m - y_m + \sum_{ij} \Gamma^m_{ij})$ unoccupied sites. The number of ways of arranging them is:

$$\frac{(N - X_m - Y_m + \Gamma^m_{bb})!}{\Gamma^m_{hh}!(x_m - \Gamma^m_{hh} - \Gamma^m_{hb})!(y_m - \Gamma^m_{hh} - \Gamma^m_{bh})!} \times \frac{1}{(N - X_m - Y_m - x_m - y_m + \sum_{ij} \Gamma^m_{ij})!}.$$

The product of all these factors gives

$$\begin{aligned} C_m &= \frac{N! X_m! Y_m! (N - X_m)! (N - Y_m)!}{(x_m - \Gamma^m_{hh} - \Gamma^m_{hb})!(y_m - \Gamma^m_{hh} - \Gamma^m_{bh})!(X_m - \Gamma^m_{bb} - \Gamma^m_{bh})!(Y_m - \Gamma^m_{bb} - \Gamma^m_{hb})!} \\ &\times \frac{1}{\left(N - X_m - Y_m - x_m - y_m + \sum_{i,j=b,h} \Gamma^m_{ij}\right)! \prod_{i,j=b,h} \Gamma^m_{ij}!}. \end{aligned} \tag{4.4}$$

The partition function is then the weighted sum of the product of C_m for different layers:

$$\begin{aligned} Z_{av} &= \frac{1}{(N!)^{2M}} \sum_{\{x_m\},\{y_m\},\{\Gamma^m_{ij}\}} \\ &\prod_m \left(C_m e^{\mu_1 x_m} e^{\mu_2 y_m} u^{\sum_{ij} \Gamma^m_{ij}} \right). \end{aligned} \tag{4.5}$$

where the sum is over all possible number of x-mers, y-mers and number of doubly occupied sites. Each term in the sum in Eq. (4.5) is of order $\exp(NM)$. Hence, for large N, M, we replace the summation with the largest summand with negligible error. To find the summand that maximizes the sum, we extremize the summand with respect to the variables that are summed over. For example, to maximize with respect to x_l, we set:

$$\frac{C(\{x_m + \delta_{m,l}\}, \{y_m\}, \{\Gamma^m_{ij}\})e^{\mu_1}}{C(\{x_m\}, \{y_m\}, \{\Gamma^m_{ij}\})} \approx 1, \tag{4.6}$$

where $C = \prod_m C_m$. Likewise, we can write equations for each of the variables.

We look for homogeneous solutions such that $\rho_x = x_m k/N$, $\rho_y = y_m k/N$, and $\gamma_{ij} = \Gamma^m_{ij}/N$ are variables that are independent of N and have no spatial dependence. Here, ρ_x and ρ_y are fractions of sites in any layer that are occupied by x-mers and y-mers respectively. In terms of these variables, Eq. (4.6) and the corresponding one obtained by maximizing with respect to y_j reduce to

$$\frac{(\rho_x - \frac{\rho_x}{k})^{k-1}(1 - \rho + \sum_{ij}\gamma_{ij})^k(\frac{\rho_x}{k} - \gamma_{hh} - \gamma_{hb})^{-1}}{(1 - \rho_x + \frac{\rho_x}{k})^{k-1}(\rho_x - \frac{\rho_x}{k} - \gamma_{bb} - \gamma_{bh})^{k-1}} = e^{-\mu_1}, \tag{4.7}$$

and

$$\frac{(\rho_y - \frac{\rho_y}{k})^{k-1}(1 - \rho + \sum_{ij}\gamma_{ij})^k(\frac{\rho_y}{k} - \gamma_{hh} - \gamma_{bh})^{-1}}{(1 - \rho_y + \frac{\rho_y}{k})^{k-1}(\rho_y - \frac{\rho_y}{k} - \gamma_{bb} - \gamma_{hb})^{k-1}} = e^{-\mu_2}, \tag{4.8}$$

where $\rho = \rho_x + \rho_y$ is the total density.

The summand in Eq. (4.5) has to be now maximized with respect to the intersection

parameters $\{\Gamma^l_{ij}\}$. On doing so, we obtain

$$\frac{[\rho_x(1-\frac{1}{k})-\gamma_{bb}-\gamma_{bh}][\rho_y(1-\frac{1}{k})-\gamma_{bb}-\gamma_{hb}]}{\gamma_{bb}(1-\rho+\sum_{ij}\gamma_{ij})} = \frac{1}{u}, \tag{4.9a}$$

$$\frac{(\frac{\rho_x}{k}-\gamma_{hh}-\gamma_{hb})(\frac{\rho_y}{k}-\gamma_{hh}-\gamma_{bh})}{\gamma_{hh}(1-\rho+\sum_{ij}\gamma_{ij})} = \frac{1}{u}, \tag{4.9b}$$

$$\frac{(\frac{\rho_x}{k}-\gamma_{hh}-\gamma_{hb})[\rho_y(1-\frac{1}{k})-\gamma_{bb}-\gamma_{hb}]}{\gamma_{hb}(1-\rho+\sum_{ij}\gamma_{ij})} = \frac{1}{u}, \tag{4.9c}$$

$$\frac{(\frac{\rho_y}{k}-\gamma_{hh}-\gamma_{bh})[\rho_x(1-\frac{1}{k})-\gamma_{bb}-\gamma_{bh}]}{\gamma_{bh}(1-\rho+\sum_{ij}\gamma_{ij})} = \frac{1}{u}, \tag{4.9d}$$

where $i, j = h, b$. Equation (4.9) can easily be solved to express γ_{bb}, γ_{hb} and γ_{bh} in terms of γ_{hh}:

$$\gamma_{bb} = (k-1)^2\gamma_{hh},\ \gamma_{bh} = \gamma_{hb} = (k-1)\gamma_{hh}, \tag{4.10}$$

and γ_{hh} satisfies the quadratic equation

$$\gamma_{hh}^2 - \gamma_{hh}\frac{\rho-\rho u-1}{k^2(1-u)} - \frac{u\rho_x\rho_y}{k^4(1-u)} = 0. \tag{4.11}$$

Equation (4.10) has a simple interpretation. Given that an x-mer and y-mer have intersected, the intersecting site is chosen from the head (h) or one of the other $k-1$ sites (b) of the k-mers randomly. In addition, the choice of h or b for the x-mer and y-mer are independent of each other. Thus, the probability of choosing 2 b's is $(k-1)^2$ times that of choosing 2 h's, and leads to the first relation in Eq. (4.10). Similar reasoning also gives the second relation in Eq. (4.10).

From Eq. (4.5), the free energy is calculated using Eq. (4.2). Eliminating the chemical potentials using Legendre transforms, we may express the free energy in terms of ρ_x, ρ_y

and u as

$$\begin{aligned} f(\rho_x, \rho_y, u) &= -\frac{k-1}{k}\sum_i \rho_i \ln \rho_i - \sum_i \left[1 - \frac{(k-1)\rho_i}{k}\right] \ln\left[1 - \frac{(k-1)\rho_i}{k}\right] \\ &\quad + \sum_i (\rho_i - k^2\gamma_{hh}) \ln(\rho_i - k^2\gamma_{hh}) + (1 - \rho + k^2\gamma_{hh}) \ln(1 - \rho + k^2\gamma_{hh}) \\ &\quad -\frac{\rho}{k} \ln k + k^2\gamma_{hh} \ln\left(\frac{k^2\gamma_{hh}}{u}\right), \end{aligned} \tag{4.12}$$

where γ_{hh} is a function of ρ_x, ρ_y and u through Eq. (4.11). This expression for the free energy turns out to be not convex everywhere. The true free energy $\bar{f}(\rho_x, \rho_y, u)$ is obtained by the Maxwell construction such that

$$\bar{f}(\rho_x, \rho_y, u) = C\mathcal{E}\Big[f(\rho_x, \rho_y, u)\Big], \tag{4.13}$$

where $C\mathcal{E}$ denotes the convex envelope. The densities ρ_x and ρ_y are free parameters. Given total density ρ, we minimize the free energy with respect to ρ_x and ρ_y subject to the constraint $\rho_x + \rho_y = \rho$. The disordered solution corresponds to $\rho_x = \rho_y$, while a solution $\rho_x \neq \rho_y$ corresponds to a nematic phase.

4.3.2 Two phase transitions

To study the phase transitions we define the nematic order parameter as

$$\psi = \frac{\rho_x - \rho_y}{\rho}. \tag{4.14}$$

A nonzero ψ corresponds to a nematic phase. The free energy when expressed as a power series in ψ, has the form

$$f(\rho_x, \rho_y, u) = A_0(\rho, u) + A_2(\rho, u)\psi^2 + A_4(\rho, u)\psi^4 + \ldots, \tag{4.15}$$

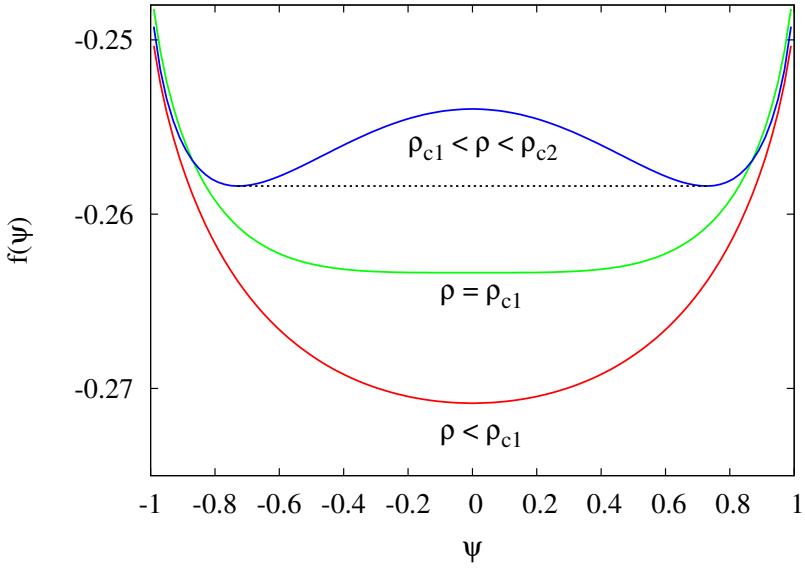

Figure 4.2: Free energy $f(\psi)$ as a function of the order parameter ψ for $\rho \approx \rho_{c1}$. The data are for $k = 6$, $u = 0.15$, and $q = 4$. The curves have been shifted for clarity. The dotted line denotes the convex envelope.

such that $f(\rho_x, \rho_y, u)$ is unchanged when $\psi \leftrightarrow -\psi$. The expressions for the coefficients $A_0(\rho, u)$, $A_2(\rho, u)$ and $A_4(\rho, u)$ are unwieldy and we do not reproduce them here. However, we find that the coefficient $A_4(\rho, u) > 0$. For small densities, the coefficient of the quadratic term $A_2(\rho, u)$ is positive and the free energy has a minimum at $\psi = 0$ corresponding to the LDD phase. However for $k \geq 4$, if u is smaller than a critical value u_c, then $A_2(\rho, u)$ changes sign continuously at a critical density ρ_{c1} and the free energy has two symmetric minima at $\psi \neq 0$, corresponding to the nematic phase. This qualitative change in the behavior of the free energy for densities close to ρ_{c1} is shown in Fig. 4.2. As density is further increased, $A_2(\rho, u)$ changes sign continuously from negative to positive at a second critical density ρ_{c2}, such that the free energy has a minimum at $\psi = 0$, corresponding to the HDD phase. The dependence of the free energy on ψ for densities close to ρ_{c2} is similar to that shown in Fig. 4.2. The variation of the order parameter ψ with density ρ is shown in Fig. 4.3 for different values of u. ψ increases continuously from zero at ρ_{c1} and decreases continuously to zero at ρ_{c2}. The average number of intersections between the rods per site, though continuous, also shows non-analytic behavior at ρ_{c1} and ρ_{c2} (see Fig. 4.4). The power series expansion of free energy in Eq. (4.15) has the same form as

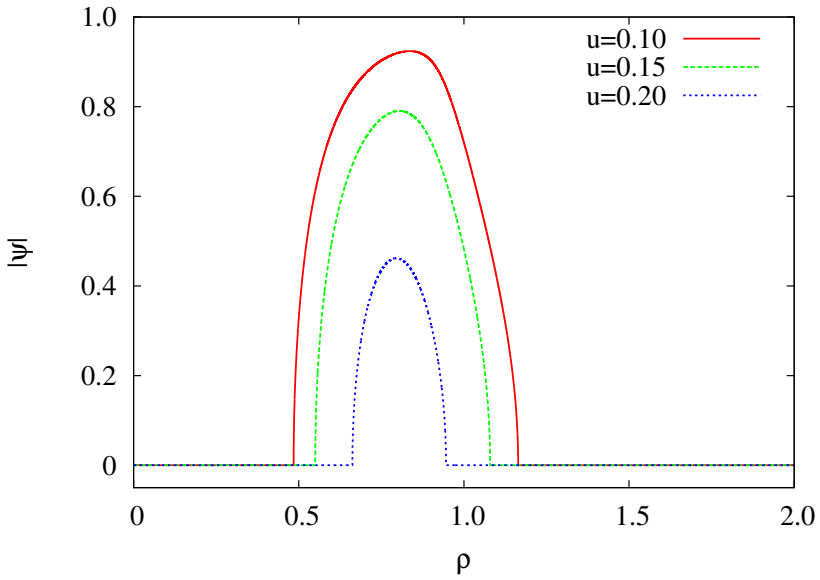

Figure 4.3: Order parameter ψ as a function of density ρ. For low and high densities, $\psi = 0$, while for intermediate densities, $\psi \neq 0$. The data are for $q = 4$ and $k = 6$.

that of a system with scalar order parameter that has two broken symmetry phases. Thus, the two transitions will be in the mean field Ising universality class. The nematic phase does not exist for $k < 4$.

The phase diagram in the ρ–u plane is determined by solving $A_2(\rho, u) = 0$ for ρ and is shown in Fig. 4.5 for different values of k. The difference between the two critical densities decreases with increasing u. Beyond a maximum value $u_c(k)$, there is no phase transition and the system remains disordered at all densities. The critical densities ρ_{c1} and ρ_{c2} may be solved as an expansion in u. For example, when $k = 4$,

$$\rho_{c1} = \frac{2}{k-1} + 2u + 12u^2 + O(u^3), \quad k = 4. \tag{4.16}$$

and

$$\rho_{c2} = 1.13148 - 2.38675u - 12.2726u^2 + O(u^3), \; k = 4. \tag{4.17}$$

It is of interest to determine ρ_{c2} for large k. For the hard rod problem, it was conjectured

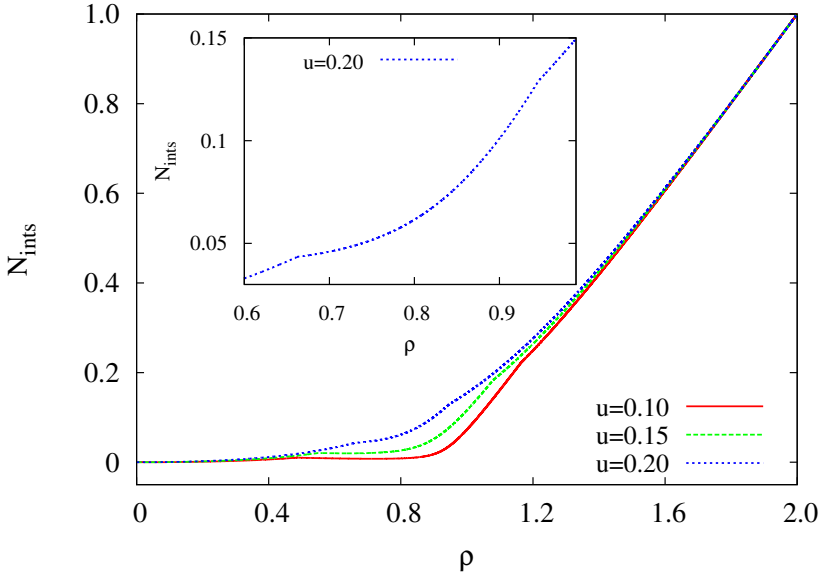

Figure 4.4: Average number of interactions per site, N_{ints}, as a function of density ρ for different values of u. Inset: The region between the two critical points is magnified. The data are for $q = 4$ and $k = 6$.

that $\rho_{c2} \approx 1 - a/k^2$, when $k \to \infty$ [20]. For our model, we find,

$$\begin{aligned} \rho_{c2} &= \frac{-1 + 2k - \sqrt{-3 + 4k}}{-1 + k}, \quad u \to 0, \\ &= 2 - \frac{2}{\sqrt{k}} + \frac{1}{k} - \frac{5}{4k^{3/2}} + \frac{1}{k^2} + O(k^{-5/2}). \end{aligned} \tag{4.18}$$

Thus the leading correction is $O(1/\sqrt{k})$, and not $O(1/k^2)$.

$u_c(k)$, the largest value of u for which the nematic phase exists, is determined by solving the equations $A_2(\rho, u) = 0$ and $dA_2(\rho, u)/d\rho = 0$ simultaneously. $u_c(k)$ increases with k (see Fig. 4.6), and approaches 1 from below as $k \to \infty$. At $u_c(k)$ two mean-field Ising critical lines meet.

4.4 k-mers on RLTL with $q = 6$

The calculation presented in Sec. 4.3 may be extended to the case when the coordination number $q \geq 6$. In this case, we associate a weight u (v) to a site occupied by two (three)

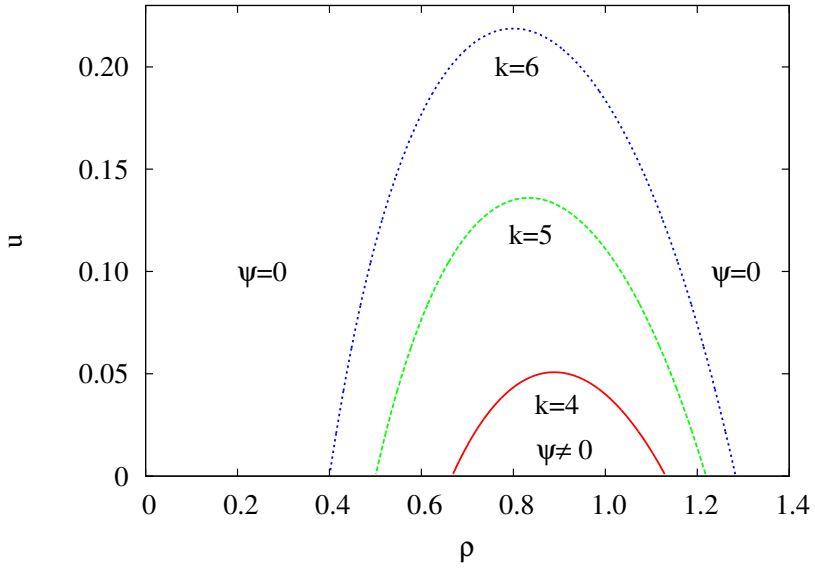

Figure 4.5: Phase diagram when $q = 4$ for different values of k.

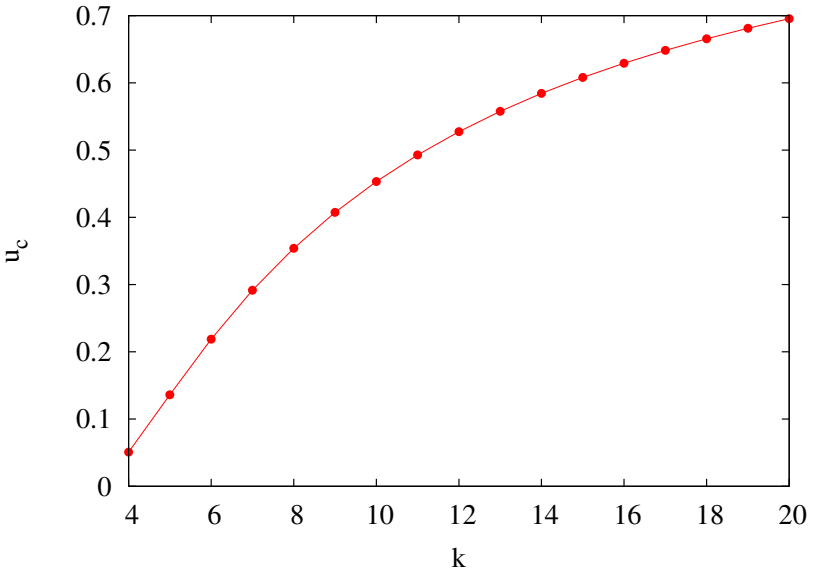

Figure 4.6: u_c, the maximum value of u for which the transitions exists as a function of k. The data are for $q = 4$.

k-mers of different types. The calculation of the free energy now involves many more combinatorial factors than for the case $q = 4$, but is straightforward.

4.4.1 Calculation of free energy

The combinatorial factor C_m for $q = 6$ may be obtained by following the same steps as in the case $q = 4$. For $q = 6$, a site can be occupied by utmost three k-mers of different types. Let Γ_{nl}^{pq} be the total number of intersections at the m-th layer between site n of a k-mer of type p and site l of a k-mer of type q. Γ_{nlm}^{pqr} denotes the total number of sites at the m-th layer shared by site n of a k-mer of type p, site l of a k-mer of type q and site m of a k-mer of type r. Here p, q and r can be x, y or z. n, l and m can be h or b depending on whether the site is the head or part of the body of the k-mer. We omit the layer index m from Γ for notational simplicity. In addition to X_m and Y_m defined in Eq. (4.3), we define

$$Z_m = \sum_{j=1}^{k-1} z_{m-j},$$

as the number of sites at the m-th layer occupied by z-mers that are extended from $(m-1)$-th layer. Let e^{μ_3} be the weight associated with a z-mer. X_m number of x-mers from $(m-1)$-th layer are connected to the X_m sites of m-th layer through X type bonds in

$$\frac{N!}{(N - X_m)!}$$

ways. After connecting the x-mers, we connect y-mers between m-th and $(m-1)$-th layer. Among the Y_m number of y-mers, $\bar{\Gamma}_{bb}^{xy}$ of them are connected to the sites at the m-th layer, which are already occupied by x-mers. Later on, while connecting z-mers, some of the sites among $\bar{\Gamma}_{bb}^{xy}$ sites might be occupied by z mers also. Thus we have $\bar{\Gamma}_{bb}^{xy} = \Gamma_{bb}^{xy} + \Gamma_{bbb}^{xyz} + \Gamma_{hbb}^{zxy}$. Remaining $(Y_m - \bar{\Gamma}_{bb}^{xy})$ sites are connected to the empty sites of the

m-th layer. The number of ways of doing this is

$$\frac{Y_m! X_m!}{\bar{\Gamma}^{xy}_{bb}!(Y_m - \bar{\Gamma}^{xy}_{bb})!(X_m - \bar{\Gamma}^{xy}_{bb})!} \times \frac{(N - X_m)!}{(N - X_m - Y_m + \bar{\Gamma}^{xy}_{bb})!}.$$

Now we connect the z mers. $\bar{\Gamma}^{xz}_{bb}$ and $\bar{\Gamma}^{yz}_{bb}$ number of z-mers from $(m-1)$-th layer are connected with the sites at the m-th layer which are occupied by x-mers and y-mers respectively. Here $\bar{\Gamma}^{xz}_{bb} = \Gamma^{xz}_{bb} + \Gamma^{yxz}_{hbb}$ and similarly, $\bar{\Gamma}^{yz}_{bb} = \Gamma^{yz}_{bb} + \Gamma^{xyz}_{hbb}$. Γ^{xyz}_{bbb} number of z-mers are connected to the sites which are already simultaneously shared by x-mers and y-mers at the m-th layer. Rest of the $(Z_m - \bar{\Gamma}^{xz}_{bb} - \bar{\Gamma}^{yz}_{bb} - \Gamma^{xyz}_{bbb})$ number of z-mers are connected to the remaining empty sites at the m-th layer. The number of ways of connecting them is

$$\begin{aligned}
&\frac{Z_m!}{\bar{\Gamma}^{xz}_{bb}!(Z_m - \bar{\Gamma}^{xz}_{bb})!} \times \frac{(X_m - \bar{\Gamma}^{xy}_{bb})!}{(X_m - \bar{\Gamma}^{xy}_{bb} - \bar{\Gamma}^{xz}_{bb})!} \\
&\frac{(Z_m - \bar{\Gamma}^{xz}_{bb})!}{\bar{\Gamma}^{yz}_{bb}!(Z_m - \bar{\Gamma}^{xz}_{bb} - \bar{\Gamma}^{yz}_{bb})!} \times \frac{(Y_m - \bar{\Gamma}^{xy}_{bb})!}{(Y_m - \bar{\Gamma}^{xy}_{bb} - \bar{\Gamma}^{yz}_{bb})!} \\
\times &\frac{(Z_m - \bar{\Gamma}^{xz}_{bb} - \bar{\Gamma}^{yz}_{bb})!}{\Gamma^{xyz}_{bbb}!(Z_m - \bar{\Gamma}^{xz}_{bb} - \bar{\Gamma}^{yz}_{bb} - \Gamma^{xyz}_{bbb})!} \times \frac{\bar{\Gamma}^{xy}_{bb}!}{(\bar{\Gamma}^{xy}_{bb} - \Gamma^{xyz}_{bbb})!} \\
\times &\frac{(N - X_m - Y_m + \bar{\Gamma}^{xy}_{bb})!}{(N - X_m - Y_m - Z_m + \bar{\Gamma}^{xy}_{bb} + \bar{\Gamma}^{yz}_{bb} + \bar{\Gamma}^{xz}_{bb} + \Gamma^{xyz}_{bbb})!}.
\end{aligned}$$

We can connect $(N - X_m)$, $(N - Y_m)$ and $(N - Z_m)$ free bonds of type X, Y and Z respectively to the empty sites at the m-th layer in

$$(N - X_m)!(N - Y_m)!(N - Z_m)!$$

ways. Now we consider the k-mers, starting from the sites at the m-th layer which are already occupied by the k-mers extended from the previous layer. Number of ways of choosing the heads of the k-mers at the m-th layer from the sites which are already occupied by two different k-mers is given by,

$$\frac{\bar{\Gamma}^{yz}_{bb}!}{\Gamma^{xyz}_{hbb}!(\bar{\Gamma}^{yz}_{bb} - \Gamma^{xyz}_{hbb})!} \times \frac{\bar{\Gamma}^{xz}_{bb}!}{\Gamma^{yxz}_{hbb}!(\bar{\Gamma}^{xz}_{bb} - \Gamma^{yxz}_{hbb})!} \times \frac{(\bar{\Gamma}^{xy}_{bb} - \Gamma^{xyz}_{bbb})!}{\Gamma^{zxy}_{hbb}!(\bar{\Gamma}^{xy}_{bb} - \Gamma^{xyz}_{bbb} - \Gamma^{zxy}_{hbb})!}.$$

Similarly two k-mers may start from the same site. We can choose such pairs of heads at the m-th layer from the sites having single k-mers passing through them in

$$\frac{(Z_m-\bar{\Gamma}^{xz}_{bb}-\bar{\Gamma}^{yz}_{bb}-\Gamma^{xyz}_{bbb})!)}{\Gamma^{xyz}_{hhb}!(Z_m-\bar{\Gamma}^{xz}_{bb}-\bar{\Gamma}^{yz}_{bb}-\Gamma^{xyz}_{bbb}-\Gamma^{xyz}_{hhb})!}\times\frac{(Y_m-\bar{\Gamma}^{xy}_{bb}-\bar{\Gamma}^{yz}_{bb})!}{\Gamma^{xzy}_{hhb}!(Y_m-\bar{\Gamma}^{xy}_{bb}-\bar{\Gamma}^{yz}_{bb}-\Gamma^{xzy}_{hhb})!}\times\frac{(X_m-\bar{\Gamma}^{xy}_{bb}-\bar{\Gamma}^{xz}_{bb})!}{\Gamma^{yzx}_{hhb}!(X_m-\bar{\Gamma}^{xy}_{bb}-\bar{\Gamma}^{xz}_{bb}-\Gamma^{yzx}_{hhb})!}$$

ways. The total number of x-mers, y-mers and z-mers starting from the m-th layer are x_m, y_m and z_m respectively. Number of ways of choosing heads of new k-mers from the sites at the m-th layer that are already occupied by single k-mers is,

$$\begin{aligned}&\frac{(Y_m-\bar{\Gamma}^{xy}_{bb}-\bar{\Gamma}^{yz}_{bb}-\Gamma^{xzy}_{hhb})!}{\Gamma^{xy}_{hb}!(Y_m-\bar{\Gamma}^{xy}_{bb}-\bar{\Gamma}^{yz}_{bb}-\Gamma^{xzy}_{hhb}-\Gamma^{xy}_{hb})!}\times\frac{(Z_m-\bar{\Gamma}^{xz}_{bb}-\bar{\Gamma}^{yz}_{bb}-\Gamma^{xyz}_{hhb}-\Gamma^{xyz}_{bbb})!}{\Gamma^{xz}_{hb}!(Z_m-\bar{\Gamma}^{xz}_{bb}-\bar{\Gamma}^{yz}_{bb}-\Gamma^{xyz}_{hhb}-\Gamma^{xyz}_{bbb}-\Gamma^{xz}_{hb})!}\\
\times&\frac{(X_m-\bar{\Gamma}^{xy}_{bb}-\bar{\Gamma}^{xz}_{bb}-\Gamma^{yzx}_{hhb})!}{\Gamma^{yx}_{hb}!(X_m-\bar{\Gamma}^{xy}_{bb}-\bar{\Gamma}^{xz}_{bb}-\Gamma^{yzx}_{hhb}-\Gamma^{yx}_{hb})!}\times\frac{(Z_m-\bar{\Gamma}^{xz}_{bb}-\bar{\Gamma}^{yz}_{bb}-\Gamma^{xyz}_{hhb}-\Gamma^{xyz}_{bbb}-\Gamma^{xz}_{hb})!}{\Gamma^{yz}_{hb}!(Z_m-\bar{\Gamma}^{xz}_{bb}-\bar{\Gamma}^{yz}_{bb}-\Gamma^{xyz}_{hhb}-\Gamma^{xyz}_{bbb}-\Gamma^{xz}_{hb}-\Gamma^{yz}_{hb})!}\\
\times&\frac{(X_m-\bar{\Gamma}^{xy}_{bb}-\bar{\Gamma}^{xz}_{bb}-\Gamma^{yzx}_{hhb}-\Gamma^{yx}_{hb})!}{\Gamma^{zx}_{hb}!(X_m-\bar{\Gamma}^{xy}_{bb}-\bar{\Gamma}^{xz}_{bb}-\Gamma^{yzx}_{hhb}-\Gamma^{yx}_{hb}-\Gamma^{zx}_{hb})!}\times\frac{(Y_m-\bar{\Gamma}^{xy}_{bb}-\bar{\Gamma}^{yz}_{bb}-\Gamma^{xzy}_{hhb}-\Gamma^{xy}_{hb})!}{\Gamma^{zy}_{hb}!(Y_m-\bar{\Gamma}^{xy}_{bb}-\bar{\Gamma}^{yz}_{bb}-\Gamma^{xzy}_{hhb}-\Gamma^{xy}_{hb}-\Gamma^{zy}_{hb})!}.\end{aligned}$$

There are $(N-X_m-Y_m-Z_m+\bar{\Gamma}^{xy}_{bb}+\bar{\Gamma}^{xz}_{bb}+\bar{\Gamma}^{yz}_{bb}+\Gamma^{xyz}_{bbb})$ unoccupied sites so far at the m-th layer. They can be divided into four groups: sites shared simultaneously by two heads of different types of k-mers, sites occupied by three heads of the k-mers of different types, sites from which single k-mers start, and completely empty sites. Number of ways to arrange them is,

$$\begin{aligned}&\frac{(N-X_m-Y_m-Z_m+\bar{\Gamma}^{xy}_{bb}+\bar{\Gamma}^{xz}_{bb}+\bar{\Gamma}^{yz}_{bb}+\Gamma^{xyz}_{bbb})!}{\Gamma^{xy}_{hh}!\Gamma^{xz}_{hh}!\Gamma^{yz}_{hh}!\Gamma^{xyz}_{hhh}!N_{em}!(x_m-\Gamma^{xy}_{hh}-\Gamma^{xz}_{hh}-\Gamma^{xy}_{hb}-\Gamma^{xz}_{hb}-\Gamma^{xyz}_{hhb}-\Gamma^{xzy}_{hhb}-\Gamma^{xyz}_{hbb}-\Gamma^{xyz}_{hhh})!}\\
\times&\frac{1}{(y_m-\Gamma^{xy}_{hh}-\Gamma^{yz}_{hh}-\Gamma^{yx}_{hb}-\Gamma^{yz}_{hb}-\Gamma^{xyz}_{hhb}-\Gamma^{yzx}_{hhb}-\Gamma^{yxz}_{hbb}-\Gamma^{xyz}_{hhh})!}\\
\times&\frac{1}{(z_m-\Gamma^{yz}_{hh}-\Gamma^{xz}_{hh}-\Gamma^{zx}_{hb}-\Gamma^{zy}_{hb}-\Gamma^{xzy}_{hhb}-\Gamma^{yzx}_{hhb}-\Gamma^{zxy}_{hbb}-\Gamma^{xyz}_{hhh})!},\end{aligned}$$

where,

$$N_{em} = N - X_m - x_m - Y_m - y_m - Z_m - z_m + \frac{1}{2}\sum_{i,j,i\neq j}\left[\Gamma^{ij}_{hh} + \bar{\Gamma}^{ij}_{bb} + 2\Gamma^{ij}_{hb}\right]$$
$$+ \Gamma^{xyz}_{bbb} + 2\left[\Gamma^{xyz}_{hhb} + \Gamma^{xzy}_{hhb} + \Gamma^{yzx}_{hhb} + \Gamma^{xyz}_{hhh}\right] + \Gamma^{xyz}_{hbb} + \Gamma^{yxz}_{hbb} + \Gamma^{zxy}_{hbb}.$$

$[\bar{\Gamma}^{ij}_{bb}]$ and $[\Gamma^{ij}_{hh}]$ are symmetric in i and j, but $[\Gamma^{ij}_{hb}]$ is not. Multiplying all these factors and writing $\bar{\Gamma}$ in terms of Γ we obtain C_m for $q = 6$. Define homogeneous, N-independent variables: $\gamma^{ij}_{nl} = \Gamma^{ij}_{nl}/N$, $\gamma^{ijk}_{nlm} = \Gamma^{ijk}_{nlm}/N$, $\rho_x = x_m k/N$, $\rho_y = y_m k/N$ and $\rho_z = z_m k/N$. ρ_x, ρ_y and ρ_z are the fraction of sites occupied by x-mers, y-mers and z-mers respectively.

We define,

$$F = \rho_x - \frac{\rho_x}{k} - \gamma^{xy}_{bb} - \gamma^{xz}_{bb} - \gamma^{yx}_{hb} - \gamma^{zx}_{hb} - \gamma^{zxy}_{hbb} - \gamma^{yxz}_{hbb} - \gamma^{yzx}_{hhb} - \gamma^{xyz}_{bbb},$$
$$G = \rho_y - \frac{\rho_y}{k} - \gamma^{xy}_{bb} - \gamma^{yz}_{bb} - \gamma^{xy}_{hb} - \gamma^{zy}_{hb} - \gamma^{zxy}_{hbb} - \gamma^{xyz}_{hbb} - \gamma^{xzy}_{hhb} - \gamma^{xyz}_{bbb},$$
$$W = \rho_z - \frac{\rho_z}{k} - \gamma^{xz}_{bb} - \gamma^{yz}_{bb} - \gamma^{xz}_{hb} - \gamma^{yz}_{hb} - \gamma^{yxz}_{hbb} - \gamma^{xyz}_{hbb} - \gamma^{xyz}_{hhb} - \gamma^{xyz}_{bbb},$$
$$f = \frac{\rho_x}{k} - \gamma^{xy}_{hh} - \gamma^{xz}_{hh} - \gamma^{xy}_{hb} - \gamma^{xz}_{hb} - \gamma^{xyz}_{hbb} - \gamma^{xyz}_{hhb} - \gamma^{xzy}_{hhb} - \gamma^{xyz}_{hhh},$$
$$g = \frac{\rho_y}{k} - \gamma^{xy}_{hh} - \gamma^{yz}_{hh} - \gamma^{yx}_{hb} - \gamma^{yz}_{hb} - \gamma^{yxz}_{hbb} - \gamma^{xyz}_{hhb} - \gamma^{yzx}_{hhb} - \gamma^{xyz}_{hhh},$$
$$w = \frac{\rho_z}{k} - \gamma^{xz}_{hh} - \gamma^{yz}_{hh} - \gamma^{zy}_{hb} - \gamma^{zx}_{hb} - \gamma^{zxy}_{hbb} - \gamma^{xzy}_{hhb} - \gamma^{yzx}_{hhb} - \gamma^{xyz}_{hhh},$$
$$D = 1 - \rho + \frac{1}{2}\sum_{i\neq j}\left[\gamma^{ij}_{bb} + \gamma^{ij}_{hh} + 2\gamma^{ij}_{hb}\right] + 2\left[\gamma^{xyz}_{bbb} + \gamma^{xyz}_{hhh} + \gamma^{xyz}_{hbb} + \gamma^{yxz}_{hbb}\right.$$
$$\left. + \gamma^{zxy}_{hbb} + \gamma^{xyz}_{hhb} + \gamma^{xzy}_{hhb} + \gamma^{yzx}_{hhb}\right].$$

γ's satisfy the following equations, obtained by the maximizing the summand of the par-

tition function with respect to the interaction parameters {Γ}:

$$\frac{FG}{\gamma_{bb}^{xy}D}=\frac{1}{u},\frac{GW}{\gamma_{bb}^{yz}D}=\frac{1}{u},\frac{FW}{\gamma_{bb}^{xz}D}=\frac{1}{u},$$
$$\frac{fg}{\gamma_{hh}^{xy}D}=\frac{1}{u},\frac{gw}{\gamma_{hh}^{yz}D}=\frac{1}{u},\frac{fw}{\gamma_{hh}^{xz}D}=\frac{1}{u},$$
$$\frac{fG}{\gamma_{hb}^{xy}D}=\frac{1}{u},\frac{gF}{\gamma_{hb}^{yx}D}=\frac{1}{u},\frac{gW}{\gamma_{hb}^{yz}D}=\frac{1}{u},$$
$$\frac{wG}{\gamma_{hb}^{zy}D}=\frac{1}{u},\frac{fW}{\gamma_{hb}^{xz}D}=\frac{1}{u},\frac{wF}{\gamma_{hb}^{zx}D}=\frac{1}{u},$$
$$\frac{fgw}{\gamma_{hhh}^{xyz}D^2}=\frac{1}{v},\frac{FGW}{\gamma_{bbb}^{xyz}D^2}=\frac{1}{v},\frac{fgW}{\gamma_{hhb}^{xyz}D^2}=\frac{1}{v},\frac{fwG}{\gamma_{hhb}^{xzy}D^2}=\frac{1}{v},$$
$$\frac{gwF}{\gamma_{hhb}^{yzx}D^2}=\frac{1}{v},\frac{wFG}{\gamma_{hbb}^{zxy}D^2}=\frac{1}{v},\frac{gFW}{\gamma_{hbb}^{yxz}D^2}=\frac{1}{v},\frac{fGW}{\gamma_{hbb}^{xyz}D^2}=\frac{1}{v}.$$

Simplifying the above equations we obtain $\gamma_{bb}^{ij}=(k-1)^2\gamma_{hh}^{ij}$, $\gamma_{hb}^{ij}=\gamma_{hb}^{ji}=(k-1)\gamma_{hh}^{ij}$, $\gamma_{bbb}^{ijk}=(k-1)^3\gamma_{hhh}^{ijk}$, $\gamma_{hbb}^{ijk}=(k-1)^2\gamma_{hhh}^{ijk}$ and $\gamma_{hhb}^{ijk}=(k-1)\gamma_{hhh}^{ijk}$. F, G, W, f, g, w, D are simplified using the above relations. Using these relations and setting $\rho_y=\rho_z$ and hence $\gamma_{hh}^{xy}=\gamma_{hh}^{xz}$, we reduce the number of independent equations for $\{\gamma\}$, given by,

$$fg=\frac{D\gamma_{hh}^{xy}}{u}, \tag{4.19}$$
$$gw=\frac{D\gamma_{hh}^{yz}}{u}, \tag{4.20}$$
$$fgw=\frac{\gamma_{hhh}^{xyz}D^2}{v}. \tag{4.21}$$

We solve these three simultaneous equations to estimate the free energy. Maximizing the summand of the partition function with respect to x_l, y_l and z_l for $q=6$ and we obtain,

$$\frac{\left[\rho_x-\frac{\rho_x}{k}\right]^{k-1}\left[1-\rho+k^2(\gamma_{hh}^{xy}+\gamma_{hh}^{xz}+\gamma_{hh}^{yz})+2k^3\gamma_{hhh}^{xyz}\right]^k e^{\mu_1}}{\left[1-\rho_x+\frac{\rho_x}{k}\right]^{k-1}[k-1]^{k-1}\left[\frac{\rho_x}{k}-k\gamma_{hh}^{xy}-k\gamma_{hh}^{xz}-k^2\gamma_{hhh}^{xyz}\right]^k}=1, \tag{4.22}$$
$$\frac{\left[\rho_y-\frac{\rho_y}{k}\right]^{k-1}\left[1-\rho+k^2(\gamma_{hh}^{xy}+\gamma_{hh}^{xz}+\gamma_{hh}^{yz})+2k^3\gamma_{hhh}^{xyz}\right]^k e^{\mu_2}}{\left[1-\rho_y+\frac{\rho_y}{k}\right]^{k-1}[k-1]^{k-1}\left[\frac{\rho_y}{k}-k\gamma_{hh}^{xy}-k\gamma_{hh}^{yz}-k^2\gamma_{hhh}^{xyz}\right]^k}=1, \tag{4.23}$$
$$\frac{\left[\rho_z-\frac{\rho_z}{k}\right]^{k-1}\left[1-\rho+k^2(\gamma_{hh}^{xy}+\gamma_{hh}^{xz}+\gamma_{hh}^{yz})+2k^3\gamma_{hhh}^{xyz}\right]^k e^{\mu_3}}{\left[1-\rho_z+\frac{\rho_z}{k}\right]^{k-1}[k-1]^{k-1}\left[\frac{\rho_z}{k}-k\gamma_{hh}^{xz}-k\gamma_{hh}^{yz}-k^2\gamma_{hhh}^{xyz}\right]^k}=1. \tag{4.24}$$

The expression of free energy for $q = 6$, in terms of uniform, N-independent variables for a fixed u and v is given by,

$$\begin{aligned} f(\rho_x, \rho_y, \rho_z, u) &= -\frac{k-1}{k}\sum_{i=1}^{q/2}\rho_i \ln\rho_i - \sum_{i=1}^{q/2}\left[1-\frac{(k-1)\rho_i}{k}\right]\ln\left[1-\frac{(k-1)\rho_i}{k}\right] \\ &+ \sum_{i=1}^{q/2}\left[\rho_i - k^2\sum_{j=1,j\neq i}\gamma_{hh}^{ij} - k^3\gamma_{hhh}\right]\ln\left[\rho_i - k^2\sum_{j=1,j\neq i}^{q/2}\gamma_{hh}^{ij} - k^3\gamma_{hhh}\right] \\ &+ \left[1-\rho+\frac{k^2}{2}\sum_{i,j=1,i\neq j}^{q/2}\gamma_{hh}^{ij} + 2k^3\gamma_{hhh}\right] \\ &\ln\left[1-\rho+\frac{k^2}{2}\sum_{i,j=1,i\neq j}^{q/2}\gamma_{hh}^{ij} + 2k^3\gamma_{hhh}\right] \\ &-\frac{\rho}{k}\ln k + \frac{k^2}{2}\sum_{i,j,i\neq j}^{q/2}\gamma_{hh}^{ij}\ln\left(\frac{k^2\gamma_{hh}^{ij}}{u}\right) + k^3\gamma_{hhh}\ln\left(\frac{k^3\gamma_{hhh}}{v}\right). \end{aligned} \tag{4.25}$$

For notational simplicity we have dropped the upper indices of γ_{hhh}^{123}.

We define the order parameter to be $\psi = (\rho_x - \rho_y)/\rho$, where we set $\rho_y = \rho_z$. We find that for $u < u_c(k)$ and $v < u$, the system undergoes two transitions as for the case $q = 4$, at critical densities ρ_{c1} and ρ_{c2}. The three dimensional ρ–u–v phase diagram may be visualized by studying the phase diagram along three different lines in the u–v plane: $v = u^2$, $v = u^3$ and $v = u^4$. The free energy, expressed as a power series in ψ, now has the form

$$\begin{aligned} f(\rho_x, \rho_y, u, v) &= A_0(\rho, u, v) + A_2(\rho, u, v)\psi^2 \\ &+ A_3(\rho, u, v)\psi^3 + A_4(\rho, u, v)\psi^4 + \ldots, \end{aligned} \tag{4.26}$$

where $A_4(\rho, u, v) > 0$ and $A_3(\rho, u, v)$ is in general nonzero. At low densities, $A_2(\rho, u, v)$ is positive and the free energy has a global minimum at $\psi = 0$. With increasing density it develops a second local minimum at $\psi \neq 0$. At ρ_{c1} the two minima become degenerate, and for $\rho_{c1} < \rho < \rho_{c2}$, the free energy has a minimum at $\psi \neq 0$, corresponding to the nematic phase. A typical example is shown in Fig. 4.7. The order parameter thus shows a discontinuity at ρ_{c1} and the transition is first order. In all the cases we have studied, we

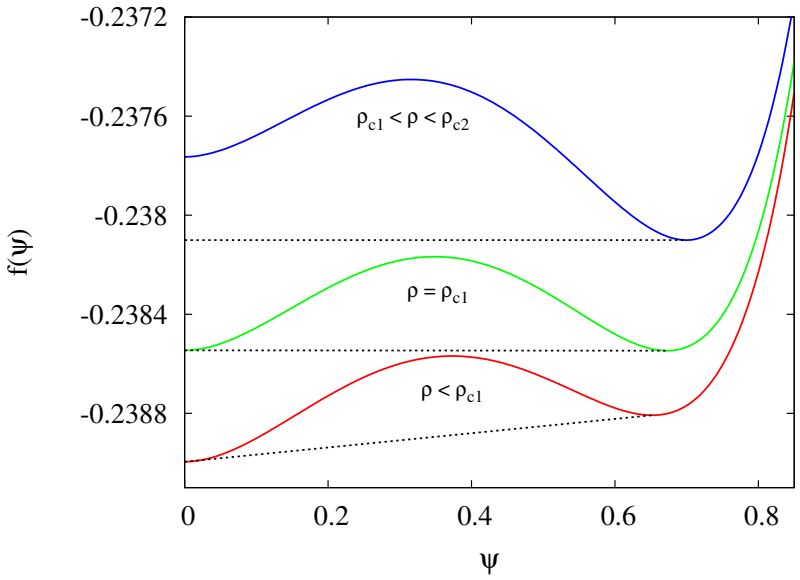

Figure 4.7: Free energy $f(\psi)$ as a function of the order parameter ψ for $\rho \approx \rho_{c1}$ when $q = 6$. The data are for $k = 6$, $v = u^2$ and $u = 0.15$. The dotted lines denote the convex envelopes.

find that the first transition from disordered to nematic phase is discontinuous.

On the other hand, the nature of the second transition from the nematic to HDD phase depends on the value of k, u and v. When $v = u^2$, the second transition is first order for all k. However, when $v = u^3$, the second transition could be first order or continuous. We find that for $k < 7$, the second transition is always first order while for $k \geq 7$, the order of transition depends on u. In Fig. 4.8, we show the variation of the order parameter ψ with density ρ for different values of u for fixed $k = 7$. The second transition is continuous for small values of u and first order for larger values of u. For the transitions that are first order, the system shows coexistence near the transition point. In the coexistence region, the system no longer has uniform density, instead has regions of the ordered and disordered phases. The order parameter for these densities are obtained from the Maxwell construction. In Fig. 4.8, the coexistence regions are marked with thick lines. Qualitatively similar behavior is seen for $k > 7$. The second transition is continuous for $u \leq u^*(k)$ and first order for $u > u^*(k)$. The value of $u^*(k)$ increases with k. When $v = u^4$, the phenomenology is qualitatively similar to that for the case $v = u^3$.

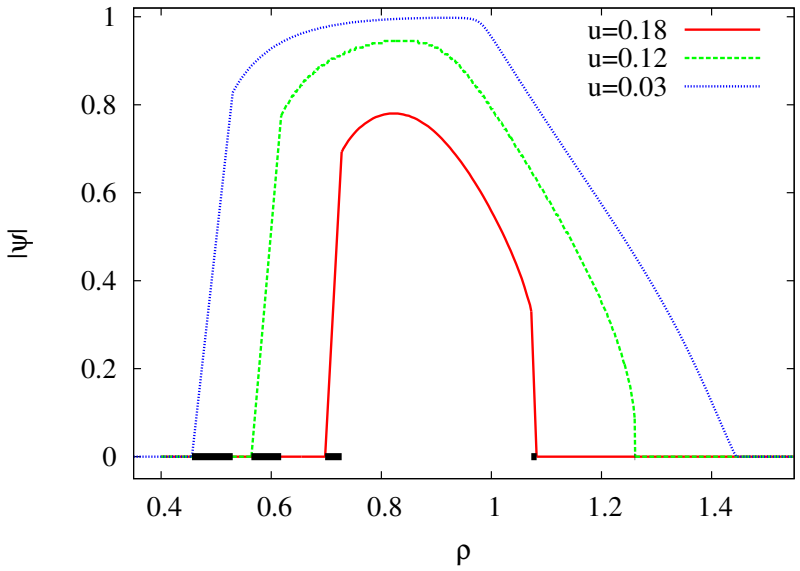

Figure 4.8: Order parameter ψ as a function of density ρ for different values of u for $k = 7$, $q = 6$, and $v = u^3$. The second transition is first order for $u > u^*(k)$ and continuous for $u \leq u^*(k)$. Here, $u^*(7) \approx 0.09563$. Regions shown by the thick lines denote coexistence region.

The first order or continuous nature of the second transition is also reflected in the average number of intersections. In Fig. 4.9, we show the variation for the number of intersections per site with density for $k = 7$ for two values of u: one corresponding to a first order and the other to continuous transition. In addition to ψ, the average number of intersections between rods per site also shows a discontinuity when the transition is first order. This discontinuity vanishes when the transition becomes continuous.

These observations are summarized in the ρ–u phase diagram for $k = 7$ shown in Fig. 4.10. Shaded portions denote the coexistence regions in the $\rho - u$ plane. For $v = u^3$ and $v = u^4$, a second order line terminates at a tricritical point beyond which the transition becomes first order.

The exponents describing the continuous transitions may be found from the Landau-type free energy, Eq. (4.26). At the first transition $A_2(\rho, u, v) > 0$ and $A_3(\rho, u, v) < 0$. At the spinodal point $A_2(\rho, u, v)$ changes sign to negative. As density is further increased $A_2(\rho, u, v)$ changes sign back to positive. When this occurs, $A_3(\rho, u, v)$ could be positive

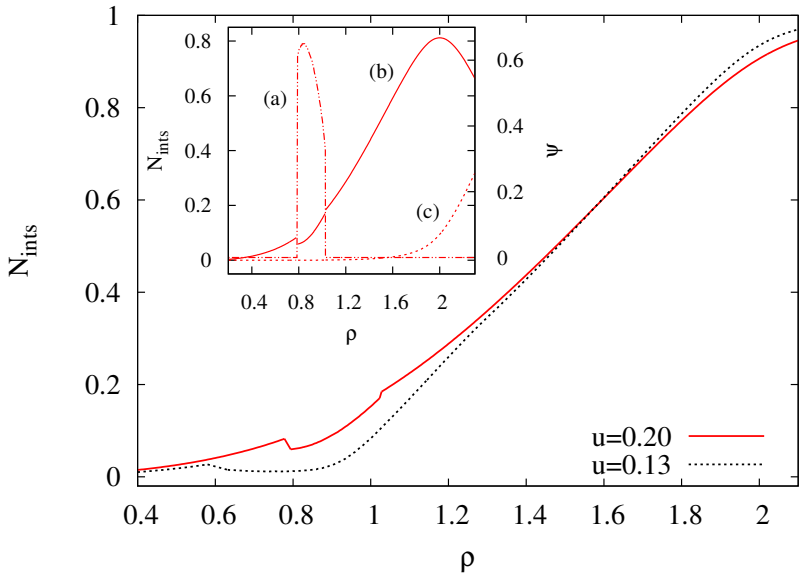

Figure 4.9: The number of interactions per site, N_{ints}, as a function of density ρ for two different values of u. The data are for $q = 6$, $k = 7$, and $v = u^4$. Inset: The variation with density of (a) order parameter ψ, (b) fraction of sites occupied by two k-mers, and (c) fraction of sites occupied by three k-mers. Here, $u = 0.20$.

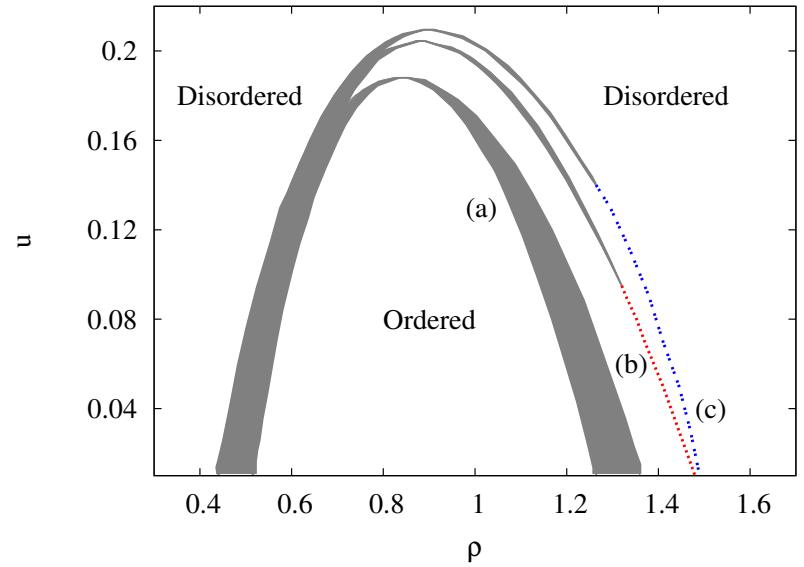

Figure 4.10: Phase diagram for $q = 6$ and $k = 7$ for (a) $v = u^2$, (b) $v = u^3$, and (c) $v = u^4$. Shaded portions denote coexistence regions. Dotted lines denote continuous transitions.

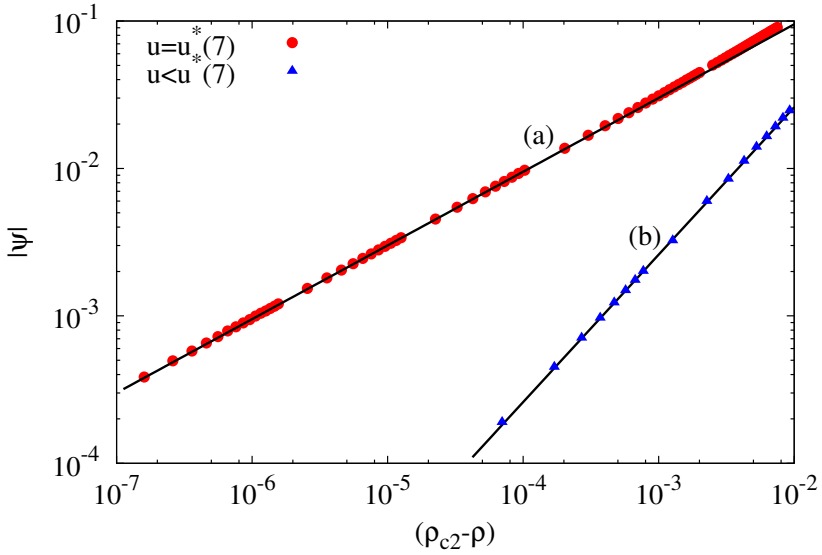

Figure 4.11: The order parameter ψ as the density ρ approaches the critical density ρ_{c2} for $u < u^*$ and at the tricritical point $u = u^*$ when $k = 7$, $q = 6$ and $v = u^3$. The solid lines are power laws (a) $(\rho_{c2} - \rho)^{1/2}$ and (b) $(\rho_{c2} - \rho)$.

or negative. If positive, then the transition will be continuous. Now the critical exponents are determined from a Landau free energy functional of the form $A_2\psi^2 + A_3\psi^3$, and hence the critical exponent $\beta = 1$, where $\psi \sim (\rho_{c2} - \rho)^\beta$ as ρ approaches ρ_{c2} from below. At the tricritical point $A_3(\rho, u, v) = 0$, and the transition is in the mean field Ising universality class with $\beta = 1/2$ (see Fig. 4.11).

4.5 Summary and discussion

In this chapter, we studied the problem of monodispersed rigid rods on the RLTL, a Bethe-like lattice where rods of different orientations are allowed to intersect with weight $u, v, \ldots$ depending on whether a site is occupied by two, three, ... k-mers. We showed that the system undergoes two phase transitions with increasing density for $k \geq k_{min}$ and appropriate choice of interaction parameters. For coordination number $q = 4$, the two transitions are continuous and in the mean field Ising universality class. For $q = 6$, while the first transition is first order, the nature of the second transition depends on the values k, u and

v, giving rise to a rich phase diagram. To the best of our knowledge, it is the only solvable model on interacting rods that shows two phase transitions.

The limit $u \to 0$ is different from $u = 0$ (the hard rod problem). When $u = 0$, the second transition in absent [26]. When $u, v > 0$, the fully packed phase is disordered by construction and if the first phase transition exists, so does a second phase transition. The relaxation of the restriction that only rods of different orientations may intersect at a lattice site does not change the qualitative behavior of the system as the high-density phase remains disordered. There are still two transitions, both in the mean field Ising universality class (when $q = 4$). However, the solution becomes more cumbersome.

Similarly, when $q = 6$, the limit $v \to 0$ is different from $v = 0$ when $u > 0$. When $v = 0$, a lattice site may occupied by utmost two k-mers of different type. In this case, the fully packed phase is not necessarily disordered and for certain values of k and u, only one transition is present with increasing density.

For hard rods on the square lattice, Monte Carlo simulations were unable to give a clear answer to the question whether the HDD and LDD phases are qualitatively similar or not. It was argued that the HDD phase on the square lattice has a large crossover length scale $\xi^* \sim 1400$, and for length scales larger than ξ^*, it is possible that the HDD phase is not qualitatively different from the LDD phase. This was based on the evidence that vacancies in the HDD phase do not form a bound state. In this chapter, by expanding the phase diagram from a one-dimensional ρ phase diagram to a multi-dimensional ρ–interaction parameters phase diagram, we showed that it is always possible to continuously transform the LDD phase into the HDD phase without crossing any phase boundary. This means that the LDD and HDD phases are qualitatively similar, at least for the model on RLTL. It would thus be worthwhile to simulate the hard rods problem on the square lattice for system sizes larger than 1400 and verify the same.

For the RLTL with coordination number $q = 4$, we showed that for large k, $\rho_{c2} \approx 2 - a/\sqrt{k} + O(k^{-1})$. This is at variance from the prediction from entropy based arguments for

the hard rod problem that ρ_{c2} approaches 1 as k^{-2} [20]. It would be interesting to resolve this discrepancy.

Chapter 5

Hard rectangles with integer aspect ratio on the square lattice

5.1 Introduction

In this chapter, we consider the system of hard rectangles of size $m \times mk$ ($m > 1$) on a two-dimensional square lattice where each rectangle occupies m (mk) lattice sites along the short (long) axis. Here, we restrict our study to the case when k is integer. The aim of this chapter would be to investigate the phase diagram of the hard rectangle system for general m and k using numerical simulations.

The model and the Monte carlo algorithm is described in Sec. 5.2. We observe four distinct phases at different densities: isotropic, nematic, columnar, and sublattice phases. These phases, suitable order parameters to characterize them, and other thermodynamic quantities are defined in Sec. 5.3. From extensive large scale simulations, we determine the rich phase diagram for $m = 2, 3$, and $k = 1, \ldots, 7$. The phase diagram for $m = 2$ is discussed in Sec. 5.4. We find that all transitions except the isotropic–columnar transition for $k = 6$ are continuous. The critical exponents and universality classes of the continuous

transitions are determined. Section 5.5 contains the details about the phase diagram and the nature of the phase transitions for $m = 3$. Section 5.6 contains a summary and a discussion of the results. The content of this chapter is published in Ref. [119].

5.2 Model and Monte carlo Algorithm

We consider a system of monodispersed hard rectangles of size $m \times mk$ on a square lattice of $L \times L$ sites with periodic boundary conditions. A rectangle can be either horizontal or vertical. A horizontal (vertical) rectangle occupies mk sites along the x (y)-axis and m sites along the y (x)-axis. No two rectangles may overlap. An activity $z = e^{\mu}$ is associated with each rectangle, where μ is the chemical potential. Here we consider the case when the aspect ratio k is integer.

The Monte carlo algorithm to study the hard rectangle system is described in Sec. 2.4.2.

5.3 Different phases

Snapshots of the different phases that we observe in simulations are shown in Fig. 5.1. First is the low-density isotropic (I) phase in which the rectangles have neither orientational nor translational order [see Fig. 5.1(c)]. Second is the nematic (N) phase in which the rectangles have orientational order but no translational order [see Fig. 5.1(d)] . In this phase, the mean number of horizontal rectangles is different from that of vertical rectangles. The third phase is the columnar (C) phase, having orientational order and partial translational order [see Fig. 5.1(e)]. In this phase, if majority of rectangles are horizontal (vertical), then their heads, or bottom-left corners, preferably lie in rows (columns) that are separated by m. Thus, it breaks the translational symmetry in the direction perpendicular to the orientation but not parallel to the orientation. Clearly, there are $2m$ symmetric C phases. In this phase the rectangles can slide much more along one lattice direction.

The fourth phase is the crystalline sublattice (S) phase with no orientational order [see Fig. 5.1(f)]. We divide the square lattice into m^2 sublattices by assigning to a site (i, j) a label $(i \mod m) + m \times (j \mod m)$. The sublattice labeling for the case $m = 2$ is shown in Fig. 5.1(a). In the S phase, the heads of the rectangles preferably occupy one sublattice, breaking translational symmetry in both the lattice directions.

From the symmetry of the system we would expect up to 7 phases. The orientational symmetry could be present or broken while the translational symmetry could be unbroken, broken along only one or both x- and y- directions. If the orientational symmetry is broken, then the translational symmetry could be broken either parallel or perpendicular to the preferred orientation. Out of the 7 possibilities, we do not observe (i) a phase with no orientational order but partial translational order, (ii) a phase with orientational order and complete translational order (iii) a smectic like phase in which orientational order is present and translational symmetry parallel to the orientation is broken.

To distinguish among the four different phases we define the following order parameter variables:

$$q_1 = n_h - n_v, \tag{5.1a}$$

$$q_2 = |\sum_{j=0}^{m^2-1} n_j e^{\frac{2\pi i j}{m^2}}|, \tag{5.1b}$$

$$q_3 = |\sum_{j=0}^{m-1} n_{r_j} e^{\frac{2\pi i j}{m}}| - |\sum_{j=0}^{m-1} n_{c_j} e^{\frac{2\pi i j}{m}}|, \tag{5.1c}$$

$$q_4 = n_0 - n_1 - n_2 + n_3, \tag{5.1d}$$

where n_h and n_v are the fraction of sites occupied by the horizontal and vertical rectangles respectively, n_i is the fraction of sites occupied by the rectangles whose heads are in i-th sublattice, where $i = 0, \ldots, m^2 - 1$. n_{r_j} is the fraction of sites occupied by the rectangles whose heads are in row $(j \mod m)$, and n_{c_j} is the fraction of sites occupied by the rectangles whose heads are in column $(j \mod m)$. The corresponding averaged order parameters are given by, $Q_i = \langle |q_i| \rangle$, where $i = 1$ to 4. All four order parameters

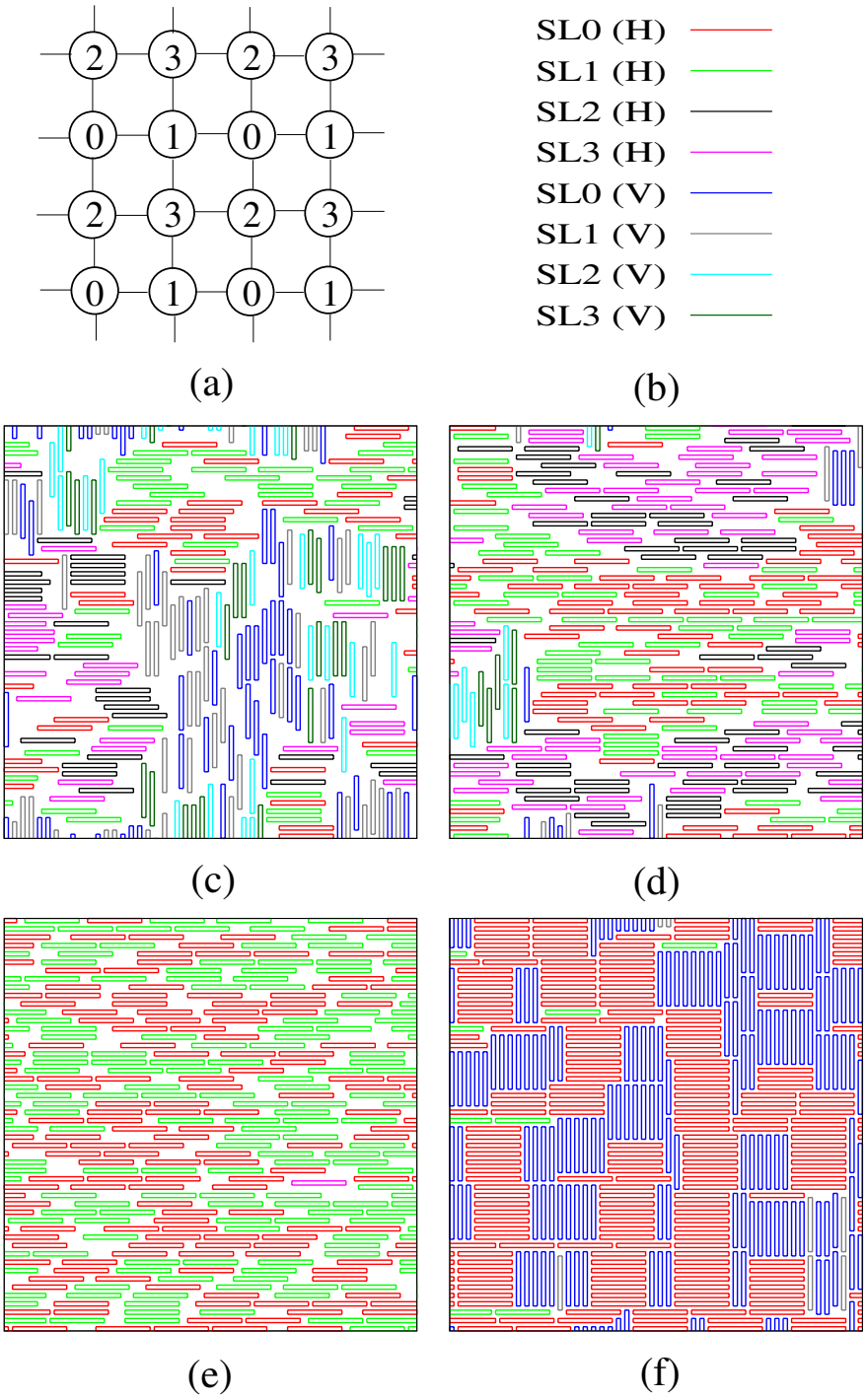

Figure 5.1: Snapshots of different phases (at different densities) in a system of 2×14 hard rectangles. (a) The four sub lattices when $m = 2$. (b) The color scheme: eight colors corresponding to two orientations, horizontal (H) and vertical (V), and heads of rectangles being on one of the four sublattices, denoted by SL0 to SL3. (c) The isotropic phase where all 8 colors are present. (d) The nematic phase, dominated by 4 colors corresponding to 4 sublattices and one orientation. (e) The columnar phase, dominated by 2 colors corresponding to two sublattices and one orientation. (f) The sublattice phase, dominated by 2 colors corresponding to one sublattice and 2 orientations.

are zero in the I phase. Q_1 is nonzero in the N and C phases, Q_2 is nonzero in the C and S phases, Q_3 is nonzero only in the C phase, and Q_4 is nonzero only in the S phase. Q_4 in Eq. (5.1d) has been defined for $m = 2$. Its generalization to $m \geq 3$ is straightforward. Density $\rho = n_h + n_v$ is the fraction of occupied sites.

We now define the thermodynamic quantities that are useful to characterize the transitions between the different phases. q_i's second moment χ_i, compressibility κ and the Binder cumulant U_i are defined as

$$\chi_i = \langle q_i^2 \rangle L^2, \tag{5.2a}$$

$$\kappa = [\langle \rho^2 \rangle - \langle \rho \rangle^2] L^2, \tag{5.2b}$$

$$U_i = 1 - \frac{\langle q_i^4 \rangle}{3 \langle q_i^2 \rangle^2}. \tag{5.2c}$$

Scaling properties of the thermodynamic quantities and the definition of the critical exponents may be found in Eq. (3.7).

5.4 Phase diagram and critical behavior for $m = 2$

In this section, we discuss the phase diagram for the case $m = 2$ and aspect ratio $k = 1, 2, \ldots 7$. The critical exponents characterizing the different continuous transitions are determined numerically.

5.4.1 Phase diagram

The phase diagram obtained from simulations for $m = 2$ and integer k are shown in Fig. 5.2. The low-density phase is an I phase for all k. The case $k = 1$ is different from other k values. For $k = 1$, the problem reduces to a hard square problem and orientational order is not possible as there is no distinction between horizontal and vertical squares.

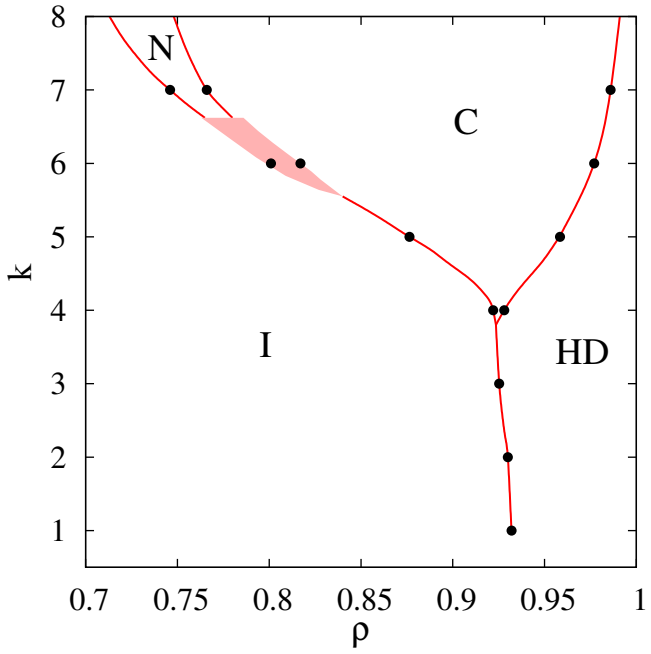

Figure 5.2: Phase diagram for rectangles of size $2 \times 2k$. I, N, C and HD denote isotropic, nematic, columnar and high-density phases respectively. The HD phase is a C phase for $k = 1$ and a S phase for $k > 1$. The data points are from simulation, while the continuous lines and shaded portions are guides to the eye. The shaded portion denotes regions of phase coexistence.

The hard square system undergoes only one continuous transition from the I phase to a C phase (having $2m$ or 4-fold degeneracy) with increasing density [99, 68, 70, 75]. Using symmetry, it can be argued that there are two types of interfacial surface tensions in this high density phase [30]. Hence, this transition belongs to the Ashkin-Teller universality class ($\beta/\nu = 7/4$ and $\gamma/\nu = 7/4$, see Refs. [80, 100, 74, 30] for recent numerical studies). For $k = 2, 3$, we find that the system undergoes one continuous transition directly from the I phase to a crystalline S phase. On the other hand, the system with $k = 4, 5, 6$ may exist in I, C, or S phases. With increasing density, the system undergoes two phase transitions: first from the I to a C phase which could be continuous or first order, and second, from the C to a S phase which is continuous. For $k = 7$, we observe three continuous transitions with increasing density: first from the I to the N phase, second into the C phase and third into the S phase. By confirming the existence of the N and C phases for $k = 8$, we expect the phase behavior for $k \geq 8$ to be similar to that for $k = 7$.

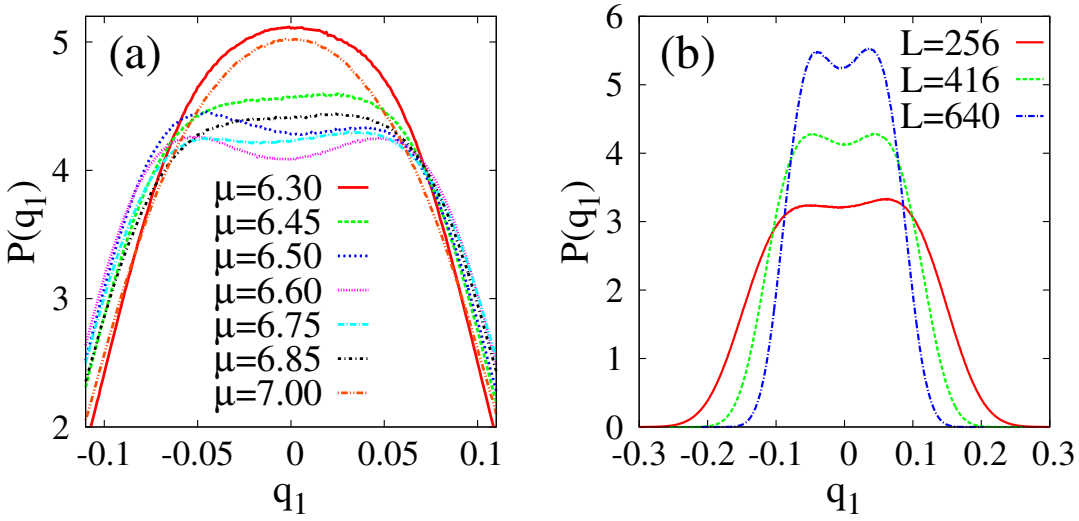

Figure 5.3: (a) The probability distribution of the order parameter q_1 for $k = 4$ at different μ values, when $L = 416$. (b) The same for different system sizes when $\mu = 6.55$.

The system undergoes more than one transition only for $k \geq k_c = 4$. We now present some supporting evidence for this claim. In Fig. 5.3 (a) we show the probability distribution of the nematic order parameter q_1, when $k = 4$, for different values of μ and fixed L, close to the I-C and the C-S transitions. For lower values of μ, the distribution is peaked around zero corresponding to the I phase. With increasing μ, the distribution becomes flat and two symmetric maxima appear at $q_1 \neq 0$ (q_3 also becomes nonzero simultaneously), corresponding to a C phase. On increasing μ further, the two maxima continuously merge into a single peak at q_1=0, corresponding to the S phase (q_3 also becomes zero and q_4 becomes nonzero). Fig. 5.3 (b) shows the distribution of q_1 for three different system sizes at a fixed value of μ for which $P(q_1)$ has two symmetric maxima at $q_1 \neq 0$. The two peaks become sharper and narrower with increasing L. We find the similar behavior for $P(q_3)$ also. From the above, we conclude that the C phase exists for $k = 4$ albeit for a very narrow range of μ. For $k = 2$ and 3 we do not observe the existence of a columnar phase and find that the probability distributions of q_1 and q_3 are peaked around zero for all μ values. Hence, we conclude that $k_c = 4$.

The N phase exists only for $k \geq 7$. This is also true for $m = 1$ [20]. To see this, notice that the I-C transition for $k = 6$ is first order (see Fig. 5.2). If a nematic phase exists for

$k = 6$, then the first transition would have been continuous and in the Ising universality class [25].

5.4.2 Critical behavior of the isotropic–sublattice (I-S) phase transition

The system of rectangles with $m = 2$ undergoes a direct I-S transition for $k = 2, 3$. At this transition, the translational symmetry gets broken along both x- and y- directions but the orientational symmetry remains preserved. We study this transition using the order parameter Q_2. Q_2 is nonzero in the S phase and zero in the I phase. In this case Q_1 and Q_3 remains zero for all values of μ. The data collapse of U_2, Q_2, and χ_2 for different values of L near the I-S transition are shown in Fig. 5.4 for $k = 2$ and in Fig. 5.5 for $k = 3$. From the crossing of the Binder cumulant data for different L, we estimate the critical chemical potential $\mu_c^{I-S} \approx 5.33$ ($\rho_c^{I-S} \approx 0.930$) for $k = 2$ and $\mu_c^{I-S} \approx 6.04$ ($\rho_c^{I-S} \approx 0.925$) for $k = 3$. The order parameter increases continuously with μ from zero as μ_c^{I-S} is crossed, making the transition continuous. The S phase has a four-fold symmetry due to the four possible sublattices. From symmetry, one can see that there are two types of interfacial surface tensions: $\sigma_{12} = \sigma_{03}$ and $\sigma_{01} = \sigma_{02} = \sigma_{23} = \sigma_{13}$), where σ_{ij} is the surface tension between the phases where majority of the rectangles have their heads on the i-th and j-th sublattices respectively. These symmetries are similar to that of the Ashkin-Teller model with 4 states and two types of surface tension energies. Thus, we expect the transition to be in the Ashkin-Teller universality class. Indeed, we find a good collapse when $\beta/\nu = 0.125 \pm 0.015$ and $\gamma/\nu = 1.75 \pm 0.03$.

Numerically, we find $\nu = 1.18 \pm 0.06$ for $k = 2$ and $\nu = 1.23 \pm 0.07$ for $k = 3$. ν being larger than 1, we do not observe any divergence in κ. This transition could have also been studied using the order parameter Q_4.

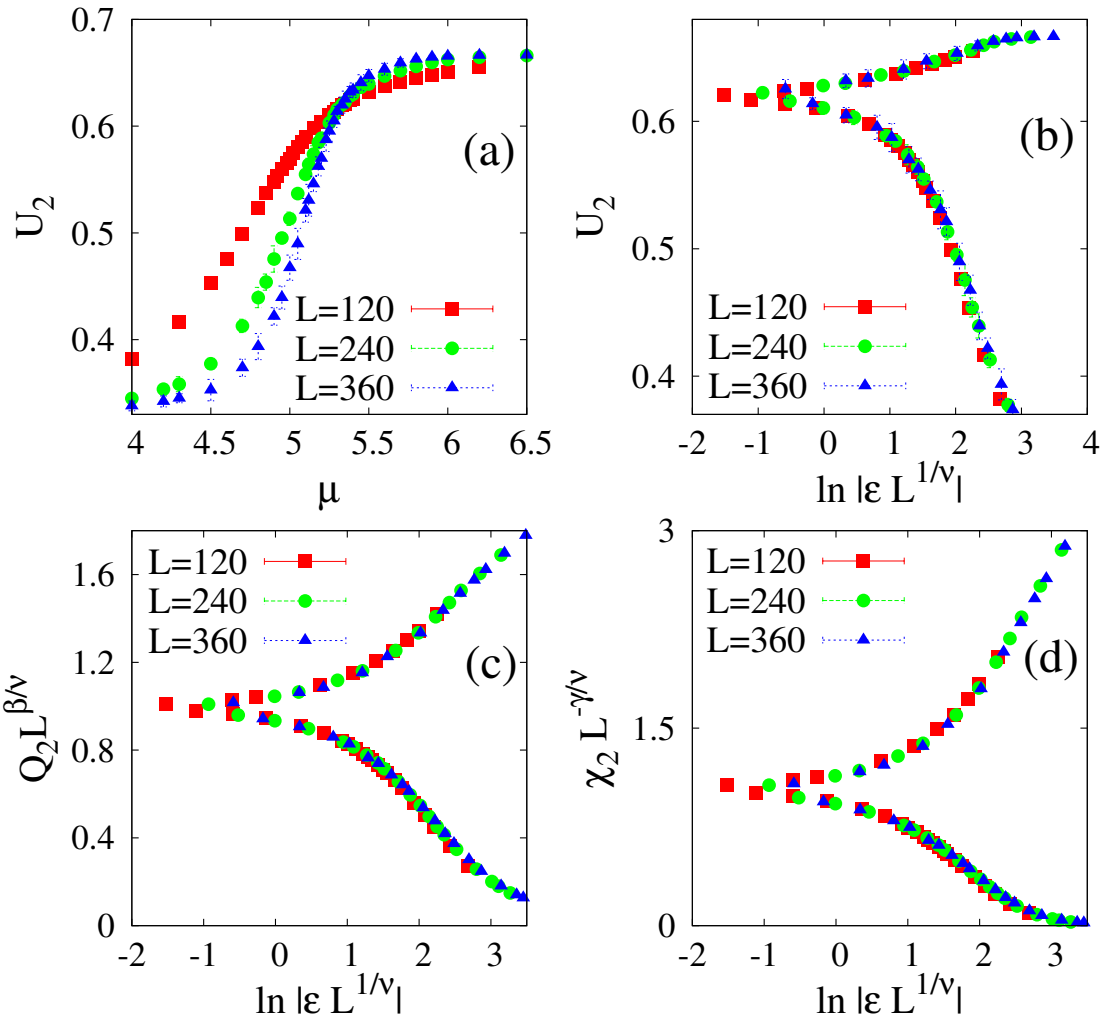

Figure 5.4: Data collapse for different L near the I-S transition for rectangles of size 2×4 ($m = 2$, $k = 2$), where $\epsilon = (\mu - \mu_c^{I-S})/\mu_c^{I-S}$. We find $\mu_c^{I-S} \approx 5.33$ ($\rho_c^{I-S} \approx 0.93$). The exponents are $\beta/\nu = 1/8$, $\gamma/\nu = 7/4$ and $\nu \approx 1.18$.

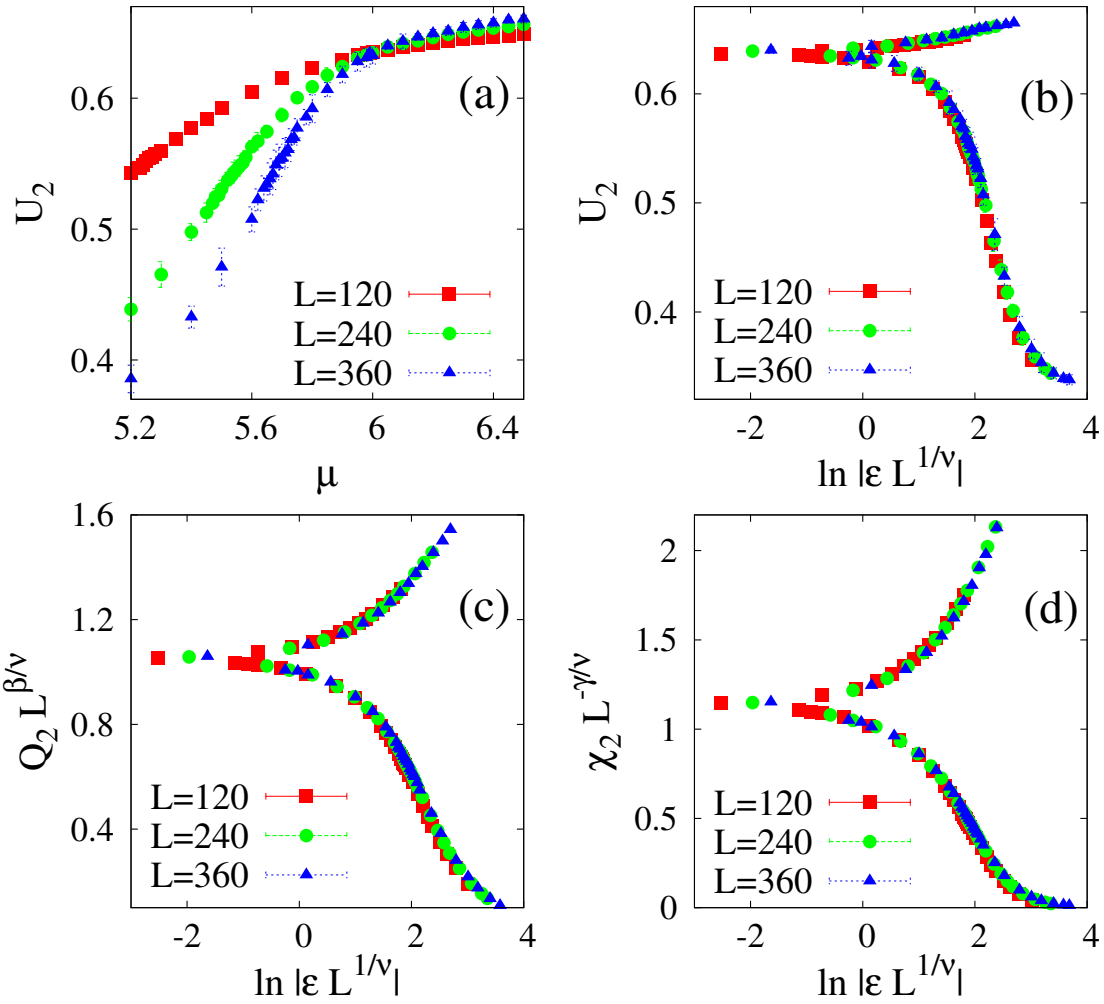

Figure 5.5: Data collapse for different L near the I-S transition for rectangles of size 2×6 ($m = 2$, $k = 3$). We find $\mu_c^{I-S} \approx 6.04$ ($\rho_c^{I-S} \approx 0.925$). The exponents are $\beta/\nu = 1/8$, $\gamma/\nu = 7/4$ and $\nu \approx 1.23$

.

5.4.3 Critical behavior of the isotropic–columnar phase (I-C) transition

The I-C transition is seen for $k = 4, 5, 6$. When $k = 4$, the C phase exists for a very narrow range of μ, making $k = 4$ unsuitable for studying the critical behavior. We, therefore, study the I-C transition for $k = 5$ (2×10 rectangles) and $k = 6$ (2×12 rectangles).

The critical behavior is best studied using the order parameter Q_3. Q_3 is nonzero only in the C phase. First, we present the critical behavior for $k = 5$. The simulation data for different system sizes are shown in Fig. 5.6. From the crossing of the Binder cumulant curves, we obtain $\mu_c^{I-C} \approx 4.98$ ($\rho_c^{I-C} \approx 0.876$). The transition is found to be continuous. There are four possible columnar states: majority of heads are either on even (r_e) or odd (r_o) rows (when horizontal orientation is preferred), or on even (c_e) or odd (c_o) columns (when vertical orientation is preferred). Again, due to this four fold symmetry and two types of surface tensions ($\sigma_{r_e r_o} = \sigma_{c_e c_o}$ and $\sigma_{r_e c_e} = \sigma_{r_e c_o} = \sigma_{r_o c_e} = \sigma_{r_o c_o}$), we expect the I-C transition to be in the Ashkin-Teller universality class. The data for different L collapse with $\beta/\nu = 0.125 \pm 0.015$, $\gamma/\nu = 1.75 \pm 0.03$ and $\nu = 0.82 \pm 0.06$ (see Fig. 5.6), confirming the same. Unlike the I-S transition for $k = 2, 3$, $\nu < 1$ and lies between the Ising and q=4 Potts points. At the I-C transition partial breaking of translational symmetry and complete breaking of rotational symmetry occur simultaneously.

The I-C transition for $k = 4$ is also continuous [see Fig. 5.3 (a)], and is therefore expected to be in the Ashkin-Teller universality class. However, there is no reason to expect that ν will be the same as that for $k = 5$.

For $k = 6$, the I-C transition is surprisingly first order. Fig. 5.7(a) shows the time profile of density near the I-C transition. At the transition point, ρ alternates between two well defined densities, one corresponding to the I phase and the other to the C phase. This is also seen in the probability distribution for density $P(\rho)$ [see Fig. 5.7(b)]. Near the I-C transition, it shows two peaks of $P(\rho)$ corresponding to the I and the C phases. Thus,

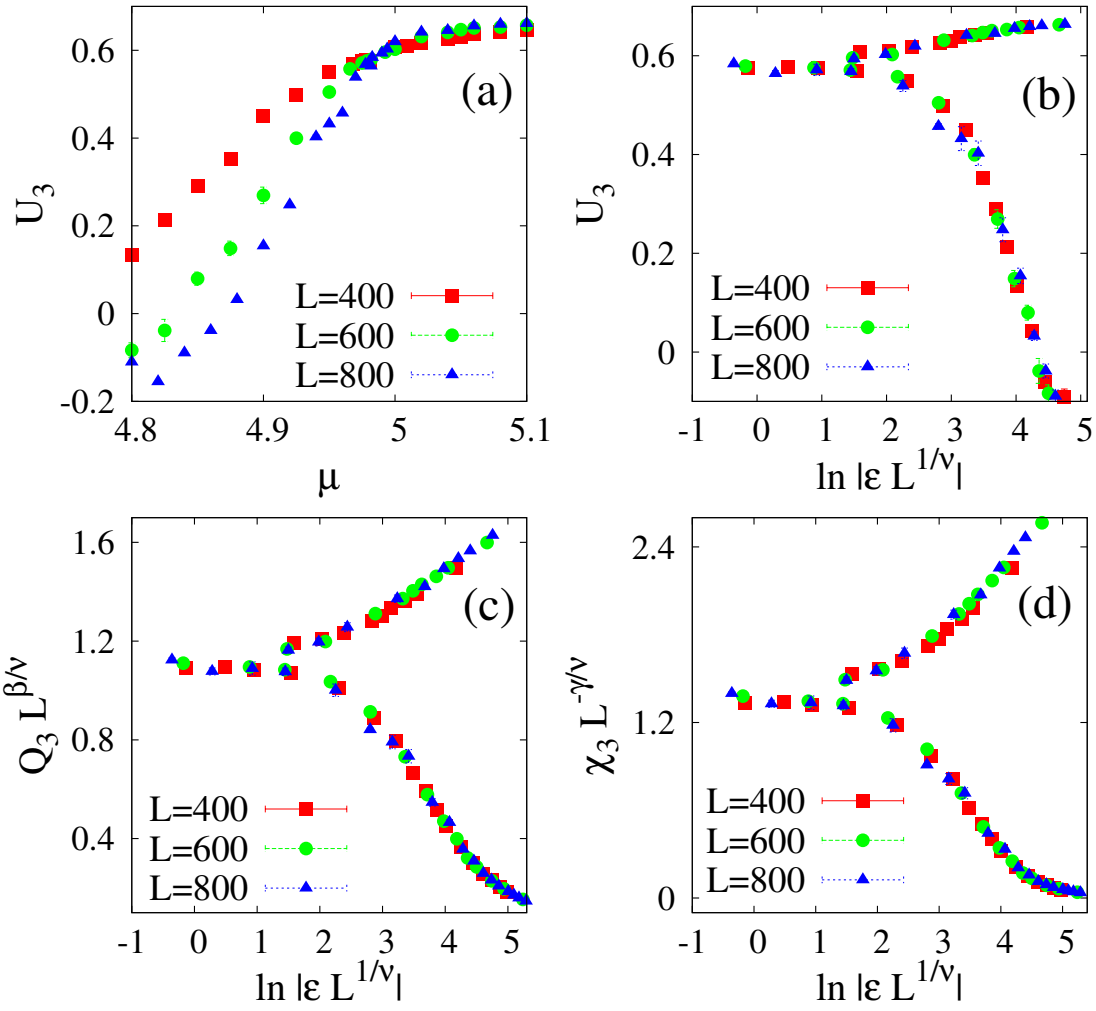

Figure 5.6: The data for different L near the I-C transition collapse when scaled with exponents $\beta/\nu = 1/8$, $\gamma/\nu = 7/4$, and $\nu = 0.82$. We find $\mu_c^{I-C} \approx 4.98$ ($\rho_c^{I-C} \approx 0.876$). Data are for rectangles of size 2×10.

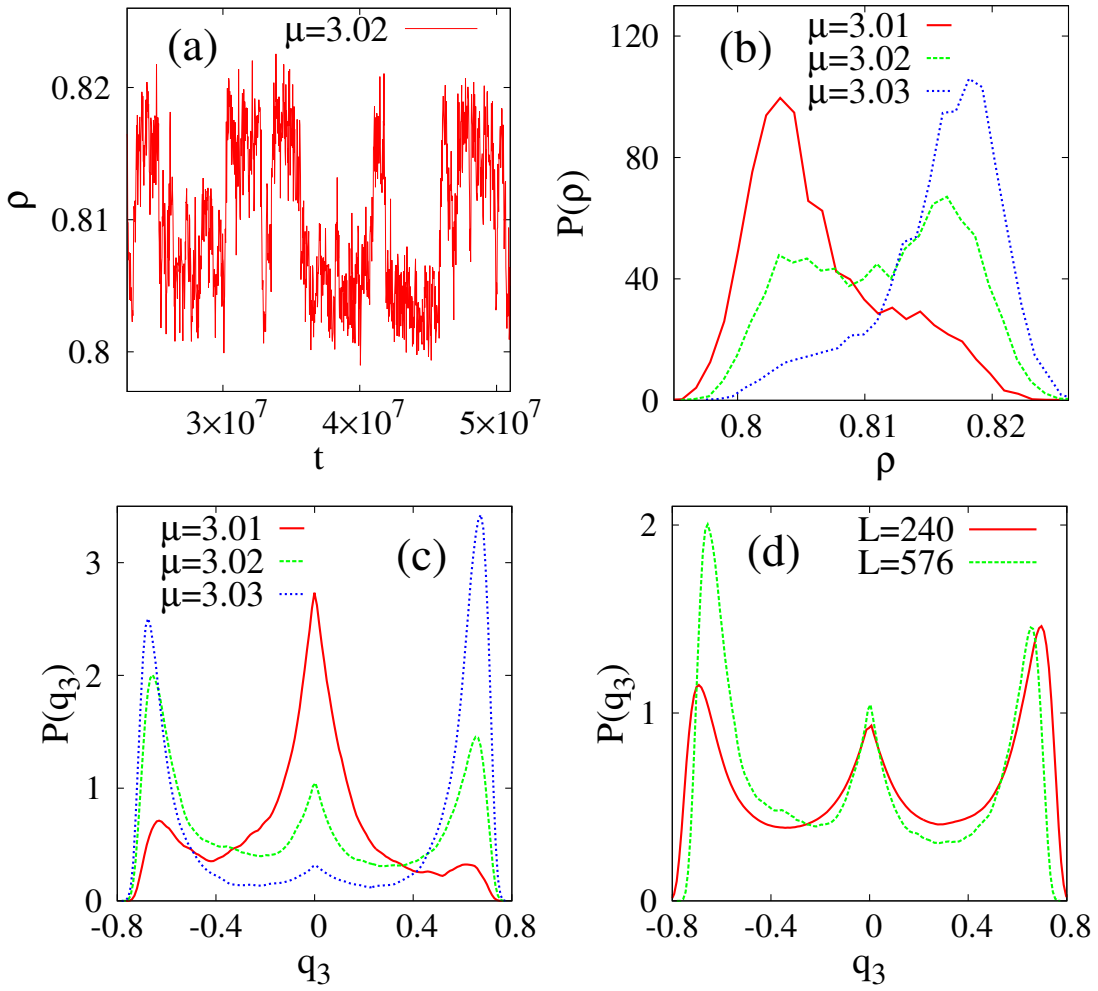

Figure 5.7: Data for the density ρ and the order parameter q_3 for rectangles of size 2×12. (a) Equilibrium time profile of ρ near the I-C transition, for $\mu = 3.02$ and $L = 720$. Probability distribution, near the I-C transition, of (b) ρ for different values of μ when $L = 576$, (c) q_3 for different values of μ when $L = 576$, and (d) q_3 for $L = 240$ ($\mu = 2.99$) and $L = 576$ ($\mu = 3.02$).

at $\mu = \mu_c^{I-C}$, the density has a discontinuity, which is shown by the shaded region in the phase diagram (see Fig. 5.2). The probability distribution of the order parameter q_3 shows similar behavior [see Fig. 5.7(c)]. Near $\mu = \mu_c^{I-C}$ the distribution shows three peaks: one at $q_3 = 0$ corresponding to the I phase and the other two at $q_3 \neq 0$, corresponding to the C phase. These peaks sharpen with increasing system size [see Fig. 5.7(d)]. At μ_c^{I-C}, the order parameter q_3 jumps from zero to a nonzero value. These are typical signatures of a first order transition. Hence, we conclude that the I-C transition may be continuous or first order depending on k.

5.4.4 Critical behavior of the isotropic–nematic phase (I-N) transition

We find that the nematic phase exists only for $k \geq 7$. We study the I-N phase transition for $k = 7$ using the order parameter Q_1. Q_1 is nonzero in the N and C phases and zero in the I phase. We confirm that the ordered phase is an N phase by checking that Q_3, which is nonzero only in the C phase, is zero. In the nematic phase, the rectangles may choose either horizontal or vertical orientation. Thus, we expect the transition to be in the Ising universality class. When $m = 1$, this has been verified using extensive Monte Carlo simulations [25]. Here, we confirm the same for $m = 2$. The data for U_1, Q_1 and χ_1 for different L collapse onto one curve when scaled with the two-dimensional Ising exponents $\beta/\nu = 1/8$, $\gamma/\nu = 7/4$, and $\nu = 1$ (see Fig. 5.8). We find $\mu_c^{I-N} \approx 1.77$ ($\rho_c^{I-N} \approx 0.746$). We note that the value of U_1 at the point where the curves for different L cross is slightly smaller than the Ising value 0.61. This suggests that larger system sizes are necessary for better collapse of the data.

5.4.5 Critical behavior of the nematic–columnar phase (N-C) transition

The N-C transition is also studied for $k = 7$, using the order parameter Q_3. Q_3 is zero in the nematic phase but nonzero in the columnar phase. At the I-N transition orientational symmetry gets broken. If the nematic phase consists of mostly horizontal (vertical) rectangles, then there is no preference over even and odd rows (columns). In the columnar phase, the system chooses either even or odd rows (columns), once the orientational symmetry is broken. Due to the two broken symmetry phases we expect this transition to be in the Ising universality class. We indeed find good data collapse when U_3, Q_3 and χ_3 for different system sizes are scaled with Ising exponents (see Fig. 5.9). The critical chemical potential or critical density is obtained from the crossing point of the binder cumulant U_3

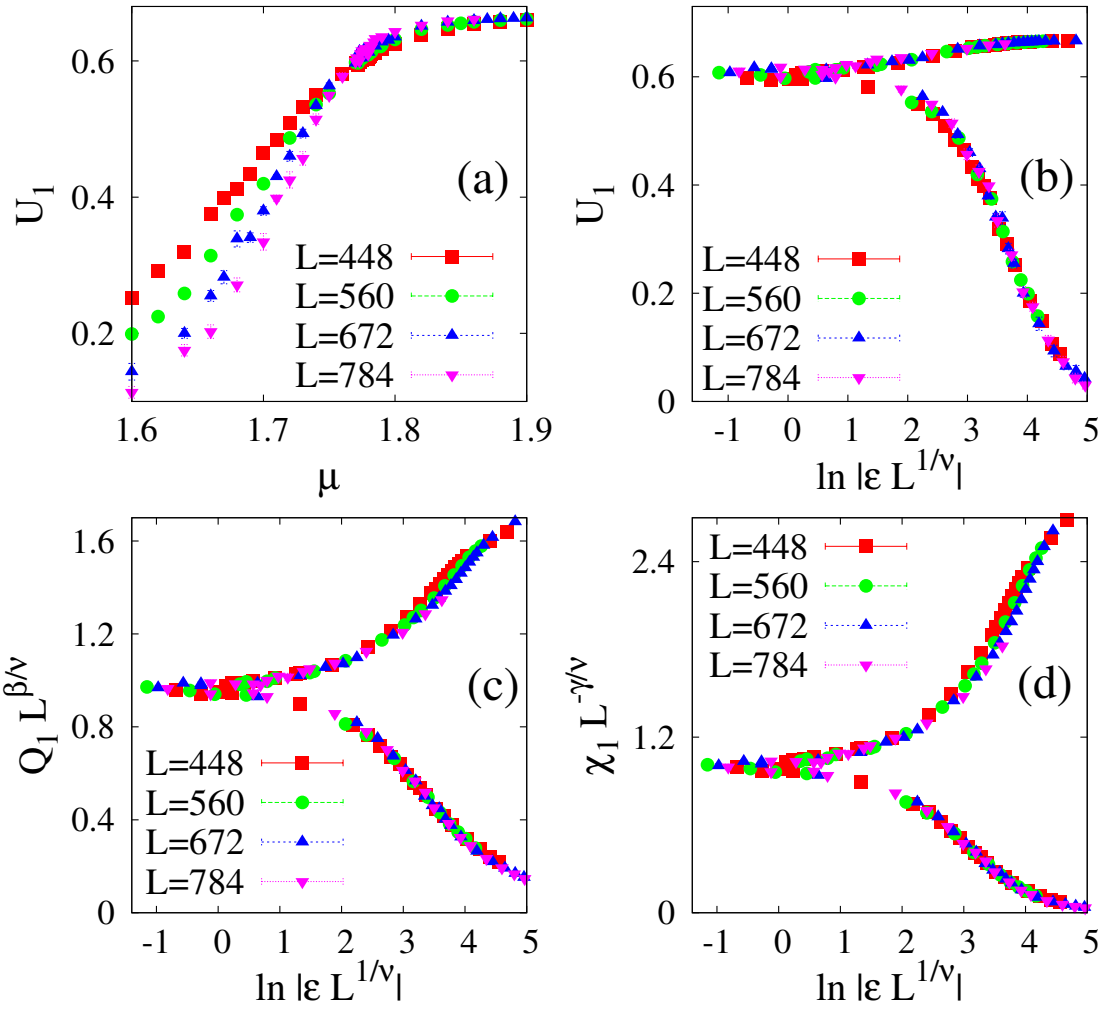

Figure 5.8: The data for different L near the I-N transition collapse when scaled with the Ising exponents $\beta/\nu = 1/8$, $\gamma/\nu = 7/4$, $\nu = 1$ and $\mu_c^{I-N} \approx 1.77$. The critical density $\rho_c^{I-N} \approx 0.746$. Data are for rectangles of size 2×14.

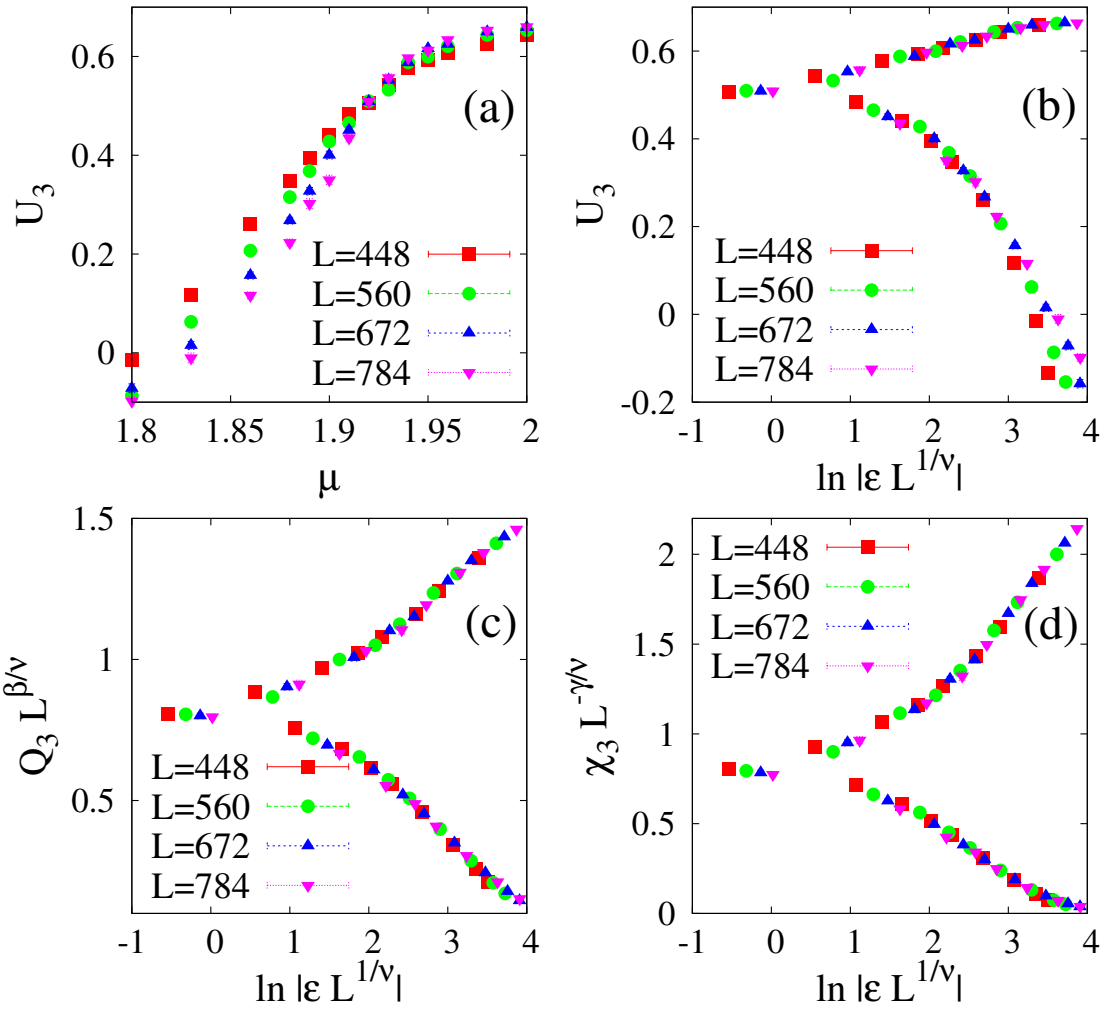

Figure 5.9: The data for different L near the N-C transition collapse when scaled with the Ising exponents $\beta/\nu = 1/8$, $\gamma/\nu = 7/4$, $\nu = 1$ and $\mu_c^{N-C} \approx 1.92$. The critical density $\rho_c^{N-C} \approx 0.766$. Data are for rectangles of size 2×14.

for different L. We find $\mu_c^{N-C} \approx 1.92$ ($\rho_c^{N-C} \approx 0.766$) for this transition. We expect the critical behavior to be same for $k > 7$.

5.4.6 Critical behavior of the columnar–sublattice phase (C-S) transition

The C-S transition exists for $k \geq 4$. This transitions is studied by choosing $k = 5$. We characterize the C-S transition using the order parameter Q_4 which is non zero only in the S phase. In the C phase, the system chooses one particular orientation and either even or

odd rows or columns, depending on the orientation. This corresponds to two sublattices being chosen among four of them. In the C-S transition the translational symmetry gets broken completely by choosing one particular sublattice, but along with that the orientational symmetry gets restored. This transition is found to be continuous. The data of U_4, Q_4 and χ_4 for different L near the C-S transition collapse well when scaled with the exponents belonging to the Ashkin-Teller universality class. The estimated critical exponents are $\beta/\nu = 1/8$, $\gamma/\nu = 7/4$ and $\nu = 0.83 \pm 0.06$ (see Fig. 5.10). Binder cumulants for different system sizes cross at $\mu_c^{C-S} \approx 9.65$ ($\rho_c^{C-S} \approx 0.958$). We expect similar behavior for $k = 4$ and 6 but possibly with different ν. The C-S transition occurs at very high density. With increasing k, the relaxation time becomes increasingly large, making it difficult to obtain reliable data for the C-S transition when $k \geq 6$.

5.5 Phase diagram and critical behavior for $m = 3$

5.5.1 Phase diagram

The phase diagram that we obtain for $m = 3$, is shown in Fig. 5.11. When $k = 1$, the corresponding hard square system has a single, first order transition from the I phase into the C phase [80]. The shaded region between two points denotes a region of phase coexistence. For $2 \leq k \leq 6$, the system undergoes two first order transitions with increasing density: first an I-C transition and second a C-S transition. This is unlike the case $m = 2$, where for $k = 2$ and 3 we find only one transition. For $k = 7$, we find three transitions as in the $m = 2$ case. The first transition from I to N phase is continuous while the second from N to C phase appears to be first order. Although we cannot obtain reliable data for the third transition into the S phase, we expect it to be first order. We note that the minimum value of k beyond which the nematic phase exists is 7 for both $m = 2$ and $m = 3$, and matches with that for $m = 1$ [20].

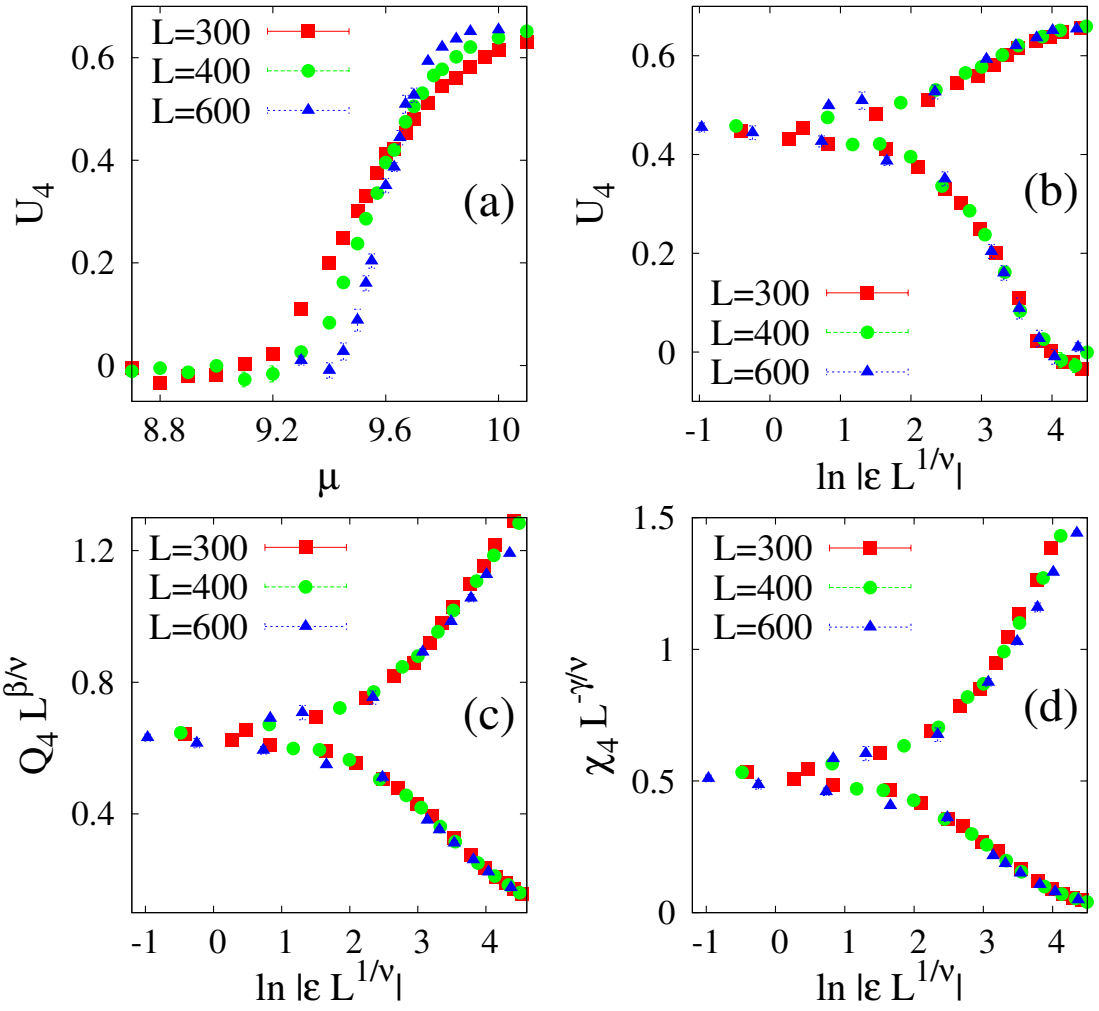

Figure 5.10: The data for different L near the C-S transition collapse when scaled with exponents $\beta/\nu = 1/8$, $\gamma/\nu = 7/4$, $\nu = 0.83$ and $\mu_c^{C-S} \approx 9.65$. The critical density $\rho_c^{C-S} \approx 0.958$. Data are for rectangles of size 2×10.

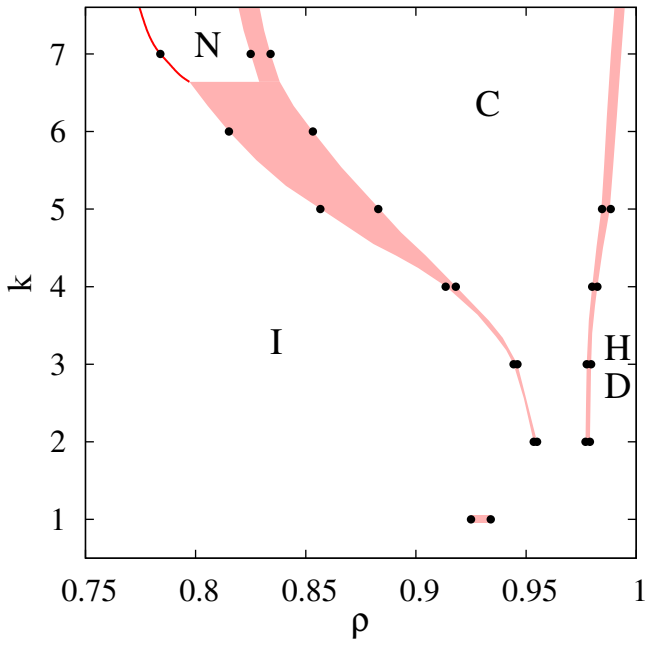

Figure 5.11: Phase diagram for rectangles of size $3 \times 3k$. HD denotes high density. The HD phase is a C phase for $k = 1$ and a S phase for $k > 1$. The data points are from simulation while the continuous line and shaded portions are a guide to the eye. The shaded portions denote regions of phase coexistence. Except the I-N transition, all the transitions are found to be first order.

5.5.2 Isotropic–columnar phase (I-C) transition

The I-C transition exists when $k \leq 6$. We study the this transition for $k = 6$, using the order parameter q_3. Now there are six possible choices for the C phase: heads are predominantly in one of the rows 0, 1 or 2 (mod 3) with all the columns equally occupied (if horizontal orientation is preferred) or in one of the columns $0, 1$ or 2 (mod 3) and all the rows are equally occupied (if vertical orientation is preferred). In this case, there are two types of surface tensions between the different ordered phase ($\sigma_{r_0r_1} = \sigma_{r_0r_2} = \sigma_{r_1r_2} = \sigma_{c_0c_1} = \sigma_{c_0c_2} = \sigma_{c_1c_2}$, and $\sigma_{r_0c_0} = \sigma_{r_0c_1} = \sigma_{r_0c_2} = \sigma_{r_1c_0} = \sigma_{r_1c_1} = \sigma_{r_1c_2} = \sigma_{r_2c_0} = \sigma_{r_2c_1} = \sigma_{r_2c_2}$). Hence, from symmetry, we can make an analogy with a spin model possessing $\mathbb{Z}_6$ symmetry and two types of surface tension energies. In this case, the nature of the transition may depend on the relative values of the surface tensions. The probability distribution of the density ρ and the order parameter $|q_3|$ for $k = 6$ near the I-C transition is shown in Fig. 5.12. The distributions are clearly double peaked at and near the transition

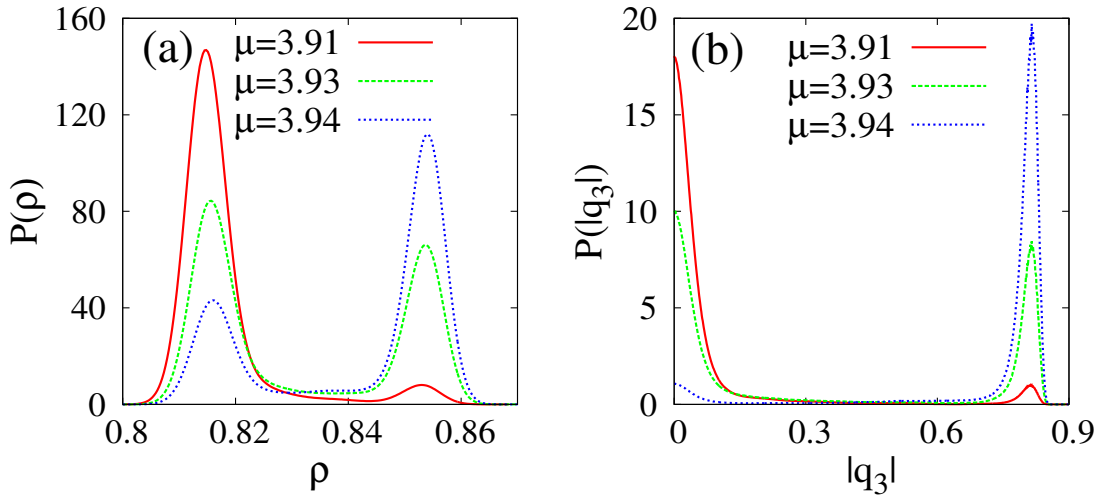

Figure 5.12: Distribution of (a) the density ρ, (b) the order parameter $|q_3|$ near the I-C transition. The data are for rectangles of size 3×18 and $L = 432$.

point, one corresponding to the I phase and the other to the C phase. We find that these peaks become sharper with increasing system size. This is suggestive of a first order phase transition with a discontinuity in both density and order parameter as μ crosses μ_c^{I-C}. The discontinuity in the density is denoted by the shaded regions of Fig. 5.11. The chemical potential at which the I-C transition occurs is given by, $\mu_c^{I-C} \approx 3.93$. Similar behavior is seen near the I-C transition for rectangles of size $3 \times 3k$ with $k = 2, 3, 4$ and 5. We observe that the discontinuity in the density increases with k.

5.5.3 Critical behavior of the isotropic–nematic phase (I-N) transition

As for $m = 2$, for $m = 3$ we find the existence of the nematic phase only for $k \geq 7$. We study the I-N transition for $k = 7$ with the order parameter q_1. It is expected to be in the Ising universality class since there are two possible choices of the orientation: either horizontal or vertical. We are unable to obtain good data collapse for Q_1, χ_1 and U_1 as the relaxation time increases with increasing m and k. Instead, we present some evidence for the transition being continuous and belonging to the Ising universality class. In Fig. 5.13 (a), the distribution q_1 near the I-N transition is shown. The two symmetric peaks of the

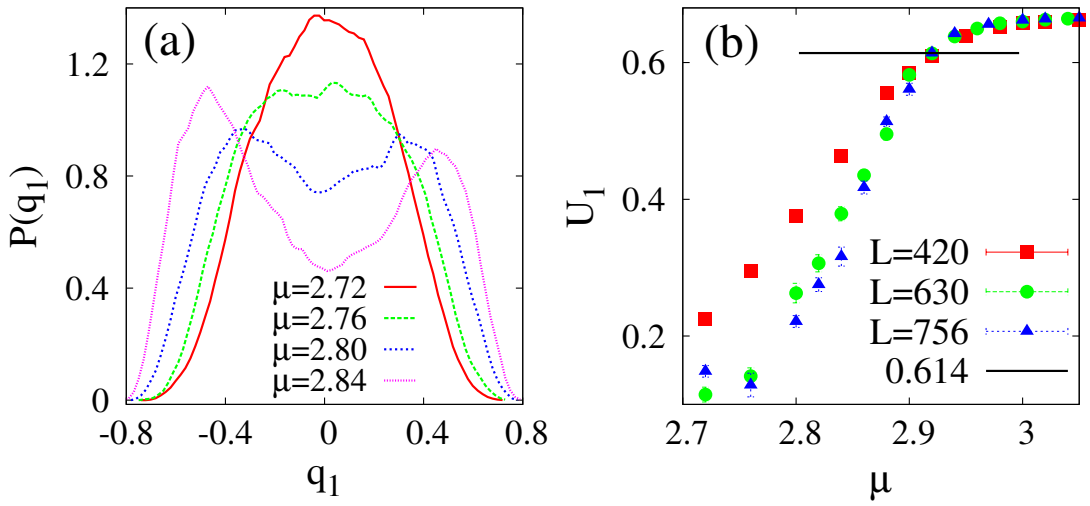

Figure 5.13: The I-N transition for rectangles of size 3×21. (a) Distribution of the order parameter q_1 near the I-N transition. The data are for $L = 420$. (b) Binder cumulant for different system sizes crosses at $\mu_c^{I-N} \approx 2.92$ ($\rho_c^{I-N} \approx 0.79$). Value of U_1 at μ_c^{I-N} is ≈ 0.61.

distribution come closer with decreasing μ and merge to a single peak. This is a signature of a continuous transition. The Binder cumulant U_1 for different system sizes cross at $\mu_c^{I-N} \approx 2.92$ ($\rho_c^{I-N} \approx 0.79$) [see Fig. 5.13 (b)]. The value of U_1 at $\mu = \mu_c^{I-N}$ is very close to the U_c value (0.61) for the Ising universality class.

5.5.4 Nematic–columnar phase (N-C) transition

The N-C transition is studied for $k = 7$ using the order parameter q_3. Contrary to our expectation that the N-C transition should be in the three-state Potts universality class, we observe a first order transition. The temporal dependence of the density near the N-C transition is shown in Fig. 5.14(a). Density jumps between two well separated values corresponding to the two different phases near the coexistence. Fig 5.14(b) shows the discontinuity in the order parameter $|q_3|$ near the transition. $P(|q_3|)$ shows two peaks of approximately equal height near $\mu_c^{N-C} \approx 3.12$. However, we are limited in our ability to obtain reliable data for 3×21 rectangles for larger system sizes, and the observed first order nature could be spurious.

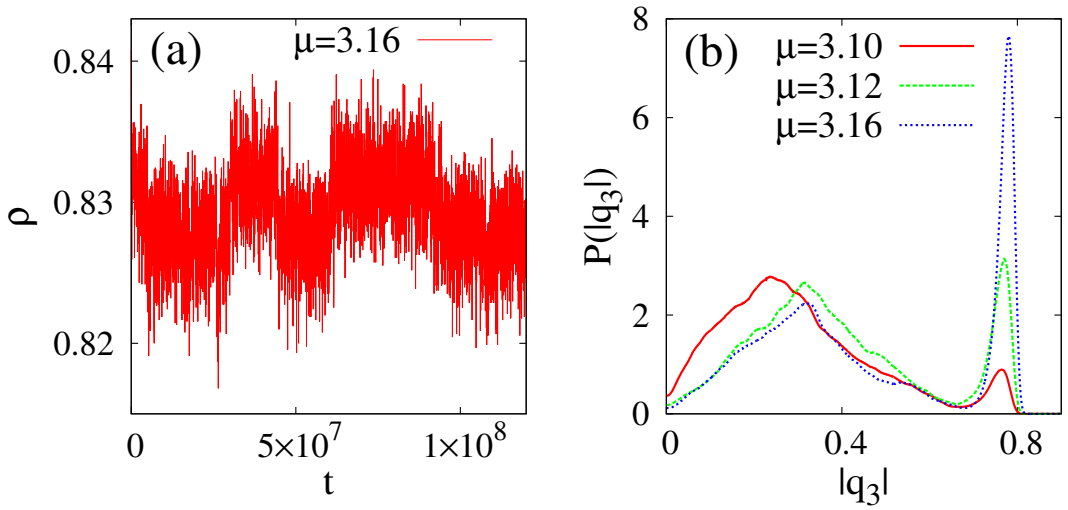

Figure 5.14: (a) Temporal variation of density ρ near the N-C transition, (b) distribution of the order parameter $|q_3|$ near the N-C transition. The data are for rectangles of size 3×21 and $L = 756$.

5.5.5 Columnar–sublattice phase (C-S) transition

The C-S transition is studied by choosing $k = 2$. We use the order parameter q_4 which is nonzero only in the S phase. The probability distribution of the density ρ and the order parameter $|q_4|$ for 3×6 rectangles near the C-S transitions is shown in Fig. 5.15. The distributions are again double peaked at and near the transition point, making the C-S transition first order. These peaks become sharper with increasing system size. The discontinuity in the density near the C-S transition is very small and can also be seen in the shaded portions of Fig. 5.11. We estimate $\mu_c^{C-S} \approx 9.33$. Similar behavior near the C-S transitions is also observed for $k > 2$, but it is difficult to get reliable data due to large relaxation times.

5.6 Summary and discussion

To summarize, we obtained the rich phase diagram of a system of hard rectangles of size $m \times mk$ on a square lattice for integer m, k using Monte Carlo simulations. For $k \geq 7$, we show that the system undergoes three entropy-driven transitions with increasing density.

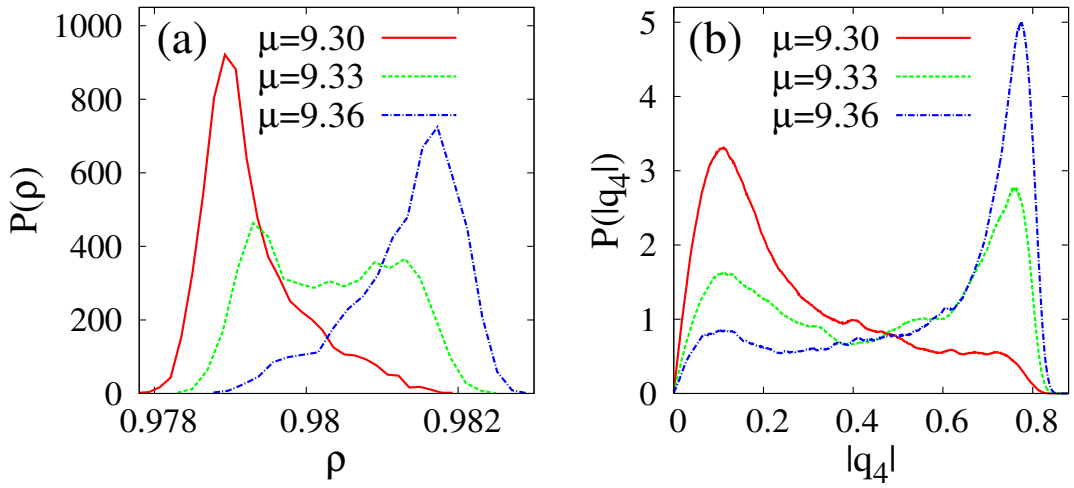

Figure 5.15: Distribution of (a) the density ρ near the C-S transition and (e) the order parameter $|q_4|$ near the C-S transition. The data are for rectangles of size 3×6 and $L = 720$.

For $m = 2$, we find that the I-N, N-C and C-S transitions are continuous, but the I-C transition may be continuous or first order, depending on k. The critical exponents for the continuous transitions are obtained using finite size scaling. The I-N and N-C transitions are found to be in the Ising universality class, while the C-S transition in the Ashkin-Teller universality class. The I-C transition is also found to be in the Ashkin-Teller universality class when continuous. For larger m, the number of possible ordered states increases and the corresponding surface tensions plays a crucial role in determining the nature of the transitions.

Surprisingly, our numerical data suggests that the nematic–columnar phase transition for $m = 3$ is first order. However, once a nematic phase with orientational order exists, there are only three possible choices for the columnar phase and a unique surface tension between these phases. By analogy with the three-state Potts model, we would expect a continuous transition, in contradiction with the numerical result. We also performed simulations for a system where the activity for vertical rectangles is zero (only horizontal rectangles are present) and observed again a first order transition. However, for 3×21 rectangles, the autocorrelation time is high and it becomes increasingly difficult to obtain reliable data. Simulations of larger systems are required to resolve this puzzle in the

future.

When $m = 2$, the I-C transition is found to be continuous for $k = 4$ and 5, but first order for $k = 6$. For $k = 6$, it is a weak first order transition and it is difficult to see the jump in density for small system sizes. It is also possible that the data is difficult to interpret because the transition point is close to a triciritcal point (the intersection of the I-N and N-C phase boundaries). It would be interesting to reconfirm the first order nature by either simulating larger systems or doing constant density Monte carlo simulations at the transition point so that phase separation may be seen. Also, determining a method to map k and ρ to the Ashkin-Teller model parameters would be useful in clarifying this issue.

Another issue that we are not able to resolve completely is the determination of the minimum value of k (say k_c) for which two transitions exist. For $m \geq 3$, we show that $k_c = 2$. When $m = 2$, our numerical data suggests that $k_c = 4$, with a direct transition from isotropic to sublattice phase for $k = 2, 3$. However, for $k = 4$, the columnar phase exists in a very narrow window of μ or ρ. Whether the columnar phase is present for $k = 2, 3$, but we are unable to resolve the transitions, is something that requires investigation with much larger system sizes.

Chapter 6

Hard rectangles with non-integer aspect ratio

6.1 Introduction

In this chapter, we study the phase diagram of the system of hard rectangles of size $m \times mk$ on the square lattice, when m and mk both are integers, but the aspect ratio k is non-integer. What are the different phases and the phase diagram when k is rational but not an integer? What are the minimum values of k beyond which the nematic and columnar phases exist? Can one get consistent bounds for those minimum k values by comparing with the case of integer k? Answering these questions will allow us to obtain the complete phase diagram for the system of hard rectangles.

We obtain the phase diagram for $m = 2$, when k is a half-integer, using large scale Monte Carlo simulations. The existence of an isotropic phase, a nematic phase, a columnar phase and a high-density phase is observed. Nature of the high-density phase depends on the length and width of the rectangles. The isotropic-columnar transition is found to be discontinuous, while the isotropic-nematic and nematic-columnar transitions are continuous.

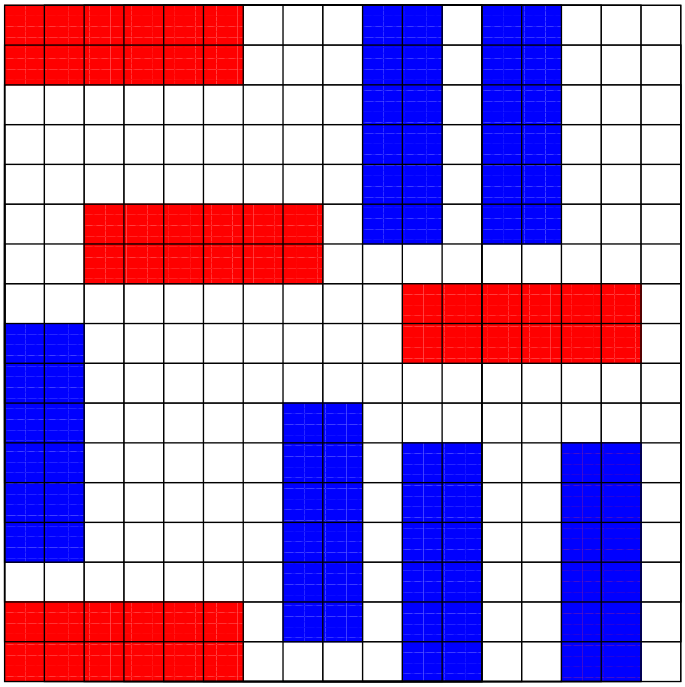

Figure 6.1: A schematic diagram showing a valid configuration for the system of hard rectangles of size 3×7 ($m = 3$, and aspect ratio $k = 7/3$).

The critical exponents are numerically estimated for the continuous transitions. We find that the columnar phase exists only when $k \geq 11/2$ for $m = 2$ and when $k \geq 13/3$ for $m = 3$. The nematic phase exists only when $k \geq 15/2$ for $m = 2$ and when $k \geq 22/3$ for $m = 3$.

The chapter is organizes as follows. In Sec. 6.2, the model is defined and the Monte Carlo algorithm is discussed. In Sec. 6.3, we describe the different phases that we observe in simulations. The phase diagram for $m = 2$ is determined using Monte carlo simulations in Sec. 6.4. Section 6.5 is devoted to study the nature of the different phase transitions occurring in the system. We study the isotropic-columnar, isotropic-nematic and nematic-columnar transitions in detail. In Sec. 6.6, we briefly discuss the phase behavior of the system when $m \geq 3$. Section 6.7 contains summary of the results obtained and discussions. The content of this chapter is published in Ref. [133].

6.2 Model and Monte carlo algorithm

Consider monodispersed hard rectangles of size $m \times mk$ on a square lattice of size $L \times L$ with periodic boundary conditions. Here, m and mk both are integers, but k is non-integer. Each rectangle is oriented either horizontally or vertically. A horizontal (vertical) rectangle occupies mk lattice sites along x (y)-direction and m lattice site along y (x)-direction. Each site may have at most one rectangle passing through it. An example of a valid configuration is shown in Fig. 6.1. We associate an activity $z = e^{\mu}$ to each rectangle, where μ is the chemical potential.

We simulate the system in the constant μ grand canonical ensemble using the efficient algorithm involving cluster moves as described in Sec. 2.4.2. A rotatable plaquettes for the flip move is now of size $R \times R$, where R is the least common multiple of m and mk. The rotatable plaquettes being larger (compared to the case for integer k) in size, have lower probability to occur during the simulations. This makes the flip move less effective, making it difficult to equilibrate the systems at high densities.

6.3 Different phases

As for integer k, we observe four different phases in the simulations: an isotropic (I) phase, a nematic (N) phase, a columnar (C) phase and a high-density (HD) phase. The I phase is disordered. In the N phase, rectangles orient preferably along the horizontal or vertical direction, but they do not have any positional order. Each row or column on an average contains equal number of bottom-left corners (heads) of the rectangles. The columnar (C) phase has orientational order and translational order only in the direction perpendicular to the nematic orientation. When $m = 2$, in the columnar phase, if the majority of the rectangles are horizontal (vertical), their heads lie mostly on either even rows (columns) or odd rows (columns). Hence, there are 4 (in general $2m$) symmetric C

phases. The I, N and C phases are observed when $m \geq 2$, for both integer and non-integer k.

The HD phase has no orientational order. But it may or may not possess translational order depending on the length and width of the rectangles. Let, the greatest common divisor of the length and width be denoted by p. We divide the square lattice into p^2 sublattices by assigning to a site (i, j) a label $(i \mod p) + p \times (j \mod p)$. In the fully packed limit, it is straightforward to verify that the heads of the rectangles occupy one of the p^2 sublattices. We expect this phase to be stable to introduction of vacancies at densities close to the full packing. If $p > 1$, the HD phase is a sublattice phase with complete translational order but no orientational order. On the other hand, when $p = 1$ (length and width are mutually prime), the HD phase is disordered with no orientational or translational order. Since existing evidence for $m = 1$ suggests that the high-density disordered phase is qualitatively similar to the low-density I phase (see Sec. 3.6 and 4.5), we expect the same to hold for $m \geq 2$ whenever the HD phase is disordered.

When $m \geq 2$ and integer k, $p = m > 1$ and the HD is known to be a sublattice phase (see Sec. 5.3), consistent with the above argument. To further confirm that the HD phase is a sublattice phase when $p > 1$, but k is a non-integer, we simulate the system of rectangles of size 4×6, for which $p = 2$. We divide the lattice into $p^2 = 4$ sublattices. The sublattice order parameter is defined as $q_4 = n_0 - n_1 - n_2 + n_3$ (consistent with the definitions in Chapter. 5), where n_i is the fraction of sites occupied by rectangles whose heads are on the i-th sublattice. It is straightforward to check that $\langle |q_4| \rangle \neq 0$ only for the sublattice phase. To show the existence of sublattice phase at high density, a large value of μ is chosen ($\mu = 10.8$), and the temporal evolution of $|q_4|$ is tracked, starting from three different initial configurations: nematic, disordered and sublattice phases (see Fig 6.2). At large times, the system reaches a stationary state that is independent of the initial configuration, ensuring equilibrium. For this choice of μ, the fraction of occupied sites ρ fluctuates around 0.962. In equilibrium, $\langle |q_4| \rangle \approx 0.580$, clearly showing the existence of a sublattice

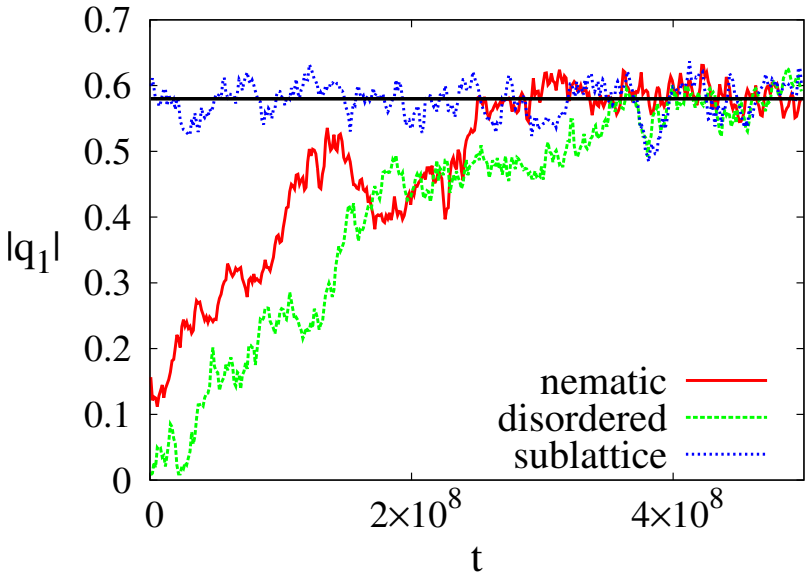

Figure 6.2: Time evolution of the sublattice order parameter q_4, starting from three different types of initial configurations: nematic, disordered, and sublattice phases. The straight line is $|q_4| = 0.580$. The data are $\mu = 10.8$ and for L=960. The equilibrium density is ≈ 0.962.

phase.

6.4 Phase diagram for $m = 2$

The phase diagram for $m = 2$ and non-integer k is shown in Fig. 6.3, where the data points are obtained from Monte Carlo simulations and the lines are guides to the eye. The low density phase is an I phase for all k. Since the length and width of the rectangles are mutually prime, $p = 1$, and the HD phase is a reentrant I phase. No phase transitions are observed when $k \leq 9/2$. The C phase exists only for $k \geq 11/2$, while the N phase exists only for $k \geq 15/2$.

We could not numerically obtain any data point on the C-HD phase boundary as it is not possible to equilibrate the systems within available computer time at high densities for $k \geq 11/2$.

The I-C transition is found to be first order for both $k = 11/2$ and $13/2$. The shaded region

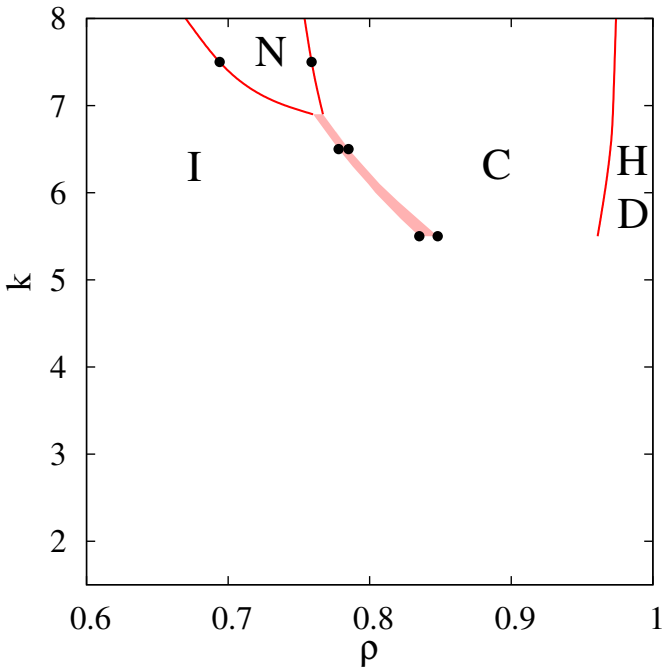

Figure 6.3: Phase diagram for rectangles of size $2\times 2k$, where k is restricted to non-integer values. I, N, C and HD denote isotropic, nematic, columnar and high-density phases respectively. The data points are from simulation, while the continuous lines and shaded portions are guides to the eye. The shaded portion denotes regions of phase coexistence.

in Fig. 6.3 denotes the region of phase coexistence at a first order phase transition. We find that the I-N and N-C transitions are both continuous. These transitions are analyzed in detail below.

6.5 Critical behavior for $m = 2$

We now study the nature of the different phase transitions for the system of $2 \times 2k$ rectangles, where k is half-integer. The I-N transition is studied by the order parameter q_1, defined as

$$q_1 = n_h - n_v, \tag{6.1}$$

where n_h and n_v are the fraction of sites occupied by the horizontal and vertical rectangles respectively. In the I phase $\langle |q_1| \rangle = 0$, while in the N phase, $\langle |q_1| \rangle \neq 0$.

The I-C and N-C phase transitions are best studied with the order parameter

$$q_3 = |n_{re} - n_{ro}| - |n_{ce} - n_{co}|, \tag{6.2}$$

where n_{re} (n_{ro}) is the fraction of sites occupied by rectangles whose heads are on the even (odd) rows, and n_{ce} (n_{co}) is the fraction of sites occupied by rectangles whose heads are on the even (odd) columns. In the I and N phases, $n_{re} \approx n_{ro}$, and $n_{ce} \approx n_{co}$, implying that $\langle |q_3| \rangle = 0$. In the C phase, either $n_{re} \neq n_{ro}$ and $n_{ce} \approx n_{co}$, or $n_{ce} \neq n_{co}$ and $n_{re} \approx n_{ro}$ implying that $\langle |q_3| \rangle \neq 0$.

The averaged order parameter is denoted by $Q_i = \langle q_i \rangle$. The other relevant thermodynamic quantities are the second moment χ_i and the Binder cumulant U_i, defined as

$$\chi_i = \langle q_i^2 \rangle L^2, \tag{6.3a}$$

$$U_i = 1 - \frac{\langle q_i^4 \rangle}{3\langle q_i^2 \rangle^2}. \tag{6.3b}$$

where $i = 2, 3$. Singular behavior of the thermodynamic quantities near a critical point and the definition of the critical exponents may be found in Eq. (3.7).

6.5.1 Isotropic–nematic (I-N) transition

We study the I-N transition for 2×15 ($k = 15/2$) rectangles using the order parameter Q_1. Since the N phase may have orientational order only in the horizontal or vertical direction, we expect the I-N transition to be in the two-dimensional Ising universality class, as has been confirmed for integer k, when $m = 1$ [25] and $m = 2, 3$ (see Sec. 5.4.4 and 5.5.3), and for systems of polydispersed rods [115, 116]. The data for U_1 for different system sizes intersect at $\mu = \mu_c^{I-N} \approx 0.945$ [see Fig. 6.4(a)]. The corresponding critical density is $\rho_c^{I-N} \approx 0.694$, which is less than $\rho_c^{I-N} \approx 0.745$ for $k = 7$ [112]. The data for U_1 [see Fig. 6.4(b)], Q_1 [see Fig. 6.4(c)], and χ_1 [see Fig. 6.4(d)] for different system sizes

collapse onto a single curve when scaled as in Eq. (3.7) with Ising exponents $\beta/\nu = 1/8$, $\gamma/\nu = 7/4$, and $\nu = 1$. For larger values of k, integer or otherwise, we expect the I-N transition to be in the Ising universality class.

6.5.2 Nematic–columnar (N-C) transition

We study the N-C transition for rectangles of size 2×15 using the order parameter Q_3. When the system makes a transition from the N phase with horizontal (vertical) orientation to the C phase, the symmetry between even and odd rows (columns) is broken. From symmetry considerations, we expect the N-C transition to be in the Ising universality class. The data for U_3 for different system sizes intersect at $\mu = \mu_c^{N-C} \approx 1.696$ [see Fig. 6.5(a)], corresponding to $\rho_c^{N-C} \approx 0.759$. The data for U_3 [see Fig. 6.5(b)], Q_3 [see Fig. 6.5(c)], and χ_3 [see Fig. 6.5(d)] for different system sizes collapse onto a single curve when scaled as in Eq. (3.7) with Ising exponents $\beta/\nu = 1/8$, $\gamma/\nu = 7/4$, and $\nu = 1$. The N-C transition in the system of 2×14 rectangles has also been shown to be in the Ising universality class (see Sec. 5.4.5), and we expect the same for $k > 15/2$.

6.5.3 Isotropic–columnar (I-C) transition

The I-C transition occurs only for rectangles of size 2×11 ($k = 11/2$) and 2×13 ($k = 13/2$). The transition is best studied using the order parameter q_3. We find that the transition is first order for both values of k. This may be established by numerically calculating the probability density functions (pdf) $P(\rho)$ of the density ρ and $P(q_3)$ of the order parameter q_3 for values of μ that are close to the transition point $\mu_c^{I-C} \approx 3.885$ for $k = 11/2$ and $\mu \approx \mu_c^{I-C} = 2.390$ for $k = 13/2$. The pdf for $k = 11/2$ and $13/2$ are shown in Fig. 6.6 and Fig. 6.7 respectively. In both the figures, the pdfs for q_3 have three clear peaks at the transition point: the two peaks at $q_3 \neq 0$ correspond to the symmetric C phases and the one at $q_3 = 0$ to the I phase. The pdf for ρ have two peaks of nearly equal height at the

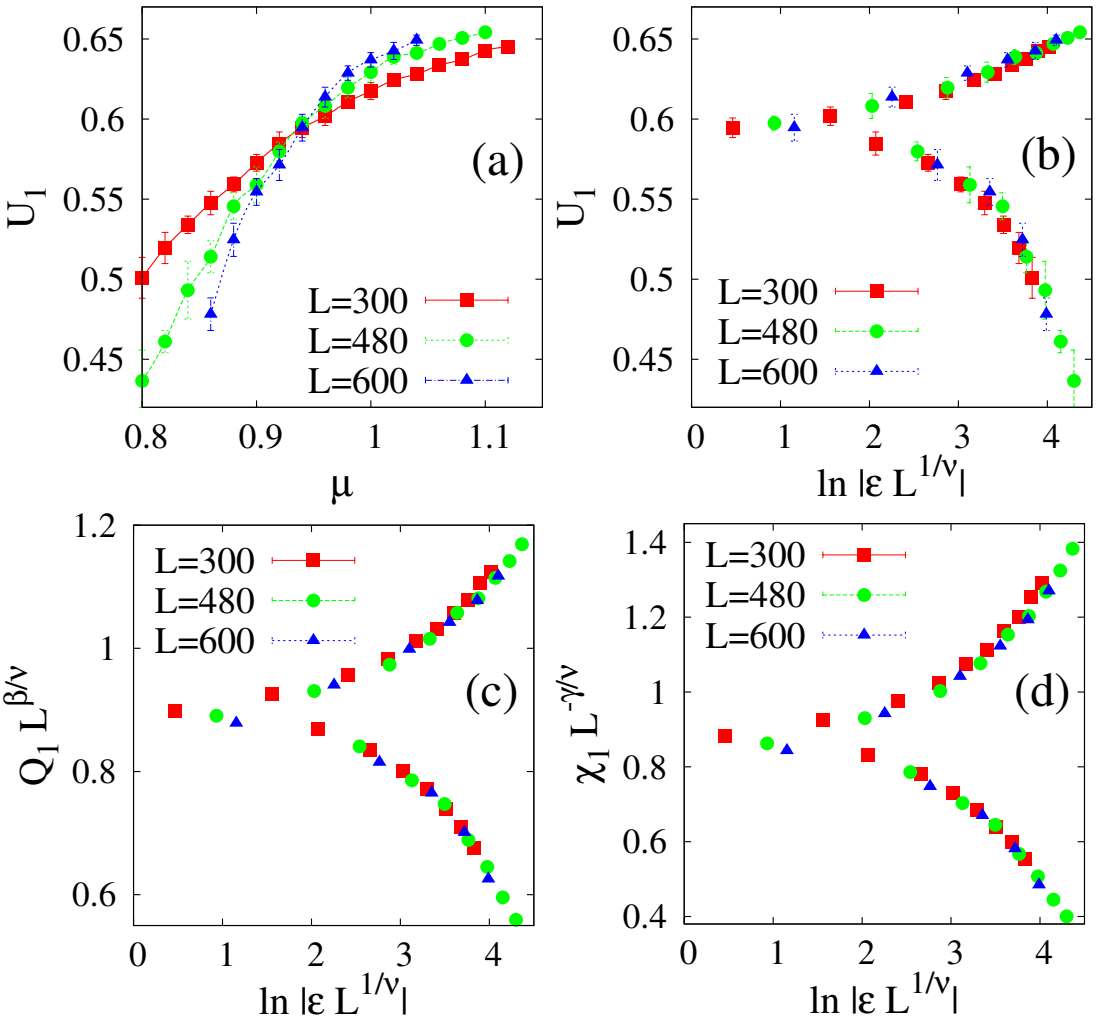

Figure 6.4: The critical behavior near the I-N transition for rectangles of size 2×15 ($k = 15/2$). (a) The data for Binder cumulant for different system sizes intersect at $\mu_c^{I-N} \approx 0.945$ ($\rho_c^{I-N} \approx 0.694$). The data for different L near the I-N transition for (b) Binder cumulant, (c) order parameter, and (d) second moment of the order parameter collapse onto a single curve when scaled as in Eq. (3.7) with the Ising exponents $\beta/\nu = 1/8$, $\gamma/\nu = 7/4$, and $\nu = 1$.

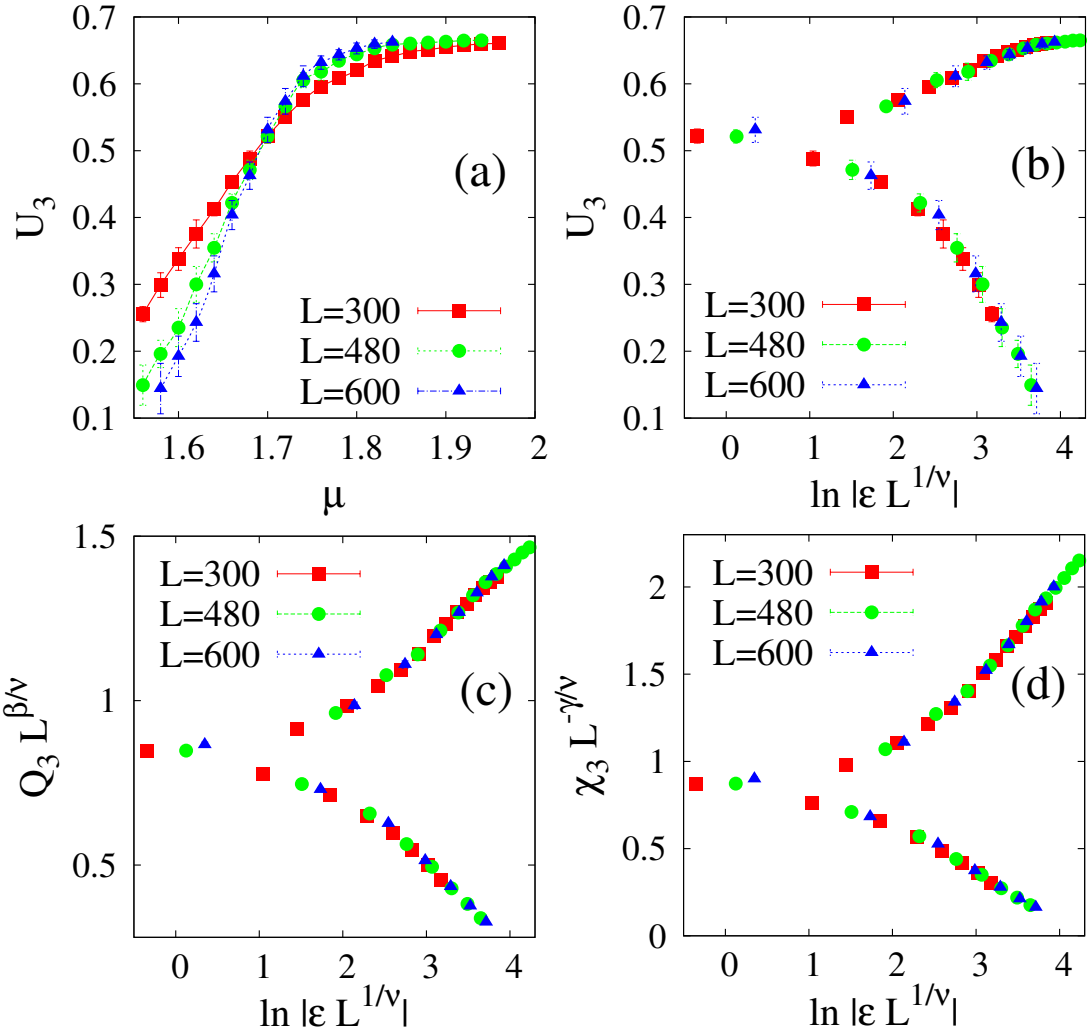

Figure 6.5: The critical behavior near the N-C transition for rectangles of size 2×15 ($k = 15/2$). (a) The data for Binder cumulant for different system sizes intersect at $\mu_c^{N-C} \approx 1.696$ ($\rho_c^{N-C} \approx 0.75$). The data for different L near the N-C transition for (b) Binder cumulant, (c) order parameter, and (d) second moment of the order parameter collapse onto a single curve when scaled as in Eq. (3.7) with the Ising exponents $\beta/\nu = 1/8$, $\gamma/\nu = 7/4$, and $\nu = 1$.

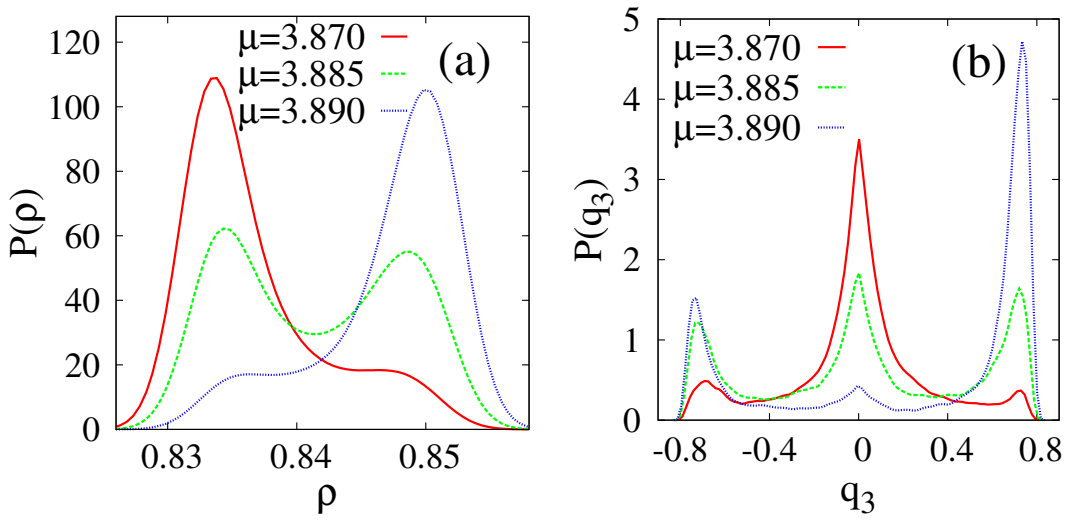

Figure 6.6: Probability density function of (a) density ρ and (b) order parameter q_3 for three values of μ near the I-C transition. The data are for rectangles of size 2×11 and $L = 440$.

transition point, though these peaks are not clearly separated for $k = 13/2$. The difference in the peak positions is equal to the jump in the density across the transition point and is shown by the shaded region in Fig. 6.3. We find that these peaks become sharper with increasing system size. These are clear signatures of a first order transition.

6.6 Phase diagram for $m \geq 3$

We expect that the phase diagram for $m \geq 3$ and non-integer k to be qualitatively similar to that for $m = 2$ with three entropy-driven transitions for large k. The HD phase is a disordered or sublattice phase depending on whether the length and width of the rectangles are mutually prime or not. For $m = 3$, we determine the the minimum value of k beyond which the C and N phases exist. There are no transitions for $k \leq 11/3$. We find that the C phase exists only for $k \geq 13/3$, while the N phase exists only for $k \geq 22/3$. When $m = 3$, the C phase has a 6-fold symmetry and there exists two types of surface tensions in the system as discussed earlier. Thus, it is difficult to guess the nature of the I-C transition without knowing the values of surface tensions. For rectangles with $k = 13/3$, we find

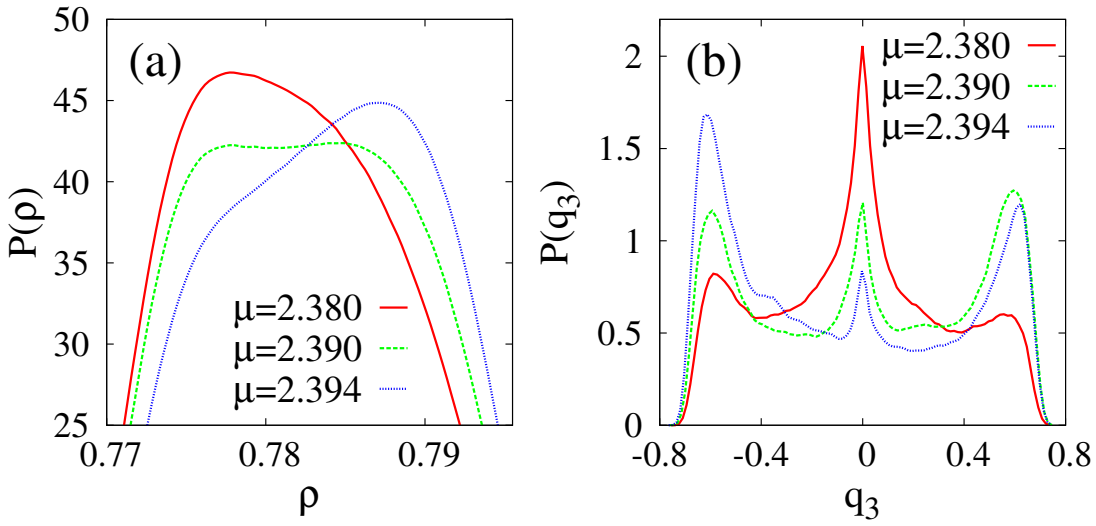

Figure 6.7: Probability density function of (a) density ρ and (b) order parameter q_3 for three values of μ near the I-C transition. The data are for rectangles of size 2×13 and $L = 416$.

that the I-C phase transition is first order in nature. The pdfs for ρ and q_3 behave similarly to that for the case of $m = 2$. The I-N transition is expected to be in Ising universality class for all m.

6.7 Summary and discussion

In this chapter, we obtained numerically the phase diagram of the system of hard rectangles of size $m \times mk$ with non-integer aspect ratio k. As for integer k, the system may exist in four different phases: isotropic, nematic, columnar or high-density phase. The high-density phase is a disordered phase when the length and width of the rectangles are mutually prime, otherwise, it is a sublattice phase.

The N phase exists only when $k \geq 15/2$ for $m = 2$ and when $k \geq 22/3$ for $m = 3$. For integer k, the N phase exists only when $k \geq 7$ for $m = 1, 2, 3$. These different lower bounds may be combined to give tighter bounds for k_{min}^{I-N}, the smallest value of k beyond which the N phase exists. We conclude that $20/3 < k_{min}^{I-N} \leq 7$. While the isotropic–columnar transition is found to be first order, the isotropic–nematic and the

nematic–columnar transitions belong to the two-dimensional Ising universality class. We could not access the columnar–high-density phase transition due to numerical limitations. The phase diagram for large m is expected to be qualitatively similar to that for $m = 2$. However, the nature of the various transitions, except the isotropic-nematic transition, may be different.

The bounds for k_{min}^{I-C}, the minimum value of k beyond which the C phase exists, are not so clear. We find that the C phase exists when $k \geq 11/2$ for $m = 2$ and when $k \geq 13/3$ for $m = 3$. On the other hand, for integer k, the C phase exists for $k \geq 4$ for $m = 2$ and when $k \geq 2$ for $m = 3$. Thus, unlike for the N phase, k_{min}^{I-C} depends both on m and whether k is a integer or not, and it is not possible to combine the bounds in terms of only m.

Chapter 7

Asymptotic phase behavior for the system of hard rectangles

7.1 Introduction

As we have seen, the system of hard rectangles of size $m \times mk$ on the square lattice undergoes three entropy-driven phase transitions with density for large aspect ratios ($k \geq 7$): first, from a low-density isotropic (I) to a nematic (N) phase, second, from the nematic to a columnar (C) phase and third, from the columnar to a high density phase. The high density phase is disordered if the length and width of the rectangles are mutually prime, else, it is sublattice (S) phase with complete positional order, but no orientational order. In this chapter, we investigate the asymptotic behavior of the isotropic–nematic, nematic–columnar and columnar–sublattice phase boundaries using a combination of numerical simulations and analytical techniques involving Bethe approximations, virial expansion, and entropy estimates.

The limit $k \to \infty$, keeping m fixed is argued to be the limit of oriented lines in the continuum. For this limiting case in three dimensions, the virial expansion truncated at

the second virial coefficient becomes exact and the critical density for the I-N transition $\rho_c^{I-N} \approx A_1 k^{-1}$ [11, 15, 134]. A_1 for oriented long rectangles in the two-dimensional continuum can be directly estimated by simulating oriented lines of length ℓ, for which it is straightforward to show that the critical number density $\approx A_1 \ell^{-2}$. From the simulations of this system with $\ell = 1$, it can be inferred that $A_1 \approx 4.84$ [97]. For $m = 1$, by simulating systems with k up to 12 on the lattice, it has been shown that $\rho_c^{I-N} \propto k^{-1}$ [112]. From the value of the critical density for $k = 10$ [112], it can be estimated that $A_1 \approx 5.02$, different from that for oriented lines [97]. There are no such similar studies for $m > 1$. The limit $m \to \infty$, keeping k fixed corresponds to the continuum problem of oriented rectangles of aspect ratio k, a model that was introduced and studied by Zwanzig using virial expansion [15]. This limit is difficult to study numerically on the square lattice.

In this chapter, by simulating systems of rectangles with aspect ratio k up to 60 (for $m = 1$), and $k = 56$ (for $m = 2$ and 3), we show that ρ_c^{I-N} is proportional to k^{-1} for $m = 1, 2$ and 3. Within numerical error, A_1 is shown to be independent of m and equal to 4.80 ± 0.05. To understand better the limit of large k, we study the I-N transition using a Bethe approximation, and a virial expansion truncated at the second virial coefficient. The critical density ρ_c^{I-N} is obtained for all m and k. When k is large, both the theories predict that $\rho_c^{I-N} \approx A_1/k$, where $A_1 = 2$. In particular, we find that within the virial expansion truncated at the second virial coefficient, ρ_c^{I-N} is independent of m, for all k. For the N-C transition, we numerically determine ρ_c^{N-C} for $m = 2$ and k up to 24 and show that for large k, $\rho_c^{N-C} \approx 0.73 + 0.23k^{-1}$. We study the N-C transition also using the same Bethe approximation to predict $\rho_c^{N-C} \approx A_2(m) + A_3(m)k^{-1}$ for $k \gg 1$, which captures the large k behavior correctly. It shows that a system of oriented rectangles with large aspect ratio in the two-dimensional continuum should exhibit both nematic and columnar phases provided $\lim_{m\to\infty} A(m) < 1$. In addition, we find that the Binder cumulant at the N-C transition is surprisingly dependent on k, and decreases as k^{-1} with increasing k. However, we show that the transition remains in the Ising universality class.

The rest of the chapter is organized as follows. Section 7.2 contains a brief description of the model, the Monte Carlo algorithm, and definitions of the phases and the relevant thermodynamic quantities of interest. In Sec. 7.3.1, we present the numerical results for the I-N transition for $m = 1, 2$ and 3. The asymptotic behavior of the N-C phase boundary for $m = 2$ and large k is determined numerically in Sec. 7.3.2. The Binder cumulant is shown to be non-universal, though exponents continue to be universal. Section 7.4.1 contains calculations of the I-N phase boundary using an ad-hoc Bethe approximation and a truncated virial expansion. In Sec. 7.4.2, we study the N-C transition analytically by estimating the entropy within the same Bethe approximation. The C-S phase boundary is studied by estimating the entropies in Sec. 7.4.3. Section 7.5 contains a summary and discussion of results. The content of this chapter is published in Ref. [119] and [135].

7.2 Model and definitions

The model of hard rectangles on the square lattice has already been discussed in the earlier chapters. We redefine it for the completeness of this chapter. Consider a system of monodispersed hard rectangles of size $m \times mk$ on a square lattice of size $L \times L$, with periodic boundary conditions. Each rectangle occupies m sites along the short axis and mk sites along the long axis, such that k is the aspect ratio. A rectangle is called horizontal or vertical depending on whether the long axis is along the x-axis or y-axis. No two rectangles may overlap. We associate an activity $z = e^{\mu}$ to each rectangle, where μ is the chemical potential.

To simulate the system, we use the grand canonical Monte carlo algorithm as discussed in Sec. 2.4.2. Here we define the order parameters and necessary thermodynamic quantities to study the I-N and the N-C transitions numerically. For the I-N transition, we use the order parameter

$$q_1 = n_h - n_v, \tag{7.1}$$

where n_h and n_v are the fraction of sites occupied by the horizontal and vertical rectangles respectively. The corresponding averaged order parameter $Q_1 = \langle |q_1| \rangle$ is zero in the I phase and nonzero in the N and C phases. The density is defined as the fraction of occupied sites. For the N-C transition, we use the order parameter

$$q_3 = |n_{re} - n_{ro}| - |n_{ce} - n_{co}|, \tag{7.2}$$

where n_{re} (n_{ro}) is the fraction of sites occupied by the rectangles whose bottom-left corners or heads are in the even (odd) rows, and n_{ce} (n_{co}) is the fraction of sites occupied by the rectangles whose heads are in the even (odd) columns. In the I and N phases, $n_{re} \approx n_{ro}$, and $n_{ce} \approx n_{co}$, and hence the corresponding averaged order parameter $Q_3 = \langle q_3 \rangle$ is zero. In the C phase, either $n_{re} \neq n_{ro}$ and $n_{ce} \approx n_{co}$, or $n_{re} \approx n_{ro}$ and $n_{ce} \neq n_{co}$, such that Q_3 is nonzero.

The second moment of the order parameter $\chi_i = \langle q_i^2 \rangle L^2$ and the Binder cumulant $U_i = 1 - \langle q_i^4 \rangle / 3 \langle q_i^2 \rangle^2$, where $i = 1$ and 3. Scaling properties of Q_i, χ_i, U_i may be found in Eq. (3.7).

7.3 Estimation of the phase boundaries using numerical simulations

7.3.1 Isotropic–nematic (I-N) phase boundary

In this section, we investigate the asymptotic behavior of the I-N phase boundary for $m = 1$, 2, and 3 by numerical simulations and show that $\rho_c^{I-N} = A_1 k^{-1}$ when $k \gg 1$, where A_1 is independent of m. Since there are two symmetric N phases (horizontal and vertical), the I-N transition for the system of hard rectangles is continuous and belongs to the Ising universality class for all m. We determine the critical density ρ_c^{I-N} from the

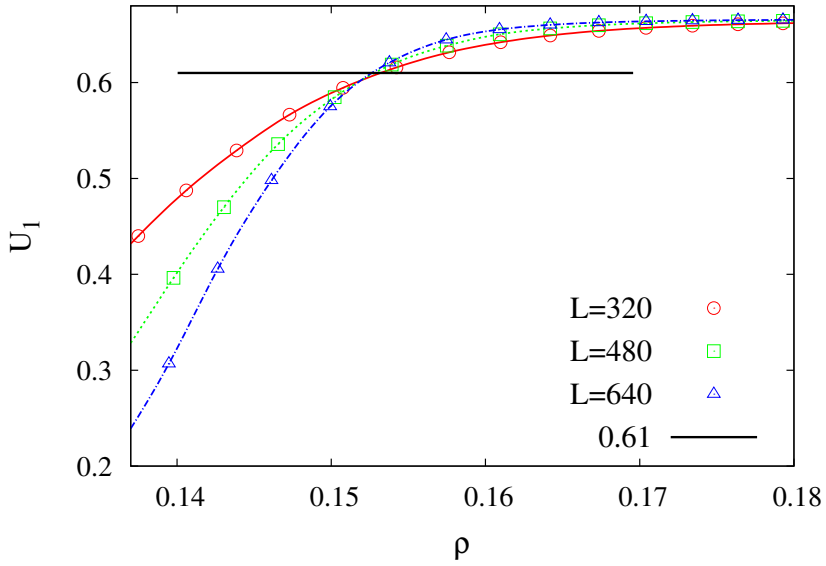

Figure 7.1: The variation of the Binder cumulant U_1 with density ρ for three different system sizes. The lines are cubic splines, fitted to the data. The value of U_1 at $\rho = \rho_c^{I-N}$ is ≈ 0.61. The data are for $m = 1$ and $k = 32$.

point of intersection of the curves of Binder cumulant with density for different system sizes. A typical example is shown in Fig. 7.1, where the variation of U_1 with density ρ is shown for three different system sizes when $m = 1$ and $k = 32$. The Binder cumulant data are fitted to a cubic spline to obtain a smooth and continuous curve for each L. This allows us to determine the point of intersection or ρ_c^{I-N} more accurately. In the example shown in Fig. 7.1, the curves for Binder cumulants for three different system sizes crosses at $\rho = \rho_c^{I-N} \approx 0.152$ and the value of the critical Binder cumulant $U_1^c \approx 0.61$. We find $U_1^c \approx 0.61$ for all values of m and k that we have studied, consistent with the value for the two-dimensional Ising model [131].

We simulate systems with aspect ratio up to $k = 60$ for $m = 1$ and $k = 56$ for $m = 2$ and 3. The critical density ρ_c^{I-N} obtained from the Binder cumulants are shown in Fig. 7.2. The data are clearly linear in k^{-1} for large k, confirming that $\rho_c^{I-N} = A_1 k^{-1}$, $k \gg 1$. In addition, the data for $m = 1, 2, 3$ asymptotically lie on the same straight line, showing that A_1 is independent of m. We estimate $A_1 = 4.80 \pm 0.05$.

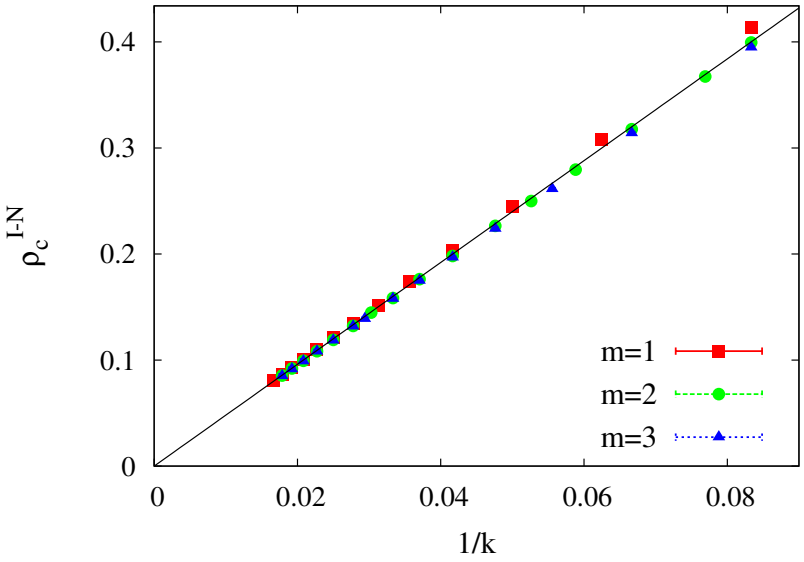

Figure 7.2: The variation of the critical density for the I-N transition ρ_c^{I-N} with k^{-1} for $m = 1, 2$ and 3. The straight line is $4.80k^{-1}$.

7.3.2 Nematic–columnar (N-C) phase boundary

In this section, we numerically study the N-C phase transition for $m = 2$ and determine the asymptotic behavior of the critical density ρ_c^{N-C} for large k. When $m = 2$, the N-C transition belongs to the Ising universality class for all k and the corresponding critical densities are determined from the intersection of Binder cumulant curves for different system sizes as discussed in Sec. 7.3.1. The critical density ρ_c^{N-C} decreases to a constant with increasing k (see Fig. 7.3). We obtain $\rho_c^{N-C} \approx 0.727 + 0.226k^{-1}$, $k \gg 1$ when $m = 2$. As ρ_c^{N-C} asymptotically approaches a constant value, it becomes increasingly difficult to get reliable data for large k.

Surprisingly, we find that the value of the critical Binder cumulant at the N-C transition point depends on the aspect ratio k. When $m = 2$, the critical Binder cumulant U_3^c decreases monotonically as a power law with k, from 0.50 when $k = 7$ to 0.18 when $k = 24$ (see Fig. 7.4). The data is fitted best with $U_3^c \approx 4.45\ k^{-1}$. Usually, for the Ising universality class, the value critical Binder cumulant at the transition point is expected to be universal (≈ 0.61) . However, there are a few examples of systems that exhibit such non

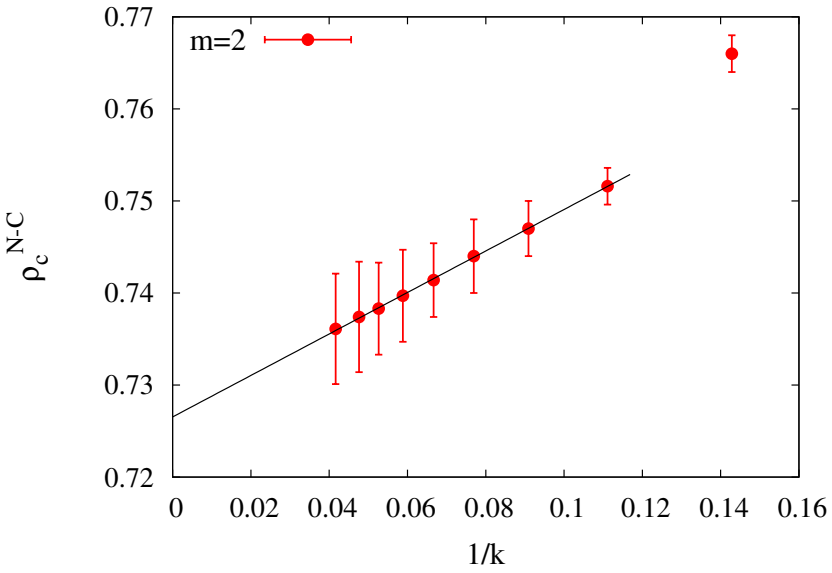

Figure 7.3: The variation of the critical density for the N-C transition ρ_c^{N-C} with k^{-1} for $m = 2$. The straight line is a linear fit to the data: $0.727 + 0.226k^{-1}$.

universal behavior [131, 136, 137]. These include the anisotropic Ising model where the critical Binder cumulant depends on the ratio of the coupling constants along the x and y directions [136], and the isotropic Ising model on rectangular lattice, where the critical Binder cumulant is a function of the aspect ratio of the underlying lattice [131]. In the latter case, $U_3^c \approx 2.46\,\alpha^{-1}$, where α is the aspect ratio of the lattice [131]. Thus, nominally $k \approx 1.8\,\alpha$.

Although U_3^c varies with k, we confirm that the critical exponents for the N-C transition remains the same as those of the two-dimensional Ising model. To do so, we determine the critical exponents for the system with $m = 2$ and $k = 13$ using finite size scaling. For this example, critical Binder cumulant is ≈ 0.35, noticeably different from that for the Ising universality class. The data for the Binder cumulant U_3 for different system sizes intersect at $\mu_c^{N-C} \approx 1.00$ [see fig. 7.5 (a)]. We find that the data for U_3, Q_3 and χ_3 for different system sizes collapse onto a single curve when scaled as in Eq. (3.7) with Ising exponents $\beta/\nu = 1/8$, $\gamma/\nu = 7/4$, and $\nu = 1$ [see Fig. 7.5 (b)–(d)]. We thus conclude that, though the critical Binder cumulant is non-universal, the transition is in the Ising universality class.

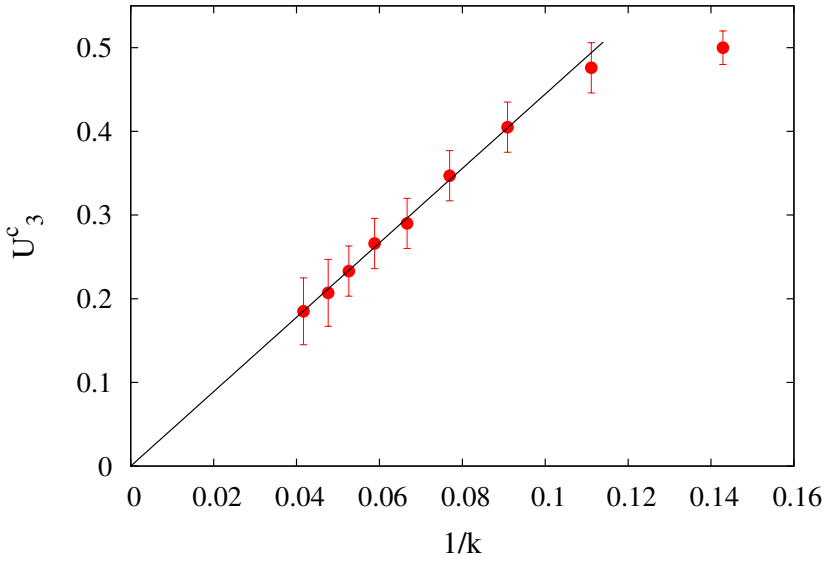

Figure 7.4: The variation of the critical Binder cumulant U_3^c at the N-C transition with k^{-1}. The straight line 4.446 k^{-1} is a linear fit to the data. The data are for $m = 2$.

7.3.3 Columnar–sublattice (C-S) phase boundary

The columnar–sublattice phase transition occurs at very high density for large k or m, resulting in a large relaxation time. It becomes very difficult to obtain reliable data within reasonable time at these densities. Hence, we could not investigate the asymptotic behavior of the columnar–sublattice phase boundary numerically.

7.4 Estimation of the phase boundaries using analytical methods

In this section, we obtain the asymptotic behavior of the phase diagram for large k using theoretical arguments.

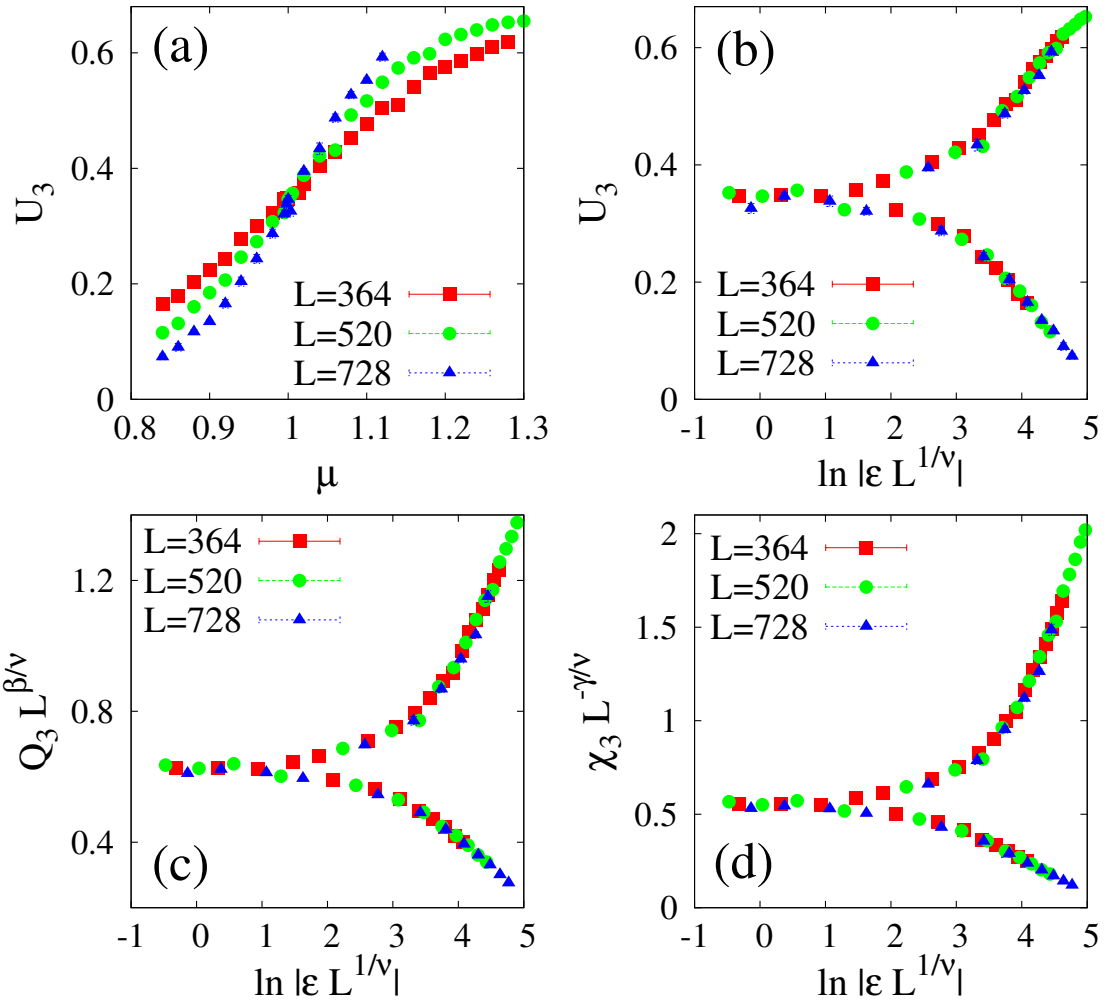

Figure 7.5: The critical behavior near the N-C transition for rectangles of size 2×26 ($k = 13$). (a) The data for Binder cumulant for different system sizes intersect at $\mu_c^{N-C} \approx 1.00$. The data for different L near the N-C transition for (b) Binder cumulant, (c) order parameter, and (d) second moment of the order parameter collapse onto a single curve when scaled as in Eq. (3.7) with the Ising exponents $\beta/\nu = 1/8$, $\gamma/\nu = 7/4$, and $\nu = 1$.

7.4.1 Isotropic–nematic (I-N) phase boundary

Here we obtain the asymptotic behavior of the isotropic–nematic phase boundary for large k using analytical methods. The critical density for the I-N phase transition, for fixed m and $k \gg 1$ may be determined by making an analogy with the continuum problem. The limit $k \to \infty$, keeping m fixed corresponds to the system of oriented lines in the continuum. For this problem $\rho_c^{I-N} \approx A_1/k$ [20, 112]. Thus, we expect $\rho_c^{I-N} \approx A_1/k$, where A_1 is independent of m. For $k = 7$, we observed only a weak dependence of ρ_c^{I-N} on m with the critical density being 0.745 ± 0.005 ($m = 1$) [112], 0.744 ± 0.008 ($m = 2$) and 0.787 ± 0.010 ($m = 3$) (see Sec. 5.4 and 5.5).

In the absence of an exact solution, we present two approximate calculations: first a Bethe approximation and second a virial expansion truncated at the second virial coefficient.

Bethe approximation

The Bethe approximation becomes exact on tree-like lattices. For $m = 1$, the model was solved exactly on the 4-coordinated random locally tree-like layered lattice (RLTL) to obtain $\rho_c^{I-N} = 2/(k-1)$ [26] or $A_1 = 2$. The RLTL also allows an exact solution to be obtained for more complicated systems like repulsive rods. However, a convenient formulation of the problem of hard rectangles on the RLTL is lacking. Therefore, we resort to an ad-hoc Bethe approximation introduced by DiMarzio to estimate the entropy of hard rods on a cubic lattice [28], and later used for studying the statistics of hard rods on different lattices [114, 112, 113]. However, a straightforward extension of this method to a system of rectangles suffers from the enumeration result depending on the order in which the rectangles are placed. A scheme that overcomes this shortcoming was suggested in Ref. [138]. Here, we adapt the calculations to study the I-N transition.

The I-N phase boundary can be determined if the entropy as a function of the densities of the horizontal and vertical rectangles is known. We estimate the entropy by computing

the number of ways of placing N_x horizontal and N_y vertical rectangles on the lattice.

First, we place the horizontal rectangles on the lattice one by one. Given that j_x horizontal rectangles have been placed, the number of ways of placing the $(j_x + 1)^{th}$ horizontal rectangle may be estimated as follows. The head of the rectangle may be placed in one of the $(M - m^2 k j_x)$ empty sites, where M is the total number of lattice sites. We denote this site by A (see Fig. 7.6). For this new configuration to be valid, all sites in the $m \times mk$ rectangle with head at A should be empty. Given A is empty, we divide the remaining $(m^2k - 1)$ sites in three groups: $(mk - 1)$ sites along the line AB, $(m - 1)$ sites along the line AC, and the remaining $(m - 1)(mk - 1)$ sites (D is an example). Let $P_x(B|A)$ be the conditional probability that B is empty given that A is empty. Then the probability that $(mk - 1)$ sites along the line AB are empty is $[P_x(B|A)]^{mk-1}$, where the subscript x denotes the direction AB. In writing this, we ignore all correlations beyond the nearest neighbor. Likewise, the probability that $(m - 1)$ sites along the line AC are empty is given by $[P_y(C|A)]^{m-1}$, where $P_y(C|A)$ is the conditional probability that C is empty given A is empty. Let $P(D|B \cap C)$ denote the conditional probability that D is empty given that B and C are both empty. Then, the probability that the remaining $(m - 1)(mk - 1)$ sites are empty may be approximated by $[P(D|B \cap C)]^{(m-1)(mk-1)}$. Collecting these different terms together, we obtain the number of ways to place the $(j_x + 1)^{th}$ horizontal rectangle

$$\begin{aligned} \nu_{j_x+1} &= (M - m^2 k j_x) \times [P_x(B|A)]^{mk-1} [P_y(C|A)]^{m-1} \\ &\times [P(D|B \cap C)]^{(m-1)(mk-1)}. \end{aligned} \tag{7.3}$$

It is not possible to determine these conditional probabilities exactly. However, they may be estimated by assuming that the rectangles are placed randomly. Given A is empty, either B might be empty or occupied by a horizontal rectangle (as no vertical rectangles have been placed yet) in m ways. Thus, given A is empty, the probability that B is also

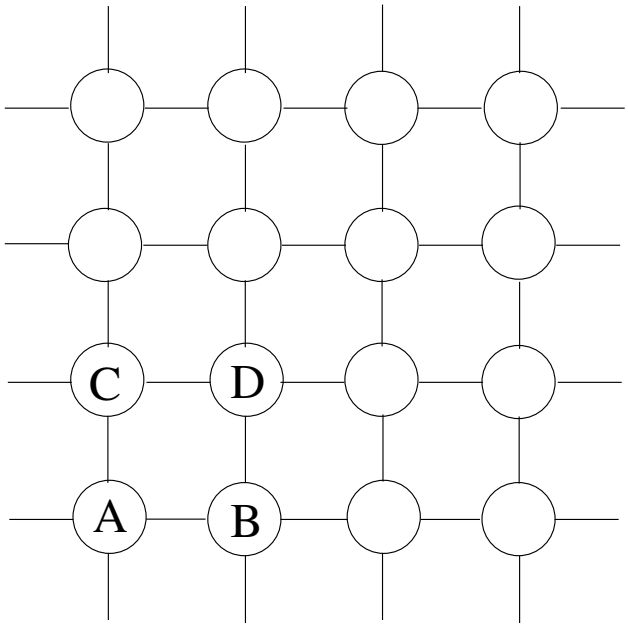

Figure 7.6: Schematic of a square lattice showing the position of the sites A-D to explain the calculation of the isotropic–nematic phase boundary.

empty, is

$$P_x(B|A) = \frac{M - m^2 k j_x}{M - m^2 k j_x + m j_x}. \tag{7.4}$$

Similarly, if A is empty, C might be empty or it might be occupied by any of the mk sites on the longer axis (passing through C) of a horizontal rectangle. Thus the probability that C is empty, given A empty is given by

$$P_y(C|A) = \frac{M - m^2 k j_x}{M - m^2 k j_x + mk j_x}. \tag{7.5}$$

Next, we estimate $P(D|B \cap C)$. If we follow a similar approach to calculate $P(D|B \cap C)$, the resultant entropy becomes dependent on the order of placement of the horizontal and vertical rectangles, and thus asymmetric with respect to N_x and N_y. To overcome this shortcoming, we follow the Bethe approximation proposed in Ref. [138] and assume

$$P(D|B \cap C) \approx \frac{P_x(C|D) P_y(B|D)}{P_{xy}(C|B)}, \tag{7.6}$$

where

$$P_{xy}(B|C) = \frac{M - m^2 k j_x}{M - m(m-1)k j_x + (m-1) j_x}, \tag{7.7}$$

is the probability that C is empty given B is empty. It can be easily seen that

$$P_x(C|D) = P_x(B|A), \tag{7.8a}$$

$$P_y(B|D) = P_y(C|A). \tag{7.8b}$$

As all the horizontal rectangles are indistinguishable, the total number of ways to place N_x of them is,

$$\Omega_x = \frac{1}{N_x!} \prod_{j_x=0}^{N_x-1} \nu_{j_x+1}. \tag{7.9}$$

Substituting Eqs. (7.4)–(7.8) into Eq. (7.3), we obtain ν_{j_x+1}. Ω_x is given by

$$\Omega_x = \frac{1}{N_x!} \prod_{j_x=0}^{N_x-1} \frac{[M - m^2 k j_x]^{m^2 k} [M - (m-1)(mk-1) j_x]^{(m-1)(mk-1)}}{[M - m(mk-1) j_x]^{m(mk-1)} [M - mk(m-1) j_x]^{mk(m-1)}}. \tag{7.10}$$

After placing N_x horizontal rectangles we would like to determine the number of ways in which N_y vertical rectangles may be placed on the lattice. Given N_x horizontal rectangles and j_y vertical rectangles have already been placed, we estimate ν_{j_y+1}, the number of ways to place the $(j_y+1)^{th}$ vertical rectangle, using the same procedure as above. Now, we may choose an empty site A (see Fig. 7.6) randomly in $(M - m^2 k N_x - m^2 k j_y)$ ways to place the head of the $(j_y+1)^{th}$ vertical rectangle. As the vertical rectangles have their longer axis along y-direction, it can be easily seen that

$$\begin{aligned} \nu_{j_y+1} &= (M - m^2 k N_x - m^2 k j_y)[P_y(C|A)]^{mk-1} \\ &\times [P_x(B|A)]^{m-1} [P(D|B \cap C)]^{(m-1)(mk-1)}. \end{aligned} \tag{7.11}$$

The expressions for the conditional probabilities will now be modified due to the presence

of both horizontal and vertical rectangles. If A is empty, C may be empty or occupied by one of the mk sites on the long axis (passing through C) of a horizontal rectangle, or by one of the m sites on the short axis (passing through C) of a vertical rectangle. Hence, given A is empty, the probability that C is also empty is

$$P_y(C|A) = \frac{M - m^2kN_x - m^2kj_y}{M - mk(m-1)N_x - m(mk-1)j_y}. \tag{7.12}$$

Similarly, the probability of B being empty, given A is empty, is

$$P_x(B|A) = \frac{M - m^2kN_x - m^2kj_y}{M - m(mk-1)N_x - mk(m-1)j_y}. \tag{7.13}$$

Now the probability that B is empty, given C is empty, is

$$P_{xy}(B|C) = \frac{M - m^2kN_x - m^2kj_y}{M - (mk-1)(m-1)(N_x + j_y)}. \tag{7.14}$$

$P(D|B \cap C)$ is determined using Eqs. (7.6) and (7.8). Substituting Eqs. (7.12)–(7.14) into Eq. (7.11), we obtain ν_{j_y+1}. The total number of ways to place N_y vertical rectangles, given that N_x horizontal rectangles have already been placed, is then

$$\begin{aligned}
\Omega_y &= \frac{1}{N_y!}\prod_{j_y=0}^{N_y-1}\nu_{j_y+1} \\
&= \frac{1}{N_y!}\prod_{j_y=0}^{N_y-1}\frac{[M - m^2k(N_x + j_y)]^{m^2k}}{[M - m(mk-1)N_x + mk(m-1)j_y]^{mk(m-1)}} \\
&\times \frac{[M - (m-1)(mk-1)N_x - (m-1)(mk-1)j_y]^{(m-1)(mk-1)}}{[M - mk(m-1)N_x - m(mk-1)j_y]^{m(mk-1)}}.
\end{aligned} \tag{7.15}$$

The total number of ways to place N_x horizontal and N_y vertical rectangles on the lattice is given by

$$\Omega = \Omega_x\Omega_y. \tag{7.16}$$

Let ρ_x and ρ_y be the fraction of the sites occupied by the horizontal and the vertical rect-

angles, given by

$$\rho_i = \frac{m^2 k N_i}{M}, \quad i = x, y. \tag{7.17}$$

Using Eqs. (7.10) and (7.15), the entropy of the system per site in the thermodynamic limit may be expressed in terms of ρ_x and ρ_y as

$$\begin{aligned} s(\rho_x, \rho_y) &= \lim_{M\to\infty} \frac{1}{M} \ln\left(\Omega_x \Omega_y\right) \\ &= -\sum_{i=x,y} \frac{\rho_i}{m^2 k} \ln \frac{\rho_i}{m^2 k} - [1-\rho] \ln [1-\rho] \\ &- \left[1 - \frac{(m-1)(mk-1)}{m^2 k}\rho\right] \ln \left[1 - \frac{(m-1)(mk-1)}{m^2 k}\rho\right] \\ &+ \sum_{i=x,y} \left[1 - \frac{(mk-1)\rho + (k-1)\rho_i}{mk}\right] \ln \left[1 - \frac{(mk-1)\rho + (k-1)\rho_i}{mk}\right], \end{aligned} \tag{7.18}$$

where $\rho = \rho_x + \rho_y$ is the fraction of occupied sites.

The entropy $s(\rho_x, \rho_y)$ is not concave everywhere. The true entropy $\bar{s}(\rho_x, \rho_y)$ is obtained by the Maxwell construction such that

$$\bar{s}(\rho_x, \rho_y) = C\mathcal{E}\left[s(\rho_x, \rho_y)\right], \tag{7.19}$$

where $C\mathcal{E}$ denotes the concave envelope.

The entropy may also be expressed in terms of the total density $\rho = \rho_x + \rho_y$ and the nematic order parameter ψ, defined as

$$\psi = \frac{\rho_x - \rho_y}{\rho}. \tag{7.20}$$

ψ is zero in the isotropic phase and nonzero in the nematic phase. At a fixed density ρ, the preferred phase is obtained by maximizing $s(\psi)$ with respect to ψ. The transition density for the I-N transition is denoted by ρ_c^{I-N}. In Fig. 7.7, we show the plot of entropy $s(\psi)$ as a function of ψ, for three different densities near the I-N transition. For $\rho < \rho_c^{I-N}$ the entropy $s(\psi)$ is maximum at $\psi = 0$ i.e $\rho_x = \rho_y$, corresponding to the isotropic phase. Beyond ρ_c^{I-N} the entropy develops two symmetric maxima at $\psi = \pm\psi_0$, where $\psi_0 = 0$ at

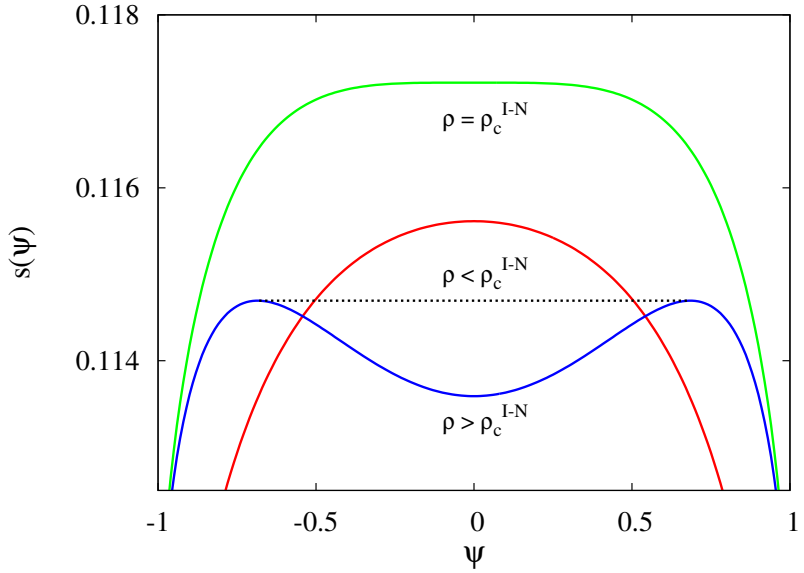

Figure 7.7: Entropy s as a function of the nematic order parameter ψ near the I-N transition ($\rho_c^{I-N} \approx 0.552$). The data are for $k = 4$ and $m = 2$. The dotted line denotes the concave envelope.

$\rho = \rho_c^{I-N}$. $\psi_0 \neq 0$ i.e. $\rho_x \neq \rho_y$ corresponds to the nematic phase. The order parameter ψ grows continuously with density ρ. This is a typical signature of a continuous transition with two equivalent broken symmetry phases. The entropy $s(\rho, \psi)$ is invariant under the transformation $\psi \leftrightarrow -\psi$ and contains only even powers of ψ, when expanded about $\psi = 0$. The critical density ρ_c^{I-N} may be obtained by solving $d^2 s/d\psi^2|_{\psi=0} = 0$ and is given by

$$\rho_c^{I-N} = \frac{2km}{mk^2 + m - k - 1}. \tag{7.21}$$

Asymptotic behavior of ρ_c^{I-N} is given by

$$\rho_c^{I-N} = \begin{cases} \frac{2}{k} + \frac{2}{mk^2} + O(k^{-3}), & k \to \infty, m \text{ fixed}, \\ \frac{2k}{1+k^2} + \frac{2k(1+k)}{(1+k^2)^2 m} + O(m^{-2}), & m \to \infty, k \text{ fixed}. \end{cases} \tag{7.22}$$

Thus, $A_1 = 2$.

When $m = 1$, the critical density $\rho_c^{I-N} = 2/(k-1)$, which matches with the exact calculation of ρ_c^{I-N} for the system of hard rods of length k on the RLTL [26]. It reflects that

the Bethe approximations becomes exact on the RLTL. For $m = 1$, the nematic phase and hence the I-N transition exists for $k \geq k_{min} = 4$. While for $m = 2$ and 3, $k_{min} = 3$, for $m \geq 4$ the nematic phase exists even for $k = 2$.

Virial expansion

In this subsection we determine ρ_c^{I-N} using a standard virial expansion truncated at the second virial coefficient. We closely follow the calculations of Zwanzig for oriented hard rectangles in the continuum [15]. The excess free energy of the system of hard rectangles (relative to the ideal gas) may be expressed in terms of the virial coefficients and the density. We truncate the series at the second virial coefficient and study the I-N transition in the limit $k \to \infty$.

Consider a system of N rectangles on the square lattice of volume V. Each rectangle may be oriented along two possible directions. Setting $\beta = 1$, the configurational sum of the system is given by,

$$Q_N = \frac{1}{N!2^N} \sum_{\mathbf{u}} \sum_{\mathbf{R}} \exp(-U_N), \tag{7.23}$$

where the sum over all possible positions and directions are denoted by $\sum_{\mathbf{R}}$ and $\sum_{\mathbf{u}}$ respectively, U_N is the total interaction energy of all rectangles. The excess free energy (relative to the ideal gas) ϕ_N of the system of rectangles having fixed orientations is defined by

$$\exp[-\phi_N(\mathbf{u})] = \frac{1}{V^N} \sum_{\mathbf{R}} \exp(-\beta U_N). \tag{7.24}$$

As the rectangles having same orientation are indistinguishable, ϕ_N depends only on the fractions of the rectangles pointing along the two possible directions. If the number of rectangles oriented along direction i is denoted by N_i, we may rewrite the Eq. (7.23) using

Eq. (7.24) as

$$\begin{aligned} Q_N &= \frac{V^N}{N!2^N} \sum_{N_1,N_2=0}^{N} \frac{N!}{N_1!N_2!} e^{-\phi_N(N_1,N_2)} \delta_{N_1+N_2,N} \\ &= \sum_{N_1=0}^{N} \sum_{N_2=0}^{N} W(N_1,N_2), \end{aligned} \tag{7.25}$$

where $\delta_{N_1+N_2,N}$ takes care of the constraint that the total number of rectangles is N and W is given by

$$W(N_1,N_2) = \frac{V^N}{2^N N_1!N_2!} \exp[-\phi_N(N_1,N_2)]. \tag{7.26}$$

In the thermodynamic limit $N \to \infty$ and $V \to \infty$, the above summation may be replaced by the largest summand W_{max} with negligible error. Thus the configurational free energy per particle is given by

$$F = -\lim_{N,V\to\infty} \frac{1}{N} \ln Q_N = -\lim_{N,V\to\infty} \frac{1}{N} W_{max}. \tag{7.27}$$

The fractions of rectangles pointing in the i -direction is denoted by $x_i = N_i/N$, such that $(x_1 + x_2) = 1$, and the number density of the rectangles is given by $N/V = \rho/m^2k$, where ρ is the total fraction of occupied sites. Equation (7.27) for the free energy may be expressed in terms of x_1 and x_2 as

$$F(x_1,x_2) = -1 + \ln 2 + \ln \frac{\rho}{m^2k} + \sum_{i=1}^{2} x_i \ln x_i + \frac{1}{N}\phi_N(\rho,x_1,x_2). \tag{7.28}$$

The virial expansion of the excess free energy ϕ_N, for a composition $\mathbf{x} = (x_1, x_2)$ of the rectangles is given by

$$-\frac{1}{N}\phi_N(\rho,\mathbf{x}) = \sum_{n=2} B_n(\mathbf{x}) \left(\frac{\rho}{m^2k}\right)^{n-1}, \tag{7.29}$$

where

$$\begin{aligned} B_n(\mathbf{x}) &= \frac{1}{Vn!}\int \sum \prod f \\ &= \frac{1}{Vn!}\sum_{j=0}^{n}\binom{n}{j}x_1^{n-j}x_2^j B(n-j,j) \\ &= \frac{1}{V}\sum_{j=0}^{n}\frac{B(n-j,j)}{(n-j)!\,j!}x_1^{n-j}x_2^j, \end{aligned} \tag{7.30}$$

where $\int \sum \prod f$ is the standard abbreviation for the cluster integrals over the irreducible graphs consisting on n rectangles with composition $\mathbf{x}$ and f denotes the Mayer functions, defined as

$$f = \exp(-U) - 1, \tag{7.31}$$

where U is the interaction energy. Due to the hard-core exclusion, we have $U = \infty$ for any intersection or overlap among the rectangles, otherwise $U = 0$. Hence

$$f = \begin{cases} -1, & \text{for any intersection} \\ 0, & \text{otherwise} \end{cases} \tag{7.32}$$

$B(n-j, j)$ denotes the sum of the irreducible n-particle graphs for the composition where $(n-j)$ rectangles are oriented along the x direction and j rectangles are along the y-direction.

As the total fraction $x_1 + x_2 = 1$, we set

$$\begin{aligned} x_1 &= x, \\ x_2 &= 1 - x. \end{aligned} \tag{7.33}$$

We consider up to the second virial coefficient and truncate the expansion in Eq. (7.29) at first order in ρ. From the definition of the virial coefficients in Eq. (7.30), we can easily

infer that they are symmetric in the following way:

$$B(n_1, n_2) = B(n_2, n_1). \tag{7.34}$$

Using Eq. (7.30) and the above symmetry property of $B(n_1, n_2)$, we can rewrite Eq. (7.29) as

$$\begin{aligned} -\frac{1}{N}\phi_N &\approx \frac{1}{2V}B(2,0)\left(\frac{\rho}{m^2k}\right)(2x^2 - 2x + 1) \\ &+ \frac{1}{V}B(1,1)\left(\frac{\rho}{m^2k}\right)(x - x^2) + O(\rho^2). \end{aligned} \tag{7.35}$$

Now we evaluate the virial coefficients. From Eq. (7.32) we can see that f has nonzero contributions only when the rods intersect. Thus the calculation of the virial coefficients on a lattice turns out as the problem of counting the number of disallowed configurations. By definition

$$\begin{aligned} B(2,0) &= B(0,2) = \int d^2R_1 \int d^2R_2 \; f_{12}(2,0) \\ &= -V \times (2mk - 1) \times (2m - 1), \end{aligned} \tag{7.36}$$

where $(2mk - 1) \times (2m - 1)$ is the number of disallowed configurations when both the rectangles are oriented along the same direction [see Fig. 7.8(a)]. Similarly

$$\begin{aligned} B(1,1) &= \int d^2R_1 \int d^2R_2 \; f_{12}(1,1) \\ &= -V \times (m + mk - 1)^2, \end{aligned} \tag{7.37}$$

where $(m + mk - 1)^2$ is the number of disallowed configurations when the two rectangles are oriented along different directions [see Fig. 7.8(b)].

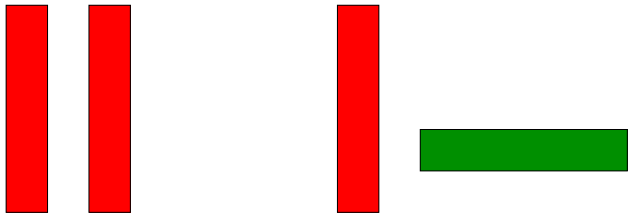

(a) (b)

Figure 7.8: Schematic diagram showing the orientations of two rectangles in the calculation of (a) $B(2,0)$ and (b) $B(1,1)$.

Substituting Eqs. (7.36) and (7.37) into Eq. (7.35), we find

$$\begin{aligned} -\frac{1}{N}\phi_N &\approx -\frac{1}{2}(2x^2-2x+1)\left(\frac{\rho}{m^2k}\right)(2m-1)(2mk-1) \\ &- (x-x^2)\left(\frac{\rho}{m^2k}\right)(m+mk-1)^2 + O(\rho^2). \end{aligned} \tag{7.38}$$

Now substituting Eq. (7.38) in Eq. (7.28), the expression for the free energy reduces to

$$\begin{aligned} F(x) &= -1+\log 2+\log\frac{\rho}{m^2k}+x\log x+(1-x)\log(1-x) \\ &+ (x-x^2)\left(\frac{\rho}{m^2k}\right)(m+mk-1)^2+(x^2-x+\frac{1}{2}) \\ &\times \left(\frac{\rho}{m^2k}\right)(2m-1)(2mk-1)+O(\rho^2). \end{aligned} \tag{7.39}$$

The preferred state at any fixed density is obtained by minimizing the free energy $F(x)$ with respect to x. For $\rho < \rho_c^{I-N}$, $F(x)$ is minimized for $x = 1/2$, corresponding to the isotropic phase, and beyond ρ_c^{I-N}, $F(x)$ is minimized for $x \neq 1/2$, corresponding to the nematic phase. Thus the system undergoes a transition from an isotropic phase to a nematic phase with increasing density. The I-N transition is found to be continuous with the critical density ρ_c^{I-N}. The expansion of the free energy $F(x)$ as a power series in x about $x = 1/2$ contains only even powers, and thus the critical density ρ_c^{I-N} may be determined by solving

$$\frac{d^2}{dx^2}F(x)|_{x=\frac{1}{2}} = 0. \tag{7.40}$$

Solving Eq. (7.40) for ρ, we find

$$\rho_c^{I-N} = \frac{2k}{(k-1)^2}, \tag{7.41}$$

which independent of m, for all k. The asymptotic behavior of ρ_c^{I-N} is given by

$$\rho_c^{I-N} = \frac{2}{k} + \frac{4}{k^2} + O(k^{-2}), \text{ when } k \to \infty. \tag{7.42}$$

Comparing Eq. (7.22) and Eq. (7.42), we see that both the Bethe approximation and the virial theory predicts $\rho_c^{I-N} \approx A_1/k$ for $k \gg 1$, where $A_1 = 2$.

7.4.2 Nematic–columnar (N-C) phase boundary

Bethe approximation

To obtain the asymptotic behavior of the N-C phase boundary, we use the same ad-hoc Bethe approximation scheme for rods due to DiMarzio [28], adapted to other shapes [138]. To estimate the phase boundary of the nematic–columnar transition for $m \times mk$ rectangles on the square lattice with $M = L \times L$ sites, we require the entropy as a function of the occupation densities of the m types of rows/columns. The calculations become much simpler, if we consider a fully oriented phase with only horizontal rectangles. Now, the nematic phase corresponds to the the phase where there is equal occupancy of each of the m types of rows, while the columnar phase breaks this symmetry and preferentially occupies one type of row. For this simplified model with only one orientation, we estimate the entropy as detailed below. We present the calculation for $m = 2$, classifying the rows as even and odd rows. Generalization to higher values of m is straight forward.

Let there be N_e (N_o) number of rectangles whose heads occupy even (odd) rows. We first place the N_e rectangles one by one on the even rows. Given that j_e rectangles have already been placed, the number of ways in which the $(j_e + 1)^{th}$ rectangle can be placed may be

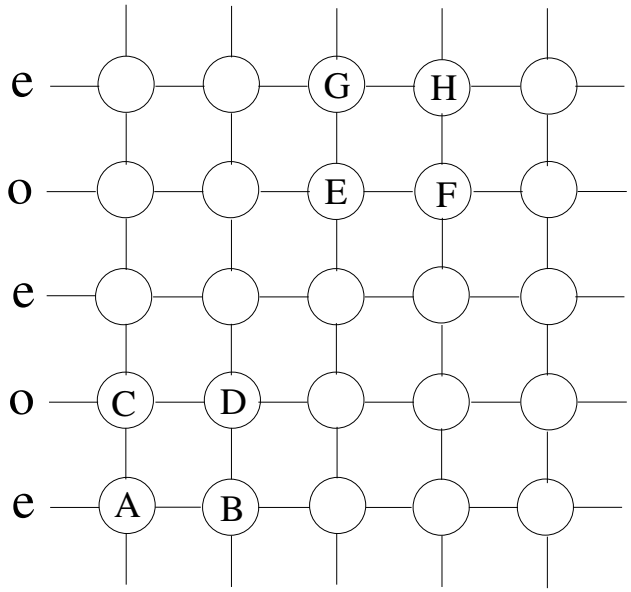

Figure 7.9: Schematic diagram showing the positions of sites A–F to aid the explanation of the calculation of the nematic–columnar phase boundary. Even and odd rows are denoted by e and o respectively.

estimated as follows. The head of the $(j_e + 1)^{th}$ rectangle has to be placed on an empty site of an even row. We denote this site by A (see Fig. 7.9). The site A may be chosen at random in $(M/2 - 2kj_e)$ ways, $M/2$ being the number of sites in even rows and $2kj_e$ being the number of occupied sites in the even rows by the j_e rectangles. We now require that the $2k - 1$ consecutive sites to the right of A are also empty. The probability of this being true is $[P_x(B|A)]^{2k-1}$, where $P_x(B|A)$ is the conditional probability that B (see Fig. 7.9) is empty given that A is empty. In terms of M and j_e, $P_x(B|A)$ is given by

$$P_x(B|A) = \frac{\frac{M}{2} - 2kj_e}{\frac{M}{2} - 2kj_e + j_e}. \tag{7.43}$$

To place the $(j_e + 1)^{th}$ rectangle, we also require that the site C (see Fig. 7.9) and the $2k - 1$ consecutive sites to the right of C are also empty. The probability of this being true is $P_y(C|A) \times P_{xy}(D|B \cap C)^{2k-1}$, where $P_y(C|A)$ is the conditional probability that C is empty given A is empty, and $P_{xy}(D|B \cap C)$ is the conditional probability that D (see Fig. 7.9) is empty given that both B and C are empty. Sites C and D belongs to an odd row. Since both

A and B are empty, C and D can be occupied only by rectangles with heads in the same odd row. But, there are no such rectangles. Therefore, $P_y(C|A) = 1$, and $P_{xy}(D|B \cap C) = 1$. Thus, given that j_e rectangles have been placed, the $(j_e + 1)^{th}$ rectangle may be placed in

$$\nu_{j_e+1} = \left(\frac{M}{2} - 2kj_e\right) \times [P_x(B|A)]^{2k-1} \tag{7.44}$$

ways. Hence, the total number of ways of placing N_e rectangles with heads on even rows is

$$\begin{aligned} \Omega_e &= \frac{1}{N_e!} \prod_{j_e=0}^{N_e-1} \nu_{j_e+1} \\ &= \frac{1}{N_e!} \prod_{j_e=0}^{N_e-1} \frac{(\frac{M}{2} - 2kj_e)^{2k}}{(\frac{M}{2} - 2kj_e + j_e)^{2k-1}}. \end{aligned} \tag{7.45}$$

Keeping the N_e rectangles with heads on even rows, we now place N_o rectangles one by one with their heads on the odd rows. Given that j_o rectangles have been placed on the odd rows, the number of ways of placing the $(j_o + 1)^{th}$ rectangle may be estimated as follows. The head of the $(j_o + 1)^{th}$ rectangle must be placed on an empty site on an odd row. We denote this site by E (see Fig. 7.9). E may be chosen in $(\frac{M}{2} - 2kN_e - 2kj_o)$ ways, where we have ignored correlations between rectangles. Here $2kN_e$ is the number of occupied sites in the odd rows due to the N_e rectangles with their heads on the even rows, and the $2kj_o$ is the number of sites occupied by j_o rectangles on odd rows. We now require that the $2k-1$ consecutive sites to the right of E are also empty. The probability of this being true is $[P_x(F|E)]^{2k-1}$, where $P_x(F|E)$ is the conditional probability that F (see Fig. 7.9) is empty given that E is empty. $P_x(F|E)$ is given by

$$P_x(F|E) = \frac{M/2 - 2kN_e - 2kj_o}{M/2 - 2kN_e - 2kj_o + N_e + j_o}, \tag{7.46}$$

where we have again ignored all correlations.

For placing the $(j_o + 1)^{th}$ rectangle, we also require that the site G (see Fig. 7.9) and the

$2k-1$ consecutive sites to the right of G are also empty. The probability of this being true is $P_y(G|E) \times P_{xy}(H|F \cap G)^{2k-1}$, where $P_y(G|E)$ is the conditional probability that G is empty given E is empty, and $P_{xy}(H|F \cap G)$ is the conditional probability that H (see Fig. 7.9) is empty given that both F and G are empty. Ignoring correlations, $P_y(G|E)$ is given by

$$P_y(G|E) = \frac{M/2 - 2kN_e - 2kj_o}{M/2 - 2kj_o}. \tag{7.47}$$

As discussed before, to overcome the problem of the resultant entropy not being symmetric with respect to N_e and N_o, we follow the Bethe approximation proposed in Ref. [138],

$$\begin{aligned} P(H|F \cap G) &= \frac{P(F \cap G|H)P(H)}{P_{xy}(G|F)P(F)}, & (7.48)\\ &\approx \frac{P_x(G|H)P_y(F|H)}{P_{xy}(G|F)}. & (7.49) \end{aligned}$$

where in Eq. (7.48), we use $P(H) = P(F)$ and in Eq. (7.49), we replace $P(F \cap G|H)P(H)$ by $P_x(G|H)P_y(F|H)$, which is an approximation.

In Eq.(7.49), from symmetry, it is easy to see that $P_x(G|H) = P_x(F|E)$ and $P_y(F|H) = P_y(G|E)$ and can be read off from Eqs. (7.46) and (7.47). To obtain an expression for $P_{xy}(G|F)$, the probability that G is empty, given that the site F is empty, we again ignore correlations. We then obtain

$$P_{xy}(G|F) = \frac{M/2 - 2kN_e - 2kj_o}{M/2 - 2kj_o + j_o}. \tag{7.50}$$

The number of ways of placing the $(j_o+1)^{th}$ rectangle is

$$\begin{aligned} \nu_{j_o+1} &= \left(\frac{M}{2} - 2kN_e - 2kj_o\right) \times P_x(F|E)]^{2k-1} \\ &\times P_y(G|E) \times [P(H|G \cap F)]^{2k-1}. & (7.51) \end{aligned}$$

Substituting for each of the quantities on the right hand side, we obtain the total number

of ways of placing the N_o rectangles on the odd rows as

$$\begin{aligned}\Omega_o &= \frac{1}{N_o!}\prod_{j_o=0}^{N_o-1} v_{j_o+1} \\ &= \frac{1}{N_o!}\prod_{j_o=0}^{N_o-1}\frac{(\frac{M}{2}-2kN_e-2kj_o)^{4k}}{(\frac{M}{2}-2kj_o)^{2k}} \\ &\quad\times\frac{(\frac{M}{2}-2kj_o+j_o)^{2k-1}}{(\frac{M}{2}-2kN_e-2kj_o+N_e+j_o)^{4k-2}}.\end{aligned} \tag{7.52}$$

We would like to express the entropy in terms of the total density ρ and the densities of occupied sites in even and odd rows, given by ρ_e and ρ_o respectively. Clearly,

$$\rho_e = \frac{4kN_e}{M}, \tag{7.53}$$

$$\rho_o = \frac{4kN_o}{M}, \tag{7.54}$$

$$\rho = \rho_e + \rho_o. \tag{7.55}$$

The entropy per site $s(\rho_e,\rho_o)$ in the thermodynamic limit is given by

$$s(\rho_e,\rho_o) = \lim_{M\to\infty}\frac{1}{M}\ln\left(\Omega_0\Omega_e\right). \tag{7.56}$$

Substituting for Ω_e and Ω_o from Eqs. (7.45) and (7.52), we obtain

$$\begin{aligned}s(\rho_e,\rho_o) &= -\sum_{i=o,e}\frac{\rho_i}{4k}\ln\frac{\rho_i}{2k} - (1-\rho)\ln(1-\rho) + \left(1-\rho+\frac{\rho}{2k}\right)\ln\left(1-\rho+\frac{\rho}{2k}\right) \\ &\quad + \sum_{i=o,e}\frac{1-\rho_i}{2}\ln(1-\rho_i) - \frac{1}{2}\sum_{i=o,e}\left(1-\rho_i+\frac{\rho_i}{2k}\right)\ln\left(1-\rho_i+\frac{\rho_i}{2k}\right).\end{aligned} \tag{7.57}$$

We express the entropy $s(\rho_e,\rho_o)$ in terms of density ρ and the order parameter ψ_{N-C}, defined as

$$\psi_{N-C} = \frac{\rho_e-\rho_o}{\rho}. \tag{7.58}$$

ψ_{N-C} is zero in the nematic phase and nonzero in the columnar phase. For a fixed value

of ρ, the equilibrium values of ρ_o and ρ_e are determined by maximizing the entropy $s(\rho, \psi_{N-C})$ with respect to ψ_{N-C}. In Fig. 7.10 we show the variation of entropy $s(\rho, \psi_{N-C})$ with ψ_{N-C} for different densities. For small values of ρ, the entropy is maximized by $\psi_{N-C} = 0$, *i.e*, $\rho_e = \rho_o$. Beyond a critical density ρ_c^{N-C}, $s(\rho, \psi_{N-C})$ is maximized by $\psi_{N-C} \neq 0$, *i.e*, $\rho_e \neq \rho_o$. ψ_{N-C} grows continuously with ρ for $\rho > \rho_c^{N-C}$, and thus the transition for $m = 2$ is continuous.

The expansion of $s(\rho, \psi_{N-C})$ in powers of ψ_{N-C} has only even powers of ψ_{N-C} since $s(\rho, \psi_{N-C})$ is invariant when $\psi_{N-C} \leftrightarrow -\psi_{N-C}$. Thus, the critical density is obtained from the condition $d^2 s/d\psi_{N-C}^2|_{\psi_{N-C}=0} = 0$. This gives

$$\begin{aligned} \rho_c^{N-C} &= \frac{-1 + 4k - \sqrt{1 - 4k + 8k^2}}{2k - 1} \\ &= (2 - \sqrt{2}) + \frac{A}{k} + O(k^{-2}), \end{aligned} \tag{7.59}$$

where $A = (\frac{1}{2} - \frac{1}{2\sqrt{2}}) > 0$. We note that as $k \to \infty$, ρ_c^{N-C} tends to a k independent value and that the transition exists for all $k \geq 2$.

We can similarly calculate the entropy for $m = 3$ and then generalize the expression of entropy for arbitrary m and k. Now, there are m densities $\rho_1, \rho_2, \ldots, \rho_m$, corresponding to the m types of rows. In terms of them, the entropy is given by

$$\begin{aligned} s(\{\rho_i\}) &= -\sum_{i=1}^{m} \frac{\rho_i}{m^2 k} \ln \frac{\rho_i}{mk} - (1-\rho)\ln(1-\rho) + \left(1 - \rho + \frac{\rho}{mk}\right) \ln\left(1 - \rho + \frac{\rho}{mk}\right) \\ &\quad + \sum_{i=1}^{m} \frac{1 - \rho + \rho_i}{m} \ln(1 - \rho + \rho_i) - \frac{1}{m} \sum_{i=1}^{m} \left(1 - \rho + \rho_i + \frac{\rho - \rho_i}{mk}\right) \\ &\quad \times \ln\left(1 - \rho + \rho_i + \frac{\rho - \rho_i}{mk}\right). \end{aligned} \tag{7.60}$$

Here, we define the order parameter to be

$$\psi_{N-C} = \frac{\rho_1 - \rho_2}{\rho}, \tag{7.61}$$

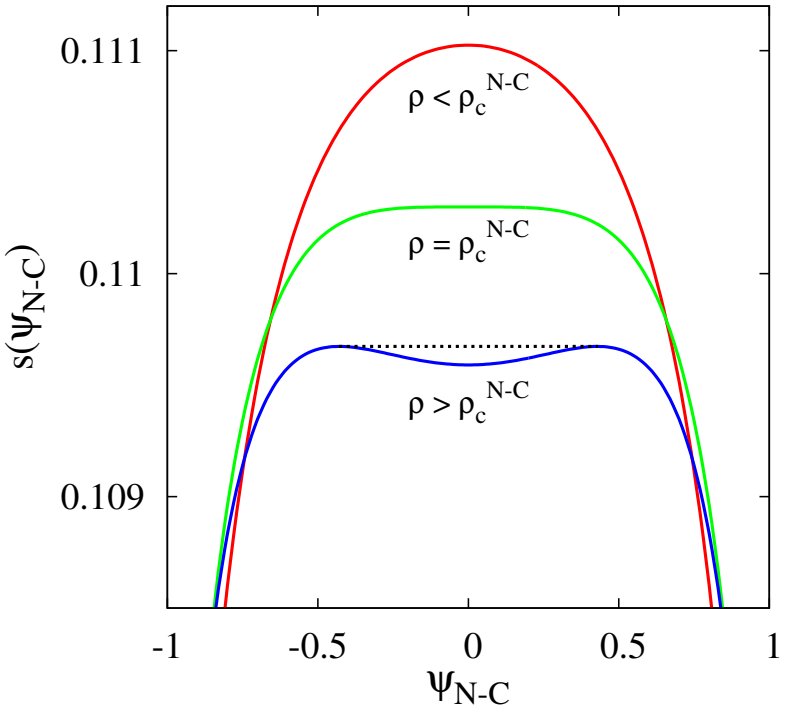

Figure 7.10: Entropy as a function of the order parameter ψ_{N-C} for $m = 2$ near the N-C transition ($\rho_c^{N-C} \approx 0.624$). The data are for $k = 4$. The dotted line denotes the concave envelope.

where we set $\rho_2 = \rho_3 = \ldots = \rho_m$. Now, $s(\psi_{N-C}, \rho)$ is not invariant when $\psi_{N-C} = -\psi_{N-C}$. Thus, when expanded in powers of ψ_{N-C}, $s(\psi_{N-C}, \rho)$ has cubic terms, making the transition first order. This is illustrated in Fig. 7.11 which shows the variation of entropy with ψ_{N-C} for different ρ near the N-C transition. For low densities $s(\psi_{N-C})$ exhibit a single peak at $\psi_{N-C} = 0$, but with increasing ρ a secondary maximum gets developed at $\psi_{N-C} \neq 0$. For $\rho = \rho_c^{N-C}$ the maximum at $\psi_{N-C} = 0$ and $\psi_{N-C} \neq 0$ becomes of equal height. Beyond ρ_c^{N-C} the global maximum of $s(\psi_{N-C}, \rho)$ jumps to $\psi_{N-C} \neq 0$, making the N-C transition to be first order.

Unlike the $m = 2$ case, there is no way to obtain an analytic expression for ρ_c^{N-C}. For m=3, the numerically determined ρ_c^{N-C} for different k is shown in Fig. 7.12. From the data, we obtain

$$\rho_c^{N-C} = 0.62875 + \frac{0.107}{k}, \quad m = 3. \tag{7.62}$$

We note that this expression has the same form as for $m = 2$ [see Eq. (7.59)].

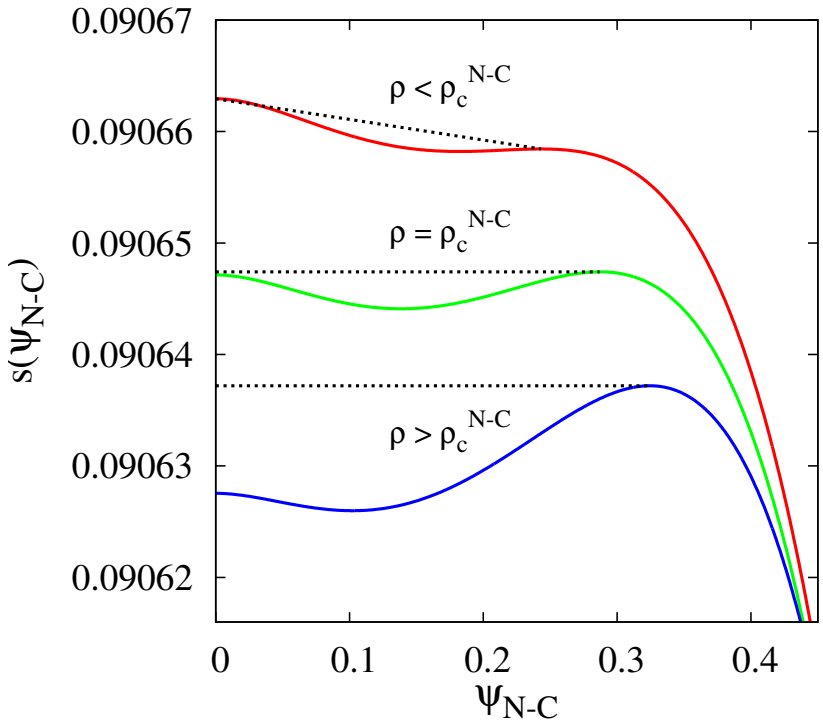

Figure 7.11: Entropy as a function of the order parameter ψ_{N-C} for m=3 near the N-C transition ($\rho_c^{N-C} \approx 0.684$). The data are for $k = 2$. The dotted lines denote the concave envelopes. The curves have been shifted for clarity.

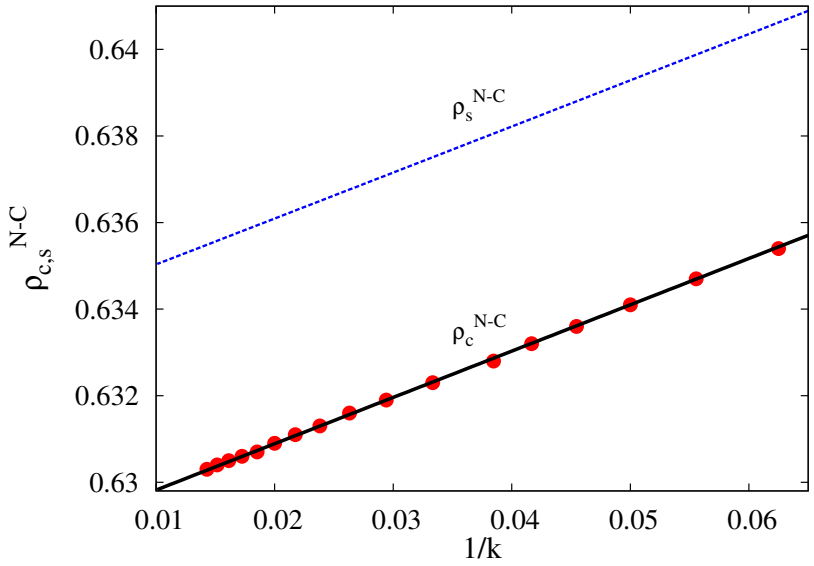

Figure 7.12: The critical density ρ_c^{N-C} and the spinodal density ρ_s^{N-C}, obtained from the Bethe approximation, as a function of $1/k$ for $m = 3$. The solid line is $0.62875 + 0.107/k$.

For $m > 3$, we proceed as follows. The transition density ρ_c^{N-C} is bounded from above by the spinodal density ρ_s^{N-C}, the density at which the entropy at $\psi_{N-C} = 0$ changes from a local maximum to local minimum. ρ_s^{N-C} is obtained from the condition $d^2s/d\psi_{N-C}^2|_{\psi_{N-C}=0} = 0$ and we obtain

$$\rho_s^{N-C} = \frac{-m + 2km^2 - m\sqrt{1 - 4k + 4k^2m}}{2(1 - m - km + km^2)} \geq \rho_c^{N-C}, \tag{7.63}$$

$$= \frac{\sqrt{m}}{1 + \sqrt{m}} + \frac{B_1(m)}{k} + O\left(k^{-2}\right),\ k \to \infty, \tag{7.64}$$

$$= 1 - \frac{1}{\sqrt{m}} + \frac{B_2(k)}{m} + O\left(m^{-3/2}\right),\ m \to \infty, \tag{7.65}$$

where $B_1(m) = \frac{1}{2(m+\sqrt{m})}$ and $B_2(k) = (1 + \frac{1}{2k})$. The spinodal density is compared with ρ_c^{N-C} in Fig. 7.12. From Eq. (7.65), it follows that $\rho_s^{N-C} \leq 1$ and tends to one when $m, k \to \infty$. The limit $m \to \infty$ corresponds to the continuum limit. In this limit $\rho_s^{N-C} \to 1$. Thus, it is not clear whether the nematic–columnar phase transition will exist in the continuum.

7.4.3 Columnar–sublattice (C-S) phase boundary

The sublattice phase at high densities exists only when the length and width of the rectangles are not mutually prime. The dependence of the C-S phase boundary on m and k may be determined by estimating the entropy for the C and S phases close to full packing. We approximate the entropy of the C phase by the entropy of the fully aligned C phase. Since the heads of the rectangles are all in either even or odd rows/columns, by ignoring the unoccupied rows/columns, the calculation of entropy reduces to a one-dimensional problem of rods. The mean number of holes in a row is $L(1 - \rho)$, and the mean number of rods (of length mk) in a row is $\frac{\rho L}{mk}$. There are L/m such rows. The number of ways of arranging the rods and holes on a row is

$$\Omega_{row} = \frac{[L(1 - \rho) + \frac{\rho L}{mk}]!}{[L(1 - \rho)]![\frac{\rho L}{mk}]!}, \tag{7.66}$$

such that the total number of ways of arranging the rectangles is $\Omega_{row}^{L/m}$. Hence, $\mathcal{S}_C$, the entropy per site of the columnar phase is given by $\mathcal{S}_C = (Lm)^{-1} \ln \Omega_{row}$, which for densities close to 1 is

$$\mathcal{S}_C \approx \frac{1-\rho}{m} \ln\left[\frac{e}{km(1-\rho)}\right] + O[(1-\rho)^2]. \tag{7.67}$$

We now estimate the entropy for the sublattice phase. At full packing, the head of each rectangle occupies one of m^2 sublattices. Ignoring the sites belonging to other sublattices, it is easy to see that each configuration of rectangles can be mapped on to a configuration of rods of length k on a lattice of size $L/m \times L/m$. Thus, the entropy per site at full packing may be estimated by solving the problem of rods [20]. We have already discussed in Sec. 1.1.3 that a lower bound on the entropy of an orientationally disordered phase on a lattice of size $\ell \times \ell$ at full coverage may be estimated by breaking the lattice into strips of size $k \times \ell$. The number of ways of covering a strip with rods of size k is given by $F_\ell \approx \lambda^\ell$, where λ is the largest root of the equation

$$\lambda^k - \lambda^{k-1} - 1 = 0. \tag{7.68}$$

Asymptotic form of the solution for $k \gg 1$ is given by,

$$\lambda = 1 + \frac{\ln k}{k} - \frac{\ln \ln k}{k} + \frac{\ln \ln k}{k \ln k} + \text{higher-order terms}. \tag{7.69}$$

Hence, the total number of ways of covering the lattice of size $\ell \times \ell$ with rods of length k is given by $\Omega = [F_\ell]^{\ell/k} \approx \lambda^{\ell^2/k}$. Now we replace ℓ by L/m and find the entropy per site of the sublattice phase at full packing for the system of rectangles as,

$$\begin{aligned} \mathcal{S}_S(\rho = 1) &= \frac{1}{L^2} \ln \Omega \\ &\approx \frac{\ln k}{m^2 k^2}, \; k \gg 1 \end{aligned} \tag{7.70}$$

For densities close to 1 ($\rho = 1 - \epsilon$) we estimate the correction term to $\mathcal{S}_S(\rho = 1)$ by

removing $\epsilon/(m^2k)$ fraction of rectangles at random from the fully packed state. Here, we ignore the entropy of the holes, assuming that the holes form bound states. This gives the entropy of the sublattice phase, close to the full packing to be approximately

$$\mathcal{S}_S \approx \frac{\ln k}{m^2k^2} - \frac{1}{m^2k}[(1-\rho)\ln(1-\rho) + \rho\ln\rho], \quad k \gg 1, \tag{7.71}$$

Comparing Eqs. (7.67) and (7.71) up to the leading order we obtain the critical density for the C-S transition to be

$$\rho_c^{C-S} \approx 1 - \frac{A_4}{mk^2}, \; k \gg 1, \tag{7.72}$$

where $A_4 > 0$ is a constant.

7.5 Summary and discussion

For $k \geq 7$, the system of long, hard rectangles of size $m \times mk$ on the square lattice undergoes three entropy-driven phase transitions with density: first from a low-density I phase to an intermediate density N phase, second from the N phase to a C phase and third from the C phase to a HD phase. The HD phase is a S phase when the length and width of the rectangles are not mutually prime. In this chapter, we study the asymptotic behavior of the I-N, N-C and C-S phase boundaries when $k \gg 1$. From extensive Monte carlo simulations of systems with $m = 1$, 2 and 3, we establish that $\rho_c^{I-N} \approx A_1/k$, for $k \gg 1$, where A_1 is independent of m and is estimated to be 4.80 ± 0.05, the numerical value being consistent with that obtained from simulation of oriented lines [97]. The maximum value of k we studied is 60, while earlier simulations having been restricted up to $m = 1$ and $k = 12$ [112]. The I-N transition was also studied analytically using an ad-hoc Bethe approximation and a truncated virial expansion. Both these theories support the numerical result $\rho_c^{I-N} \approx A_1/k$, for $k \gg 1$, where A_1 is independent of m. Within both these theories, we obtain $A_1 = 2$.

The Bethe approximation, while taking into account nearest neighbor correlations, ignores other correlations and there appears to be no systematic way of improving the calculations to obtain better estimates of A_1. On the other hand, the virial expansion truncated at the second virial coefficient is known to become exact in three dimensions when $k \to \infty$. But in two dimensions, higher order virial coefficients contributes significantly. To confirm this, we computed the higher order virial coefficients. As $B_2 \sim k^2$ [see Eqs. (7.37)], in the limit $k \to \infty$, $B_2 \times \rho/k \sim O(1)$. We can rewrite Eq. (7.29) as

$$\begin{aligned} -\frac{1}{N}\phi_N(\mathbf{x}) &\approx B_2(\mathbf{x})\frac{\rho}{m^2k} + \frac{B_3(\mathbf{x})}{[B_2(\mathbf{x})]^2}\left[B_2(\mathbf{x})\frac{\rho}{m^2k}\right]^2 \\ &+ \frac{B_4(\mathbf{x})}{[B_2(\mathbf{x})]^3}\left[B_2(\mathbf{x})\frac{\rho}{m^2k}\right]^3 + O(\rho^4). \end{aligned} \tag{7.73}$$

When $k \gg 1$, it can be verified that $B_3 \sim O(k^3)$ and hence $B_3/[B_2]^2 \sim O(1/k)$. Quite interestingly we find $B_4 \sim O(k^6)$ and $B_4/[B_2]^3 \sim O(1)$. Thus B_4 will have non negligible contribution to ρ_c^{I-N}. In general $B_{2n} \sim O(k^{4n-2})$, implying all the even virial coefficients will have non negligible contributions. Usually, the number of diagrams required to compute higher order virial coefficients increase rapidly with order. However, here the number of diagrams are of order one. Hence, it may be possible to determine A_1 exactly by taking into account all the even virial coefficients.

We also investigated the asymptotic behavior of ρ_c^{N-C} both numerically and analytically. By performing numerical simulations for $m = 2$, we find $\rho_c^{N-C} \approx 0.73 + 0.23k^{-1}$ when $k \gg 1$. The Bethe approximation predicts: $\rho_c^{N-C} \approx A_2(m) + A_3(m)/k$, for $k \gg 1$ which is in qualitative agreement with the numerical results. Recently, similar behavior is also observed using truncated high activity expansion. Further, asymptotic dependence of A_2 and A_3 on m is also obtained [139]. But numerical study of the large m behavior is restricted due to large relaxation times at high densities.

Entropy estimates of the columnar and sublattices phases gives, the critical density for the C-S transition $\rho_c^{C-S} \approx 1 - A_4/(mk^2)$ for $k \gg 1$, where A_4 is a constant. However, we

could not numerically verify this claim as it becomes difficult to equilibrate the system at densities close to one due to the presence of long-lived metastable states. The limit $m \to \infty$, keeping k fixed corresponds to the continuum limit of oriented rectangles. In this limit, $\rho_c^{C-S} \to 1$, implying that the sublattice phase will not survive in continuum. But we expect the nematic and columnar phases to exist.

Density-functional theory calculations for a system of hard rectangles with restricted orientation in the continuum, confined in a two-dimensional square nanocavity, predicts that the system will exhibit nematic, smectic, columnar and solid-like phases, where the solid-like phase has both orientational and complete positional order [140]. In contrast, we do not find any evidence of smectic or solid-like phases when m or k tend to ∞, the continuum limit. In particular, on lattices the maximal density phase of a monodispersed system does not have orientational order [10, 20].

We showed that the critical Binder cumulant for the N-C transition decreases as k^{-1} with increasing the aspect ratio k of the rectangles. The critical Binder cumulant in the Ising model on rectangular geometry decreases as α^{-1}, where α is the aspect ratio of the lattice [131]. Whether a mapping between k and α exists is an open question. Curiously, the critical Binder cumulant is zero when $k \to \infty$ (or $\alpha \to \infty$). In the Ising model, this has been interpreted as the absence of transition on one-dimensional geometries [131]. However, the hard rectangle system shows a transition at $k \to \infty$. It is possible that in this limit, the fluctuations at the transition become Gaussian.

Chapter 8

Conclusion and future directions

In this chapter, we summarize the main results of the thesis and list some open problems. We considered the system of hard rectangles of size $m \times mk$ on lattices and studied its phase diagram in detail.

In **Chapter 2**, we described a Monte carlo algorithm to study the systems of hard extended objects on lattices by implementing it for the system of hard rods ($m = 1$) and rectangles ($m > 1$). The algorithm overcomes the problem of large relaxation times at high densities and is easily generalizable for hard particles of other shapes. In addition, the algorithm is highly parallelizable which makes it efficient to study large system sizes and higher-dimensional systems. Various parallel computing techniques were also discussed.

In **Chapter 3**, we studied the system of monodispersed hard rods ($m = 1$) on lattices which is known to exhibit a nematic phase at intermediate densities for $k \geq 7$. We showed the existence of a second transition from the nematic phase to a high density disordered phase with increasing density for $k = 7$ on both square and triangular lattices, and examined the nematic–disordered transition in detail using Monte carlo simulations. The nematic phase becomes unstable at high activities. This metastability of the nematic order is explained within the classical Kolmogorov-Johnson-Mehl-Avrami nucleation theory. The transition is found to be continuous on both the lattices. On the square lattice, the critical

behavior of this transition differs from that of the first transition (low-density disordered–nematic), which raises the question whether the high-density disordered phase is similar to the low-density disordered phase. Nature of the high-density disordered phase is investigated by studying the correlations, cluster size distribution, stack distribution and spatial distribution of holes. Existence of a crossover length scale $\xi^* \gtrsim 1400$ is observed on the square lattice, within which the correlations decay algebraically. The distribution of stacks and holes exhibits similar behavior in the low and high-density disordered phases. Although the estimated critical exponents differ from those of the Ising model, we could not rule out a crossover to the Ising universality class for length scales $\gg \xi^*$. On the triangular lattice, the critical exponents of the nematic–disordered transition are consistent with the first transition, belonging to the three-state Potts universality class. Unlike the square lattice case, here, we do not find any extended regime where the correlations decay algebraically.

In **Chapter 4**, we studied the model of monodispersed repulsive rods of length k on the random locally tree-like layered lattice to better understand the high density phase. In this model, rods of different orientations are allowed to intersect, but with an energy cost. We solved the model exactly to compute the free energy and showed that for $k \geq 4$, the system undergoes two transition with increasing density: first from a low-density disordered to a nematic phase and second from the nematic to a high-density disordered phase. When the coordination number is 4, both the transitions are found to be continuous, belonging to the mean field Ising universality class. For even coordination number larger than 4, while the first transition becomes discontinuous, the nature of the second transition depends on the length of the rod and the intersection parameters. From the phase behavior, we argue that one may go from the low-density disordered phase to the high-density disordered phase without encountering any phase transition, implying both the phases have similar symmetry. Hence, we concluded that the high-density phase is a reentrant disordered phase.

Transition	*Nature*
Isotropic-sublattice (I-S)	Ashkin-Teller universality
Isotropic-columnar (I-C)	Ashkin-Teller universality or first order
Isotropic-nematic (I-N)	Ising universality
Nematic-columnar (N-C)	Ising universality
Columnar-sublattice (C-S)	Ashkin-Teller universality

Table 8.1: Table showing nature of different phase transitions for $2\times 2k$ rectangles, where k is integer. Universality classes of the continuous transitions are given.

Chapter 5 was devoted to study the equilibrium phase behavior of the system of monodispersed hard rectangles of size $m \times mk$ on a square lattice using numerical simulations. Here, we restricted the aspect ratio k to be integer. When $m = 2$ and 3, for $k \geq 7$, with increasing density, the system transits successively from isotropic (I) to nematic (N) to columnar (C) to solid-like sublattice (S) phase. When $k < 7$, the N phase is absent. For $2 \leq k < 7$ when $m \geq 3$, and for $4 \leq k < 7$ when $m = 2$, the system undergoes two transitions with increasing density: first from the I phase to the C phase and second, from the C phase to the S phase. The C phase does not exist for $k = 2, 3$ when $m = 2$, and the system makes a direct transition from the I phase to the S phase. We also determined the nature of the different phase transitions. When $m = 2$, all the transitions are found to be continuous except the I-C transition, which is continuous for $k = 5$ and discontinuous for $k = 6$. Universality classes for the different continuous transitions are summarized in Table 8.1. For $m = 3$, the I-N transition remains in the Ising universality class, but the other transitions become first order.

In **Chapter 6**, we numerically obtained the phase diagram of the system of hard rectangles of size $m \times mk$ with non-integer aspect ratio k. The system may exist in four different phases: I, N, C or high density (HD) phases. The HD phase is a disordered phase when the length and width of the rectangles are mutually prime, else, it is a S phase with complete positional order. The N phase is found to exist only when $k \geq 15/2$ for $m = 2$ and when $k \geq 22/3$ for $m = 3$. We obtained tighter bounds for k_{min}^{I-N}, the smallest value of k beyond which the N phase exists. We concluded that $20/3 < k_{min}^{I-N} \leq 7$. The bounds for k_{min}^{I-C}, the

minimum value of k beyond which the C phase exists, are not so clear. We find that the C phase exists when $k \geq 11/2$ for $m = 2$ and when $k \geq 13/3$ for $m = 3$. On the other hand, for integer k, the C phase exists for $k \geq 4$ for $m = 2$ and when $k \geq 2$ for $m = 3$. Thus, unlike for the N phase, k_{min}^{I-C} depends both on m and whether k is a integer or not, and it is not possible to combine the bounds in a tighter form. When $m = 2$, the I-C transition is found to be first order, while both the I-N and N-C transition are continuous and belong to the Ising universality class. The phase diagram for large m is expected to be qualitatively similar to that for $m = 2$, but the nature of the different transitions, except the isotropic–nematic transition, may be different.

Chapter 7, contains the study of the asymptotic behavior of the isotropic–nematic (I-N), nematic–columnar (N-C) and columnar–sublattice (C-S) phase boundaries for the hard rectangles system using Monte carlo simulations and analytical calculations. By simulating systems up to $k = 60$ for $m = 1$ and $k = 56$ for $m = 2$ and 3, we showed that the critical density for the I-N transition $\rho_c^{I-N} \approx A_1/k$, when $k \gg 1$, where A_1 is independent of m and equals to 4.80 ± 0.05. The N-C phase boundary is studied numerically for $m = 2$ and k up to 24. We estimate $\rho_c^{N-C} \approx 0.73 + 0.23k^{-1}$ for large k. Binder cumulant for the N-C transition is found to be non-universal and decreases as k^{-1} for $k \gg 1$. However, the critical exponents belong to the Ising universality class for all k. Numerical simulations of the C-S phase transitions for large k is constrained by large relaxation times at high densities.

The I-N phase boundary is also studied analytically using virial expansion truncated at the second virial coefficient and Bethe approximation. Within both the theories we obtained $\rho_c^{I-N} \approx A_1/k$ for $k \gg 1$, where $A_1 = 2$. In particular, using virial expansion we find ρ_c^{I-N} to be independent of m, for all k. Bethe approximation for the N-C transition predicts $\rho_c^{N-C}(m) \approx A_2(m) + A_3(m)\ k^{-1}$, which is qualitatively in agreement with the numerical finding. But within the Bethe approximation, $A_2(m = 2) \approx 0.59$ and $A_3(m = 2) \approx 0.15$. We studied the C-S transition using entropy estimates and obtained $\rho_c^{C-S} \approx 1 - A_4/mk^2$

for $k \gg 1$, where A_4 is a constant.

Future directions: Here we discuss some open problems and future directions based on the studies in this thesis.

The system of hard rods ($m = 1$) undergoes two successive transitions with increasing density: first from a low-density disordered to a nematic phase and second from the nematic to a high-density disordered phase. Although we showed that the low-density and the high-density disordered phases are qualitatively similar on the RLTL, the question whether these two phases are similar on the square lattice is still not answered satisfactorily. The numerically obtained critical exponents for the second transition differ from those of the first transition. However, the simulations for $m = 1$ presented in this thesis are done without incorporating the flip move. Performing the simulations with the flip move reduces the autocorrelation time and should improve the data at high densities, leading to better estimates of the critical exponents for the second transition.

At full packing or zero monomer density, the phase of the system of k-mers on a bipartite lattice is critical with algebraic decay of correlation. The correlation exponent is exactly known only for dimers ($k = 2$) [64]. For trimers ($k = 3$), it was shown to be different from that of dimers [67]. The immediate question would be, how the correlation at full packing depends on k? One possible direction to solve this problem is to follow the Coulomb gas method. It involves two major steps: first, mapping the fully packed system of k-mers to a height model and then, fixing the renormalized couplings to write an effective action for the coarse-grained height field which can be treated with the theory of Coulomb gas with electric and magnetic charges. The couplings are a priori unknown. For dimers, the couplings may be fixed using the exact solution. However, there exists no exact solution for $k > 2$. The height representation for trimers may constructed using a two-dimensional vector field [67]. But it still remains unresolved how to fix the couplings for the k-mer problems without using the exact solution. One may look how it is done for fully packed loop model [141, 142].

Does the critical behavior of the nematic–disordered phase transition at high densities get affected by the critical properties at full packing? In other words, do the critical exponents of this transition depend on k? It would be very interesting to study the nematic–disordered transition for $k > 7$ on the square lattice and verify this issue. Also, further studies are needed to determine if the correlations in the high-density disordered phase decay exponentially for distances greater than ξ^*.

One may also study the problem of repulsive rods on the square lattice using numerical simulations. The algorithm presented in Sec. 2.4.1 is generalizable to the case when intersections are allowed. Confirming whether the qualitative behavior is similar to that seen for the RLTL would be interesting. Measuring the exponents for the second transition might be easier for such a model as the critical density would be away from the fully packed limit.

The RLTL is suitable for studying hard-core models of anisotropic particles. An example is polydispersed systems of hard rods which can show multiple phases [143, 144]. Its solution on the RLTL would make rigorous some of the qualitative features of the problem. Another interesting problem is that of percolation of a system of long rods. Using simulations, the dependence of the critical percolation threshold on the rod length, and the probabilities of horizontal and vertical rods being present, has been conjectured [145, 146]. These conjectures may be checked on the RLTL through an exact solution.

The hard rectangle model may be generalized in different directions. One could consider the model on other lattices like the triangular lattice. Here, the parallelograms may orient themselves along three possible lattice directions. For each orientation, the rectangles may have two different slants (as the shorter side of the rectangle may be oriented along two possible lattice directions). In this case, we expect the phase diagram to be qualitatively similar to that for the square lattice. However, as there are three broken symmetry phases corresponding to the three directions, the I-N transition would be in the three-state Potts universality class, as opposed to Ising universality class for the square lattice. However,

the N-C transition would be same as that for the square lattice. Now, the number of symmetric C phases increases from $2m$ to $6m$ or $3m$. The S phase will now have $2m^2$ symmetric states, the extra factor of 2 being due to the two different slants corresponding to each orientation. As the number of possible states increases with m, it becomes harder to argue the nature of the transitions a priori.

Extension to hard cuboids on cubic lattice would result in a much richer phase diagram that remains to be explored. Is the high-density phase a layered phase? Does a smectic-like phase exist at intermediate densities? What is the complete phase diagram? The algorithm for rectangles (see Sec. 2.4.2) is easily implementable in three dimensions. In this case, one needs to implement efficient parallel programming techniques. GPU seems to be a potential candidate to explore this problem.

The $m = 1$ case (hard rods) is the only instance where the existence of a nematic phase may be proved rigorously [24]. Can one come up with such proof to show that the high-density phase for hard rods has no order? To the best of our knowledge, there exists no proof of existence of phases with partial translational order like the columnar phase. The hard rectangle model seems an ideal candidate to prove its existence. Recently, the nematic–columnar transition for the hard rectangle gas has been studied using a high-activity expansion in inverse fractional powers of the fugacity [139]. The terms in the expansion are more tractable in the limit $k \gg 1$. This limiting case is a good candidate for proving the existence of the columnar phase.

Another generalization is to study polydispersed system of hard rods or rectangles to obtain the phase diagrams for different mixtures. The Monte carlo algorithm presented for the system of monodispersed rectangles may easily be generalized for polydispersed case. Entropy per site of the fully ordered nematic phase for the monodispersed system at full coverage is zero in the thermodynamic limit, favouring the orientationally disordered phase at high densities. Polydispersity leads to nonzero nematic entropy at full packing. Thus, it would be intersecting to see whether the orientational order is stable

at full packing for any mixture. In the continuum, polydispersity may result in reentrant nematic phase or two distinct nematic phases, and broadening of phase coexistence region [98, 96]. It would be interesting to see which features persist in the lattice version. In this context, one may also study the effect of introducing aligning interaction between the rectangles that stablises the orientational order.

Recently, the mixture of hard dimers and squares, exhibiting a rich phase diagram with a Kosterlitz-Thouless transition and a line of Ashkin-Teller criticality separating the different phases, has been studied using a transfer matrices based Monte carlo algorithm which enabled the study even at full packing [31]. This opens up many possibilities including the study of the systems with different mixtures of hard rectangles, rectangles with attractive interaction between them, such as between two neighboring rectangles on the same row or column. Including attractive interaction results in phases with broken orientational and transitional symmetry even for dimers [107, 108].

Virial expansion truncated at the second virial coefficient predicts $\rho_c^{I-N} \approx A_1/k$ for $k \gg 1$, where $A_1 = 2$. However, from Monte carlo simulations, we found $A_1 = 4.80 \pm 0.05$, for $k \gg 1$. This discrepancy indicates that the second virial theory is not exact in the limit $k \to \infty$ in two dimensions. We found that the higher order virial coefficients can't be neglected in this case, as all the even virial coefficients have non-negligible contribution. But none of the odd virial coefficients contribute in the limit $k \to \infty$. In general, number of diagrams required to calculate virial coefficients increases very rapidly with the order of the coefficient. Quite interestingly, we found that in this case the number of diagrams are of order one, which opens up the possibility of calculating A_1 exactly by taking into account the contribution of the higher order even virial coefficients.

Using entropy estimates, we found that for hard rectangles, the critical density for the C-S transition $\rho_{C-S}^c \approx 1 - A_4/mk^2$. It would be interesting to verify this conjecture and determine the prefactor by Monte carlo simulations. It may be easier to verify the conjecture for the system of hard rods ($m = 1$). But, further improvement in the algorithm is needed.

One possible direction is the modification suggested in Ref. [31].

The phase diagram when the aspect ratio of the rectangles is irrational remains an open question. In this case, it has been conjectured that there could be more transitions at densities close to full packing, when the disordered phase will become unstable to a nematic or columnar phases [20]. This question, as well as finding tighter bounds on k for existence of different phases are best answered by obtaining the phase diagram of hard rectangles with restricted orientation in two-dimensional continuum, when the aspect ratio may be continuously tuned.

Bibliography

[1] P. N. Pusey and W. van Megen *Nature*, vol. 320, p. 340, 1986.

[2] X. Wen, R. B. Meyer, and D. L. D. Caspar *Phys. Rev. Lett.*, vol. 63, p. 2760, 1989.

[3] E. Grelet *Phys. Rev. Lett.*, vol. 100, p. 168301, 2008.

[4] A. Kuijk, D. V. Byelov, A. V. Petukhov, A. v. Blaaderen, and A. Imhof *Faraday Discuss.*, vol. 159, p. 181, 2012.

[5] M. P. B. van Bruggen, F. M. van der Kooij, and H. N. W. Lekkerkerker *J. Phys. Condens. Matter*, vol. 8, p. 9451, 1996.

[6] K. Zhao, R. Bruinsma, and T. G. Mason *Proc. Natl. Acad. Sci.*, vol. 108, p. 2684, 2011.

[7] Y. Maeda, T. Niori, J. Yamamato, and H. Yokoyoma *Thermochimica Acta*, vol. 431, p. 87, 2005.

[8] W. G. Hoover and F. H. Ree *J. Chem. Phys.*, vol. 49, p. 3609, 1968.

[9] B. J. Alder and T. E. Wainwright *J. Chem. Phys.*, vol. 27, p. 1208, 1957.

[10] P. G. de Gennes and J. Prost, *The Physics of Liquid Crystals*. Oxford: Oxford University Press, 1995.

[11] L. Onsager *Ann. N.Y. Acad. Sci.*, vol. 51, p. 627, 1949.

[12] P. Bolhuis and D. Frenkel *J. Chem. Phys*, vol. 106, p. 666, 1997.

[13] D. E. Taylor, E. D. Williams, R. L. Park, N. C. Bartelt, and T. L. Einstein *Phys. Rev. B*, vol. 32, p. 4653, 1985.

[14] D.-J. Liu and J. W. Evans *Phys. Rev. B*, vol. 62, p. 2134, 2000.

[15] R. Zwanzig *J. Chem. Phys.*, vol. 39, p. 1714, 1963.

[16] P. J. Flory *Proc. R. Soc.*, vol. 234, p. 73, 1956.

[17] R. L. C. Vink *Eur. Phys. J. B*, vol. 72, p. 225, 2009.

[18] A. Donev, J. Burton, F. H. Stillinger, and S. Torquato *Phys. Rev. B*, vol. 73, p. 054109, 2006.

[19] K. Zhao, C. Harrison, D. Huse, W. B. Russel, and P. M. Chaikin *Phys. Rev. E*, vol. 76, p. 040401, 2007.

[20] A. Ghosh and D. Dhar *Eur. Phys. Lett.*, vol. 78, p. 20003, 2007.

[21] O. J. Heilmann and E. Lieb *Commun. Math. Phys.*, vol. 25, p. 190, 1972.

[22] H. Kunz *Phys. Lett. A*, vol. 32, p. 311, 1970.

[23] O. J. Heilmann and E. H. Lieb *Phys. Rev. Lett.*, vol. 24, p. 1412, 1970.

[24] M. Disertori and A. Giuliani *Commun. Math. Phys.*, vol. 323, p. 143, 2013.

[25] D. A. Matoz-Fernandez, D. H. Linares, and A. J. Ramirez-Pastor *Eur. Phys. Lett*, vol. 82, p. 50007, 2008.

[26] D. Dhar, R. Rajesh, and J. F. Stilck *Phys. Rev. E*, vol. 84, p. 011140, 2011.

[27] A. Casey and P. Harrowell *J. Chem. Phys.*, vol. 103, p. 6143, 1995.

[28] E. DiMarzio *J. Chem. Phys.*, vol. 35, p. 658, 1961.

[29] T. Nath and R. Rajesh *Phys. Rev. E*, vol. 90, p. 012120, 2014.

[30] K. Ramola, *Onset of Order in Lattice Systems: Kitaev Model and Hard Squares*. PhD thesis, Tata Institute of Fundamental Research, Mumbai, 2012.

[31] K. Ramola, K. Damle, and D. Dhar *Phys. Rev. Lett.*, vol. 114, p. 190601, 2015.

[32] D. Frenkel *Physica A*, vol. 263, p. 26, 1999.

[33] S. Fraden, G. Maret, D. L. D. Caspar, and R. B. Meyer *Phys. Rev. Lett.*, vol. 63, p. 2068, 1989.

[34] Z. Dogic and S. Fraden *Langmuir*, vol. 16, p. 7820, 2000.

[35] A. Kuijk, A. v. Blaaderen, and A. Imhof *J. Am. Chem. Soc.*, vol. 133, p. 2346, 2011.

[36] P. Bak, P. Kleban, W. N. Unertl, J. Ochab, G. Akinci, N. C. Bartelt, and T. L. Einstein *Phys. Rev. Lett.*, vol. 54, p. 1539, 1985.

[37] A. Patrykiejew, S. Sokolowski, and K. Binder *Surf. Sci. Rep.*, vol. 37, p. 207, 2000.

[38] C. Avendano and F. A. Escobedo *Soft Matter*, vol. 8, p. 4675, 2012.

[39] B. Dünweg, A. Milchev, and P. A. Rikvold *J. Chem. Phys.*, vol. 94, p. 3958, 1991.

[40] M. T. M. Koper *J. Electroanal. Chem.*, vol. 450, p. 189, 1998.

[41] D. S. Gaunt and M. E. Fisher *J. Chem. Phys.*, vol. 43, p. 2840, 1965.

[42] F. H. Ree and D. A. Chesnut *J. Chem. Phys.*, vol. 45, p. 3983, 1966.

[43] Z. Ràcz *Phys. Rev. B*, vol. 21, p. 4012, 1980.

[44] D. Dhar *Phys. Rev. Lett.*, vol. 49, p. 959, 1982.

[45] D. Dhar *Phys. Rev. Lett.*, vol. 51, p. 853, 1983.

[46] D. C. Brydges and J. Z. Imbrie *J. Stat. Phys.*, vol. 110, p. 503, 2003.

[47] G. Parisi and N. Sourlas *Phys. Rev. Lett.*, vol. 46, p. 871, 1981.

[48] O. Derzhko and J. Richter *Phys. Rev. B*, vol. 70, p. 104415, 2004.

[49] M. E. Zhitomirsky and H. Tsunetsugu *Phys. Rev. B*, vol. 75, p. 224416, 2007.

[50] D. S. Rokhsar and S. A. Kivelson *Phys. Rev. Lett.*, vol. 61, p. 2376, 1988.

[51] R. Baxter *Ann. Comb.*, vol. 3, p. 191, 1999.

[52] K. Georgiou, E. Kranakis, and D. Krizanc *Discrete Math.*, vol. 309, p. 5120, 2009.

[53] E. Eisenberg and A. Baram *J. Phys. A*, vol. 33, p. 1729, 2000.

[54] M. Weigt and A. K. Hartmann *Eur. Phys. Lett*, vol. 62, p. 533, 2003.

[55] E. Eisenberg and A. Baram *Eur. Phys. Lett*, vol. 71, p. 900, 2005.

[56] E. Caglioti, V. Loreto, H. J. Herrmann, and M. Nicodemi *Phys. Phys. Lett*, vol. 79, p. 1575, 1997.

[57] B. C. Barnes, D. W. Siderius, and L. D. Gelb *Langmuir*, vol. 25, p. 6702, 2009.

[58] A. J. Ramirez-Pastor, T. P. Eggarter, V. D. Pereyra, and J. L. Riccardo *Phys. Rev. B*, vol. 59, p. 11027, 1999.

[59] F. Romá, A. J. Ramirez-Pastor, and J. L. Riccardo *Langmuir*, vol. 19, p. 6770, 2003.

[60] C. Gruber and H. Kunz *Commun. Math. Phys.*, vol. 22, p. 133, 1971.

[61] P. W. Kasteleyn *Physica*, vol. 27, p. 1209, 1961.

[62] M. E. Fisher *Phys. Rev.*, vol. 124, p. 1664, 1961.

[63] H. N. V. Temperley and M. E. Fisher *Philos. Mag.*, vol. 6, p. 1061, 1961.

[64] M. E. Fisher and J. Stephenson *Phys. Rev.*, vol. 132, p. 1411, 1963.

[65] N. Allegra and J.-Y. Fortin *Phys. Rev. E*, vol. 89, p. 062107, 2014.

[66] A. Verberkmoes and B. Nienhuis *Phys. Rev. Lett.*, vol. 83, p. 3986, 1999.

[67] A. Ghosh, D. Dhar, and J. L. Jacobsen *Phys. Rev. E*, vol. 75, p. 011115, 2007.

[68] A. Bellemans and R. K. Nigam *J. Chem. Phys.*, vol. 46, p. 2922, 1967.

[69] H. Meirovitch *J. Stat. Phys.*, vol. 30, p. 681, 1983.

[70] P. A. Pearce and K. A. Seaton *J. Stat. Phys.*, vol. 53, p. 1061, 1988.

[71] T. M. Haas *J. Stat. Phys.*, vol. 54, p. 201, 1989.

[72] A. Baram and M. Fixman *J. Chem. Phys.*, vol. 101, p. 3172, 1994.

[73] J. Heringa and H. W. J. Blöte *Physica A*, vol. 251, p. 224, 1998.

[74] X. Feng, H. W. J. Blöte, and B. Nienhuis *Phys. Rev. E*, vol. 83, p. 061153, 2011.

[75] K. Ramola and D. Dhar *Phys. Rev. E*, vol. 86, p. 031135, 2012.

[76] R. J. Baxter *J. Phys. A*, vol. 13, p. L61, 1980.

[77] O. J. Heilmann and E. Praestgaard *J. Stat. Phys*, vol. 9, p. 23, 1973.

[78] R. Dickman *J. Chem. Phys.*, vol. 136, p. 174105, 2012.

[79] J. L. Jacobsen *J. Phys. A*, vol. 40, p. 1439, 2007.

[80] H. C. M. Fernandes, J. J. Arenzon, and Y. Levin *J. Chem. Phys.*, vol. 126, p. 114508, 2007.

[81] J. Bouttier, P. D. Francesco, and E. Guitter *J. Phys. A*, vol. 35, p. 3821, 2002.

[82] M. Assis, J. L. Jacobsen, I. Jensen, J.-M. Maillard, and B. M. McCoy *J. Phys. A*, vol. 47, p. 445001, 2014.

[83] D. Frenkel and B. M. Mulder *Mol. Phys*, vol. 55, p. 1171, 1985.

[84] D. Frenkel, H. N. W. Lekkerkerker, and A. Stroobants *Nature*, vol. 332, p. 822, 1988.

[85] J. A. C. Veerman and D. Frenkel *Phys. Rev. A*, vol. 45, p. 5632, 1992.

[86] M. A. Bates and D. Frenkel *J. Chem. Phys*, vol. 109, p. 6193, 1998.

[87] Z. Dogic and S. Fraden *Phys. Rev. Lett.*, vol. 78, p. 2417, 1997.

[88] P. A. Buining and H. N. W. Lekkerkerker *J. Phys. Chem.*, vol. 97, p. 11510, 1993.

[89] A. Czogalla, D. J. Kauert, R. Seidel, P. Schwille, and E. P. Petrov *Nano Lett.*, vol. 15, p. 649, 2015.

[90] J. P. Straley *Phys. Rev. A*, vol. 4, p. 675, 1971.

[91] D. Frenkel and R. Eppenga *Phys. Rev. A*, vol. 31, p. 1776, 1985.

[92] M. D. Khandkar and M. Barma *Phys. Rev. E*, vol. 72, p. 051717, 2005.

[93] M. A. Bates and D. Frenkel *J. Chem. Phys*, vol. 112, p. 10034, 2000.

[94] K. W. Wojciechowski and D. Frenkel *Comput. Methods Sci. Tech.*, vol. 10, p. 235, 2004.

[95] A. Baumgärtner *J. Phys. A*, vol. 17, p. L971, 1984.

[96] Y. Martínez-Ratón and J. A. Cuesta *J. Chem. Phys*, vol. 118, p. 10164, 2003.

[97] T. Fischer and R. L. C. Vink *Eur. Phys. Lett.*, vol. 85, p. 56003, 2009.

[98] N. Clarke, J. A. Cuesta, R. Sear, P. Sollich, and A. Speranza *J. Chem. Phys*, vol. 113, p. 5817, 2000.

[99] R. J. Baxter, *Exactly Solved Models in Statistical Mechanics*. London: Academic Press, 1982.

[100] M. E. Zhitomirsky and H. Tsunetsugu *Phys. Rev. B*, vol. 75, p. 224416, 2007.

[101] F. Alet, Y. Ikhlef, J. L. Jacobsen, G. Misguich, and V. Pasquier *Phys. Rev. E*, vol. 74, p. 041124, 2006.

[102] R. E. Hartwig *J. Math. Phys.*, vol. 7, p. 286, 1966.

[103] P. Fendley, R. Moessner, and S. L. Sondhi *Phys. Rev. B*, vol. 66, p. 214513, 2002.

[104] H. W. J. Blöte and H. J. Hilhorst *J. Phys. A*, vol. 15, p. L631, 1982.

[105] C. L. Henley *J. Stat. Phys.*, vol. 89, p. 483, 1997.

[106] B. Nienhuis, *Phase transitions and Critical Phenomena*, vol. 11. ed C. Domb and J. L. Lebowitz, London: Academic Press, 1987.

[107] F. Alet, J. L. Jacobsen, G. Misguich, V. Pasquier, F. Mila, and M. Troyer *Phys. Rev. Lett*, vol. 94, p. 235702, 2005.

[108] S. Papanikolaou, D. Charrier, and E. Fradkin *Phys. Rev. B*, vol. 89, p. 035128, 2014.

[109] A. Giuliani, V. Mastropietro, and F. L. Toninelli *arXiv:1502.02302*, 2015.

[110] D. A. Huse, W. Krauth, R. Moessner, and S. L. Sondhi *Phys. Rev. Lett.*, vol. 91, p. 167004, 2003.

[111] D. A. Matoz-Fernandez, D. H. Linares, and A. J. Ramirez-Pastor *Physica A*, vol. 387, p. 6513, 2008.

[112] D. A. Matoz-Fernandez, D. H. Linares, and A. J. Ramirez-Pastor *J. Chem. Phys.*, vol. 128, p. 214902, 2008.

[113] D. H. Linares, F. Romá, and A. J. Ramirez-Pastor *J. Stat. Mech.*, p. P03013, 2008.

[114] P. Centres and A. Ramirez-Pastor *Physica A*, vol. 388, p. 2001, 2009.

[115] D. Ioffe, Y. Velenik, and M. Zahradnik *J. Stat. Phys.*, vol. 122, p. 761, 2006.

[116] J. F. Stilck and R. Rajesh *Phys. Rev. E*, vol. 91, p. 012106, 2015.

[117] J. Kundu, R. Rajesh, D. Dhar, and J. F. Stilck *AIP Conf. Proc.*, vol. 1447, p. 113, 2012.

[118] J. Kundu, R. Rajesh, D. Dhar, and J. F. Stilck *Phys. Rev. E*, vol. 87, p. 032103, 2013.

[119] J. Kundu and R. Rajesh *Phys. Rev. E*, vol. 89, p. 052124, 2014.

[120] W. Krauth and R. Moessner *Phys. Rev. B*, vol. 67, p. 064503, 2003.

[121] P. Virnau and M. Müller *J. Chem. Phys.*, vol. 120, p. 10925, 2004.

[122] B. Chapman, G. Jost, and R. van der Pas, *Using OpenMP*. Cambridge: MIT Press, 2007.

[123] J. Sanders and E. Kandrot, *CUDA by Example*. Boston: Addison Wesley, 2010.

[124] R. A. Ramos, P. A. Rikvold, and M. A. Novotny *Phys. Rev. B*, vol. 59, p. 9053, 1999.

[125] P. A. Rikvold and B. M. Gorman *Annual Reviews of Computational Physics*, vol. 1, p. 149, 1994.

[126] P. G. de Gennes and J. Prost, *Proceedings of 33rd Fundamentals of Computer Science (FOCS)*. Los Alamitos, CA: (IEEE Computer Society, Los Alamitos, CA, 1992), 1992.

[127] W. P. Thurston *Amer. Math. Monthly*, vol. 97, p. 757, 1990.

[128] C. M. Fortuin and P. W. Kasteleyn *Physica*, vol. 57, p. 536, 1972.

[129] W. Janke and A. M. J. Schakel *Nuclear Physics B*, vol. 700, p. 385, 2004.

[130] Y. Deng, H. W. J. Blöte, and B. Nienhuis *Phys. Rev. E*, vol. 69, p. 026123, 2004.

[131] G. Kamieniarz and H. W. J. Blöte *J. Phys. A*, vol. 26, p. 201, 1993.

[132] J. Kundu and R. Rajesh *Phys. Rev. E*, vol. 88, p. 012134, 2013.

[133] J. Kundu and R. Rajesh *Eur. Phys. J. B*, vol. 88, p. 133, 2015.

[134] G. J. Vroege and H. N. W. Lekkerkerker *Rep. Prog. Phys.*, vol. 55, p. 1241, 1992.

[135] J. Kundu and R. Rajesh *Phys. Rev. E*, vol. 91, p. 012105, 2015.

[136] W. Selke and L. N. Shchur *J. Phys. A*, vol. 38, p. L739, 2005.

[137] W. Selke *J. Stat. Mech.*, p. P04008, 2007.

[138] E. P. Sokolova and N. P. Tumanyan *Liq. Cryst.*, vol. 27, p. 813, 2000.

[139] T. Nath, J. Kundu, and R. Rajesh *arXiv:1411.7831*, 2014.

[140] M. González-Pinto, Y. Martínez-Ratón, and E. Velasco *Phys. Rev. E*, vol. 88, p. 032506, 2013.

[141] J. Kondev, J. de Gier, and B. Nienhuis *J. Phys. A*, vol. 29, p. 6489, 1996.

[142] J. L. Jacobsen and J. Kondev *Nucl. Phys. B*, vol. 532, p. 635, 1998.

[143] A. Speranza and P. Sollich *Phys. Rev. E*, vol. 67, p. 061702, 2003.

[144] M. Fasolo and P. Sollich *Phys. Rev. Lett.*, vol. 91, p. 068301, 2003.

[145] P. Longone, P. M. Centres, and A. J. Ramirez-Pastor *Phys. Rev. E*, vol. 85, p. 011108, 2012.

[146] Y. Y. Tarasevich, N. I. Lebovka, and V. Laptev *Phys. Rev. E*, vol. 86, p. 061116, 2012.